UNIVERSIDAD COMPLUTENSE DE MADRID
FACULTAD DE CIENCIAS FÍSICAS
Departamento de Física de la Tierra y Astrofísica

TESIS DOCTORAL

Seasonal climate prediction for the wind energy sector: methods and tools for the development of a climate service

Predicciones climáticas estacionales para el sector de la energía eólica: métodos y herramientas para el desarrollo de un servicio climático

MEMORIA PARA OPTAR AL GRADO DE DOCTOR

PRESENTADA POR

Verónica Torralba Fernández

Director

Francisco J. Doblas-Reyes

Madrid
Ed. electrónica 2019

UNIVERSIDAD COMPLUTENSE DE MADRID
FACULTAD DE CIENCIAS FÍSICAS
Departamento de Física de la Tierra y Astrofísica

TESIS DOCTORAL

Seasonal climate prediction for the wind energy sector: methods and tools for the development of a climate service

---

Predicciones climáticas estacionales para el sector de la energía eólica: métodos y herramientas para el desarrollo de un servicio climático

Memoria para optar al grado de doctor presentada por

Verónica Torralba Fernández

Director
Francisco J. Doblas-Reyes

Tutor
Elsa Mohino Harris

Madrid, 2019

Cover and book design:
Isadora Christel

The author acknowledges the **Barcelona Supercomputing Center-Centro Nacional de Supercomputación (BSC-CNS)** for its support for the development of this thesis.

This thesis has been funded by the **RESILIENCE** (CGL2013-41055-R) project supported by the Spanish Ministerio de Economía y Competitividad (MINECO), the **EUPORIAS** (GA 308291) and **SPECS** (GA 308378) projects supported by the European Programme FP7. Further financial support has been provided by the COPERNICUS action **CLIM4ENERGY**-Climate for Energy (C3S 441 Lot 2), the New European Wind Atlas (**NEWA**) project (funded by the Spanish Ministerio de Economía y Competitividad (MINECO) and by the European ERA-NET Plus NEWA) and by the **S2S4E** (GA 776787) HORIZON 2020 project.

Agradecimientos

Haciendo balance de los años de doctorado, me doy cuenta de la gran evolución que he tenido tanto a nivel personal como profesional. Sin embargo, esta evolución no hubiera sido posible sin todas las personas, que me han ayudado a superar cada uno de los obstáculos que he ido encontrando. Por ese motivo quiero utilizar estas páginas para agradecerles a todos ellos.

Quiero empezar dando las gracias al director de esta tesis. Paco, no sería capaz de poner por escrito todo lo que me has enseñado durante el doctorado. Es sorprendente que muchas de estas enseñanzas no tengan nada que ver con la predicción climática. Tu pasión por este trabajo, tu alto nivel de exigencia y tu capacidad para transformar las dificultades en oportunidades son un referente para mí. Espero haber estado a la altura.

También quiero agradecer a Elsa por haber sido el mejor nexo con la Universidad. Que siempre hayas estado disponible para resolver cualquier duda me ha facilitado mucho las cosas en estos años. Además, durante la realización del trabajo fin de máster, tuve la suerte de poder trabajar con Belén y contigo y de adquirir unos conocimientos sobre la variabilidad climática que me han sido muy útiles para el desarrollo de esta tesis.

Nube, aunque no seas la primera de la lista seguramente eres la persona más importante que he conocido durante estos años de doctorado. Muchas gracias por haber confiado siempre en mi capacidad para sacar adelante esta tesis, por ser una gran amiga y uno de mis apoyos fundamentales.

Cuando llegué a Barcelona a conocer al grupo de IC3 (a la CFU) no tenía ninguna expectativa concreta, pero al hablar con Melanie tuve la sensación de que ese era un buen sitio para mí. Mel, gracias por haber estado conmigo durante los dos primeros años. Fue una suerte trabajar contigo. Espero que tu visión sobre los servicios climáticos se haya plasmado en esta tesis.

Además de Nube y Mel, el tiempo en IC3 y después en BSC no hubiera sido lo mismo sin Javi Vegas, Chloé, Mingu, Nico, Pierre-Antoine, y Uri. Muchas gracias por vuestra disponibilidad para ayudarme en cualquier cosa, por haberme dejado aprender de vosotros y por haber hecho mejor mi día a día.

Ya en BSC, he podido ver el trabajo tan duro que ha supuesto crear un grupo de servicios climáticos. Albert, gracias por tu esfuerzo y confianza durante estos años. Muchas gracias también a Isadora que siempre ha estado dispuesta a ayudarme con mis pósters y presentaciones y también por compartir conmigo muchos momentos. Aunque también sé que esta línea no es suficiente para agradecerte el haber sacado tiempo de tus vacaciones y fines de semana para el diseño de esta tesis. Muchas gracias al resto del grupo de Earth System Services, que siempre se han interesado por la evolución de esta tesis. Ha sido un placer trabajar con todos vosotros. En particular, quiero agradecer a las personas con las que he podido colaborar más: Andrea, Jaume, Raül, Nicola, Llorenç, Marta y Bala. Gracias por estar siempre disponibles para ayudar en lo que hiciera falta.

También quiero agradecer todos los miembros del departamento de Earth Sciences ya que hacen que trabajar en este grupo sea un privilegio. Muchas gracias al grupo del café, que incluso ahora que no estamos tan cerca buscan la manera de que no se pierdan las buenas costumbres. Gracias a los PhDs de Torre Girona y en especial a Bianca por hacer que el exilio fuera más llevadero. Muchas gracias también a Mar y Gabi por estar siempre disponibles para ayudar en todo y resolver cualquier duda. Y gracias a Javi García por sus palabras de ánimo y por buscar tiempo para discutir cualquier resultado.

Quiero dar las gracias a Daniel Cabezón y a Sergio Lozano por compartir sus conocimientos sobre energía eólica, los cuales han sido muy importantes para el desarrollo de este trabajo.

Además de todas estas personas, esta tesis no hubiera sido posible sin el apoyo de mi familia y mis amigos.

Muchas gracias a mis amigas de toda la vida, a María y a Sonia porque aunque no les he dedicado mucho tiempo durante estos años siempre han estado muy cerca de mí. También quiero agradecer a la familia de Sonia porque siempre me ha ayudado y me ha tratado como si fuera una más de la casa. Gracias a todos mis amigos de la licenciatura, en particular a Paula, Cristina y Ade que han compartido muchos momentos conmigo durante estos años en Barcelona.

Gracias a mis padres por ser tan buenas personas y por haberme enseñado lo fundamental. ¡Os quiero mucho! Muchas gracias a mis hermanas

(creo que la mayoría de buenos momentos que he tenido en mi vida son gracias a vosotras). Gracias Elena por cuidar de todos y por haberme regalado (vale Javi, ¡tú también!) a mi sobrino Carlos, que es sin duda a quién más he echado de menos durante este tiempo en Barcelona. Gracias Laura por ser tan especial y por estar siempre pendiente de mí. También agradezco a mis abuelas por su cariño incondicional y por ser un ejemplo de fortaleza. Muchas gracias a mi abuelo Pablo por haber estado siempre orgulloso de mí y porque estoy segura de que le hubiera gustado mucho ver esta tesis. Gracias a Dioni, Rosi, Isidora, Patri y Dani por apoyarme en todo, por acogerme en vuestra familia y por las visitas a Barcelona.

Y por último a Sergio. No sé cómo hubiera sobrevivido a esto sin ti. Gracias por ser como eres, por estar siempre conmigo, por tu energía incombustible y también por todos los momentos que hemos vivido en estos años.

Contents

Acknowledgements iv

List of figures xii

List of tables xvii

List of acronyms xviii

Abstract xx

Resumen xxiv

Chapter* 1: *Introduction 2

1.1 Seasonal forecasts 2

1.1.1 Climate prediction framework 3

1.1.2 Sources of predictability at seasonal timescales 4
1.1.3 Seasonal forecast systems 9
1.1.4 Uncertainty in seasonal forecasts 10
1.1.5 Seasonal forecast products 12
1.2 Making seasonal forecasts actionable 15
1.2.1 Climate services context 16
1.2.2 Steps for the climate services development 17
1.2.3 Climate services based on seasonal forecasts 20
1.3 Seasonal forecasts for wind energy 21
1.3.1 Wind energy as a climate-sensitive sector 21
1.3.2 Current forecasting options in the wind industry 22
1.3.3 Tailoring seasonal forecasts for wind energy applications 24
1.4 Scientific challenges for the development of a wind energy climate service 24
1.5 Objectives 28
1.6 Thesis structure 29

Chapter 2: Data description and methodology 34

2.1 Seasonal forecast system: ECMWF System 4 34
2.2 Observational references: reanalyses 37
2.3 Wind at 10-m and temperature at 2-m 39
2.4 Forecast quality assessment 40
2.5 Leave-one-out cross-validation 41

Chapter 3: Systematic errors and trends in the seasonal forecasts 48

3.1 Methodology 49
3.1.1 Climatology and bias 49
3.1.2 Moments of the probability distribution 50
3.1.3 Shapiro-Wilk test 52
3.1.4 Linear trends 52

3.2 Seasonal mean climatology and bias 53
3.2.1 Spatial variability of the mean wind speed 53
3.2.2 ECMWF System 4 seasonal biases 55
3.3 Moments of the probability distribution 58
3.3.1 Standard deviation 58
3.3.2 Skewness and kurtosis 59
3.4 Normality test applied to the seasonal distributions 62
3.5 Long-term variability 64
3.5.1 Trends as a function of the season 65
3.5.2 Trends of the extreme wind speed 67
3.5.3 Coherence of the trends from different reanalyses 70
3.5.4 Trends in the seasonal predictions 72
3.6 Conclusions 76

Chapter 4: Seasonal prediction of wind energy relevant climate indices 82

4.1 Methodology 83
4.1.1 ENSO and NAO indices 83
4.1.2 Storm track definition 85
4.1.3 Metrics 86
4.2 Seasonal predictability of wind energy relevant climate indices 87
4.3 Evaluation of the extra-tropical storm tracks 87
4.4 Teleconnections of wind energy relevant climate indices 94
4.4.1 ENSO impact on wind speed and temperature 94
4.4.2 NAO impact on wind speed and temperature 100
4.4.3 Storm tracks impact on wind speed and temperature 102
4.5 Conclusions 106

Chapter 5: Euro-Atlantic weather regimes for wind energy applications 112

5.1 Methodology 113
5.1.1 Data processing 113
5.1.2 Weather regime computation 114
5.1.3 Metrics for the weather regime evaluation 116

5.2 Weather regimes in ERA-Interim 118
5.3 Reconstructing impact variables with WRs 124
5.4 Seasonal forecast verification of weather regimes 126
5.4.1 Spatial patterns 126
5.4.2 Skill of the predicted weather regimes 129
5.5 Conclusions 131

Chapter **6**: *Bias adjustment and verification for wind energy applications* 138

6.1 Methodology 140
6.1.1 Bias adjustment and reconstruction methods 140
6.2 Bias adjustment impact on the wind speed forecast quality 143
6.3 Reconstruction of the 10-m wind speed from the Niño-3.4 index 151
6.4 Seasonal predictions of extreme wind speeds 156
6.4.1 Definition of wind extreme indices 156
6.4.2 Systematic errors in the seasonal forecasts of extreme winds 158
6.4.3 Predictability of the wind speed seasonal extremes 160
6.5 Conclusions 160

Chapter **7**: *Conclusions and perspectives* 166

7.1 Conclusions 167
7.2 Future work 173
7.3 Final remarks 175

Appendix **A**: *Metrics for the forecast quality assessment* 180

Appendix **B**: *Additional figures* 192

Appendix **C**: *List of publications* 236

References 240

List of Figures

Chapter 1: Introduction 2

Figure 1 – Time horizon of different short-to-medium range forecasts, climate predictions and climate projections 3
Figure 2 – Scheme illustrating the role of different parts of the Earth's climate system (atmosphere, land surface and ocean) as sources of predictability 5
Figure 3 – Graphic illustrating the main characteristics of the ENSO in its positive phase 6
Figure 4 – Graphic illustrating the main characteristics of the NAO in its positive phase 7
Figure 5 – Schematic of a probabilistic forecast 11
Figure 6 – ECMWF System 4 near-surface wind speed probabilistic forecast of most likely tercile category, for DJF 2016/2017 13
Figure 7 – WMO Global Producing Centres for Long-Range Forecasts 14
Figure 8 – Graphic illustrating the Global Framework for Climate Services vision 18

Figure 9 – Diagram with a simplified climate services chain 19
Figure 10 – Global wind energy cumulative installed capacity (MW) from 2007 to 2017 21
Figure 11 – Stages of wind farm development, the stakeholders involved at each stage and temporal horizons of the climate information used 23
Figure 12 – Mindmap with the potential fields of application of seasonal forecasts in the wind energy sector 25

Chapter 2: Data description and methodology 34

Figure 13 – Diagram of the ECMWF System 4 seasonal forecast system 36
Figure 14 – Schematic illustration of the leave-one-out cross-validation method . . 42

Chapter 3: Systematic errors and trends in the seasonal forecasts 48

Figure 15 – Hypothetical probability density functions to illustrate the concepts of of a) standard deviation, b) skewness and c) kurtosis 51
Figure 16 – Seasonal mean climatology of the 10-m wind speed (m/s) from ERA-Interim in the 1981-2015 period 54
Figure 17 – Mean bias of the ECMWF System 4 seasonal predictions (ensemble mean) of 10-m wind speed (m/s) and 2-m air temperature (K) 57
Figure 18 – Standard deviation of the 10-m wind speed (m/s) in ECMWF System 4 and ERA-Interim 60
Figure 19 – Skewness and kurtosis of the 10-m wind speed 61
Figure 20 – P-values of the Shapiro-Wilk goodness-of-fit normality test. 63
Figure 21 – Normalised linear trends (% per decade) of the 10-m wind speed from ERA-Interim 66
Figure 22 – Normalised linear trends (% per decade) of the 850 hPa wind speed from ERA-Interim 67
Figure 23 – Linear trends (m/s per decade) comparison of the 10^{th} and 90^{th} percentiles of the 10-m wind speed from ERA-Interim 69
Figure 24 – Coherence maps between the ERA-Interim, JRA-55 and MERRA-2 reanalyses in the a) 10-m and b) 850 hPa c) 10^{th} percentile and d) 90^{th} percentile wind speed trends 71
Figure 25 – Normalised linear trend (% per decade) of the ECMWF System 4 seasonal forecasts of 10-m wind speed 73

Figure 26 – Coherence maps between the trends of the ECMWF System 4 seasonal forecasts of 10-m wind speed trends and those produced by a) ERA-Interim, b) JRA-55 and c) MERRA-2. 74

Chapter 4: Seasonal prediction of wind-energy relevant indices 82

Figure 27 – Niño 3.4 and NAO indices and spatial patterns 84
Figure 28 – Summary of the methodology used to explore the teleconnections in the ERA-Interim reanalysis and ECMWF System 4 seasonal predictions 86
Figure 29 – Pearson correlation coefficient between the ECMWF System 4 ensemble mean of the a) Niño-3.4 and b) NAO indices and the corresponding indices from the ERA-Interim reanalysis 88
Figure 30 – ERA-Interim climatological storm track intensity (hPa) 89
Figure 31 – Comparison of the climatological storm track intensity (hPa) of a) ERA-Interim and b) ECMWF System 4 90
Figure 32 – Bias (hPa) between the storm tracks predicted by the ECMWF System 4 and the ERA-Interim reanalysis 92
Figure 33 – Bias (hPa) between the storm tracks predicted by the ECMWF System 4 and the ERA-Interim reanalysis for different lead months 93
Figure 34 – One-point correlation maps between the 10-m wind speed (left column) and 2-m air temperature (right column) with the Niño-3.4 index 95
Figure 35 – Lead time dependency of the DJF differences between the ECMWF System 4 seasonal forecasts and ERA-Interim in the one-point correlation maps of the 10-m wind speed and the Niño-3.4 index . . . 98
Figure 36 – Lead time dependency of the DJF differences between the ECMWF System 4 seasonal forecasts and ERA-Interim in the one-point correlation maps of the 2-m temperature and the Niño-3.4 index . . . 99
Figure 37 – One-point correlation maps between the 10-m wind speed and 2-m air temperature with the NAO index 101
Figure 38 – One-point correlation map between the 10-m wind speed with the NAST and NPST indices 103

Figure 39 – One-point correlation map between the 2-m air temperature with the NAST and NPST indices 104

Chapter 5: Euro-Atlantic weather regimes for wind energy applications 112

Figure 40 – Workflow used to perform weather regime classifications for each month of the year from daily sea level pressure anomalies 115
Figure 41 – Composites of the averaged sea level pressure anomalies (hPa), belonging to each one of the clusters obtained by the KM classification in winter months 121
Figure 42 – Composites of the averaged 10-m wind speed (m/s), belonging to each one of the clusters obtained by the KM classification in winter months. 122
Figure 43 – Composites of the averaged 2-m air temperature (K), belonging to each one of the clusters obtained by the KM classification in winter months. 123
Figure 44 – Pearson correlation between the reconstructed 10-m wind speed (first row) and 2-m air temperature (second row) based on weather regimes and the original variables from ERA-Interim 125
Figure 45 – Spatial correlation between the ECMWF System 4 seasonal predictions and ERA-Interim reanalysis monthly weather regimes patterns obtained by the KM and RMSD methods 127
Figure 46 – Spatial correlation between the ECMWF System 4 seasonal predictions and ERA-Interim reanalysis composites of the 10-m wind speed and 2-m temperature with monthly WRs obtained by the KM and RMSD methods 128
Figure 47 – Pearson correlation between the ECMWF System 4 seasonal predictions and ERA-Interim reanalysis monthly frequencies of occurrence corresponding to the WRs obtained by the KM method and RMSD methods 130

Chapter 6: Bias adjustment and verification for wind energy applications 138

Figure 48 – Time series of 10-m wind speed from ECMWF System 4 and ERA-Interim reanalysis in winter (DJF) for a region in Canada 144
Figure 49 – Fair ranked probability skill score (FRPSS) for tercile events of 10-m wind speed forecasts from ECMWF System 4 and ERA-Interim reanalysis in winter (DJF) 145

Figure 50 – Reliability diagrams of 10-m wind speed forecasts from ECMWF System 4 and ERA-Interim reanalysis in winter (DJF) for a region in Canada. 148
Figure 51 – Rank histograms of 10-m wind speeds forecasts from ECMWF System 4 and ERA-Interim reanalysis in winter (DJF) for a region in Canada . 150
Figure 52 – Pearson correlation between the ERA-Interim data and the seasonal forecasts of 10-m wind speed from a) ECMWF System 4 b) reconstruction from the Niño-3.4 index "in sample" and c) reconstruction from the Niño-3.4 index in cross-validation 152
Figure 53 – Pearson correlation between the 10-m wind speed from ECMWF System 4, the reconstructed 10-m wind speed predictions from the Niño-3.4 index and the differences between them 154
Figure 54 – Percentage of points in a Canadian region with different correlation ranks in the 10-m wind speed seasonal predictions from ECMWF System 4 and those reconstructed from the Niño-3.4 index 155
Figure 55 – Illustration of the methodology used to compute extreme wind speed indicators 157
Figure 56 – Bias of the ECMWF System 4 seasonal forecasts of the 10-m wind speed extreme indicators 159
Figure 57 – Pearson correlation of the ECMWF System 4 seasonal forecasts of the 10-m wind speed extreme indicators 161

List of Tables

Table 1 – Summary with the main specifications of the systems employed by the current WMO Global Producing Centers for Long-Range Forecasts. (Source: https://www.wmolc.org/contents2.php?sm_id=1&tm_id=1&cdepth=3&upnum=6&ca_id=116&s1=4&s2=1&t1=4). 15

Table 2 – Summary of the main characteristics of the three reanalysis datasets used in the present study. 40

Table 3 – Goodness-of-fit tests: Pearson χ^2, JP-slope and JP-convex statistics formulated by Jolliffe and Primo (2008) and their p-values in brackets. They have been computed from the rank histograms (Figure 51) of 10-m wind speed forecasts from ECMWF System 4 in winter (DJF) for the period 1981-2012. . 150

List of acronyms

C3S Copernicus Climate Change

CDF Cumulative Density Function

CRPSS Continuous Ranked Probability Skill Score

DJF December-January-February

ECWMF European Centre for Medium-Range Weather Forecasts

ENSO El Niño-Southern Oscillation

$\boldsymbol{faq90}_{clim}$ fraction of time above the 90^{th} percentile

$\boldsymbol{fbq10}_{clim}$ fraction of time below the 10^{th} percentile

FCRPSS Fair Continuous Ranked Probability Skill Score

FRPSS Fair Ranked Probability Skill Score

GFCS Global Framework for Climate Services

GHG Greenhouse Gases

GPCLRF Global Producing Centre for Long-Range Forecasts

JJA June-July-August

JMA Japan Meteorological Agency

KM K-means clustering approach

MAM March-April-May

NASA National Aeronautics and Space Administration

NAST North Atlantic Storm Track

NAO North Atlantic Oscillation

NCEP National Center for Environmental Prediction

NPST North Pacific Storm Track

PCA Principal components analysis

PDF Probability Density Function

q10 10^{th} percentile

q90 90^{th} percentile

RMSD Root-mean-square distance

RPSS Ranked Probability Skill Score

SLP Sea Level Pressure

SON September-October-November

SST Sea Surface Temperature

WMO World Meteorological Organization

WR Weather Regimes

Abstract

Introduction

Seasonal forecasts have shown high potential for their application in different socioeconomic sectors (e.g. energy, agriculture, transport, tourism, health, ...). Nevertheless, the deployment of these forecasts in different decision-making processes requires that the seasonal forecasts are adapted to be easily integrated into different applications. To satisfy this need, the climate services research line has recently emerged to transform climate information into products that can be used by the society and the industry. One of the sectors that could benefit the most from seasonal forecasts is the wind energy sector. Wind energy is one of the most important sources of renewable energy for the mitigation of climate change effects on the society.

Despite the numerous economic and environmental benefits related to this source of renewable energy, its integration in the energy market presents several challenges. One of the factors affecting wind energy development is climate variability, which is at the origin of fluctuations in the wind speed and air temperature. Forecasting these fluctuations at different timescales is crucial for the efficient management of the wind energy resources and the integration of the wind energy systems into the electric network. Nowadays, short term forecasts (from minutes up to a few days) and climate projections (from 30 years up to a century) are used in different decision-making processes and activities in the wind energy sector. However, those decisions that require information about the evolution of wind energy

resources in the upcoming months or seasons are based on the assumption that the future climate conditions will be a repetition of the past. An alternative to this approach is the use of seasonal forecasts, which allow anticipating climate events, some of them might have never occurred before.

Objectives

The main goal of this thesis is to provide a robust evaluation of the opportunities and limitations of the use of seasonal forecasts in a climate service tailored to improve wind energy applications. This goal will be achieved by two specific objectives.

1 To describe the systematic errors affecting the seasonal forecasts of wind speed and air temperature and the evaluation of the forecast quality of wind energy relevant climate indices in the ECMWF System 4 seasonal forecast system.

2 To investigate the potential of the seasonal forecasts for the development of pioneering products tailored to benefit the wind energy sector by providing more accurate information than current approaches do.

Main results

- The seasonal forecasts of 10-m wind speed and 2-m air temperature show systematic errors in the mean, standard deviation, skewness, kurtosis and also in the long-term trends. These systematic errors depend on the reanalyses used as an observational reference. This evidences the uncertainty affecting reanalysis datasets, particularly in the case of the 10-m wind speed.

- The high correlation values obtained for the indices used to describe the inter-annual variability of the El Niño-Southern Oscillation (through the Niño-3.4 index) and the North Pacific storm tracks (NPST index) illustrate the good levels of seasonal skill in the Pacific. However, the ECMWF System 4 does not produce skilful information in the North Atlantic, as shown by the low correlation values in the seasonal forecasts of the North Atlantic Oscillation (NAO index) and the storm tracks in the North Atlantic (NAST index).

- Weather regimes (WRs) have been defined for each individual month of the year in the Euro-Atlantic region. The sea level pressure-based WRs' frequency of occurrence has been used to reconstruct the 10-m wind speed and 2-m air temperature. The reconstructed variables display high correlations with the original variables in key regions for the wind industry, such as the North Sea. This evidences that WRs are a useful tool to understand the climate variability.

- WRs for the seasonal forecasts have been obtained with two alternative methodologies: the k-means analysis and the minimum root-mean-square distance. The seasonal forecasts of the WRs are only skilful in the first forecast

month (regardless of the method used to perform the classification), as it is when the WR frequency of occurrence shows positive skill.

- The comparison of three statistical bias adjustment approaches (simple, calibration and quantile mapping) applied on the seasonal forecasts of 10-m wind speed shows a similar impact on the forecast quality. However, the calibration method produces adjusted seasonal forecasts with marginally more reliable probabilities. Consequently, this method is recommended to adjust the forecasts to be included in an operational climate service.

- The usefulness of hybrid empirical-dynamical models has been illustrated for a region in Canada. The seasonal forecasts of 10-m wind speed have been reconstructed from the ECMWF system 4 seasonal forecasts of the Niño-3.4 index and the empirical relationship between this index and the 10-m wind speed in the reference dataset. The reconstructed seasonal forecasts show enhanced skill as a consequence of the improved representation of the ENSO teleconnections to wind speed in that region.

Conclusions

The scientific contributions of this PhD thesis represent an innovation in the use of climate information for the creation of tailored products to benefit the wind energy sector. The main lessons learnt from this work, as outlined below, should be considered for the future generation of seasonal forecast systems and related climate services for wind energy.

- The choice of a bias adjustment method should take into account not only the systematic errors in the mean but in other moments of the distribution. Besides, it is important to take into account the uncertainty affecting the observational references by employing more than one reference dataset.

- The predictability of the Niño-3.4 and NPST indices reveals that these indices are good candidates to be used as predictors in a hybrid model that combines dynamical predictions with the empirical relationships of these indices with the wind speed and air temperature based on observations.

- The two different methodologies used to derive seasonal forecasts of WRs are complementary. While the k-means classification method is useful to investigate systematic errors in the atmospheric circulation, the assignation based on the minimum root-mean-square distance is useful to generate an easily interpretable product.

- Seasonal forecasts tailored to the wind energy sector have to include an indication of their quality compared with a benchmark forecast. Furthermore, these forecasts should have similar statistical properties to the observational references. Consequently, forecast quality assessment and bias adjustment are essential steps in the development of a wind energy climate service.

Resumen

Introducción

Las predicciones climáticas estacionales han mostrado un gran potencial para su aplicación en distintos sectores socioeconómicos (energía, agricultura, transporte, turismo, salud,etc). Sin embargo, la integración de estas predicciones en procesos de toma de decisión requiere que éstas sean adaptadas para poder ser utilizadas de una manera automática y sencilla en distintas actividades. Con el fin de satisfacer esta necesidad ha surgido la línea de investigación de los servicios climáticos, que tiene como objetivo la transformación de información climática en productos que puedan beneficiar a la sociedad y la industria. Uno de los sectores que puede obtener un mayor beneficio de las predicciones estacionales es el sector de la energía eólica, que es una de las fuentes de energía renovable más importantes para la mitigación de los efectos del cambio climático.

A pesar de la gran cantidad de beneficios ambientales y económicos asociados a esta fuente de energía renovable, su penetración en el mercado energético conlleva grandes retos. Uno de los factores que influye en el desarrollo del sector eólico es la variabilidad climática, ya que ésta es la responsable de las fluctuaciones en la velocidad del viento y la temperatura. La predicción de estas variaciones a distintas escalas temporales es esencial para la gestión eficiente de los recursos eólicos y para la integración de los sistemas eólicos en la red eléctrica. Por ese motivo, las predicciones a corto plazo (entre diez minutos y unos días) y las proyecciones de cambio climático (desde 30 años a una década) son herramientas utilizadas actualmente en este

sector. No obstante, en aquellas decisiones que requieren información sobre la evolución del clima en los próximos meses o estaciones, se considera que las condiciones climáticas futuras serán una repetición de las que hubo en el pasado. Una alternativa a esta suposición, es la utilización de predicciones climáticas estacionales, las cuales son capaces de anticipar eventos que no han ocurrido en el pasado.

Objetivos

La meta principal de esta tesis doctoral es proporcionar una evaluación de las oportunidades y limitaciones de las predicciones estacionales para su utilización en el desarrollo de un servicio climático dirigido a beneficiar al sector eólico. Para alcanzar esta meta se proponen dos objetivos específicos:

1 Evaluación del sistema de predicción estacional System 4 del ECMWF mediante la descripción de los errores sistemáticos en la velocidad del viento y la temperatura y del análisis de la calidad de las predicciones de índices climáticos relevantes para la industria eólica.

2 Investigación del potencial de las predicciones estacionales para el desarrollo de productos novedosos que permitan anticipar variaciones en los recursos eólicos y que mejoren la información utilizada actualmente para los procesos de toma de decisión.

Resultados principales

- Las predicciones estacionales de la velocidad del viento y de la temperatura del aire presentan errores sistemáticos en la media, desviación estándar, asimetría, curtosis y también en las tendencias. Estos errores sistemáticos varían dependiendo de la referencia observacional utilizada, lo que muestra el papel tan importante que juega la incertidumbre que afecta a los distintos reanálisis, y en particular a la variable velocidad del viento.

- Las predicciones estacionales de los índices climáticos que permiten caracterizar la variabilidad inter-anual de "El Niño-Southern Oscillation" (índice Niño-3.4) y las "storm track" en el Pacífico (índice NPST) tienen valores altos de correlación, lo que evidencia la gran capacidad predictiva del sistema de predicción ECMWF System 4 en el Pacífico. Sin embargo, los índices de la "North Atlantic Oscillation" (índice NAO) y de las "storm tracks" en el Atlántico Norte (índice NAST) presentan valores de correlación bajos que indican que ECMWF System 4 tiene dificultades para proporcionar información fiable en esta región.

- Los regímenes de tiempo en la región Euro-Atlántica se han definido individualmente para cada mes del año y sus frecuencias de ocurrencia han sido utilizadas para reconstruir el viento y la temperatura. Este método de reconstrucción proporciona variables que

tienen una alta correlación con las variables originales en regiones importantes para la industria eólica como el mar del Norte. Este resultado demuestra que los regímenes de tiempo son una herramienta útil para entender la variabilidad en los recurso eólicos.

- Los regímenes de tiempo basados en predicciones estacionales han sido calculados mediante dos métodos diferentes: clasificación "k-means" y asignación con el criterio de la distancia cuadrática media mínima. Sin embargo, ambos métodos producen regímenes de tiempo que sólo son fiables en el primer mes de la predicción, ya que es el único mes para el que las frecuencias de ocurrencia de los regímenes en las predicciones estacionales muestran correlaciones positivas con las frecuencias de la referencia observacional.

- La comparación del efecto de tres métodos estadísticos (método simple, calibración y asignación de cuantiles) para el ajuste de los sesgos en las predicciones estacionales de la velocidad del viento ha demostrado que estos métodos tienen un impacto similar en la calidad de las predicciones. No obstante, el método de calibración proporciona unas predicciones ajustadas con probabilidades ligeramente más creíbles. Por lo tanto, se ha determinado que este método es el más adecuado para la generación de predicciones que vayan a ser integradas en un servicio climático operacional.

- La utilidad de modelos híbridos que combinan predicciones dinámicas con relaciones empíricas se ha ilustrado para una región de Canadá. En esta región las predicciones estacionales de viento han sido reconstruidas a partir de las predicciones estacionales del índice Niño-3.4 y de la relación empírica de este índice con el viento en la referencia observacional. Las predicciones reconstruidas presentan un aumento de su predecibilidad respecto a las predicciones originales como consecuencia de la mejora en la representación de las teleconexiones del ENSO con la velocidad del viento.

Conclusiones

Las contribuciones científicas de esta tesis doctoral ilustran un uso innovador de las predicciones estacionales para la creación, por primera vez, de productos climáticos orientados al sector eólico. Las conclusiones más relevantes deberían ser tenidas en cuenta en el desarrollo de las generaciones futuras de sistemas de predicción estacional así como de los servicios climáticos asociados al sector energético. Estas conclusiones son las siguientes:

- La elección del método más adecuado para corregir los errores sistemáticos de las predicciones estacionales debe tener en cuenta tanto los sesgos en la media como en otras propiedades estadísticas de la distribución de las variables velocidad del viento y temperatura. Además, es fundamental la consideración de la incertidumbre asociada a la selección de la base de datos de referencia.

- Las dos metodologías utilizadas para calcular regímenes de tiempo en las predicciones estacionales son complementarias. El método “k-means” es un diagnóstico muy útil para identificar los errores sistemáticos de los sistemas de predicción estacional en la caracterización de los regímenes de tiempo, mientras que el método basado en la asignación con la distancia cuadrática media mínima es apropiado para generar un producto que pueda ser utilizado fácilmente.

- La caracterización de la calidad de las predicciones así como el ajuste de sus sesgos son dos aspectos fundamentales en el desarrollo de un servicio climático para el sector eólico. Las predicciones estacionales adaptadas deben incluir información acerca de su valor añadido respecto a una predicción de referencia. Además, estas predicciones tienen que tener propiedades estadísticas similares a las referencias observacionales para poder ser interpretadas y utilizadas correctamente por los usuarios de la industria eólica.

01 Introduction

01 Introduction

This chapter sets the framework of the thesis in six sections. An overview of the state-of-the-art in seasonal climate forecasting in presented section 1.1. This section is followed by a description of how seasonal forecasts could be used for the development of a climate service in section 1.2. The vulnerability of the wind energy sector to climate conditions and the potential benefits of integrating seasonal forecasts in this sector are discussed in section 1.3. The scientific challenges in the use of seasonal forecasts for the development of climate information tailored to the wind energy sector are exposed in section 1.4. Section 1.5 details the objectives and section 1.6 describes the structure of the chapters included in this PhD thesis.

1.1 Seasonal forecasts

The climate system is a highly complex structure consisting of five major components: atmosphere, hydrosphere, cryosphere, lithosphere and biosphere, which interact with each other. Forecasting approaches seek to simulate the evolution of the different components of the climate system over a wide range of timescales. This evolution is the result of the combination of internal dynamics (i.e. natural climate variability) and external forcings such as the human-induced climate change (Solomon 2007).

Forecasts can be classified into three major categories depending on their time horizon:

short to medium range forecasts, climate predictions (subseasonal, seasonal, and decadal) and climate projections. This thesis focuses on climate predictions at seasonal timescales (i.e. seasonal forecasts).

1.1.1 Climate prediction framework

The time horizons covered by each type of forecast are illustrated in Figure 1. Although this classification can help to identify which are the most useful forecasts for each specific application, the boundaries between these categories are usually blurred, as some of the physical processes responsible for the climate variability are common among the timescales and the improvements in one particular forecast category can benefit forecasts covering a different timescale (Brunet et al. 2010).

Short to medium range forecasts, usually known as weather forecasts, predict the evolution of phenomena with ranges from minutes to a few days ahead. They are produced with advanced representations of atmospheric processes at spatial resolutions of a few kilometres (Mariotti et al. 2018). These forecasts strongly depend on the detailed description of the observed conditions at their starting point which is usually defined as initial conditions[1]) (National Academies of Sciences and Medicine 2016). It is generally considered not possible to make detailed weather forecasts beyond two weeks due to the unavoidable uncertainty in the initial conditions that grows after a certain time. This

[1] The initial conditions for atmospheric forecasts are obtained through data assimilation, a way of combining short-range forecasts with observations to obtain an optimal estimate of the state of the atmosphere.

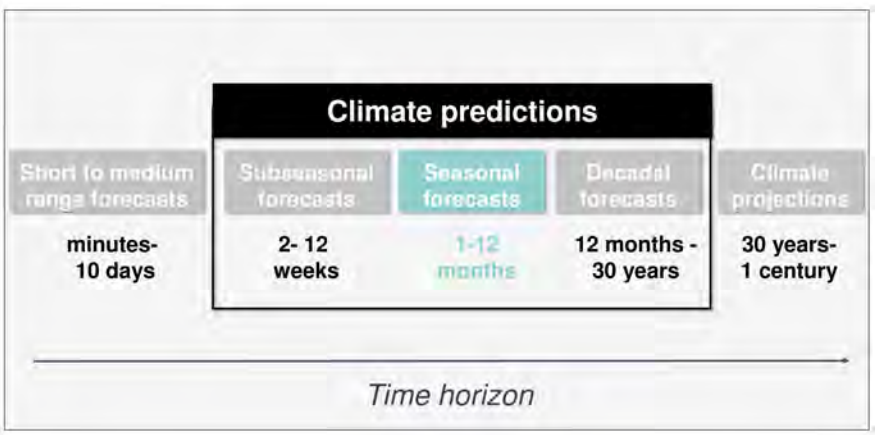

Figure 1 – Time horizon of different short to medium range forecasts, climate predictions and climate projections. Seasonal forecasts are highlighted as they are the forecasts used in this thesis.

is a consequence of the chaotic nature of the climate system in combination with errors in the formulation of the forecast models (Lorenz 1963).

At the other end of the time horizon, climate projections estimate the possible fluctuations of climate from several decades or even a century ahead (Figure 1). Projections are produced by climate models based on retrospective and future estimations of external climate forcings such as aerosol emissions and greenhouse gases, without taking into account information about the state of the climate system at the time of releasing the information (Meehl et al. 2009; Doblas-Reyes et al. 2013a; Kirtman et al. 2013).

The gap between weather forecasts and climate projections is covered by climate predictions. Their goal is to reproduce the future evolution of some aspects of the climate system including both externally forced and internally generated components. Despite the limited predictability beyond two weeks related to the chaotic nature of the climate system, climate predictions are feasible because they take advantage of the interactions between the atmosphere and the components of the climate system such as the ocean, which has a strong thermal capacity and long-term memory, but also from the land surface that vary at slower timescales. These slow variations enable predictability from one month to a few seasons ahead (Figure 2). Besides, climate predictions do not attempt to forecast the actual day-to-day variability of the climate system as the weather forecasts do (Meehl et al. 2009; Kirtman et al. 2013), but the average evolution of some climate variable over the coming weeks (subseasonal), months (seasonal), or years and decades (decadal).

During the recent years, several international initiatives have promoted the development of the subseasonal (Vitart 2004; Vitart et al. 2012; Robertson et al. 2015) and decadal forecasts (Smith et al. 2007; Van Oldenborgh et al. 2012; García-Serrano and Doblas-Reyes 2012; Doblas-Reyes et al. 2013a). However, the use of the forecasts at subseasonal and decadal time horizons is still in their infancy. By contrast, seasonal forecasts, have been developed during more than 30 years (Cane et al. 1986; Stockdale et al. 1998; Van den Dool 2007). Seasonal forecasts range between more than one month and slightly longer than one year into the future. These forecasts can provide information about the probability of particular climate conditions to occur (i.e. how likely it is that the coming season will be warmer or colder than normal). As it has been previously mentioned, the physical basis for such estimates arises from the slow variations of different climate system components.

1.1.2 Sources of predictability at seasonal timescales

A definition of climate predictability has been given by Doblas-Reyes et al. (2013b):

> *"Climate predictability is the extent to which an informative prediction is possible if an optimum procedure is used."*

In other words, predictability is a feature of the

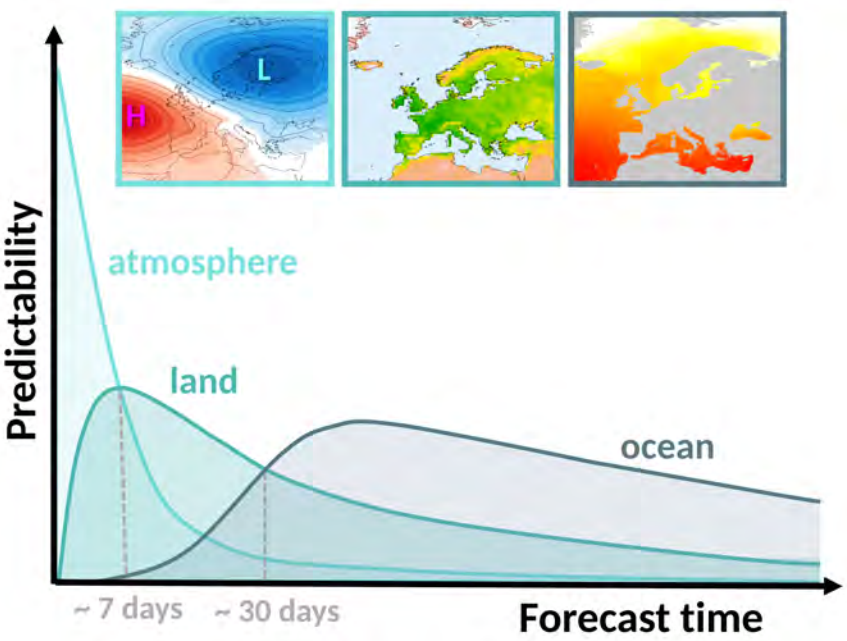

Figure 2 – Scheme illustrating the role of different parts of the Earth's climate system (atmosphere, light turquoise; land surface, turquoise; ocean, dark turquoise) as sources of predictability (vertical axis). For short forecast times, knowing the initial state of the atmosphere counts the most. At 2-week to 4-week forecast times, knowledge of the land surface is also needed. Forecasting more than 30 days ahead typically requires a good knowledge of the ocean (Adapted from: Mariotti et al. 2018).

climate system itself rather than the ability of the forecast systems to make skilful predictions in practice (Kirtman et al. 2013). As explained before, for seasonal predictions, the initial conditions involve phenomena that extend beyond the atmosphere to include details on the state of the ocean and land surface. These long-lived phenomena have much longer variability timescales than the dominant atmospheric instabilities, which enables predictability of climatic anomalies beyond approximately one month to at least a few seasons (National Research Council 2010).

The main potential sources of predictability at seasonal timescales are described below.

ENSO[2]. El Niño-Southern Oscillation (ENSO) is the dominant mode of variability at seasonal timescales, as it can be predicted several seasons in advance (e.g. Palmer and Anderson 1994; Goddard et al. 2001; Smith et al. 2012). ENSO is an ocean-atmosphere coupled phenomenon characterised by anomalous warm sea surface

[2] The acronym ENSO is used to describe the coupling between the oceanic phenomenon known as El Niño (EN) and the atmospheric component which is the Southern Oscillation (SO).

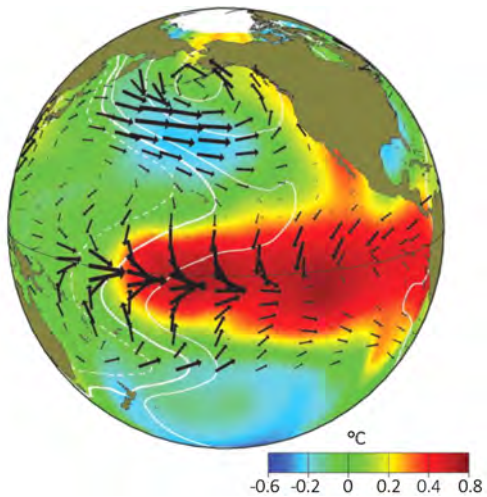

Figure 3 – Graphic illustrating the main characteristics of the ENSO in its positive phase. SST (colour shading and scale in °C), SLP (contour interval is 0.5 mb, with solid contours negative and dashed contours positive pressure levels), and surface wind stress (vectors, with the longest vector equivalent to ∼1 N m^{-2}) anomaly patterns derived rom a linear regression against SST anomalies averaged over 6°N–6°S, 90°W–180° in the eastern and central equatorial Pacific. (Source: McPhaden et al. (2006)).

temperature (SST) in the tropical Pacific caused by a weakening of the trade winds in its positive phase called El Niño (Figure 3). The negative phase of ENSO is La Niña, and it exhibits opposite anomalies. These fluctuations of the SST are accompanied by the Southern Oscillation (SO), which is the atmospheric component of ENSO, and it is usually described by positive anomalies in the sea level pressure (SLP) over Indonesia and the western tropical Pacific and negative anomalies in the eastern tropical Pacific for El Niño conditions (Walker G.T. 1932; Zebiak and Cane 1987; Wang et al. 2017b). Although the ENSO centre of action is located in the tropical Pacific (Figure 3), this phenomenon has an influence on the climate conditions worldwide. The period of ENSO events ranges between 2–7 years. Despite this periodicity, ENSO acts as a source of predictability at subseasonal, seasonal and decadal timescales (National Research Council 2010). Due to the crucial role ENSO plays in the seasonal variability, the assessment of the forecast quality of the seasonal forecasts of ENSO has been usually employed as a proxy of the overall seasonal forecast quality (Stockdale et al. 2011).

Tropical Oceans. Low-frequency SST variations in the tropical Atlantic and Indian oceans are also the source of important climate anomalies throughout the globe. In the tropical Atlantic, the seasonal predictability is related to the persistence of SST anomalies in that region and the associated changes in atmospheric circulation and rainfall (Kushnir et al. 2006). In the Indian basin, the tropical SST in the western region can be skillfully predicted two seasons in advance and the Indian Ocean dipole (i.e. the zonal mode of SST variability in the tropical Indian ocean) can be predicted between one and two seasons ahead (Zhao and Hendon 2009; Zhu et al. 2015).

North Atlantic. Part of the variability in the North Atlantic region at different timescales can be described by the North Atlantic Oscillation (NAO), which is the leading mode of variability

in this region (Hurrell and Deser 2010). The NAO is characterised by an anomalous SLP gradient between Iceland and the Azores. During the NAO positive phase (Figure 4) he SLP gradient is intensified and the westerlies are reinforced showing a northeastward trajectory. This increases the advection of warm and humid air, which leads to warm conditions over northwestern Europe and eastern United States and cold in Greenland and southern Europe. The negative phase of the NAO shows a weakened SLP gradient and more zonally distributed westerlies reducing the advection of warm air over Europe (Wallace and Gutzler 1981; Hurrell et al. 2003). Due to the important role that NAO plays in the Atlantic basin (and the surrounding continents), there are many studies focused on the seasonal predictability of the NAO (e.g. Doblas-Reyes et al. 2003; Scaife et al. 2014; Wang et al. 2017b). However, the development of the NAO involves atmospheric processes that are difficult to predict (e.g. Barnes and Hartmann 2010). This has prevented some seasonal forecast systems to produce skilful seasonal forecasts of the NAO (Kushnir et al. 2006; Kim et al. 2012). Nevertheless, the development of the NAO can also be remotely forced by large-scale disturbances affecting the North Atlantic region such as ENSO, Arctic sea ice, or the stratosphere (Brönnimann 2007; Kidston et al. 2015; Semenov and Latif 2015). These processes could be used as predictors to improve the seasonal skill in the North Atlantic region (e.g. Scaife et al. 2014; Baker et al. 2018).

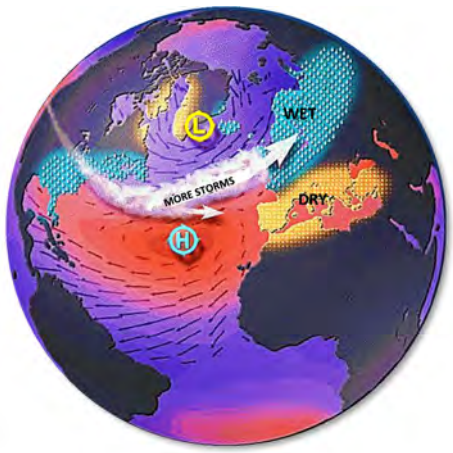

Figure 4 – Graphic illustrating the main characteristics of the NAO in its positive phase. The positive NAO is characterised by a stronger than usual pressure difference between the Icelandic low (L) and the Azores high (H) leading to more storms crossing the North Atlantic. Regions with warm and wet conditions are shown as blue regions (eastern North America and northern Europe) but regions with cold and dry conditions are highlighted in orange (southern Europe). The intensity and direction of the wind is depcicted as vectors. (Source: https://www.ldeo.columbia.edu/res/pi/NAO/ by Martin Visbeck).

Land surface. Some studies have demonstrated the existence of regions where the skill of air temperature can be increased by the land surface initialisation (Dutra et al. 2010; Prodhomme et al. 2016; Ardilouze et al. 2017). This improvement is due to intense land-atmosphere coupling processes such as the soil moisture and the snow. Soil moisture has a strong persistence that lasts several months and modifies the atmosphere through changes in the surface energy budget. These changes, in turn, modify

the energy fluxes between the surface and the atmospheric boundary layer (Hirschi et al. 2011). In addition, snowpack anomalies during winter also act as a source of predictability. Snowpack anomalies lead to large runoff during the snowmelt season, which affects the atmosphere by changing the surface albedo (Cohen and Fletcher 2007).

Sea ice. Sea ice seasonal predictability mainly raises from the persistence of the sea ice anomalies, but also from the sea ice interaction with other climate system components such as the ocean or the atmosphere (Guemas et al. 2016). Until recently, seasonal forecast systems have used climatological or persistent sea ice conditions. However, due to the importance of the sea ice for the seasonal predictability, recent seasonal prediction systems include both initialisation and dynamical evolutions of sea ice, which have enhanced the seasonal skill over mainly the Arctic (Saha et al. 2014; MacLachlan et al. 2015). Nevertheless, the initialisation of climate models with appropriate sea ice conditions has contributed to the correct simulation of extreme events at mid-latitudes (Acosta Navarro et al. 2018).

Stratosphere. During the early winter season in extra-tropical regions, one of the most important sources of predictability is the stratosphere (e.g Thompson et al. 2002). Variations in the stratospheric circulation such as those originated by the quasi-biennial oscillation (QBO) or by the sudden-stratospheric warmings (SSW) may precede and affect anomalies at the Earth's surface that can last several months (Sigmond et al. 2013; Scaife et al. 2016). The QBO is a quasi-periodic oscillation of the equatorial zonal wind in the tropical stratosphere, and it can be accurately forecasted many months in advance (Boer 2009). The SSWs are rapid breakdowns of the westerly flow (or polar vortex) in the polar winter stratosphere that are followed by long-lived circulation anomalies in the lower stratosphere. Although recent advances in the vertical resolution of the atmospheric models could be used to improve the representation of the QBO or SSW, the understanding of the processes responsible of the stratosphere downward influence still needs to be improved. The misrepresentation of these processes by the current seasonal forecast systems could lead to a weak signal at the surface and an underestimation of the skill (Stockdale et al. 2015).

GHG and aerosols. Changes in the atmospheric composition due to the increase of greenhouse gases (GHGs) and changes in the aerosol load present a major human-related component associated with anthropogenic activities that might be predictable (National Research Council 2010). Although the variability in the concentration of aerosols and GHGs is crucial for long-term climate prediction, they can also have an impact on seasonal forecasting. In particular, those seasonal forecast systems including variations in the GHG and aerosol concentrations show improved forecast quality associated with a better representation of the climate trends (Doblas-Reyes et al. 2006; Liniger et al. 2007).

1.1.3 Seasonal forecast systems

The origins of the seasonal forecast systems are strongly linked to the advances in the understanding of the air-sea interactions (e.g. Walker G.T. 1932; Charney et al. 1981; Hoskins and Karoly 1981). The first systems were developed to produce seasonal forecasts of ENSO, as this is the most important source of predictability at seasonal timescales (Cane et al. 1986; Graham et al. 1987; Barnston and Ropelewski 1992).

These seasonal forecasts were based on empirical models. For example, Davis (1978) used empirical orthogonal functions (EOFs) to show that boreal winter SLP anomalies over the North Pacific could be predicted from October SST anomalies. Empirical models aim to statistically describe the physical relationship between the predictand and the predictor (Mason and Baddour 2008). The predictand is the target variable and the predictor is usually a large-scale climate phenomenon. Statistical methods such as the multiple linear regression-based techniques (Eden et al. 2015), empirical orthogonal functions (EOFs; Van Oldenborgh et al. 2005), analogs (Van den Dool 1994), maximum covariance analysis (MCA; Coelho et al. 2006) or canonical correlation analysis (CCA; Barnston and Ropelewski 1992) have been used for the generation of empirical forecasts at seasonal timescales. The output of these empirical models has similar statistical properties to the observations, which is an important requirement for the use of these forecasts in societal applications. Nevertheless, these models are not able to simulate the nonstationarities leading to climate system fluctuations. For that reason, empirical seasonal forecasts are mostly used as a baseline for dynamical models, but also to improve forecasts obtained from dynamical models by reducing the effects of their systematic errors[3] (Eden et al. 2015).

Seasonal forecasts produced in operational centres are usually generated by process-based seasonal forecast systems. The first dynamical systems were based on atmospheric models with prescribed surface conditions (Bengtsson et al. 1993, e.g.), but without taking into account the coupled dynamics (i.e. ocean, sea ice, snow cover and soil moisture were based on climatology). However, the most recent dynamical forecast systems consist of coupled atmospheric and oceanic global circulation models (GCMs), that include models simulating different components of the climate system such as land surface models. These systems attempt to reproduce several physical and thermo-dynamical processes that involve two-way linear and non-linear interactions between the atmosphere, ocean, land surface and sea ice (Edwards 2011; Flato 2011). However, there are some processes crucial for the large-scale climate dynamics that cannot be directly simulated by these systems, because either they

[3]The systematic errors can be defined as the deviations between forecasts and the observational reference. Especially, the systematic error between the forecast climatology and the climatology of the observational reference is known as mean bias.

are not well understood or involve subgrid scales that are not explicitly represented in the models (Doblas-Reyes et al. 2013b). This leads to the representation of these processes in the form of parameterisations, that, together with the initialisation, represent the two major sources of uncertainty affecting the output of the coupled forecast systems (Edwards 2011). The most recent forecast systems also include biogeochemical models[4], which simulate chemical and biological processes as well as their impact on the climate system (e.g Flato 2011). However, the incorporation of these biogeochemical models in the operational seasonal forecast systems is in its early stages (Ford et al. 2018).

Seasonal forecast systems that represent the dynamics of the atmosphere, ocean and land are expected to produce better seasonal forecasts than statistical approaches as they are able to simulate several linear and nonlinear interactions and have the potential to reproduce feedbacks in the climate system related to climate change (Van Oldenborgh et al. 2005). However, the development of dynamical systems often contains considerable errors and biases that limit the forecast usefulness in most regions and seasons (Eden et al. 2015). For that reason, the combination of empirical and dynamical models is starting to gain relevance to produce higher quality seasonal forecasts (e.g. Kim et al. 2015).

[4]These models are usually known as Earth System Models (Flato 2011).

1.1.4 Uncertainty in seasonal forecasts

The two main sources of uncertainty in dynamical climate prediction are the lack of perfect knowledge of initial conditions and the inability to perfectly model the climate system (Slingo and Palmer 2011). The initial conditions are obtained through the combination of short-range forecasts with observations to obtain an optimal estimate of the state of the climate system. The uncertainty in the initial conditions is related to observation errors or data assimilation assumptions. Although these errors might be small, they can lead to large errors in the forecasts due to the chaotic nature of the climate system (Lorenz 1963). An additional source of uncertainty in the forecasts is related to the limited resolution, simplified parameterisations and unresolved non-linear processes in the forecast systems. To deal with these uncertainties coming from multiple sources seasonal forecasts are usually issued in a probabilistic way.

To generate probabilistic forecasts (Figure 5), the best-guess initial conditions are slightly perturbed to take into account the initial condition uncertainty (Slingo and Palmer 2011). From these perturbed initial conditions an ensemble of individual forecasts, which are usually defined as ensemble members, is obtained. This approach produces a prediction of the forecast uncertainty, which can be measured by the ensemble dispersion (Figure 5). Forecast uncertainty is a combination of the observational error and the uncertainty coming

from the unresolved physical processes in the seasonal forecast systems. A deterministic forecast, which does not take into account the forecast uncertainty, can be obtained from the best-guess initial conditions or by computing the ensemble mean as the average of all the ensemble members. However, the fact that the deterministic forecast does not include uncertainty information limits severely the usefulness of this type of prediction.

Probabilistic forecasts including information about their uncertainty and quality can be of high value for a number of applications (Alessandrini et al. 2013; Doblas-Reyes et al. 2013b). In particular, the probabilistic forecasts can help decision makers to better inform their decisions on whether or not to take any action given the probability forecast of an event. By contrast, deterministic forecasts can be misleading, as they fail to provide information about the forecast uncertainty.

The time evolution of the systematic errors is defined as the drift, which results from the systematic amplification of the initial condition and model error as the forecast time increases caused by the nonlinearities related to the

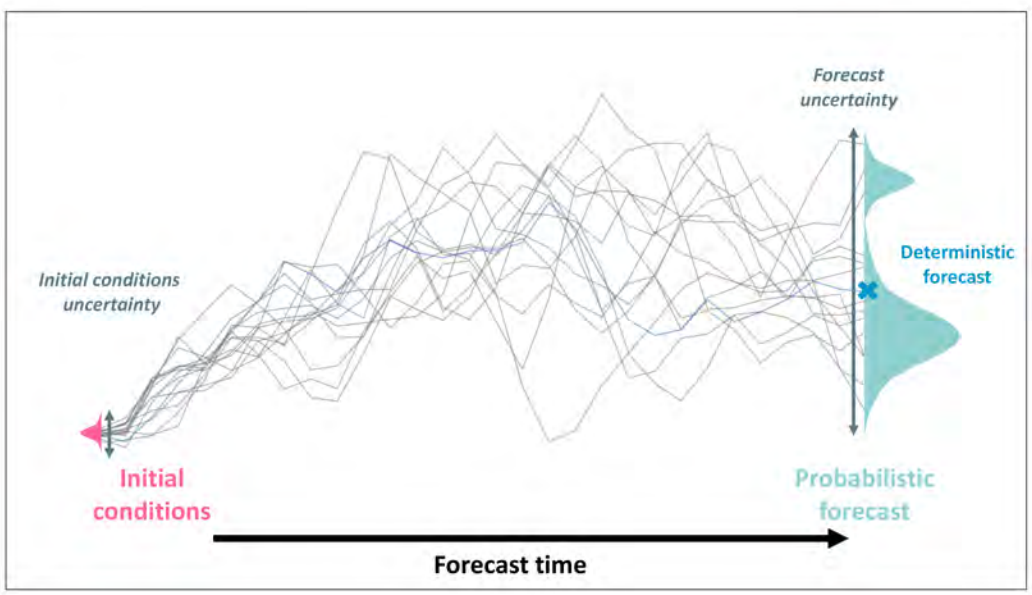

Figure 5 – Schematic of a probabilistic forecast. The thin grey lines show the time evolution of the individual forecasts (i.e ensemble members). The initial condition distribution is represented in pink and probability forecast distribution is represented in green. The spread of those distributions (vertical grey line) indicates the uncertainty in the initial conditions and in the forecast. The deterministic forecast is represented as a blue cross.

chaotic nature of the climate system (Slingo and Palmer 2011). The systematic errors can be observed in the comparison of the mean and the variability of the climate variables with those of the observational reference, as well as in the distribution of the forecast probabilities. For the characterisation and adjustment of these systematic errors, a set of retrospective forecasts (i.e. hindcasts) is needed. Hindcasts are usually made available to the users along with the forecasts as they are essential to evaluate the forecast quality in addition to the robust estimation and adjustment of the systematic errors. None of these steps can be based on an individual forecast.

1.1.5 Seasonal forecast products

Climate prediction is considered a particularly expensive computational exercise because these predictions need to be probabilistic, which requires running ensembles of simulations, and need a set of hindcasts for, at least, twenty years (Mariotti et al. 2018). However, the combination of improvements in the current computational capabilities of the different centres producing seasonal forecasts with the growing need of these forecasts for societal applications has promoted the production of seasonal forecasts by several operational centres. Most of the seasonal forecasts are generated by dynamical climate forecast systems, but a wide range of forecasting strategies and systems are used within the community. It has been proven that this diversity is not just beneficial but also necessary (e.g Weigel et al. 2008). The output of these systems are usually employed for the generation of several climate products, which combine the seasonal forecast itself with the scientific knowledge to provide guidance to the users for its interpretation.

One example of a climate product based on seasonal forecasts is the most likely tercile map illustrated in Figure 6. The most likely tercile map is a widely used tool to visualise probabilistic seasonal climate forecasts. This map shows the probability of the most likely category (below-normal, normal or above normal in this case) for the seasonal forecasts of 10-m wind speed in the 2016 boreal winter. The categories are formulated with respect to the climatological upper and lower terciles, which define equiprobable categories that contain on average 1/3 of the events over the typically 1981-2015 reference period. The probabilities derived from the seasonal forecast output are complemented with forecast quality metrics (e.g. fair ranked probability skill score defined in Appendix A), which allows identifying in which regions the seasonal forecasts provide more useful information than the information used by default for decision-making.

To coordinate the international efforts in this field and improve the accessibility and usability of the seasonal predictions, the World Meteorological Organization (WMO) has designated thirteen institutions as Global Producing Centres for Long-Range Forecasts (GPCLRFs) (Figure 7). These GPCLRFs have committed to generating regularly (typically

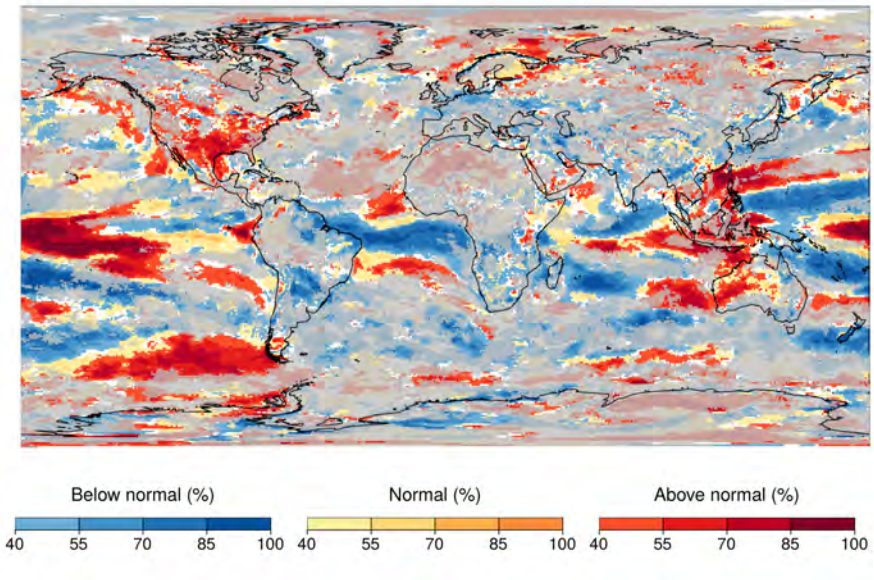

Figure 6 – ECMWF System 4 near-surface wind speed probabilistic forecast of most likely tercile category, for December-January-February 2016-2017. The seasonal predictions have been issued on the 1^{st} of November. The most likely category (below normal, normal, and above normal) and its percentage of probability to occur is shown. White colour indicates that the forecast probabilities are below 40% for all three categories. Transparent colours have been used to mask those regions where the fair ranked probability skill score is below zero. The reference dataset is ERA-Interim and the climatological period 1981-2015.

once a month) a set of products based on seasonal forecasts and their verification. The seasonal forecasts produced by each GPCLRFs have to follow specific standards[5] in terms of the temporal resolution, forecast horizon or target variables, but they also include a comprehensive set of verification metrics.

The seasonal forecasts from these centres have different specifications (i.e. ensemble size, forecast horizon or hindcast length) as detailed in Table 1, but all the seasonal forecast products delivered by each GPCLFs are collected, standardised and distributed by the WMO Lead Center for Long-Range Forecasts[6].

In addition to the GPCLRFs, there are initiatives such as the Copernicus Climate Change Service (C3S[7]) that also publish seasonal forecast products based on data from several state-of-

[5] A full description of these standards can be found under the WMO web page: http://www.wmo.int/pages/prog/wcp/wcasp/gpc/gpc.php.

[6] Seasonal forecasts from the WMO Lead Center are distributed through this webpage https://www.wmolc.org/

[7] Copernicus Climate Change Service web page: https://climate.copernicus.eu/.

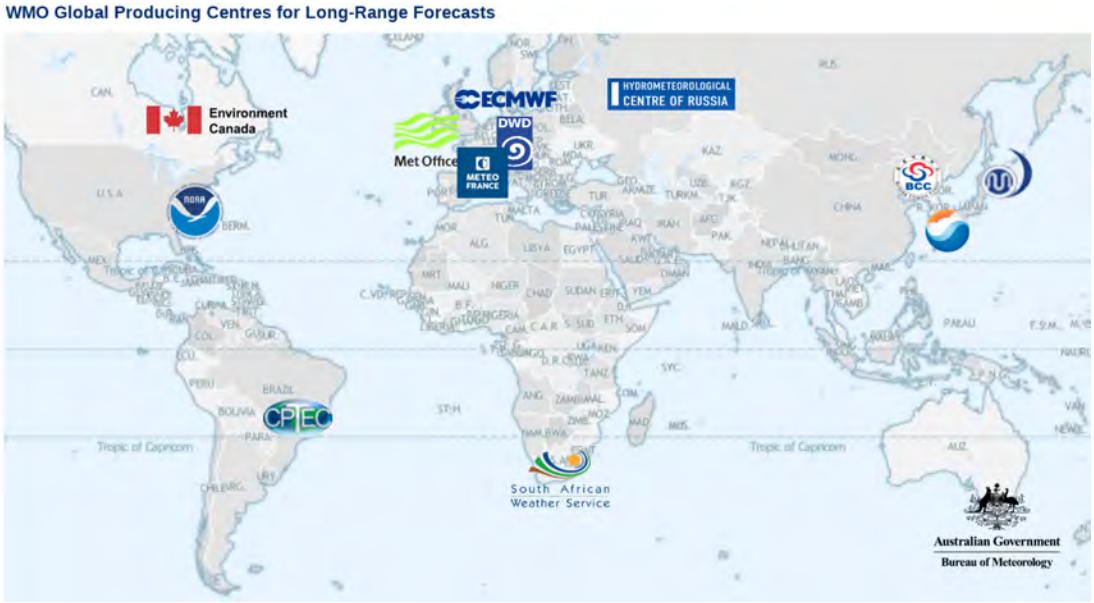

Figure 7 – WMO Global Producing Centres for Long-Range Forecasts that follow the procedures/standards in the delivery of operational seasonal forecasts (Source: http://www.wmo.int/pages/prog/wcp/wcasp/gpc/gpc.php.).

the-art seasonal forecast systems on a regular basis. The main goal of this European initiative is to make climate information freely available to users through a Climate Data Store[8] that offers a wide range of high-quality climate datasets, together with the tools needed to process the data online.

Despite the high number of institutions and initiatives delivering operational seasonal forecasts of a full set of variables in a global domain, most of the seasonal forecast products only include information about ENSO, near-surface temperature and precipitation, as these variables were identified in the past as the most relevant for society (Goddard et al. 2001). However, the ability of the seasonal forecast systems to skilfully predict additional variables of societal interest such as near-surface wind speed has remained virtually unexplored.

This limitation together with the lack of consistency shown by the different centres in the representation of climate products such as the most likely tercile map (Figure fig:mostlikely) makes very difficult the understanding and use of the climate information by some users (Davis et al. 2016). Besides, the different timing in the release of these products, the lack of awareness about which centres are producing

[8]Climate Data Store access: https://cds.climate.copernicus.eu

Table 1 – Summary with the main specifications of the systems employed by the current WMO Global Producing Centers for Long-Range Forecasts. (Source: https://www.wmolc.org/contents2.php?sm_id=1&tm_id=1&cdepth=3&upnum=6&ca_id=116&s1=4&s2=1&t1=4).

CENTERS	SYSTEM	PERIOD	FORECAST HORIZON (MONTHS)	MEMBERS	COUPLED
BEIJING	BCC_CSM1.1	1991-2010	13	24/24	Yes
CPTEC	AGCM Kuo	1979-2010	7	15/10	No
ECMWF	SEAS5	1981-2016	7/13	51/25	Yes
EXETER	GLOSEA5-GC2	1993-2015	6	42/644	Yes
MELBOURNE	POAMA-2	1980-2011	9	33/99	Yes
MONTREAL	CanCM3/4	1981-2010	12	20/20	Yes
MOSCOW	SL-AV	1981-2010	4	20/10	No
PRETORIA	SCM	1982-2009	9	40/10	Yes
SEOUL	GLOSEA5-GC2	1991-2010	6	42/15	Yes
TOKIO	JMA/MRI-CPS2	1979-2014	7	51/10	Yes
TOULOUSE	MF-System 6	1991-2014	7	51/15	Yes
WASHINGTON	CFS_v2	1981-2010	9	40/20	Yes
OFFENBACH	GCFS1	1981-2015	12	30/15	Yes

seasonal forecasts or the different protocols for the data download are other factors leading to the underutilisation of seasonal forecasts by the users (Davis et al. 2016; Soares and Dessai 2016).

1.2 Making seasonal forecasts actionable

Several organisations and decision makers have started to demand a different kind of climate information to improve society's resilience to climate hazards and to better manage the risks and opportunities arising from climate variability and change (Hewitt et al. 2013; Vaughan and Dessai 2014).

Despite the interest on the climate information and its potential benefit for different applications, there are several barriers that have prevented the integration of climate information on decision-making processes (Lemos et al. 2012).

The potential users of the climate information are usually confused by the diverse array of institutions and climate products available (Vaughan and Dessai 2014) as described in the previous sub-section. In addition, users may have unrealistic expectations of how climate knowledge fits their decision-making (Lemos et al. 2012). To promote the deployment of climate information in different socio-economic sectors is crucial to explain which are the opportunities and limitations of the climate information currently available and to demonstrate how this information can be used to improve different decision-making processes (Goddard et al. 2010). Consequently, if the climate information is properly tailored and contextualised, this could be understood by those users who are not climate experts.

From this need to translate and interpret the climate information generated by climate scientists into tailored products and tools that can be integrated into practical applications the climate services research discipline has recently emerged.

1.2.1 Climate services context

Several definitions and interpretations of the climate services term can be found in the literature. Some of these definitions have been collected in (Brasseur and Gallardo 2016). Particularly, the European commission (Street 2016) has defined climate services as:

> *"The transformation of climate-related data — together with other relevant information — into customised products such as projections, forecasts, information, trends, economic analysis, assessments (including technology assessment), counselling on best practices, development and evaluation of solutions and any other service in relation to climate that may be of use for the society at large."*

The main goal of the climate services is to enable better management of the risks of climate variability and to improve the resilience and adaptation to climate change through the development and incorporation of climate information into planning, policy and practice at the global, regional and national scale (Hewitt et al. 2012).

Due to the importance of the development of climate services for both society and industry, this research line has gained a great relevance in the past few years and it has become the focus of major international coordination and development activities (Buontempo et al. 2014). The increase of international efforts promoting the application of climate-based information by governments and societal sectors led the WMO to propose the creation of the Global Framework For Climate Services (GFCS) initiative during the World Climate Conference-3 in 2009[9]. The GFCS became effective in 2012 when its implementation plan was approved by the

[9]The conference statement could be read here: http://www.wmo.int/gfcs//sites/default/files/WCC-3_Statement_07-09-09%20mods.pdf

governments worldwide (Hewitt et al. 2012). The GFCS has three main goals: 1) the reduction of the vulnerability of society to climate variability and change by improving the accessibility and quality of the current climate services, 2) the strengthening of the engagement between users and providers and 3) the mainstreaming of climate information for decision-making. The efforts of the GFCS are focused on five priority areas that are represented in Figure 8 (agriculture and food security, water, health, energy and disaster risk reduction). These priority areas have been selected by the GFCS because they address basic issues and present the most immediate opportunities for the society (GFCS 2014). However, the number of priority areas could evolve and the needs of the users in other areas might be also addressed. For example, in 2015 energy was added as a GFCS priority area (i.e. three years later than the other four initial priority areas).

The implementation of the GFCS initiative is based on the five main components (Hewitt et al. 2012) and on the linkages between them. A short description of these components is provided below:

1. Climate information system: mechanisms to store, assess and distribute climate information.

2. Observations and monitoring: the collection of different kinds of observations (physical, chemical, socio-economic) and of adequate quality and quantity to produce climate services information.

3. User interface platform: a web-based tool that can guarantee effective communication between users and climate services providers.

4. Research, modelling and prediction: scientific knowledge essential to advance in climate science (climate predictions and projections) and in the development of climate-based applications that meet user needs.

5. Capacity development: the foundation that links and supports the four other components and the systematic development of the institutions, infrastructure and human resources needed for effective climate services.

In parallel to the GFCS, the European Commission has established a climate services roadmap framework (Street 2016) to foster the climate services sector at european level. This roadmap proposes a strategic agenda to enhance existing investments, focusing on solution-oriented activities and specific actions using current funding programmes (e.g. Horizon 2020[10]) to bridge the gap between users and researchers. The three main challenges included in the roadmap are: to enable the market growth, to build on the market framework and to enhance the quality and relevance of climate services (Street 2016).

1.2.2 Steps for the climate services development

The transformation of climate data into products that can be easily integrated into decision-

[10]Horizon 2020 is the financial instrument aimed at securing Europe's global competitiveness.

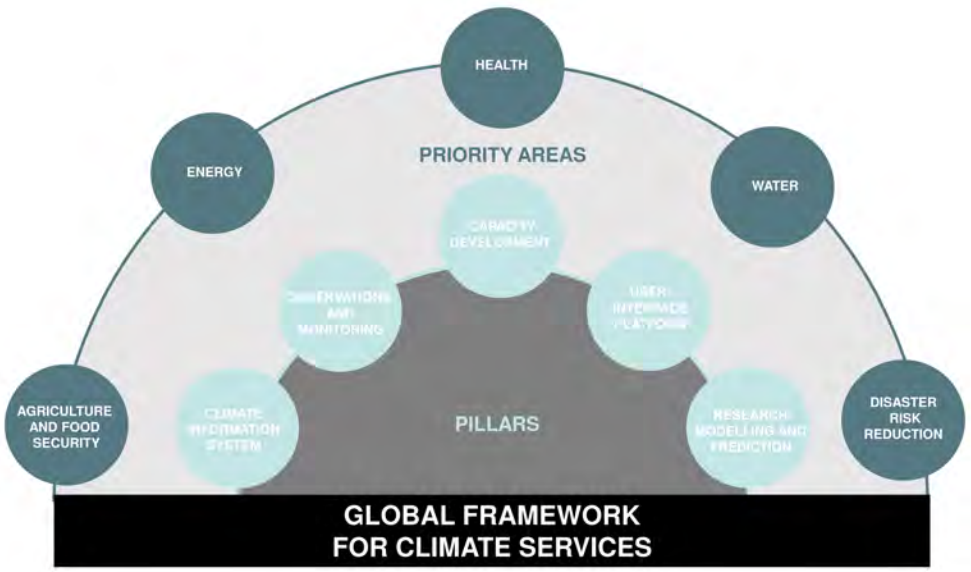

Figure 8 – Graphic illustrating the Global Framework for Climate Services (GFCS) vision. GFCS focuses on five main priority areas: agriculture and food security, water, health, energy and disaster risk reduction. The implementation of the GFCS will be implemented through five pillars: climate services information system, observations and monitoring, user interface platform, research modelling and prediction and capacity development. (Source: https://www.wmo.int/gfcs/about-gfcs).

making can be described through a basic climate services development chain based on the GFCS components (Figure 9). The effective production of climate services includes: the use of the best quality state-of-the-art climate data (e.g. observations, reanalysis, seasonal forecasts, ...) that can be employed in the production of scientifically credible, salient and legitimate climate information (Cash et al. 2003) able to satisfy the users' needs (i.e. climate information and knowledge). This information should be available through user-friendly access mechanisms that ensure the effective communication in both directions (e.g. user interface platform). Besides, the service has to include information about the interpretation of the different climate-based products to guide their application in decision-making processes.

The development of a climate service is a two-way process in which each stage is improved by the feedback obtained in both the previous and following stages. For example, the implementation of a user interface platform could be improved if the users identify some limitations when it is implemented in their decision-making process.

The different roles involved in climate services development have been also depicted in Figure

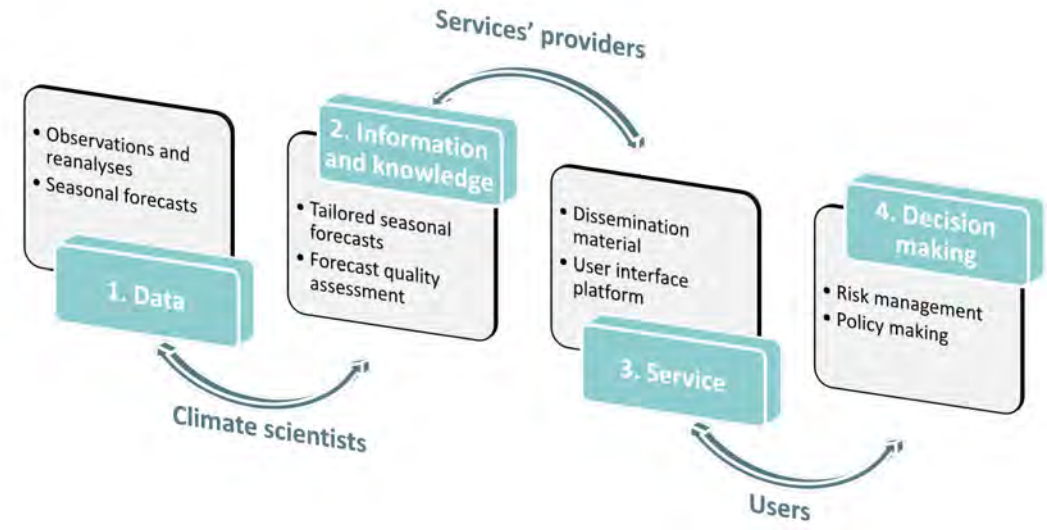

Figure 9 – Diagram with a simplified climate services chain. The development of a climate service includes the data provision, the development of knowledge and tailored information and the integration of that information into a service that can assist in decision-making processes. A couple of examples illustrating each step of the chain have been included. The main roles in each step of the climate services chain have been also included (i.e. climate scientists, services' providers and users), but the interaction among the different profiles is an essential requirement for the development of an effective climate service. The arrows indicate the climate service development is a two-way process.

9. The transformation of the climate data into tailored information and knowledge is usually performed by climate scientists. Some examples of the kind of information produced by climate scientists include knowledge about the uncertainty and quality of the specific datasets, the development of user-friendly indicators that can be more informative than the essential climate variables or the development of impact models. To guide this applied research, the interaction of climate scientists with climate services providers is essential.

Climate services' providers act at national, regional or local levels in a range of sectors (Vaughan and Dessai 2014) and they include different profiles (e.g. communication specialists, social scientists, designers, ...). Services providers must be aware of state-of-the-art climate research, datasets and products (Brooks 2013). For that reason they work very closely with climate scientists. Besides, they have to collaborate with users to identify specific decision-making processes in which climate information can help, and also improve the usability of the service. However, it is sometimes difficult for climate services providers to understand how to communicate,

visualise or distribute climate information to support decision-making in different sectors, and ultimately facilitate its uptake in decision-making. This has been recognised as one of the major limitations for the widespread use of climate services (Christel et al. 2018). To overcome this problem, the engagement between users and climate services providers has been proposed (Hewitt et al. 2012; Hering et al. 2014). This would benefit both parts, providers can learn about users' needs and users understand how to handle uncertainty with confidence.

Climate services' users are those whose actions (e.g. decisions, policies) are more likely to be influenced by the provision of a specific set of climate information and knowledge (Buontempo et al. 2018). These users can be found in humanitarian organisations, government offices, international agencies and also in the private sector (Vaughan and Dessai 2014). The level of expertise of these users ranges from those that are routinely dealing with uncertain outcomes (i.e the kind of information that can be provided with the seasonal forecasts) to those who need information in a format that facilitated yes/no decision-making. Due to this wide variety of users, climate information should be tailored to the specific user and decision to be made.

Hence, the key for the success of climate services relies on their ability to address risks and opportunities at relevant timescales with tailored solutions informed by high-quality data products (Goddard 2016), but also on the collaboration of multidisciplinary teams working together in the co-development of the climate services.

1.2.3 Climate services based on seasonal forecasts

The climate variability at seasonal timescales is particularly one of the factors playing an important role in many climate-sensitive sectors (Doblas-Reyes et al. 2013b). For that reason, the different institutions and industrial sectors have already adopted different approaches to estimate the future evolution of the seasonal climate conditions and to adapt and mitigate the climate related risk. One of the most widely used method has been the consideration that future climate variability will be similar to the long-term estimates from the past conditions (Goddard et al. 2010). However, future climate may not be a repetition of the past conditions, particularly in a climate change context. Therefore these approaches could lead to incorrect decisions. In these cases, climate predictions could be more helpful to provide insight into the future evolution of climate conditions.

Information from seasonal forecasts can help to identify vulnerabilities and risks, facilitate strategic climate adaptation actions, improve the ability to make decisions earlier, avoid subjective decision-making, take precautionary action and reduce potential costs. Nevertheless, the high demand of climate information and the great improvements in terms of provision and accessibility to the seasonal forecast products (due to the WMO GPCLRF and C3S initiatives) have not been sufficient for the penetration of these forecasts in the different activities carried out by governments and industrial sectors.

Seasonal forecasts provide a probabilistic estimate of how essential climate variables such as temperature or precipitation may develop in the coming months and seasons and, thus, can help to inform, focus and improve decision-making (Soares and Dessai 2016). However, the large amount of probabilistic information raising from seasonal forecast systems, which is usually un-tailored and difficult to understand by non-expert public, make difficult the integration of these forecasts in decision-making processes. Hence, the reduction of society's vulnerability to seasonal climate related-risks requires the contextualisation and interpretation of the seasonal forecast data, as well as the development of tailored products and tools based on this source of climate information (Hewitt et al. 2013).

Despite the limitations for the integration of seasonal forecasts in decision-making processes, their potential has started to be explored in several socio-economic sectors, such as agriculture (Crane et al. 2010; Rodriguez et al. 2018), energy (De Felice et al. 2015; Torralba et al. 2017b), transport (Palin et al. 2016), disaster risk management (Hobday et al. 2018), water management (Dutra et al. 2014) or health (Lowe et al. 2016).

1.3 Seasonal forecasts for wind energy

1.3.1 Wind energy as a climate-sensitive sector

Energy generation and the planning of operations are strongly affected by meteorological and climate conditions. Energy systems could considerably improve their resilience to weather extremes, climate variability and change, as well as their full chain of operations during their entire life-cycle if they take into account weather and climate information. For that reason, energy has been identified as one of the priority areas by the GFCS, as the use of climate information at different timescales can be highly beneficial to this sector (WMO 2017). The main goal of the GFCS in the energy priority area is to increase the sustainable development and to favour the use of renewable energy resources. This would be achieved through climate information that can help energy users to take informed decisions with potential cost savings to their operations.

The 21st Congress of the Parties for the United

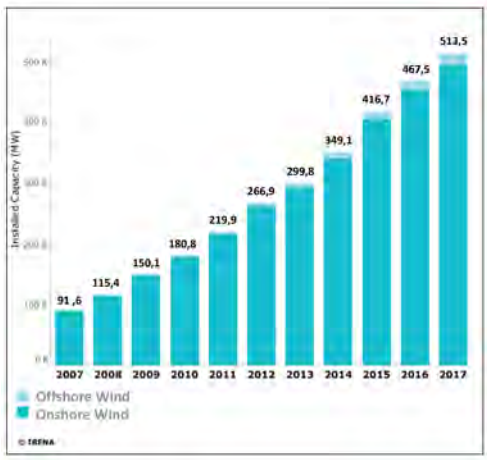

Figure 10 – Global wind energy cumulative installed capacity (MW) from 2007 to 2017. Dark/light blue represents onshore/offshore wind energy. (Source: IRENA https://www.irena.org/wind).

Nations Framework Convention on Climate Change (COP21[11]) agreement has recently proposed several policies to promote energy efficiency and replace fossil fuels with renewable sources of energy (Lane 2016). The demand for renewable sources has increased due to the need to mitigate the climate change resulting from anthropogenic greenhouse gas emissions, the interest in the creation of new economic opportunities, and the provision of energy access to people living in areas without access to other sources of energy (IEA 2017). Furthermore, renewable energy has been the fastest growing source of electricity globally in 2017, meeting a quarter of global energy demand growth last year (IEA 2018).

Wind energy is the cheapest option for new sources of power-generating capacity and is the second-leading source of renewable energy worldwide, only exceeded by hydropower in terms of installed capacity (Pryor and Barthelmie 2010; Santos et al. 2015). In recent years, wind power has experienced rapid growth in terms of installed capacity (Figure 10), reaching a total of 513 GW installed worldwide in 2017. As a consequence, wind energy has become a key element of the electricity supply in many parts of the world (WWEA 2016).

One of the major challenges faced by the wind industry is its vulnerability to the climate variability (Pryor and Barthelmie 2010). As any other renewable energy source, wind energy comes from natural sources, therefore stronger-than-normal wind speeds could lead to safety problems, and lower-than-normal wind speeds could lead to important losses in case wind resources cannot satisfy the electricity supply. Therefore, the use of weather and climate information is a crucial factor for the expansion of the wind industry.

1.3.2 Current forecasting options in the wind industry

Forecasts of the wind energy resources at different timescales represent a key piece of the decision-making processes. The GFCS has defined several focus areas in the energy sector which can benefit the most from the use of climate information (WMO 2017). In the wind energy sector these focus areas correspond to different stages in the lifetime of a wind farm illustrated in 11. Forecasts at different time horizons (Figure 1) can be used to produce climate information at each one of this stages, and some of them are currently being widely used by the wind industry.

Weather forecasts (from minutes up to a few days) have been traditionally used by the wind industry because near-surface winds and thus energy production strongly depend on mesoscale and synoptic-scale variability (Pryor and Barthelmie 2010; Graff et al. 2014). Wind turbines only can operate within a range of wind speed thresholds (2-30 m/s), and above the high threshold, power production is ramped down to

[11] More details on COP21 can be found here: https://unfccc.int/process-and-meetings/conferences/past-conferences/paris-climate-change-conference-november-2015/cop-21

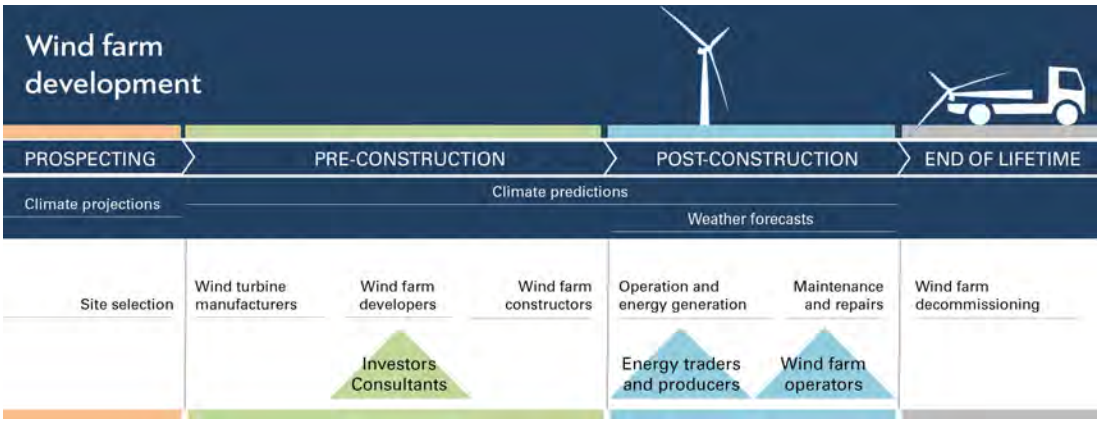

Figure 11 – Stages of wind farm development, the stakeholders involved at each stage and temporal horizons of the climate information used. While weather forecasts are limited to two weeks, climate predictions extend further into the future, from seasons up to decades, and climate projections are longer-term, from decades up to centuries. (Source: Terrado et al. 2017).

protect the wind turbine from heavy loading. Hence, weather forecasts are very relevant during the post-construction phase, particularly for wind farm operators (Foley et al. 2012).

The need for climate information that is representative of the next few decades has raised the interest of wind industry in climate projections, particularly they are becoming widely used during the prospecting phase. Climate projections are usually combined with historical data for the evaluation of the long-term wind energy resources in a particular region. This information is used for the selection of a wind farm location and to guide investments (Hueging et al. 2013; Vautard et al. 2014; Reyers et al. 2015).

With a focus on timescales from a few weeks up to a decade into the future, current energy practices use an approach that is based on the future climate being a repetition of an estimate of the current climatological behavior (Garcia-Morales and Dubus 2007). This approach has several caveats, such as the inability to predict events that never happened before or the low chances that a particular season show exactly the same conditions than an average of the past decades.

Recent advances in the science of climate prediction that cover the gap between weather forecasting and climate change projections can be considered as an alternative to the state-of-the-art by providing climate information that helps users to move beyond using only climatological information. This information will be particularly relevant during the pre-construction phase of a wind farm, when decadal predictions can benefit wind farm developers

and constructors by informing them about the future evolution of the energy yield and also to the investors by providing information about the return on investments. During the post-construction phase, subseasonal and seasonal forecasts can also provide added value to the operation and maintenance tasks and financial operations.

1.3.3 Tailoring seasonal forecasts for wind energy applications

Despite the potential applications of climate predictions for the wind energy sector, the use of this kind of predictions by this industry is still in its infancy. Particularly, climate predictions at seasonal timescales have experienced a great development in the recent years, and they are now providing skilful forecasts for extra-tropical regions where no substantial skill was found before (Scaife et al. 2014). This has promoted their use for other energy sources (Garcia-Morales and Dubus 2007; De Felice et al. 2015). However, there are few instances of their application in the wind energy context (Clark et al. 2017; Torralba et al. 2017b).

The probabilistic seasonal predictions can be used as a tool to inform wind energy users with greater accuracy than current approaches, because they include information about their uncertainty. Improved climate information that includes seasonal forecasts could be beneficial for different wind energy applications (Figure 12).

The intermittent nature of wind makes very difficult to keep the balance between supply and demand (Pinson 2013), therefore, the use of forecasts at several timescales could help to avoid blackouts. Financial activities and energy trading can also take advantage of the seasonal predictions to anticipate the cash flow and the savings of some costs due to a better anticipation of market changes. Decision-making processes related to operations and maintenance of the wind farms can be optimised. For example, they can benefit the planning of maintenance works in offshore wind farms if they are scheduled during periods for which the wind energy resources are expected to be lower-than-normal, as it is in these cases when the impact on the wind generation will be lower. Electricity grid operators can also use seasonal forecasts to estimate the future production generated by the wind farms, an information that can be employed as input for load-balance models (Füss et al. 2013; Najafi et al. 2016). This framework can favor greater penetration of wind energy sector into markets.

1.4 Scientific challenges for the development of a wind energy climate service

The scenario described is of great interest for the wind energy and climate science communities but little progress has been made in practice. Some wind energy users have perceived the advantage of using seasonal forecasts because they are aware that some of their competitors are using this kind of information. However, the added value of the seasonal forecasts for their

activities is still not obvious for them (Soares and Dessai 2016). To promote the integration of the seasonal forecasts in the wind energy community, the forecasts should be tailored to the potential applications and decision-making context. However, as the development of climate services based on seasonal forecasts is a very new research discipline, several gaps of knowledge have been identified.

Due to the lack of long enough homogeneous time series of historical data from observational measurements, both the wind energy and climate forecasting communities rely on global reanalysis datasets for different activities. Reanalysis products are the result of the assimilation of observations from different sources into an atmospheric model that generates evenly distributed global data. Wind energy users usually employ these sources of data for the characterisation of the long-term variability in the wind energy resources (Kirchner-Bossi et al. 2015; Cannon et al. 2015). Nevertheless, for some users, it is difficult to identify the most suitable dataset for their specific needs (Gregow et al. 2015). The same problem is found by climate scientists, who also need an observational reference for the characterisation of the climate variability

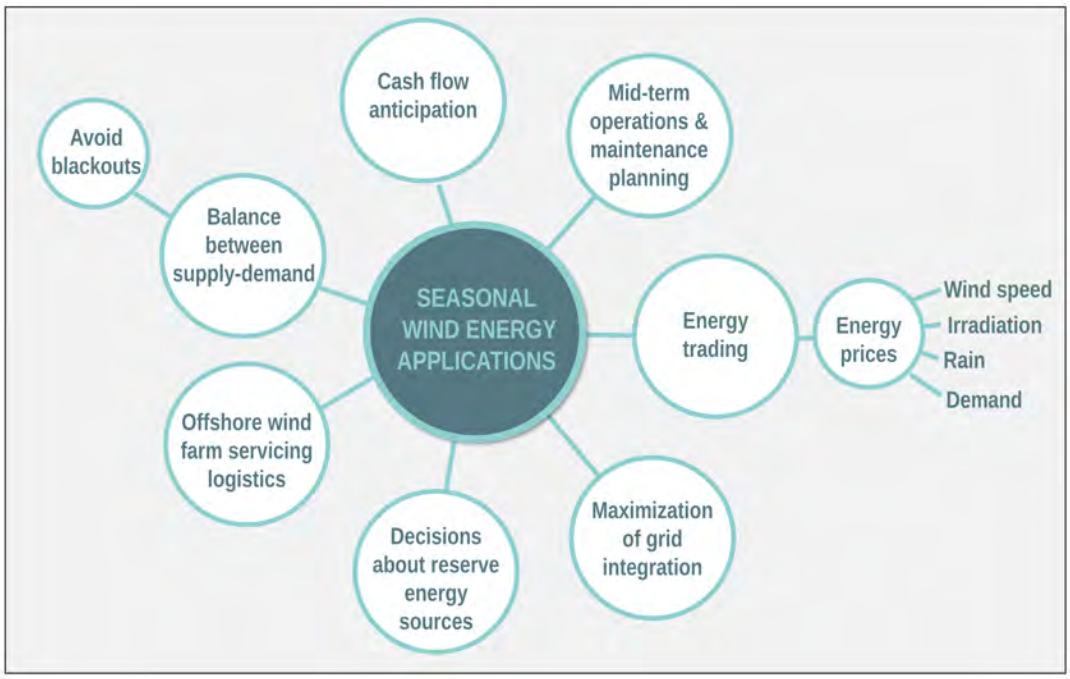

Figure 12 – Mindmap with the potential fields of application of seasonal forecasts in the wind energy sector. (Courtesy of Marta Terrado).

and the assessment of the seasonal forecasts quality. Despite several intercomparison studies between different reanalyses and observations available in the literature, previous research only focused on specific regions and variables such as temperature and precipitation (Lorenz and Kunstmann 2012; Simmons et al. 2014). However, the intercomparison of the uncertainty affecting wind speed from different reanalyses at the global scale is not readily available. The characterisation of the limitations of different reanalyses would be helpful for the assessment of the users' vulnerability to inconsistencies in the observational references and to increase the robustness of the forecast quality assessment, which is usually based on one specific observational dataset without taking into account its uncertainty (Torralba et al. 2017a).

Wind energy resources are very sensitive to climate variability at several timescales. The quantification and understanding of the climate response to large scale atmospheric patterns may help to predict anomalous fluctuations in wind energy resources some months in advance (Brayshaw et al. 2011; Couto et al. 2015). For that reason, users from the wind energy sector have started to show interest in the physical mechanisms leading to inter-annual climate variability of wind energy resources in specific regions. As large scale patterns such as ENSO and NAO are some of the drivers of the inter-annual climate variability, the capacity of the seasonal forecast systems to simulate these patterns and their impact on temperature and precipitation have been already explored (e.g. Kim et al. 2012; Molteni et al. 2015). Nevertheless, the representation of the impact of these phenomena on wind speed variability by the current seasonal forecast systems has not been undertaken yet. The investigation of the seasonal predictability of these large-scale phenomena and their related climate conditions could be beneficial to increase user confidence in the seasonal forecast system representation of relevant climate variables (Sillmann et al. 2017). Besides, some large scale phenomena are more predictable than smaller scale anomalies, which could be exploited to improve the seasonal forecasts of wind energy relevant variables.

The inter-annual climate variability can be also described in terms of the daily atmospheric circulation by means of weather regimes, which are defined as quasi-stationary atmospheric circulation patterns (Vautard 1990). It has been recently demonstrated that weather regimes are playing a dominant role in wind power fluctuations on the European wind power (Grams et al. 2017). Consequently, the prediction of those weather regimes some months in advance can be very useful for the wind industry. However, the capabilities of the seasonal forecast systems to simulate the weather regime variability and their impact on wind energy resources remain largely unexplored.

One of the major limitations for the deployment of seasonal forecasts in different societal sectors are the systematic errors. Users need seasonal forecasts with similar statistical properties to those in the observational references,

particularly if these forecasts need to be combined with impact models, which usually rely on past observations. Therefore, systematic errors make these forecasts directly unusable unless they are post-processed to have statistical features as close as possible to those observed. Although there are several bias adjustment approaches that have been applied in the seasonal forecasting context (e.g. Zhao et al. 2017; Manzanas et al. 2019), the suitability of these approaches to be applied over seasonal forecasts of wind speed has not been explored yet. The identification of a methodology that can improve the forecast quality of wind speed is an essential step for the development of a climate service tailored to wind energy applications (Torralba et al. 2017b).

Although wind energy users are advanced in the use of forecasts and climate information (Buontempo 2018), these users usually employ weather forecasts for their activities. For that reason, some users expect that seasonal forecasts provide information about the precise climate conditions in a specific moment, as weather forecasts do. However, as it has been previously mentioned, seasonal forecasts usually inform about the probability of the specific wind speed or temperature being in the below normal, normal or above normal categories in the upcoming month or season. Hence, to avoid misleading interpretations, it is important that tailored seasonal forecasts include some guidance about their probabilistic interpretation. For this purpose different forecast quality metrics that can provide a comprehensive view of seasonal forecast quality, inform about the ability of seasonal forecast systems to provide better information than current approaches used by the wind energy managers (i.e. climatology), and illustrate their potential to add value to wind energy applications are required.

Despite the interest of the wind energy community in the seasonal forecasts of mean wind speed, they also need more detailed information about the highest or lowest wind speed in a season. However, this kind of indicators is not currently delivered by seasonal forecast systems. To satisfy this need, the definition of wind extreme indicators and the investigation about their potential to provide usable information for wind energy activities need to be explored.

This PhD thesis aims at addressing these challenges by proposing different products and knowledge for the wind industry that contribute to the full development of a climate service. This information will be delivered through a user-interface platform that allows effective communication with the users. Hence, the main focus of this thesis is on the process of producing climate forecast information relevant to wind energy applications rather than creating decision support tools that can assist in decision-making processes.

1.5 Objectives

The overall aim of this thesis is the assessment of the opportunities and limitations of a state-of-the-art seasonal forecast system for the development of climate products that can be used by wind energy users. This aim is addressed through two general objectives and specific activities.

1 Description of the systematic errors affecting the seasonal forecasts of wind speed and air temperature and the forecast quality assessment of wind energy relevant climate indices in the ECMWF System 4 seasonal forecast system.

- Characterisation of the systematic errors in the main statistical properties and long-term trends of the wind speed and air temperature.
- Quantification of the uncertainty affecting the observational references currently employed by the wind energy sector for long-term resource evaluation and as a reference for the seasonal forecast quality assessment.
- Investigation of ECMWF System 4 seasonal forecast system ability to reproduce wind energy relevant large-scale processes (ENSO, NAO and storm tracks) leading to climate variability and fluctuations in the wind energy resources in remote regions.

2 To investigate the potential of the seasonal forecasts for the development of pioneering products tailored to benefit the wind energy sector by providing more accurate information than the currently used approaches.

- Definition of a weather regime classification that can be used to understand the wind speed and temperature variability in terms of changes in their frequency of occurrence and skill assessment at seasonal timescales.
- Evaluation of the suitability of different bias adjustment techniques to produce seasonal forecasts of wind speed with similar statistical properties to the observational reference.
- Description of the different aspects of the seasonal forecast quality (i.e skill and reliability) to inform about the added value of these forecasts compared to benchmark forecasts.
- Definition of extreme wind speed indicators that can be used to anticipate the highest and lowest wind speed values in a particular season

1.6 Thesis structure

This thesis has been organised in seven chapters that aim at achieving the described goals. **Chapter 1** provides an overview of the state-of-the-art in seasonal forecasting and explains why seasonal forecasts can be beneficial for the wind energy sector in a climate services context. **Chapter 2** describes the data and the common methods employed throughout the thesis.

The characterisation and investigation of the systematic errors in ECMWF System 4 have been carried out in chapters 3 and 4. Systematic errors in the statistical properties and long-term trends of the wind energy relevant variables (10-m wind speed and 2-m temperature) have been described in **chapter 3** by comparing the ECMWF System 4 seasonal forecasts with three observational references (ERA-Interim, JRA-55 and MERRA-2 reanalyses). **Chapter 4** evaluates the seasonal predictability of ENSO, NAO and storm tracks and their impact on wind energy relevant variables. The main goal is to investigate the ECMWF System 4 systematic errors in the teleconnections and to understand the overall seasonal forecast quality as planned in objective 1.

The development of products and methodologies that can be used for the penetration of the seasonal forecasts in wind energy applications have been provided in chapters 5 and 6. The usefulness of a weather regime classification for each month of the year in the context of the wind energy sector and the seasonal predictability of these weather regimes are investigated in **chapter 5**. In **chapter 6**, the impact of three different bias adjustment approaches and a reconstruction method on the quality of the 10-m wind speed seasonal forecasts is explored. Chapter 6 also includes the definition and forecast quality assessment of extreme wind speed indicators.These chapters describe the results of the activities planned in objective 2.

The main scientific contributions derived from this PhD thesis and the ideas for the continuation of this work are discussed in **chapter 7**.

Finally, three appendices have been also included to support the information given in the chapters. **Appendix A** describes the forecast quality assessment metrics employed throughout the thesis. **Appendix B** is a catalogue with the extra figures supporting the main chapters. **Appendix C** outlines the publications in which the author has been involved during the preparation of this PhD thesis.

All the software developed and used in this work is publicly available, including a detailed documentation, through the gitlab repository of the Department of Earth Sciences of the Barcelona Supercomputing Center (https://earth.bsc.es/gitlab/es) and the CRAN repository (https://cran.r-project.org/web/packages/s2dverification/index.html).

02

Data description and methodology

02 Summary

Objective

To describe the main properties of the datasets and variables used throughout this thesis and the common strategy for the forecast quality assessment and leave-one-out cross-validation method.

Methodology

- The 10-m wind speed and the 2-m air temperature are studied as they are the most relevant variables for the wind industry. They affect energy generation and demand, respectively. These variables need to be interpolated from the model levels to a near-surface constant height level and each dataset employs a different methodology to perform this interpolation, which can lead to differences among the datasets.
- The uncertainty related to the choice of one specific dataset as the observational reference is quantified by considering three state-of-the-art reanalyses: ERA-Interim, JRA-55 and MERRA-2.
    - The ERA-Interim reanalysis is produced by European Centre for Medium-Range Weather Forecast (ECMWF) with a spatial resolution of 0.75º x 0.75º and a period ranging 1979 to present.
    - The JRA-55 reanalysis is generated in the Japan Meteorological Agency (JMA) with a 0.56º x 0.56º spatial resolution covering the period 1958 to present.
    - The MERRA-2 reanalysis is a product delivered by National Aeronautics and Space Administration (NASA) with a spatial resolution of 0.63º x 0.50º in the period 1980-present.
- The seasonal forecasts produced by the ECMWF System 4 are used. These forecasts have 51 ensemble members, a forecast time horizon of seven months and spatial resolution of approximately 80 km. In this work the combination of the hindcasts and forecasts from the operational ECMWF System 4 has been employed.
- The different post-processing approaches applied in this thesis (i.e. bias adjustment and reconstruction) are performed in 'leave-one-out cross-validation'. When post-processing is applied in cross-validation, the observation in the same year as the forecast to be post-processed is not considered for the estimation of the parameters employed in the post-processing method. The cross-validation is applied to mimic an operational context in which there are no available observations for the target period of the prediction (e.g the upcoming season).

- To investigate the usefulness of the seasonal forecasts in comparison to the approaches currently employed by the wind industry, the estimation of the forecast quality based on their past performance through several forecast quality metrics is assessed (described in Appendix A along with the different significance tests employed in this thesis).
- Two different aspects of the forecast quality are explored: skill and reliability. Skill measures the quality of the forecasts compared to some benchmark forecast, which in the case of the wind energy sector is usually a climatological forecast. Reliability quantifies the correspondence between the forecast probabilities and the observed frequency of occurrence. Reliability is an essential property for the wind energy users that employ probabilistic information for their decision-making processes.

02 Data description and methodology

This chapter presents a detailed description of the seasonal forecast systems (section 2.1) and observational references (section 2.2) employed in the thesis as well as a discussion of the reasons behind the choice of these datasets. To illustrate the current capabilities of the seasonal predictions to produce relevant information for wind energy users, the 10-m wind speed and 2-m air temperature variables have been used. The methods employed in each dataset to derive the surface variables are briefly explained in section 2.3. Although the specific methods and metrics used to explore the different aspects of the seasonal predictions are described within each chapter, the general strategy for the forecast quality assessment followed throughout the thesis is explained in section 2.4. This section is complemented by a detailed description of the metrics in Appendix A. The forecast quality assessment step is crucial when seasonal forecasts are used in decision-making processes because any forecast product without an indication of its quality based on past performance does not have any real value (Doblas-Reyes et al. 2013b). Finally, sction 2.5 describes the leave-one-out cross-validation method which has been applied in different contexts of this thesis.

2.1 Seasonal forecast system: ECMWF System 4

The European Center for Medium-Range Weather Forecasts (ECMWF) is at the forefront of the seasonal forecasting since the mid-1980s, when experimentation on ensemble forecasting for the monthly time scale was

started (Buizza and Leutbecher 2015, and references therein). The first ECMWF seasonal forecast system was based on an atmosphere-ocean coupled model released in 1997 that provided a successful forecast of the major 1997-98 El Niño event (Stockdale et al. 1998). From this first coupled system (referred to as System 1) a new generation of seasonal forecast systems have been produced: System 2 in 2001, System 3 in 2007, System 4 in 2011 and SEAS5 in 2017.

The seasonal forecasts used in this thesis are those from ECMWF System 4 (Molteni et al. 2011), which was the ECMWF's operational system until the end of 2017 when it was upgraded from System 4 to SEAS5[1]. Despite the fact that several centres are currently producing seasonal predictions (Table 1), ECMWF System 4 has been selected for this thesis because it has a large set of hindcasts and ensemble size, which are important characteristics to obtain robust results and to demonstrate the potential of the current seasonal predictions to provide useful information for wind energy applications. An additional aspect that has been taken into account for the selection of the seasonal forecast system is the availability of the seasonal predictions of 10-m wind speed, which is the essential variable for the wind energy community. For example, the well-known seasonal forecast system CFS-v2 (Saha et al. 2014) is unsuitable for the purpose of this thesis because it does not provide predictions of high-frequency 10-m wind speed for a long hindcast dataset.

ECMWF System 4 components and its most relevant properties are summarised in Figure 13. ECMWF System 4 is based on a global coupled model that comprises the ECMWF atmospheric model, the Integrated Forecast System (IFS) CY36R4 with a T255 spectral truncation (horizontal resolution of approximately 80 km) and 91 vertical levels reaching up to 0.01 hPa. The atmospheric model also includes the H-TESSEL land-surface model. This atmospheric model is coupled to the ocean model NEMO (Nucleus for European Modeling of the Ocean) version 3.3. The ocean model uses a grid with a horizontal resolution of around 1° in the extratropics with equatorial refinement and 42 levels in the vertical. The atmosphere and ocean are coupled using a version of the OASIS-3 (Ocean Atmosphere Sea Ice Soil) coupler developed at the CERFACS (Centre Européen de Recherche et de Formation Avancée en Calcul Scientifique).

Information about the current state of the earth system is introduced in the global coupled model by the initial conditions. In the atmospheric model, initial conditions are based on ERA-Interim for the period 1981 to 2010. For this period the H-TESSEL land surface model used in IFS Cy36r4 is run in offline mode with forcing data from ERA-Interim and the initial conditions for the ocean are based on the ORA-S4 ocean reanalysis. From the 1st January 2011 onwards (when ECMWF System 4 is operational), the

[1] The full description of the SEAS5 seasonal forecast system and its changes with regrad to System 4 can be found here: https://www.ecmwf.int/en/forecasts/documentation-and-support/long-range.

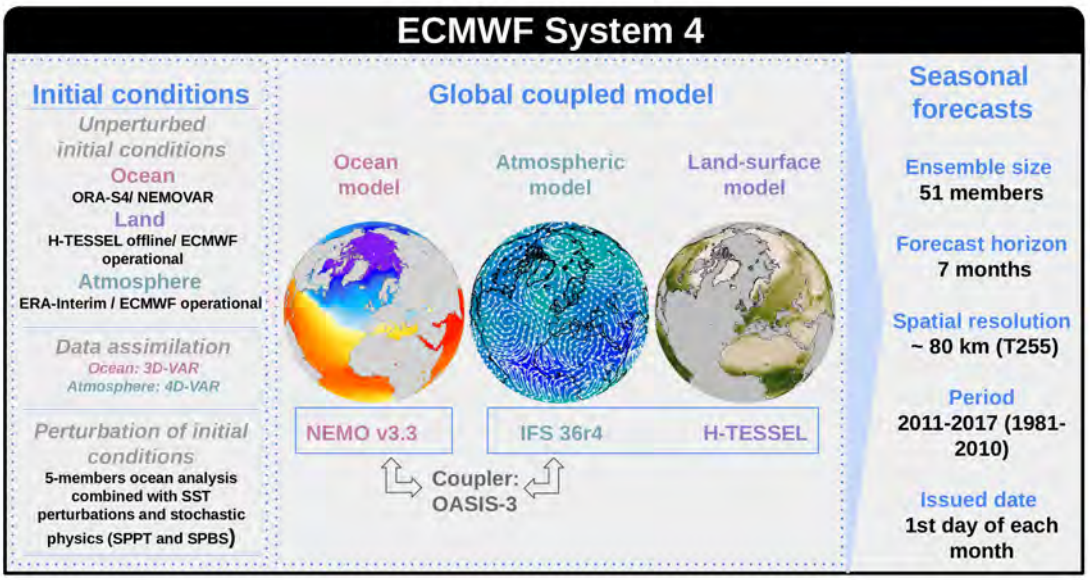

Figure 13 – Diagram of the ECMWF System 4 seasonal forecast system. This is based on the information provided in (Molteni et al. 2011).

atmospheric and land surface initial conditions are based on the ECMWF operational analysis and the ocean initial conditions are obtained from the NEMOVAR ocean analysis system. Data assimilation to generate these initial conditions is based on a four dimensional variational scheme (4D-VAR) and the first guess at appropriate time Three dimensional variational scheme (3D-VAR) strategies in the atmosphere and ocean components, respectively. The 4D-VAR data assimilation strategy can be considered a temporal extension of the 3D-VAR method.

ECMWF System 4 is run in ensemble prediction mode. As it has been explained in chapter 1, ensemble predictions are a way to deal with uncertainties in the climate system, in particular, those associated with the imperfections of the initial conditions and in the model formulation (Slingo and Palmer 2011). Ensembles allow estimating a prediction of the forecast uncertainty (measured by the ensemble dispersion), along with the prediction itself. The initial conditions are perturbed to characterise the uncertainty of the system. In particular, in ECMWF System 4 perturbations are generated by the combination of 5 members from the ocean analysis and SST perturbations, plus the use of atmospheric singular vectors. In addition, two schemes of stochastic physics, the stochastically perturbed

physical tendencies (SPPT) and stochastically perturbed backscatter (SPBS) schemes, are used during the simulation with different seeds for each ensemble member. The impact of these stochastic physical parameterisations on the ECMWF System 4 is discussed in Weisheimer et al. (2014).

The operational System 4 forecasts are produced with 51 members. The simulations are issued the first day of each month and they span up to seven months into the future with a spatial resolution of approximately 80 km. These predictions have been operationally produced from the 1^{st} of January 2011 up to November 2017, but a set of hindcasts have been generated for the 1^{st} of every month in the 1981-2010 period. The data from these hindcasts is available to users of the real-time forecast data, to allow them to calibrate their own real-time forecast products using their own techniques, to develop tailored products for their specific needs and to evaluate the quality of the forecasts.

These hindcasts are identical to the real-time forecasts except that the ensemble size is only 15 rather than 51. However, for the predictions with start dates of the 1^{st} February, May, August and November, the hindcast ensemble size was extended up to 51 members to allow for verification of the seasonal forecasts based on hindcasts having the same properties of the real-time forecasts. For that reason, the 51 members of the hindcasts have been employed for the forecast quality assessment of chapter 6. However, in those analyses performed for all the months of the year, the 15 members available for all start dates have been employed for consistency.

The evaluation of the seasonal predictions has been performed by concatenating hindcasts with operational forecasts in the period 1981-2016. This could have some implications in the results as the forecasts and hindcasts are not initialised with the same products, however the combination of hindcasts and forecasts allows to increase the length of the sample and consequently the robustness of the analyses. The impact of the ensemble size and hindcast length on forecast quality assessment and bias adjustment in the context of the seasonal predictions have been explored in Manzanas et al. (2019), where it is demonstrated that the ensemble size is playing a marginal role while hindcast length is a crucial factor.

2.2 Observational references: reanalyses

The performance of the seasonal predictions is commonly evaluated by their comparison against a reference dataset in the past. The choice of the reference dataset should be based on its capacity to represent the reality. Nevertheless, the problems related to the lack of long-enough historical data records and the unavailability of observational measurements in remote regions have promoted the use of reanalyses for the verification of climate predictions at the global scale.

Reanalyses have also demonstrated their potential usefulness for wind energy applications (Kirchner-Bossi et al. 2015; Cannon et al. 2015;

Staffell and Pfenninger 2016) as they are useful tools to understand some aspects of the climate variability, particularly in those regions where there are observational limitations.

Reanalysis products are the result of the assimilation of observations from different sources into an atmospheric model that generates evenly distributed global data. Changes in the observational type or coverage can produce low-frequency variations and trends in the reanalyses that can be difficult to isolate from the actual climate variability (Simmons et al. 2014), although special homogenisation techniques to avoid such effects have been developed in the last decades (Auer et al. 2005). The limited observations used in the reanalyses are not the only source of uncertainty affecting these products. There are also unavoidable errors in the assimilation systems that can have an impact on the quality of the reanalyses (Reichler and Kim 2008). To quantify the individual reanalysis uncertainty and identify robust signals that could be distinguished from artefacts in the observational data sources a multi-reanalysis approach has been adopted in this thesis.

Given the sparsity of global wind observations, and being aware that reanalysis estimates can often be far from observational point values, the reanalyses have been used as the best available estimate of wind speed and temperature in this thesis, but always recognising its limitations. Three state-of-the-art reanalysis datasets that have been generated by different institutions are employed: ERA-Interim, the Japanese 55-year Reanalysis (JRA-55) and the Modern Era Retrospective Analysis for Research and Applications-2 (MERRA-2).

ERA-Interim (Dee et al. 2011): uses the 4D-VAR approach in the ECMWF IFS atmospheric model to assimilate observational data from many sources to produce an evenly distributed gridded observational dataset with a cycle updated every six hours. The data are available as six-hourly fields produced with a T255 spectral truncation on a reduced Gaussian grid that corresponds to $\sim 0.75^{o}$x0.75^{o} (a horizontal resolution of 79 km) and 60 vertical levels from the surface up to 0.1 hPa.

JRA-55 (Kobayashi et al. 2015): is produced by the Japan Meteorological Agency (JMA) operational data assimilation system, which is based on the operational system as of December 2009 with a 4D-VAR scheme with a six-hourly update cycle. This reanalysis starts in 1958 and provides data with six-hourly temporal resolution, a T319 spectral truncation ($\sim$55 km) and 60 hybrid vertical levels. The spatial resolution of 1.25^{o} x 1.25^{o} is used in this work instead of the original 0.5625^{o} x 0.5625^{o} resolution because it is the only resolution for which data at 850 hPa level are available.

MERRA-2 (Molod et al. 2015): is the most recent reanalysis produced by NASA's Global Modelling and Assimilation Office (GMAO). It uses the Goddard Earth Observing System-5 (GEOS-5) atmospheric model with a 3D-VAR data assimilation scheme with a six-hourly update cycle. The data used in this thesis are hourly fields produced by an incremental

analysis update procedure (Bloom et al. 1996) that allows for products with higher-frequency than those six-hourly products generated directly from the analysis. The horizontal resolution corresponds to 0.625º x 0.5º and it has 72 sigma vertical levels available.

The most important properties of these reanalysis have been summarised in Table 2.

The main limitation of these datasets is their resolution, which results in their inability to represent local processes that are relevant to specific power plants. However, they provide (and for this reason reanalyses are widely used by the renewable energy research and operations community) an estimate of the resource available at regional scales over long periods. The resolution of these datasets is also similar to the resolution of the ECMWF System 4 seasonal predictions, which makes these products suitable for the forecast quality assessment.

2.3 Wind at 10-m and temperature at 2-m

The most relevant variables in a wind energy context are wind speed and temperature. While the wind speed provides information about the available wind energy resources, the temperature is directly linked to the energy demand. These are relevant aspects from the wind energy community because one of the challenges for renewable energy sources is to balance offer with demand. Traditionally seasonal forecast systems do not produce operational forecasts of wind speed at turbine height levels. Instead, wind speed and temperature are made available near the surface (10-m or 2-m) or at different pressure levels. It is difficult to interpolate directly to hub height as the physical height of the pressure levels is not constant over time and the interpolation also needs other variables like stability. For that reason, wind speed and temperature at 10-m and 2-m respectively have been selected for this thesis. It might be possible for the forecast systems to deliver wind speed at hub height, but the interpolation effort will make sense once the renewable energy community is informed about the benefits and drawbacks of seasonal forecast systems.

The near-surface wind speed (ws_{10m}) used in this study has been computed as the module of the zonal (u_{10m}) and meridional components (v_{10m}) of wind speed 10-m level by following this equation:

$$ws_{10m} = \sqrt{{u_{10m}}^2 + {v_{10m}}^2} \qquad (2.1)$$

This computation has been done with the instantaneous six-hourly values for ECMWF System 4, ERA-Interim and JRA-55 and from hourly data for MERRA-2. The seasonal forecasts of the 2-m air temeprature are directly produced by ECMWF System 4 and also for the reanalysis products.

Wind speed at 10-m and the 2-m air temperature provided by reanalyses and by the seasonal forecast system used here are interpolated from winds and temperatures at specific model levels. The evaluation of the wind speed and

Table 2 – Summary of the main characteristics of the three reanalysis datasets used in the present study.

Name	ERA-Interim	JRA-55	MERRA-2
Institution	ECMWF	JMA	NASA
Assimilation system	IFS Cy31r2	JMA's operational system (version Dec 2009)	GEOS-5
Assimilation scheme	4D-VAR	4D-VAR	3D-VAR
Horizontal resolution	0.75° x 0.75°	0.5625° x 0.5625°	0.625° x 0.5°
Vertical levels	60 levels (0.1 hPa)	60 levels (0.1 hPa)	72 levels (0.01 hPa)
Time resolution	6h	6h	1h
Period	1979-present	1958-present	1980-present

temperature from these data products can be affected by the different methodologies used to infer these variables from the lowest model level (Decker et al. 2012; Rose and Apt 2016).

ERA-Interim and ECMWF System 4 use different versions of the IFS atmospheric model, IFS CY31r2[2] and IFS CY36r4[3], respectively. However, both versions employ the same methodology to derive the 10-m wind speed and 2-m air temperature. Wind at 10-m and air temperature at 2-m in MERRA-2 are interpolated with the Helfand and Schubert scheme (Helfand and Schubert 1995) based on Monin-Obhukhov similarity theory that includes the effects of a viscous sublayer for heat and moisture transport over all surfaces except land (Molod et al. 2015). In the JRA-55 reanalysis the wind speed at 10-m and the temperature at 2-m are estimated with a univariate two-dimensional optimal interpolation process under the assumption of neutral stability from the lowermost level (Kobayashi et al. 2015).

Each reanalysis employs a different methodology for the computation of the 10-m wind speed and 2-m air temperature, but the most important difference is that JRA-55 is considering neutral stability in the surface layer while the ERA-Interim and MERRA-2 reanalyses use stability-dependent approaches.

[2] https://www.ecmwf.int/sites/default/files/elibrary/2007/9221-part-iv-physical-processes.pdf

[3] https://www.ecmwf.int/sites/default/files/elibrary/2010/9233-part-iv-physical-processes.pdf

2.4 Forecast quality assessment

Seasonal forecasts, as in any other forecasting process, have to be systematically compared to a

reference to assess their quality in a multifaceted process known as forecast quality assessment (Mason and Baddour 2008). The estimation of the forecast quality based on its past performance is a fundamental step to the prediction problem (Doblas-Reyes et al. 2013b) because it allows quantifying the added value of the forecasts relative to other prediction approaches. Two types of forecasts are considered in this thesis: deterministic and probabilistic. The latter is considered more complete because probabilistic forecasts provide a forecast along with an estimate of its uncertainty. At the same time, the forecast quality estimates also have uncertainty. Three sources of uncertainty in scoring metrics of probabilistic forecasts should be considered: improper estimates of probabilities from small-sized ensembles, an insufficient number of forecast cases, and imperfect reference values due to observational errors.

A way to investigate these problems is to use several scoring measures to offer a comprehensive picture of the forecast quality of the system (Jolliffe and Stephenson 2012) and to apply statistical inference as often as required. A wide range of verification metrics is available in the literature (e.g. Jolliffe and Stephenson 2012), but those metrics suitable to verify the seasonal forecast products that are distributed among the wind energy users have been selected.

The forecast quality estimates based on the performance of the system in the past may guide users about the expected performance of the future forecasts (Weisheimer and Palmer 2014), always with the caveat that the predictability of the climate system might change over time. The skill assessment used to investigate the quality of the seasonal forecasts compared to a benchmark forecasts. The skill metrics for both deterministic (ensemble mean) and probabilistic predictions which are considered in this thesis are: correlation coefficient, fair ranked probability skill score, fair continuous ranked probability skill score.

Reliability measures the agreement between the forecast probabilities for an event (e.g wind speeds exceeding the upper tercile) and the observed frequency of occurrence of that particular event. Reliability analysis of probabilistic forecast systems remains as a prime concern for the wind energy sector, as well as for any user of probabilistic predictions, due to the risks and uncertainties involved in the prediction of wind resources (Chaudhry and Hughes 2012). In this thesis, the reliability has been explored through rank histograms and reliability diagrams that have been computed for specific regions by pooling all the forecasts in all the grid points in the region. A detailed description of these metrics and their interpretation have been included in Appendix A.

2.5 Leave-one-out cross-validation

The bias-adjustment and reconstruction parameters (chapters 5 and 6) are usually determined by comparing the past forecasts with the observations, which are based on the same dataset that is available for verification. However, if the verifying observations are not

independent of the data used for the statistical training, this may lead to forecast quality estimates that are positively biased (Mason and Baddour 2008). To avoid using the same data for the derivation of the post-processing parameters and for the validation of the seasonal forecasts, it is generally considered to be best practice the use of leave-one-out cross-validation in all stages of the prediction formulation and the forecast quality assessment (Wilks 2011). An example of the cross-validation procedure over a sample with six elements has been illustrated in Figure 14.

In a cross-validation framework, the original sample is divided into L equal sized subsamples. In each of the L iterations (folds), one of these subsamples is used for test and the remaining L−1 subsamples are retained for training. This generates a sample of size L (output data) covering the whole period, which is subsequently compared against the reference dataset. Leave-one-out cross-validation is a special case of cross-validation where the number of folds (L) equals the number of instances in the data set.

When seasonal forecasts are provided as probabilities based on the ensemble members in a retrospective period (e.g. 1981-2015), probabilities should be computed in cross-validation as this method can effectively emulate how these forecasts would have been in a hypothetical operational context. For example, to compute the seasonal forecast probabilities of the wind speed being below-normal, normal or above normal in DJF 1993 the terciles should be

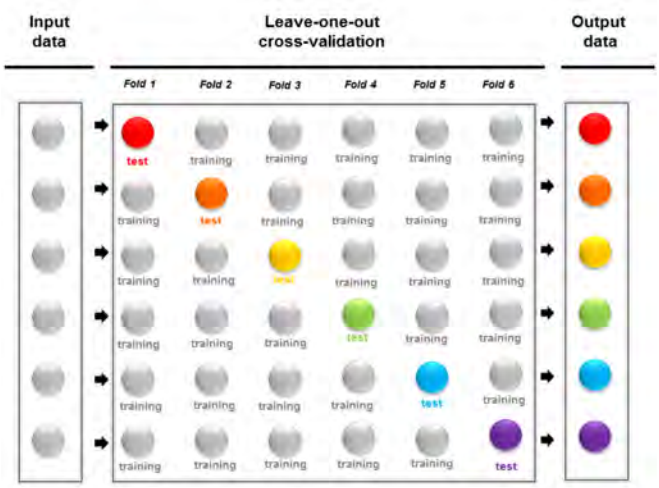

Figure 14 – Schematic illustration of the leave-one-out cross-validation method. In this example, a sample with six elements (L=6) is shown. In each iteration, one element has been used as the test and the remaining L-1 elements are used as training data.

computed from the combination of the seasonal forecast wind speed for DJF in the period 1981-1992 and those for the period 1994-2016 (i.e. excluding 1993, as it is the target year). Then the probabilities are obtained as the percentage of ensemble members in DJF 1993 below the lower tercile, those between the lower and upper terciles and the percentage of ensemble members exceeding the upper tercile. To obtain the probabilities of the seasonal forecast for the full period, this procedure is repeated for each year in the 1981-2015 period, which has a substantial computational cost.

03

Systematic errors and trends in the seasonal forecasts

03 Summary

Objective

To assess the statistical properties of the 10-m wind speed and 2-m air temperature, which are the essential variables affecting wind energy production and energy demand. This information allows describing the climate variables with a few parameters, which are often used in those energy applications with limited computational resources. The purpose of the comparison of the statistical properties of these variables in the seasonal predictions and different observational datasets is twofold. Firstly, the identification of systematic errors. Secondly, the estimation of the uncertainty coming from the reanalysis datasets currently employed as references for the long-term wind energy resource evaluation.

Methodology

- Statistical parameters: climatology, bias, standard deviation, skewness, kurtosis, Shapiro-Wilk normality test and linear trends.

Results

- Biases in the ECMWF System 4 are lower for the seasonal predictions of 10-m wind speed than for 2-m air temperature. However, the wind speed biases show a higher sensitivity to the reanalysis employed as a reference than for temperature.
- Standard deviation, skewness and kurtosis show different patterns in predictions and observations for both variables. However, these parameters show more spatial variations in the reanalyses than in the ECMWF System 4 seasonal forecasts. Furthermore, in most of the regions, the normality hypothesis cannot be rejected either for wind speed or temperature distributions.
- Near-surface wind speed trends show a strong seasonal variability that is in agreement with the results of the winds at 850 hPa. This connection between the wind speed at both levels reflects that the changes in the large scale circulation can be playing a dominant role in these trends.
- Trends of the 90^{th} percentile of the wind speed are stronger than those obtained for the 10^{th} percentile. This indicates a faster change of the high wind speed values than of the low wind speeds as a consequence of the changes in the shape of the wind speed distribution with time.

- The intercomparison of the wind speed trends from different reanalyses shows that there are many regions where all the datasets produce similar trends, thus the results are robust. This result has also been obtained for the 2-m air temperature trends where the three reanalyses agree on the trends in most of the regions over land. However, discrepancies have also been found, such as the intense wind speed declining for the JRA-55 data. These intense negative trends in JRA-55 appear as a consequence of a bias in the model used to produce the reanalysis which is not fully corrected in the data assimilation process.
- Trends in the ECMWF System 4 seasonal forecasts of wind speed and temperature are much less intense than in the reanalyses and, in some regions, they have different sign.

Conclusions

- Inconsistencies among the wind speed values in the different reanalyses could have an important impact for wind energy users as these datasets have been traditionally employed in several wind energy applications for which the evaluation of the climatology and long-term wind speed variability is required.
- Differences in the statistical parameters used for the comparison of the distribution in predictions and observations should be considered when bias adjustment approaches are applied to reduce the systematic errors affecting the products distributed among the users.
- Near-surface wind speed trends can be produced by changes in the atmospheric circulation. Trends as intense as those observed are not reproduced by ECMWF System 4. However, the reasons for this underestimation require further investigation.

Publications

Some of the results discussed in this chapter have been published in:

- **Torralba, V.**, F. J. Doblas-Reyes, and N. Gonzalez-Reviriego, 2017: Uncertainty in recent near-surface wind speed trends: a global reanalysis intercomparison. *Environmental Research Letters*, 12 (11), 114019, doi: 10.1088/1748-9326/aa8a58.

Furthermore, this chapter also presents the contributions of the author of this thesis to:

- Marcos, R., N. Gonzalez-Reviriego, **V. Torralba,** A. Soret, F.J. Doblas-Reyes, 2018: Characterization of the near surface wind speed distribution at global scale: ERA-Interim reanalysis and ECMWF seasonal forecasting System 4. *Climate Dynamic*s, 13, doi: 10.1007/s00382-018-4338-5.

03 Systematic errors and trends in the seasonal forecasts

The understanding of the uncertainty in climate variables is crucial for appropriate risk estimation of the wind energy resources. This kind of activities needs global information that requires the use of large datasets and expensive computational resources (Zhou and Smith 2013). For that reason, uncertainty estimates are obtained through the description of the probability distribution of the main variables affecting wind energy production and demand, such as wind speed and temperature. This way, the knowledge of a couple of variables can be used as guidance for the development of policies favouring sustainable adaptation initiatives that avoid poor investment decisions (Fant et al. 2016).

Despite the potential usefulness of this information, most of the studies in this sense have been tailored to explore the distributions for some particular regions (Monahan 2006; Zhou and Smith 2013). Only a few works explore the wind speed distribution at a global scale (Kiss and Jánosi 2008; Carta et al. 2009; Ouarda et al. 2016). Regarding the temperature probability distribution, much research has been devoted to the analysis of extreme events of temperature (e.g. Harmel et al. 2002; Donat and Alexander 2012) in the context of the antrophogenic climate change. Thus, these assessments have been mainly focused on the tails of the probability distribution of the temperature. However, the global assessment of the distribution parameters of the seasonal temperature is still lacking.

The assessment of the distributions' moments and their deviations from normality are

useful diagnostic tools for comparing climate datasets. However, these analyses should be complemented with an evaluation of the long-term variability of the different climate variables because they can help to identify temporal inconsistencies in the datasets. For that reason, in this chapter, the trends of wind speed and temperature are analysed.

Chapter 3 focuses on the comparison of the main moments of the 10-m wind speed and 2-m air temperature distributions between the ECMWF System 4 seasonal predictions and in three reanalyses (ERA-Interim, JRA-55 and MERRA-2). Besides, the assessment of the long-term variability of these two variables in the different datasets has been also performed. This exploratory analysis can be useful to identify discrepancies and similarities in the distribution of the observed and predicted climate variables that can inform about some aspects of the uncertainty affecting the verification of seasonal predictions (Jolliffe and Stephenson 2012). The trends of the near-surface temperature have not been included here, because they have already been widely investigated and documented in the scientific literature (Boer 2009; Vose et al. 2012; Simmons et al. 2014), but the results for the temperature trends in the datasets employed in this thesis have been included in the Appendix B (Figure B10).

The chapter is organised into five sections. Section 3.1 details the statistical parameters that have been used in this chapter. Section 3.2. includes the assessment of the seasonal variations of the wind speed mean climatology and the description of the differences between predictions and different observational sources. In section 3.3 higher-order moments of the probability distribution (standard deviation, skewness and kurtosis) are explored. Then, the resemblance of the seasonal wind speed and temperature distributions with the normal distribution is discussed in section 3.4. Finally, the evaluation of the long-term trends has been included in section 3.5. Some of the results discussed in this chapter have been published in Marcos et al. (2018) and in Torralba et al. (2017a).

3.1 Methodology

The characterisation of the main properties of the wind speed and temperature probability distribution in the reanalyses and in the ECMWF System 4 seasonal forecasts has been performed by the computation of different statistical parameters: the first-order moments (climatology and bias), higher-order moments (standard deviation, skewness and kurtosis), Shapiro-Wilk normality test and climate trends.

3.1.1 Climatology and bias

The climatology of the 10-m wind speed and 2-m air temperature has been computed as the time average over the 1981-2015 period for each grid point and season (DJF, MAM, JJA and SON) and for each reanalysis. For the seasonal predictions, the climatology has been computed as the ensemble mean of the 51 member seasonal

average for the 1-month lead time predictions (i.e. when the target season is DJF, the predictions initialised the 1^{st} of November are used). Differences between the climatology of the seasonal predictions and the corresponding of the reference dataset are commonly called mean biases. As it has been mentioned in chapter 1, these biases are caused by the imperfect model representation of the climate processes in the climate forecast systems, initialisation uncertainty and imperfections in the model parameterisations (Weigel et al. 2008).

The mean bias has been computed as follows:

$$bias = \frac{1}{N}\sum_{i=1}^{N}(\hat{y}_i - x_i) \tag{3.1}$$

Where $\hat{y}_i$ is the ensemble mean of the seasonal forecast, x_i is the value used as a reference at the i^{th} time step and N is the total number of time steps ($i = 1,...,N$).

3.1.2 Moments of the probability distribution

The properties of the distribution described by the standard deviation, skewness and kurtosis are illustrated in Figure 15.

These parameters have been computed differently in the seasonal forecasts and in the reanalyses. For the seasonal forecasts, the statitstical parameters have been obtained from the distribution based on the 51 members in the 35 years (1981-2015) for each season and grid point. The ERA-Interim standard deviation has been computed in a similar way, although for that dataset there are not ensemble members available, so the distribution is generated with 35 values per season and grid point.

Standard deviation: is a measurement of the distribution variability around the mean. The inter-annual standard deviation in the seasonal predictions and observations of 10-m wind speed and the 2-m air temperature has been computed as the square root of the average squared difference between the data points z_j $(j = 1,2,...,J)$ of the distributions and its mean $(\bar{z})$:

$$\sigma = \sqrt{\frac{1}{J-1}\sum_{j=1}^{J}(z_j - \bar{z})^2} \tag{3.2}$$

The number of data points (i.e. sample length) is equal to the number of year when the standard deviation is estimated for the reanalyses ($J = N$), but when it is computed for the seasonal forecasts, the sample also includes the number of members ($J = N \cdot M$). The normal distribution has $\sigma = 1$ (Figure 15a, *grey area*), values of $\sigma < 1$ indicate that the data tend to be close to the mean (Figure 15a, *pink curve*) and $\sigma > 1$ show that the data spread over a large range of values (Figure 15a, *blue curve*).

Skewness: allows assessing if low and high extremes are equally probable. Skewness has been used to characterise the degree of asymmetry of the wind speed and temperature distributions in comparison with the normal distribution and it can be defined as:

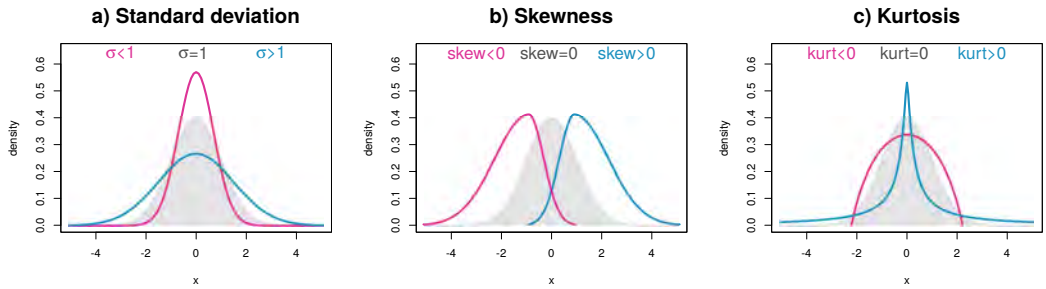

Figure 15 – Hypothetical probability density functions to illustrate the concepts of: a) standard deviation (sd), b) skewness (skew) and c) kurtosis (kurt). Grey probability distribution illustrates the typical standard deviation, skewness and of kurtosis of a normal distribution. More details are given in the text (section 3.3).

$$skew = \frac{1}{J}\sum_{j=1}^{J}\left[\frac{z_j - \bar{z}}{\sigma}\right]^3 \tag{3.3}$$

Where σ is the standard deviation of the data points z_j $(j = 1,2,...,J)$ of the distribution and $\bar{z}$ is the mean of the sample.

The normal distribution has skewness equal to zero with similar tails in both sides of the mean (Figure 15b, *grey area*), but a distribution with negative skewness has an asymmetric left tail extending out towards more negative values (Figure 15b, *pink line*) and the positive skewness indicates that the distribution has an asymmetric right tail extending out to more positive values (Figure 15b, *blue line*).

Kurtosis: is used to characterise the distribution tails. Kurtosis is helpful to investigate if the distributions of wind speed and temperature are heavy-tailed (positive kurtosis) and tend to have outliers or if the outliers are less probable than in a normal distribution (negative kurtosis). It has been computed by following this equation:

$$kurt = \left(\frac{1}{J}\sum_{j=1}^{J}\left[\frac{z_j - \bar{z}}{\sigma}\right]^4\right) - 3 \tag{3.4}$$

where $\bar{z}$ is the mean and σ is the standard deviation of the data points z_j $(j = 1,2,...,J)$.

As the kurtosis for a standard normal distribution is equal to three, to quantify the deviations of the distribution kurtosis in comparison with the standard normal distribution, kurtosis has been scaled by substratcting a value of three. This definition of kurtosis is often referred to as "excess kurtosis". Then the kurtosis equal to zero will denote that the distribution shows the same kurtosis as the normal distribution. When the kurtosis is negative the distribution has shorter tails than the normal distribution (Figure 15c, *pink line*). When the kurtosis is positive then the distribution has longer tails than the normal

distribution (Figure 15c, *blue line*).

3.1.3 Shapiro-Wilk test

Shapiro-Wilk normality test (Shapiro and Wilk 1965) has been selected for the normality assesment. The test evaluates the normality of a specific distribution and it does not need the specification of the mean and the variance such as the traditional Kolmogorov-Smirnov test (Steinskog et al. 2007).

The null hypothesis contrasted in the Shapiro-Wilk test is whether the distribution of the z_j $(j = 1,2,...,J)$ data comes from a normally distributed population. The statistic used is defined as follows:

$$W = \frac{\sum_{j=1}^{J} a_j z_j}{\sum_{j=1}^{J} (z_j - \bar{z})^2} \tag{3.5}$$

where the $z_{(j)}$ are the ordered sample values (z_1 is the smallest) and the a_j parameters are constants that depend on the mean, variance and covariance matrix (Royston 1982). For a sample size J > 3, the analytical form of the null distribution of W is not available, but it has been approximated as in Shapiro and Wilk (1968). The confidence level at the 90% has been established for this work meaning that when the p-value is equal or below 0.1 then the null hypothesis of normality is rejected.

The p-values obtained for the ERA-Interim seasonal values and the ECMWF System 4 seasonal predictions are not directly comparable because goodness-of-fit tests results can be affected by sample size differences (Steinskog et al. 2007). To take into account this effect the Fisher's method (Brown 1975) which combines p-values has been applied over the seasonal predictions as these predictions have 51 ensemble members. Fisher's method is based on the independent p-values obtained from M tests (p_m, $m = 1,2,\ldots,M$). Under the null hypothesis that the p-values follow a uniform distribution the test statistic Z is defined as:

$$Z = -2 \sum_{m=1}^{M} log_e p_m \tag{3.6}$$

where p_m is the probability that the variable exceeds the observed value under the null hypothesis that p-values follow a uniform distribution. Z is distributed as a chi-square distribution with $2M$ degrees of freedom where M is the number of independent tests performed (Brown 1975).

In this case, the Shapiro-Wilk test has been applied for each ensemble member individually, then 51 p-values have been obtained ($M = 51$). The Fisher's method (Equation 3.6) has been applied to combine the information in the 51 p-values to obtain a single outcome.

3.1.4 Linear trends

The linear trends have been estimated from linear regression of the z variable (10-m wind speed and 2-m air temperature in this work) with time ($i = 1981,...,2015$) as an independent

variable. This model can be expressed as:

$$z(i) = b_0 + b_1 i \tag{3.7}$$

The slope (b_1) indicates the linear rate of change of the variable. Positive values correspond to increasing trends whereas negative values indicate decreasing trends. The linear trends of the 10-m wind speed have been normalised by the climatological values (i.e. the mean value of the variable over time) and expressed as a percentage of change per decade. This transformation is performed to facilitate the interpretation of the wind speed trends, as wind speed is much more intense over the ocean than over land, with large spatial variations over the continents. A t-test (described in Appendix section A.3.1b) has been applied to assess if these trends are significantly different from zero at the 95% confidence level.

3.2 Seasonal mean climatology and bias

3.2.1 Spatial variability of the mean wind speed

The seasonal wind speed climatology is used in several wind energy decision-making processes. For example to explore if a particular location is suitable for the installation of a wind farm or to explore the investment return feasibility. As these decision-making processes require information about the mean conditions of wind energy resources, the global characterisation of the mean wind speed is helpful to describe the average conditions in particular locations and seasons. Although the climatology of the temperature is also important for the estimation of the energy demand, this section is only focused in the wind speed because the climatology of near-surface temperature has been already discussed in the scientific literature (e.g. Legates and Willmott 1990).

The most noticeable feature in a wind speed climatology is the land-sea contrast with higher wind values over the ocean than over the continents (Bett and Thornton 2015; Stopa et al. 2013). The wind speed values reach 10.5 m/s in some oceanic regions, but over land, they generally range between 4.5 and 6.5 m/s. These higher values over the ocean than over land are related to the roughness over continental areas that produces higher friction and slows down wind speeds.

The strongest seasonal cycle of the wind speed is observed in the North Pacific and North Atlantic (Figure 16a). The wind speeds in that regions are named westerlies winds (Fan et al. 2014) because they flow poleward out of the subtropical high-pressure cells in the Northern Hemisphere and are shifted to the right and thus blow from the southwest. They have their maximum values in winter due to the influence of the intense meridional temperature gradient in that season. Over land, the maximum wind speed values in winter also appear in the Northern Hemisphere mid-latitudes, particularly in the central United States, central-eastern Europe, western Asia and the Himalayas. Although some regions such as Greenland, Australia and the low latitudes in the Southern Hemisphere also display high wind speed values, they do not have such a strong

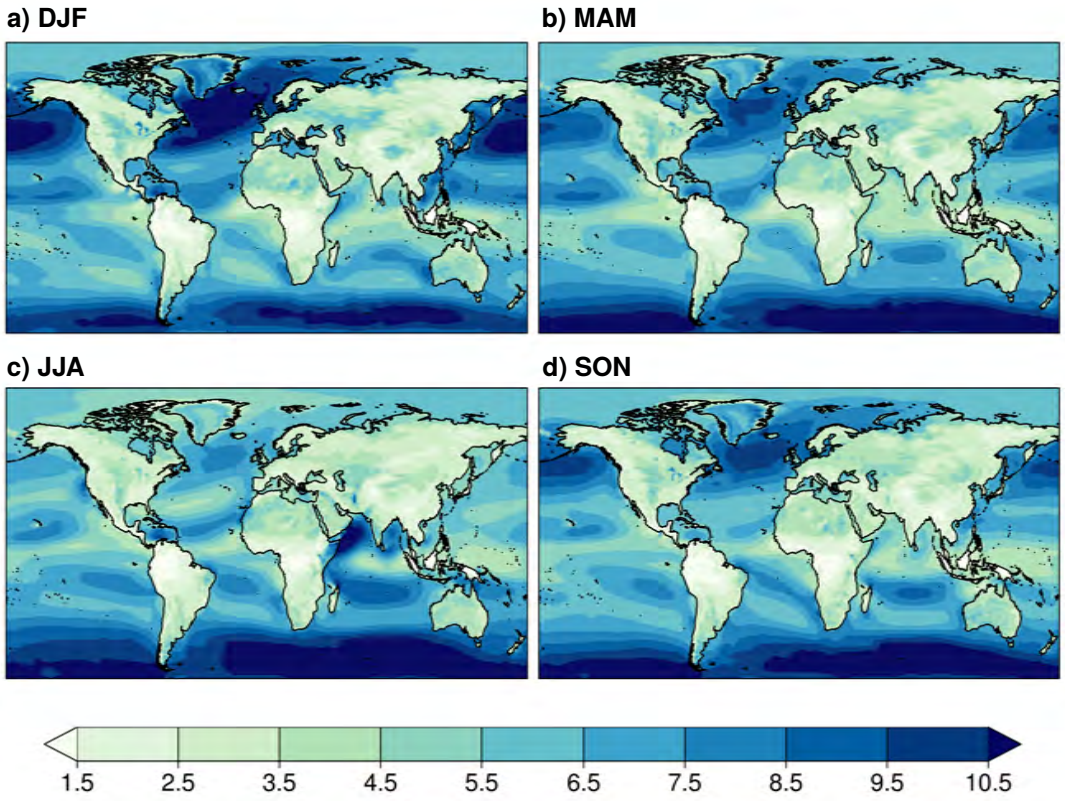

Figure 16 – Seasonal mean climatology of the 10-m wind speed (m/s) from ERA-Interim in the 1981-2015 period. They correspond to the following seasons: a) DJF, b) MAM, c) JJA and d) SON.

seasonal cycle.

In the boreal summer (Figure 16c) the wind speeds over the North Atlantic and North Pacific reach minimum values and the maximum wind speeds that appear in low latitudes at the Southern Hemisphere in all seasons spread towards the north. The highest wind speeds over the tropical Atlantic are shifted to the North following the seasonal migration of the Inte-Tropical Convergence Zone. The most remarkable characteristic in this season is the maximum wind speed values over the Indian ocean that appear as a response to the Indian monsoon. The influence of the monsoon can also be appreciated in eastern Ethiopia, Somalia and western India where the cross-equatorial level jet cause the maximum wind speeds of up to 8.5 m/s over land in this season (Joseph and Sijikumar 2004).

In spring and autumn, the geographical

distribution of the wind speed values is very similar (Figure 16b,d), although in MAM the wind speeds are slightly higher in some regions of the Northern Hemisphere, such as central United States, than in the Southern Hemisphere. Both seasons show the highest wind speeds in the North Atlantic and North Pacific with wind speeds over 9.5 m/s, but still lower than in DJF (Figure 16c).

These results evidence tha the higher values of wind speed are produced in the boreal winter in the Northern Hemisphere, but they have a strong seasonal cycle both over land and the ocean that produces large variations of the wind speed values throughout the year. These seasonal variations of wind speed are mainly related to changes in the pressure systems originated by the variations in the amount of received insolation in the different regions of the planet which in turn, produce the atmospheric circulation variability (Petersen et al. 2010).

The seasonal variations of the wind speed in the ERA-Interim dataset are similar to the climatology of the ECMWF System 4 seasonal predictions of wind speed (Figure B1) and those in JRA-55 and MERRA-2 (Figure B2), which have been included in the Appendix B.

3.2.2 ECMWF System 4 seasonal biases

The climatology of the seasonal predictions differs from the climatology of the observational reference. The analysis of these differences (i.e biases) is very important from the modelling point of view because they provide information about the systematic errors of the seasonal forecast systems. But also the bias assessment is crucial from the user perspective because some users tend to take the forecasts directly from the forecast systems (Jolliffe and Stephenson 2012) and the underestimation of these substantial unconditional errors will lead to incorrect decision-making processes.

The biases of the ECMWF System 4 seasonal predictions of wind speed and temperature relative to ERA-Interim, JRA-55 and MERRA-2 have been illustrated for the DJF season (predictions initialised the 1^{st} of November) in Figure 17. This season has been selected for illustration because it is when the wind energy resources show higher variability, and hence when the vulnerability of wind energy users is higher.

In general, the lowest wind speed biases are obtained when ERA-Interim is employed as a reference (Figure 17, top-left panel) with values ranging between -1.2 and 1.2 m/s. Positive biases, higher than 0.8 m/s, are located over tropical Pacific, eastern Asia while negative biases lower than -0.8 m/s are over Himalayas region. These results are consistent among the different datasets, although their magnitude change as a consequence of the differences in the mean wind speed characteristic of each reanalysis dataset. Strong positive biases in regions close to the Pacific Ocean and eastern Asia could be due to a positive coupled feedback between winds and SST, as too strong winds can lead to an excess of upwelling, producing colder SST, which in turn produces stronger

zonal winds (Magnusson et al. 2013). The North Sea shows a slight positive bias, as does the Caribbean region and they can be due to the poor representation of ECMWF System 4 of the Gulf Stream caused by low ocean model resolution (Magnusson et al. 2013), for that reason this bias is obtained for the three observational references (Figure 17,top row).

Wind speed biases obtained for JRA-55 (Figure 17, middle-right panel) are larger over land than over the ocean, with differences between ECMWF System 4 and the wind speeds from JRA-55 reaching 2 m/s. These positive differences are mainly related to the underestimation of the 10-m wind speed by the JRA-55 reanalysis over land, which has been attributed to the deficiencies in deriving wind speed for that particular reanalysis (Japanese Meteorological Agency, personal communication). In the JRA-55 data assimilation system, the regions where the vegetation type is categorised as trees show a negative near-surface wind speed bias. This bias appears due to the lowermost atmospheric level, the one interacting with land surface processes, being placed too high over regions with trees, reducing considerably the wind speed in the interpolation from there down to the altitude of 10 metres, which is not fully corrected in the data assimilation process.

By contrast, over the oceans, the highest wind speed biases are obtained when MERRA-2 is used as a reference with values around 0.8 m/s. Over land, the maximum biases found when MERRA-2 is used are identified in northern North America, northern South America and central Africa, where ECMWF System 4 overestimates the wind speed. Results for ERA-Interim and JRA-55 are similar, but with different magnitudes. There are instead some regions where the biases are different for each reference. For example, positive biases (around 0.4 m/s) are identified over the Iberian Peninsula when ERA-Interim is used as a reference, but these values reach 2 m/s when the JRA-55 dataset is employed, and negative biases (values between -0.8 and -0.4 m/s) are obtained when the climatology of the seasonal predictions of 10-m wind speed is compared to the ERA-Interim reanalysis wind speed.

The spatial distributions of the wind speed biases in different seasons (not shown) are very similar to that for DJF, although some differences are identified. For example, the high positive bias in the tropical Pacific reaches maximum values in JJA. Over land, the positive bias in northern North America is reduced in other seasons, and the positive bias in northern South America is shifted to the south in the boreal summer.

Mean biases of the 2-m air temperature (Figure 17, right column) are more prominent over land than over the ocean. ECMWF System 4 underestimates the mean values of the 2-m air temperature in comparison to the reanalyses in the oceans, but also in the Southern Hemisphere. Over land, the most important biases are observed in the Northern Hemisphere: western North America, North Africa and southwestern Asia with a negative bias higher than -2.4 m/s. This result is also consistent within

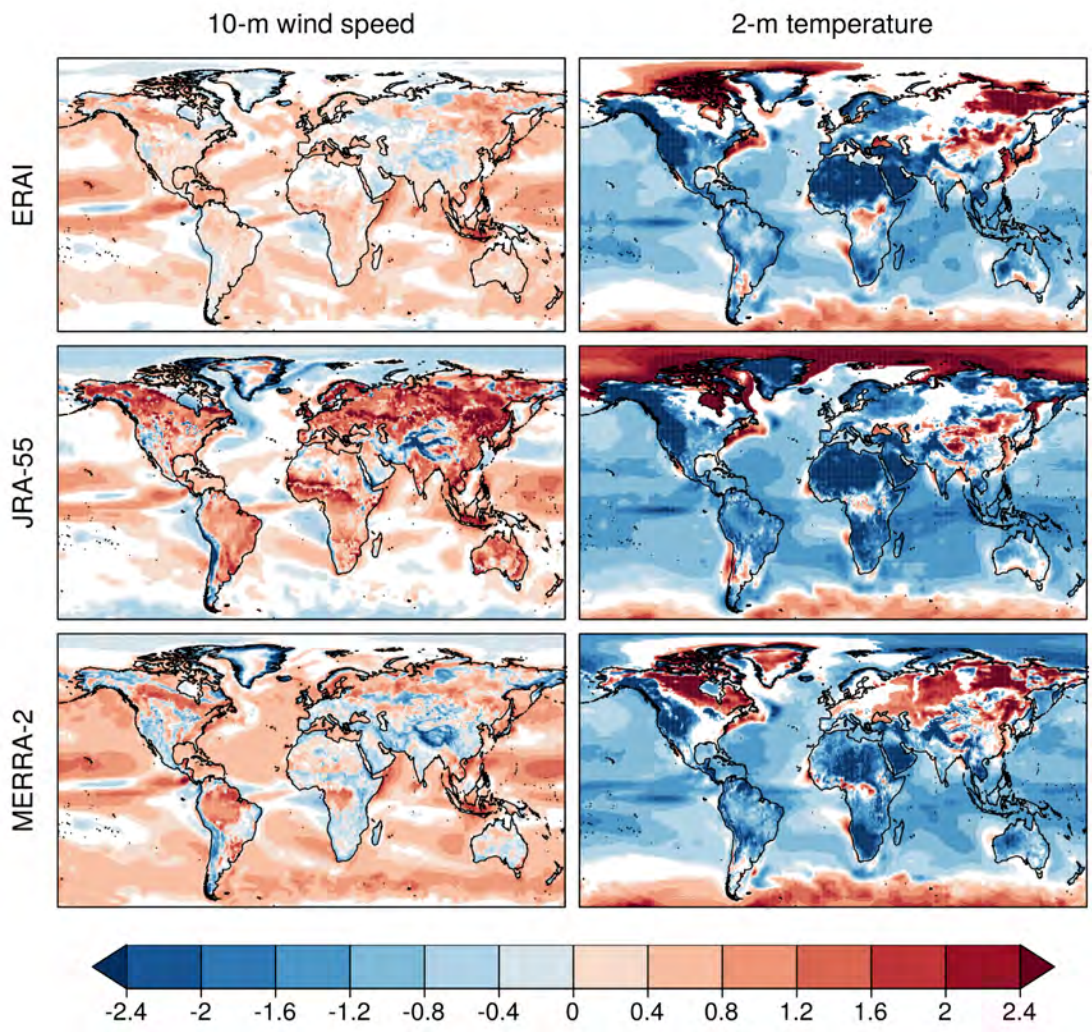

Figure 17 – Mean bias of the ECMWF System 4 seasonal predictions (ensemble mean) of 10-m wind speed (m/s) (left column) and 2-m air temperature (^{o}C) (right column). They correspond to the boreal winter (DJF) over the period of 1981- 2015. ECMWF System 4 seasonal predictions have been initialised the 1^{st} of November. Three observational references have been employed: ERA-Interim, JRA-55 and MERRA-2. White areas correspond to non-significant biases (t-test at a 95% confidence level).

the three reanalyses, but some differences can also be identified. For example in Greenland, the biases when ERA-Interim is employed are not significant in several regions, for JRA-55 biases are very intense and negative, while for MERRA-2, those biases are positive. Also for North America and Europe positive biases when MERRA-2 is used as reference indicate that ECMWF System 4 overestimates the temperature values in comparison with MERRA-2, but it underestimates the temperatures provided by the ERA-Interim and JRA-55.

The negative bias in western North America disappears in JJA when the ECMWF System 4 overestimates the air temperature in most of the North American region (not shown). Seasonal variations in the bias of temperature are also identified in northern Asia, where the positive and intense bias can be only identified in DJF.

These results illustrate that the use of several observational references for the evaluation of the seasonal predictions is crucial, particularly for the assessment of 10-m wind speed seasonal forecasts. Although the differences between the three reanalysis datasets are lower for 2-m air temperature, there are still some regions such as North America or Europe, which are key regions for the wind industry, where the differences between the bias for the air temperature are high and, consequently, the uncertainty coming from these observational references needs to be taken into account.

Given the important drift typical of climate forecasting, the biases as a function of the different lead months have been also considered. The results have been included in the Appendix B (Figures B3 and B4) where it is illustrated that for longer leads, the biases of wind speed and temperature increase as the systematic errors of the seasonal predictions grow.

3.3 Moments of the probability distribution

The discrepancies between predictions and observations are usually quantified as the difference in their means. However, there are more aspects of the distribution that should be considered in this comparison. The understanding of the differences in other parameters of the distribution can be useful to correctly interpret forecast uncertainty and quality. To provide a further description of the wind speed and temperature distributions their second, third and four main moments, which correspond to the standard deviation,the skewness and the kurtosis, have been computed.

3.3.1 Standard deviation

The wind speed standard deviation for DJF in the winter season is illustrated in Figure 18. The results of (σ_{S4}) (Figure 18a) show the maximum values over the oceans, particularly in the North Atlantic, North Pacific and over Indonesia, where the standard deviation of the wind speed is higher than 1 m/s. Over land, the highest standard deviation is also identified in regions of the Northern Hemisphere, such as central North America and Europe. Although these standard deviation values only reach 0.6

m/s which means that the distribution of wind speed in that regions is narrower than a normal distribution.

To investigate if the standard deviation of the seasonal predictions of wind speed (σ_{S4}) (Figure 18a) is similar to the standard deviation of the wind speeds from ERA-Interim (σ_{ERA-I}) the ratio of the standard deviations ($\sigma_{S4}/\sigma_{ERA-I}$) has been computed for each grid point and the result for winter is shown in Figure 18b. The predominant blue areas reflect the ECMWF System 4 underestimation of the wind speed variability compared with the values obtained from ERA-Interim. The understimation affects the tropical Pacific, but it shows the strongest effect over land, particularly in Northern Europe and Siberia. By contrast, overestimation of the standard deviation appears in some areas such as the tropical Atlantic or the Indian Ocean which indicates that the year-to-year variations of the predicted wind speed are higher than the observed wind speeds in that regions.

The differences between the inter-annual variability of the 10-m wind speed and 2-m air temperature seasonal predictions with those obtained for JRA-55 and MERRA-2 have been also explored and the results have been included in the Appendix B (Figure B5). These results show that the discrepancies among the reanalyses to represent the inter-annual variability are stronger for the 10-m wind speed than for the air temperature. ECMWF System 4 underestimates the standard deviation of the 10-m wind speed from JRA-55 in most of the regions over land, a result which is obtained not only for DJF but for all the seasons (not shown). The seasonal forecast system also overestimates the 10-m wind speed inter-annual variability over northern South America in comparison with that for MERRA-2 (Figure B5). These results show some variations for other seasons. For example, the standard deviation of the wind speed is overestimated by ECMWF System 4 in summer in several land areas over the Northern Hemisphere, and also in autumn in North America. This different performance among the reanalyses is another example of the importance of considering more than one observational reference.

3.3.2 Skewness and kurtosis

The skewness and kurtosis are the third and fourth order moments of the distribution of a variable. Although the mean and the standard deviation (first and second moments of the distribution, respectively) have the same units as the climate variables, the skewness and kurtosis are non-dimensional quantities. These parameters are referred to as shape parameters and can be helpful for the identification of appropriate probability models to describe the variable (Von Storch and Zwiers 2002).

Skewness values of the seasonal predictions of the wind speed distributions from ERA-Interim (Figure 19a) and the wind speeds from ECMWF System 4 (Figure 19c) have been compared in boreal winter, although similar results have been obtained for the different seasons (not shown).

The pattern of the wind speed skewness obtained

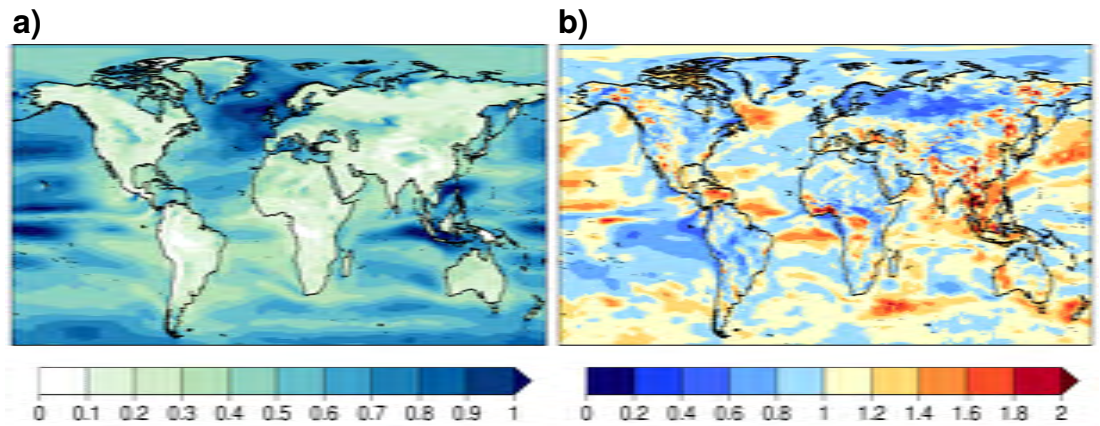

Figure 18 – Standard deviation of the 10-m wind speed (m/s) in ECMWF System 4 and in ERA-Interim. a) Standard deviation of the seasonal predictions from ECMWF System 4 (σ_{S4}), b) Standard deviation ratio ($\sigma_{S4}/\sigma_{ERA-I}$) of the 10-m wind speed seasonal predictions (ECMWF System 4) to the ERA-Interim reanalysis. This corresponds to the boreal winter (DJF) over the period 1981-2015. ECMWF System 4 seasonal predictions have been initialised the 1^{st} of November.

for ERA-Interim (Figure 19c) is very noisy, which reflects the higher spatial variability of this parameter at the global scale. Nevertheless, the seasonal predictions of wind speed (Figure 19a) exhibit a clearer skewness pattern with positive values in most of the regions. This shows that the predicted wind speed distribution at seasonal timescales has a tail that extends towards high values, therefore the probability of severe wind speed values is higher than low extremes in most of the regions. Only in a region over the tropical Pacific higher frequency of low wind speeds than for high wind speed values has been found, as indicated by skewness values are lower than two.

The kurtosis of the wind speed from the ERA-Interim reanalysis (Figure 19d) is generally negative, which indicates that the wind speed distribution has shorter tails and less extreme outliers than the normal distribution. The seasonal predictions of the wind speeds (Figure 19d) show a similar pattern to the ERA-Interim but the values of the kurtosis are lower than in the predictions. This shows that the tails of the predictions are more similar to the normal distribution than the tails of the wind speed distribution from ERA-Interim. Although both datasets show a noisy pattern, they agree in the values of the kurtosis above two in the tropical Pacific, which depicts the high frequency of extremes in that particular area.

Results of skewness and kurtosis for the JRA-55 and MERRA-2 reanalyses have been included in the Appendix B (Figure B6) where the discrepancies among the skewness and kurtosis illustrate that the uncertainty of the observational

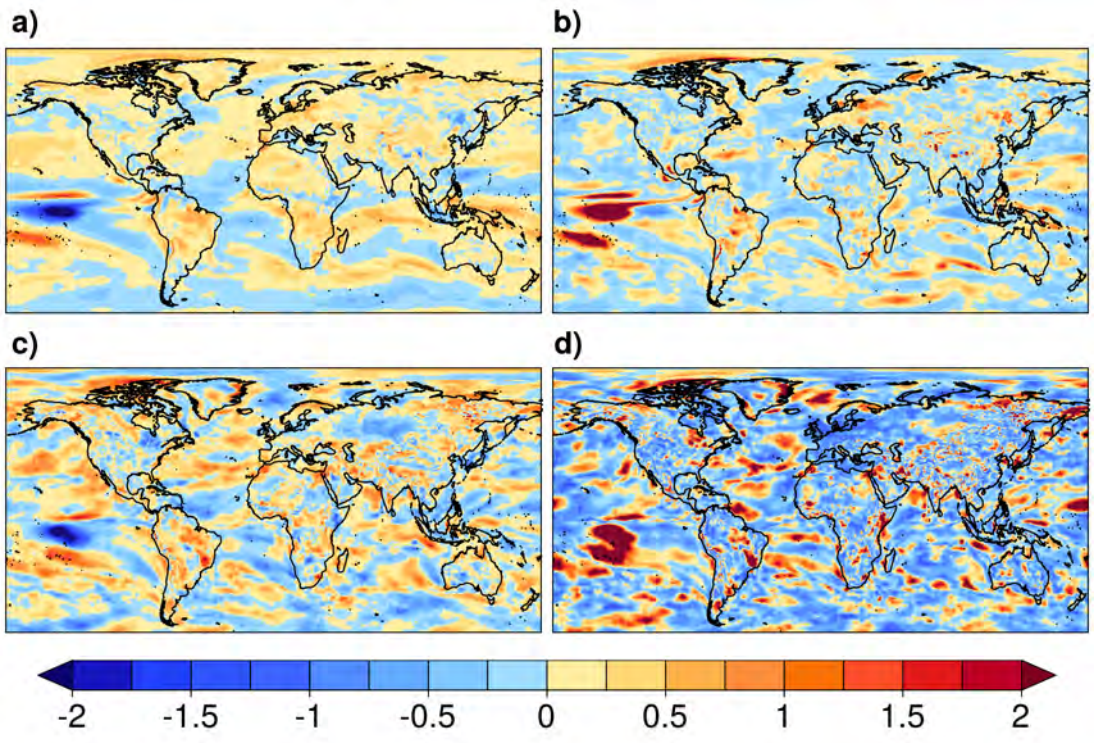

Figure 19 – Skewness and kurtosis of the 10-m wind speed a) skewness of the 10-m wind speed from ECMWF System 4, b) kurtosis of the 10-m wind speed from ECMWF System 4, c) skewness of the 10-m wind speed from ERA-Interim, and d) kurtosis of the 10-m wind speed from ERA-Interim. This corresponds to the boreal winter (DJF) over the period of 1981-2015. ECMWF System 4 seasonal predictions have been initialized the 1^{st} of November.

references is not only in the mean value of the wind speed but also in higher moments of the distributions.

The skewness and kurtosis for 2-m air temperature can be also found in the Appendix B (Figure B7). They show analogue results to those obtained for 10-m wind speed, with more noisy patterns for the reanalyses than for the seasonal predictions. Reanalyses and seasonal predictions agree in the positive skewness values obtained for South America, indicating a higher probability of high temperatures than for low temperatures in that region. The ECMWF System 4 shows a negatively skewed distribution of temperature in Europe and Asia. In the reanalyses most of these regions also show negative skewness, although there are some regions such as the Mediterranean or Iberian peninsula where positive skewness values can be found.

The kurtosis in the temperature distribution is negative in most of the regions (Figure B7). Nevertheless, some regions with positive kurtosis such as northern South America, where ECMWF System 4 and MERRA-2 can be identified, although this is not obtained for ERA-Interim or JRA-55. Discrepancies in the kurtosis of temperature between the seasonal predictions and the reanalyses are obtained for Europe, where the seasonal predictions show positive kurtosis while the reanalyses displays negative values.

The three parameters analysed in this section: standard deviation, skewness and kurtosis have shown that the seasonal forecast system ECMWF System 4 and the ERA-Interim dataset have differences that cannot be adjusted with a simple standard correction of the mean (Marcos et al. 2018). This is important because those methodologies that only adjust the mean of the predictions with the observations could produce corrected forecasts with very different statistical properties to those observed, which could prevent wind energy users to include these predictions in their decision-making processes. Hence, the application of statistical post-processing methods that modify higher moments of the distributions is recommended.

3.4 Normality test applied to the seasonal distributions

The deviations of the seasonal wind speed and temperature distributions from the normal distribution is a crucial aspect from the wind energy point of view, because the evaluation of wind energy resources over large areas involve large datasets and expensive computational requirements. Hence, it is useful to represent wind speed through probability density functions with a few key parameters (Steinskog et al. 2007; Zhou and Smith 2013). The measurement of the distribution deviations from normality can help identify the expression of non-linear processes and if they are properly reproduced by the climate forecast systems. This information is also important for the selection of a bias adjustment methodology because some of them are designed for normally distributed data.

Skewness and kurtosis are useful indicators of the deviations from normality but these parameters are very sensitive to outliers, therefore the Shapiro-Wilk goodness-of-fit normality test has been also used to describe the deviations from normality of the distributions (Jolliffe and Stephenson 2012). This test has been applied for the seasonal ERA-Interim wind speed and temperature (Figure 20a,b, respectively), but also for the seasonal predictions of those variables. The results for the rest of reanalyses and for 2-m air temperature have been included in the Appendix B (Figure B8).

The normality hypothesis cannot be rejected in most of the regions (Figure 20) where red areas are predominant. However, in some inter-tropical regions for the ERA-Interim wind speed and temperature values (Figure 20c,d), such as in the Tropical Pacific, this normality hypothesis has been rejected. Over land, the largest area

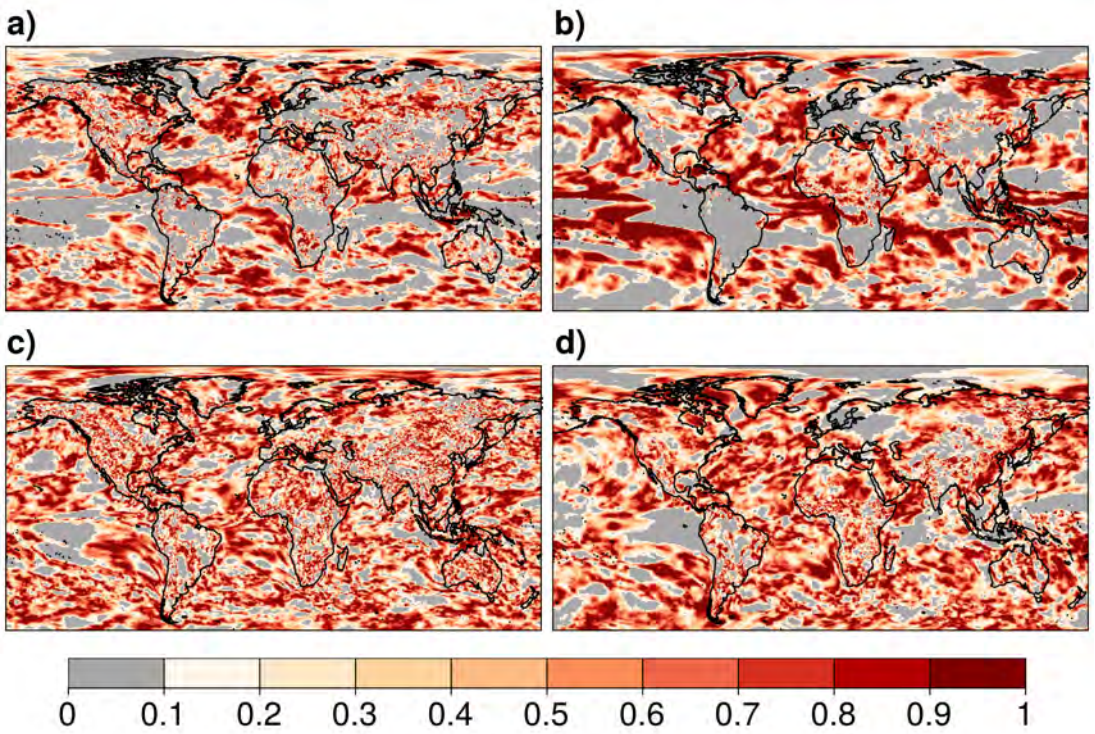

Figure 20 – P-values of the Shapiro-Wilk goodness-of-fit normality test. ECMWF System 4 a) 10-m wind speed and b) 2-m air temperature, and ERA-Interim c) 10-m wind speed and d) 2-m air temperature. This corresponds to the boreal winter (DJF) over the period of 1981-2015. ECMWF System 4 seasonal predictions have been initialised the 1^{st} of November.

with p-values under 0.1 for the temperature (Figure 20d) is in Europe, but also for some regions of South America where the hypothesis can be rejected (Figure 20d).

The number of regions where the normality is discarded increase for the seasonal predictions of wind speed and temperature (Figure 20a,b). The null hypothesis has been rejected for wind speed over some regions of North America, most of South America, but also Europe, South Africa and central Asia (Figure 20a). The seasonal distribution of the temperature from ECMWF System 4 seasonal predictions rejects the normality hypothesis for South America, some regions of Europe and south Africa (Figure 20b).

The different patterns obtained for the observed and predicted distributions of wind speed and temperature are in agreement with the results obtained for the skewness and kurtosis (section

3.3). They also reveal that the differences between the distributions in both datasets are not negligible and that should be considered when bias adjustment techniques are applied over the seasonal predictions of these specific variables (Marcos et al. 2018).

3.5 Long-term variability

The characterisation and the identification of the uncertainty in the trends can be helpful for wind energy decision-making, such as risk minimisation and resource evaluation. Observational studies have indicated the existence of wind speeds trends (Young et al. 2011; McVicar et al. 2012), but the causes of these trends are not fully understood. The main limitation for a proper assessment of the trends is the lack of a long observational dataset needed to produce robust results. To address this issue reanalysis products can be used (Vautard et al. 2010; Bett and Thornton 2015). Nevertheless, changes in the observational type or coverage can produce spurious low-frequency variations and trends in the reanalyses that can be difficult to isolate from the actual climate variability. To take into account this limitation, the use of more than one reanalysis has been recommended (Vose et al. 2012; Simmons et al. 2014). The ability to reproduce wind speed trends has been explored for the ERA-Interim, JRA-55 and MERRA-2 reanalyses. This has been complemented with the assessment of whether the ECMWF System 4 forecast system reproduces similar results to those obtained for the reanalyses. The analysis of the trends in the seasonal forecasts is important for their verification because inconsistencies with the observed trends will impact several aspects of the forecast quality. The trends have also been estimated for the 10^{th} and the 90^{th} percentile of the wind speed, because as it has been shown in section 3.3.2 where skewness and kurtosis have been explored, this variable displays asymmetry with many spatial variations. The characterisation of the trends will help to understand changes in the frequency of extreme events in recent decades.

The trends of near-surface air temperature have already been widely investigated in the scientific literature (Boer 2009; Vose et al. 2012; Simmons et al. 2014). For that reason, the results of the consistency among the reanalysis to represent the 2-m air temperature (Figure B11) along with the seasonal trends in all the datasets have been included in the Appendix B (Figure B12). The coherence among the reanalyses to represent the 2-m air temperature is superior to that observed for the 10-m wind speed (Figure B11), as indicated by most of the regions over land showing positive and significant trends in all the seasons. Exceptions to the positive trends are found for Siberia in DJF, northern North America in MAM and Australia in DJF and MAM. Inconsistencies among the reanalyses are obtained in the tropical Atlantic where the temperature trends are very small, which result in positive and negative non-significant trends in each dataset.

3.5.1 Trends as a function of the season

The ERA-Interim wind speed trends are illustrated in Figure 21. The spatial patterns of these trends have a strong seasonal variability. Globally, positive trends appear over the oceans, particularly in the tropical regions. These positive trends can be caused by the strengthening of the Walker circulation attributed largely to climate change (England et al. 2014). However, in the North Pacific in all the seasons and in the subtropical North Atlantic in JJA and SON only a significant negative trend is found (Figure 21). The global increase in wind speed over the oceans, which is much more noticeable in the tropical Pacific than in other basins, is in agreement with the results described by different authors (Young et al. 2011; Zheng et al. 2016) for a dataset based on satellite altimeter measurements and wind data from Cross-Calibrated Multi-Platform (CCMP) ocean Surface Wind Velocity Product for Meteorological and Oceanographic Applications (Atlas et al. 2011).

Over land, a strong positive trend in northern South America, and an overall negative trend, which is more visible over Europe, India and western Africa, are found (Figure 21). In western North America positive and significant trends are noticeable in boreal spring (Figure 21b). The negative and significant wind speed trends over Europe are stronger in DJF and SON (Figure 21b). This negative trend has been already identified in different observational sources and even climate simulations and it has been attributed to several factors: changes in the surface roughness related to the recent increase in vegetation cover in such area, variability of aerosol emissions, or changes in the atmospheric circulation (Vautard et al. 2010; Bichet et al. 2012; McVicar et al. 2012; Sterl et al. 2015). A non-uniform behaviour of the trends over Asia in most seasons and regions has been observed, although a declining wind speed appears in the Indian subcontinent all year round.

An increase of wind speed is found in several continental areas, such as the northern part of South America (Figure 21b), which displays the highest positive wind speed trends inland for the four seasons. Over western North America, positive and significant trends are noticeable in boreal spring (Figure 21b), but their sign change in JJA (Figure 21c). In Asia a non-uniform behaviour is found in most seasons and regions.

The wind speed trends have also been estimated for JRA-55 and MERRA-2 (Figure B11) and they lead to similar conclusions to those described for ERA-Interim, although the JRA-55 trends tend to be systematically larger, particularly over land. To identify if the trends displayed by the reanalyses can be due to changes in the atmospheric circulation or to other forcings like changes in the aerosols or the roughness length, the seasonal trends of the wind speed at 850 hPa for the ERA-Interim reanalyses have been computed (Figure 22). The corresponding results for JRA-55 and MERRA-2 are included in the Appendix (Figure B12). These figures show that the similarity of the trends between the three reanalyses is higher for

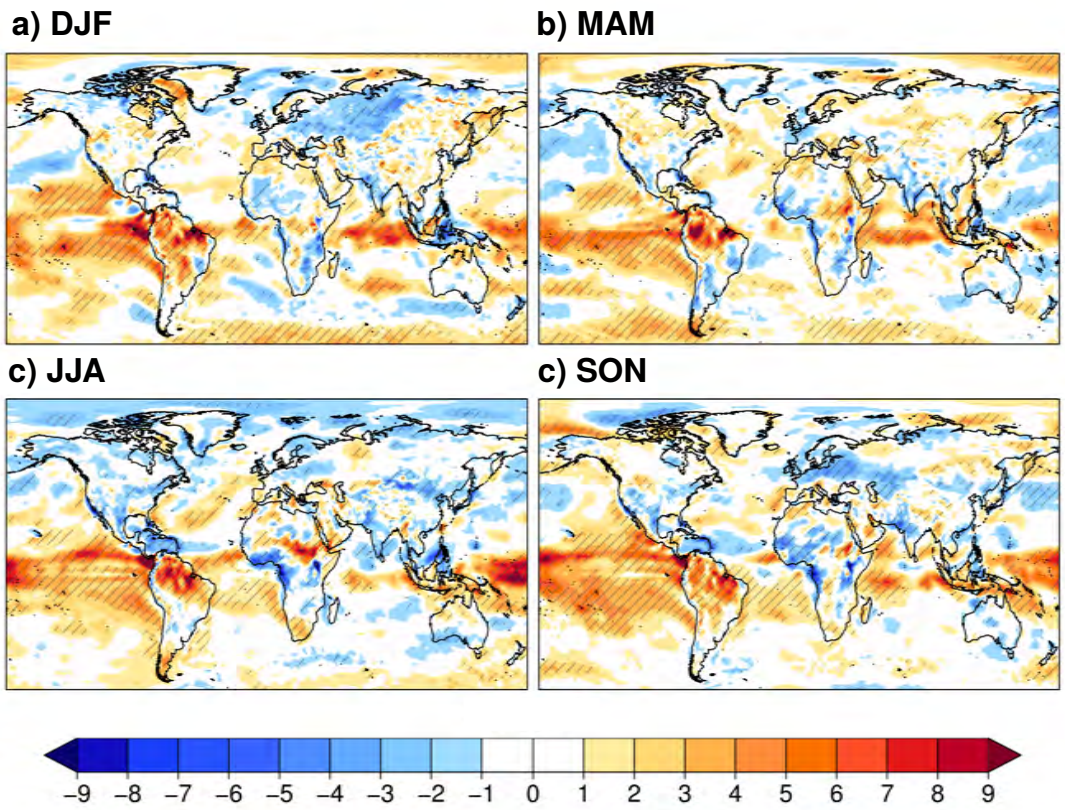

Figure 21 – Normalised linear trends (% per decade) of the 10-m wind speed from ERA-Interim. These normalised trends are calculated as the linear trend of ERA-Interim 10-m wind speed divided by its seasonal climatology over the period 1981-2015 in a) DJF, b) MAM, c) JJA, and d) SON. Hatched regions show areas where the trends are significant (t-test at a 95% confidence level).

the 850 hPa than for the 10-m wind speed, which illustrates the extra challenge that dealing with the near-surface winds implies.

There is a strong correspondence between the trends in both levels, although they tend to be stronger at 850 hPa, particularly over the ocean. The tropical Pacific and the Indian oceans display positive wind speed trends at 850 hPa in all seasons, while the tropical Atlantic shows higher positive wind speed trends mainly in DJF (Figure 22a) and MAM (Figure 22b) than the 10 m trends in the same region and season (Figure 21a,b, respectively). Substantial differences in the trends between the 850 hPa and 10 m levels are only found in two regions over land, namely northern South America where positive trends are stronger at 850 hPa than at 10-m, and central Africa where the positive trends at 10 m become

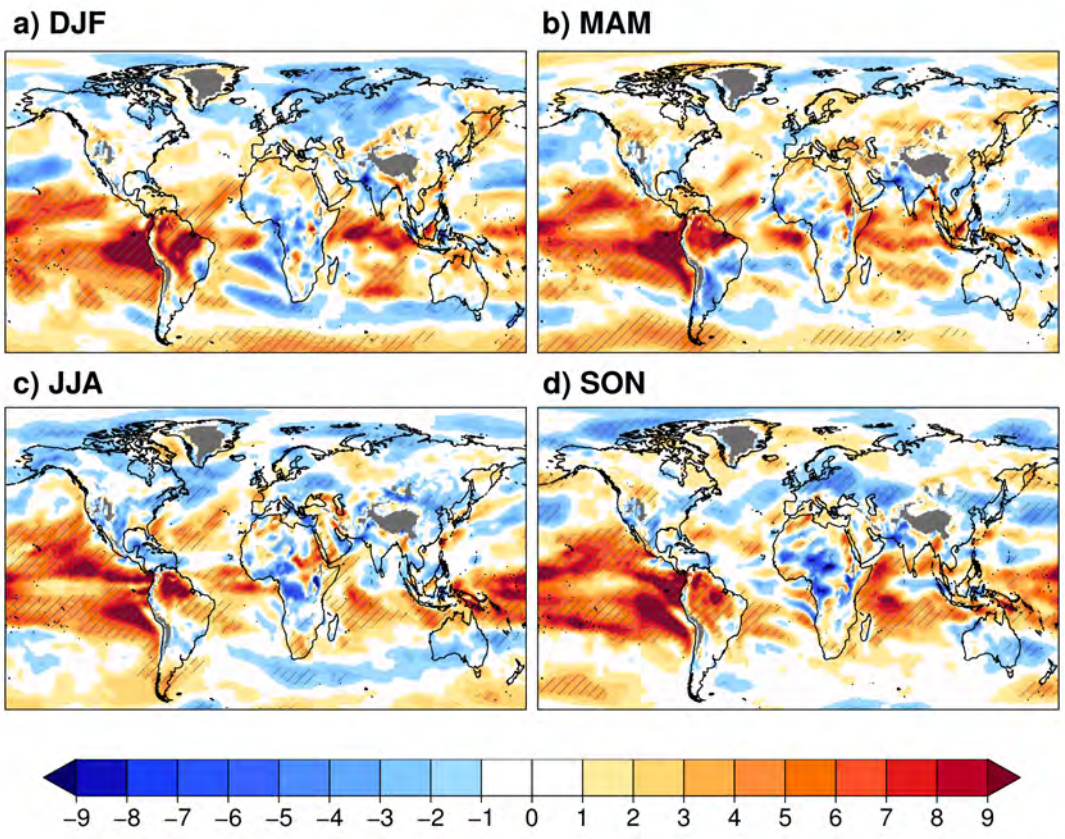

Figure 22 – Normalised linear trends (% per decade) of the 850 hPa wind speed from ERA-Interim. These normalised trends are calculated as the linear trend of ERA-Interim 850 hPa wind speed divided by its seasonal climatology over the period 1981-2015 in a) DJF, b) MAM, c) JJA, and d) SON. Hatched regions show areas where the trends are significant (t-test at a 95% confidence level).

negative at 850 hPa in most seasons. The agreement among the trends in the two analysed levels illustrates the link between the near-surface wind speed trends and the atmospheric circulation and allows attributing a large part of the near-surface trends to changes in the large-scale circulation.

3.5.2 Trends of the extreme wind speed

The characterisation of extreme wind speeds can provide extra information about the long-term changes in the frequency of unusual events and in the shape of the wind speed distribution. The trends of the 10^{th} and 90^{th} percentiles of the high frequency 10-m wind speed, which have been

taken as indicators of the unusual values within the season, have been illustrated in Figure 23 for DJF. The 10^{th} and 90^{th} percentile have been computed over the six-hourly data separately for each particular month and year and then averaged over the corresponding season. The assessment of the extreme wind speed trends has also been carried out for other seasons and reanalyses (Figures B13, B14, B15), which shows the strong seasonal variability of the trends already illustrated in Figure 21.

Positive trends are observed for both 10^{th} and 90^{th} percentiles (Figure 23a,b) over the oceans, which are stronger over the tropics than the extratropics. This is consistent with previous results (Young et al. 2011, 2012) and with the trends for the mean wind (Figure 21a). The tropical Pacific displays higher wind speed trends for the 10^{th} percentile than for the 90^{th} percentile, suggesting a change in the skewness of the whole distribution. The central North Pacific shows a decreasing trend of the 10^{th} percentile that is less intense than for the 90^{th} percentile.

Positive and significant trends over the Indian ocean are much more intense for the 90^{th} percentile than for the 10^{th} percentile, which evidences that high wind speeds increase faster than low wind speeds over that basin. Some differences are found in the spatial pattern of the trends for each index over the Atlantic basin, although both indices show positive and significant trends over the tropical Atlantic. By contrast, the structure is different between the two indices over the western North Atlantic, where trends for the 90^{th} percentile are stronger than for the 10^{th} percentile. These differences appear for other seasons too (Figure 23) and suggest changes in the structure of the wind speed distribution with time. Similar behaviour is found in the Western North Pacific, the Sea of Okhotsk and around Japan. In South America, the 90^{th} percentile shows positive trends, similar to those found in the mean wind speed for that region (Figure 21a). However, the increasing trend of the 10^{th} percentile is weaker than the widespread increasing trend of the 90^{th} percentile.

Stronger trends are obtained for the 90^{th} percentile of the wind speed than for the 10^{th} percentile also over land. To better illustrate the trends of these extreme indices in the European region, a point located in Poland [51.7° N, 18.9° E] has been selected and the corresponding time series of the 90^{th}, 50^{th} and 10^{th} percentile are shown in Figure 23c. The three time series show inter-annual variability with a decreasing trend of the wind speed. The highest negative trend corresponds to the 90^{th} percentile, which means that higher wind speeds have decreased faster than their median and low wind speeds in the last years, leading to a slight compression of the six-hourly wind speed distribution.

A general agreement between the sign of the trends in the 10^{th} and 90^{th} percentiles. For example, northern South America (positive trends), northeastern Europe, southeastern Africa or India (negative trends) show trends with the same sign for the 10^{th} and 90^{th} percentile, and this sign is also consistent

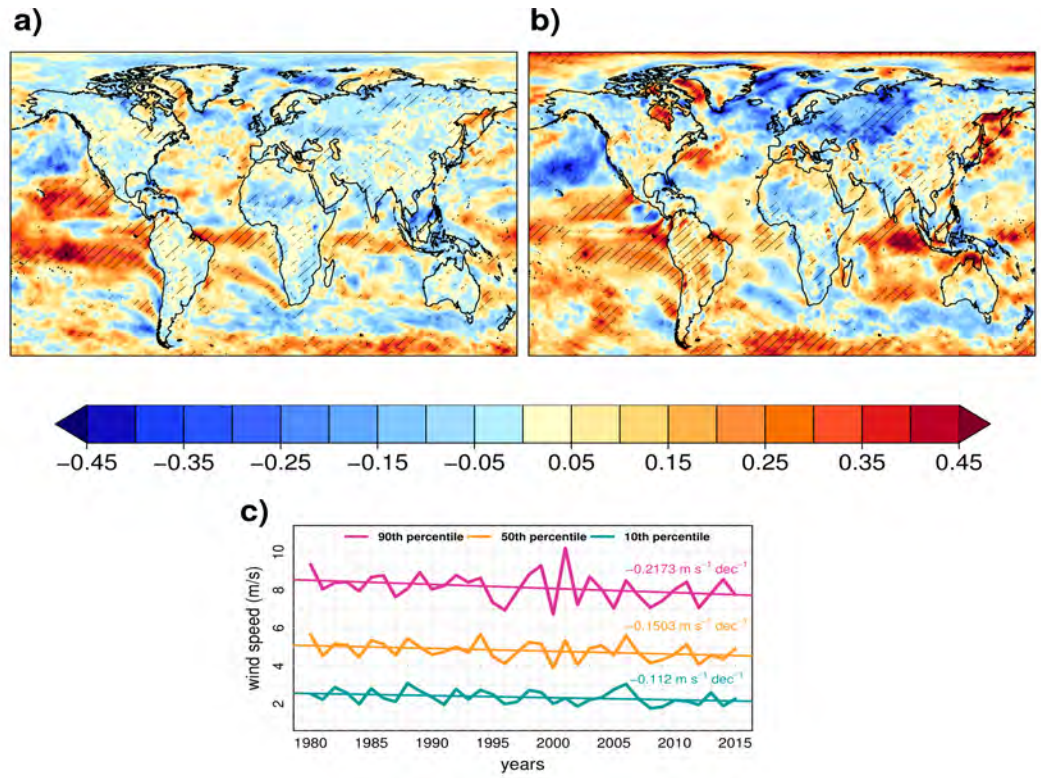

Figure 23 – Linear trends (m/s per decade) comparison of the 10^{th} and 90^{th} percentiles of the 10-m wind speed from ERA-Interim. a) Linear trend of the 10^{th} percentile, b) linear trend of the 90^{th} percentile. These trends correspond to DJF in the period 1981-2015. Hatched regions indicate where the trends are significant (t-test at a 95% confidence level), c) time series of the 90^{th} (pink line), 50th (orange line) and 10^{th} (green line) percentiles for a location in Poland [51.7º N, 18.9º E].

with the corresponding for the mean 10-m wind speed previously discussed (Figure 21). However, most of the regions show light colours, showing that the trends agree in their sign but they are not significant. The most obvious differences between the trends obtained with the two indices over land appear in southern South America, central United States, Eastern Europe, central Africa and Western Asia. The trends of central United States in DJF display different sign for both percentiles, but generally, they are not statistically significant. The increase in the 90^{th} percentile of wind speed has been previously identified (Pryor and Barthelmie 2010) and attributed to the limitations of the reanalyses, which tend to underestimate the long-term variability of wind speed in that region. Particularly, the trends of the 90^{th} percentile of the wind speed show a stronger decrease than the 10^{th} percentile.

3.5.3 Coherence of the trends from different reanalyses

The discrepancies of the wind speed trends from each reanalysis are difficult to grasp from the individual maps. For this reason a simple method to summarise the information and convey a coherent message is shown in Figure 24 for DJF. Coloured regions correspond to those locations where the reanalyses agree in the increasing or decreasing long-term behaviour of the wind speed over the last decades.

A positive and significant increase of the 10-m wind speed in boreal winter is reproduced by the three reanalyses over the tropical oceans (Figure 24a). These positive wind speed trends could be linked to the changes in the global circulation, in particular, the recent strengthening of the Walker circulation (England et al. 2014). Over land, the reanalyses show a robust negative trend over Eurasia, India, the Sahel and southern Africa. Wind increases are not robust and show patchy patterns. The decreasing wind speeds in South Africa have already been noticed in reanalysis products and attributed to the changes in the large-scale circulation (Nchaba et al. 2016). Although the trends in the Northern Hemisphere continents have been described in section 3.5.1 for the ERA-Interim reanalysis, the agreement between the three reanalyses indicates that some of the mechanisms proposed previously as potential drivers of the wind speed trends, such as changes in land use or aerosol concentrations, cannot be the only explanation of the negative trends because they are dealt with in different ways by each reanalysis. An alternative explanation of the decreasing trends might lay in changes in the large-scale circulation. If the large-scale circulation play a role, similar trends would be observed in the free troposphere. This is illustrated in Figure 24b, where the agreement of the 850 hPa wind speed trends among the different reanalyses is displayed. Over land, the three reanalyses provide similar results at both levels. The main differences between the trends in the two levels (Figure 24a,b) are the negative trends in the South Atlantic at 850 hPa. Most of the white areas correspond to regions with complex topography because it is where the MERRA-2 wind speed data are usually not available at 850 hPa since the assimilation system does not extrapolate data to levels with pressure larger than the surface pressure.

Figure 24b also shows that there are several regions (e.g. northern South America or Australia) where the three reanalyses do not agree in the sign of the trends in winter. These disagreements can be due to low and non-significant trends, hence, either a positive or a negative small trend is possible but also there are different sources of uncertainty affecting the trends. Among the uncertainty sources that can produce such discrepancies can be considered the different ways in which low-level wind speeds are derived, the observational sources included, or the corrections for the instrumental drifts that can generate inconsistencies in the observations.

The discrepancies between the reanalysis products are particularly strong between JRA-55

on one side and ERA-Interim and MERRA-2 on the other. The large trend generally found for the JRA-55 reanalysis over land (Figure B11) has been suggested to be attributable to deficiencies in deriving wind speed for that particular reanalysis (Japanese Meteorological Agency, personal communication) as it has been explained in section 3.1.2. In the JRA-55 there is a negative wind speed bias near-surface that is not fully corrected with the data assimilation. Besides, changes in the availability of observations can have an impact on the data used for the correction, resulting in large differences in wind speed

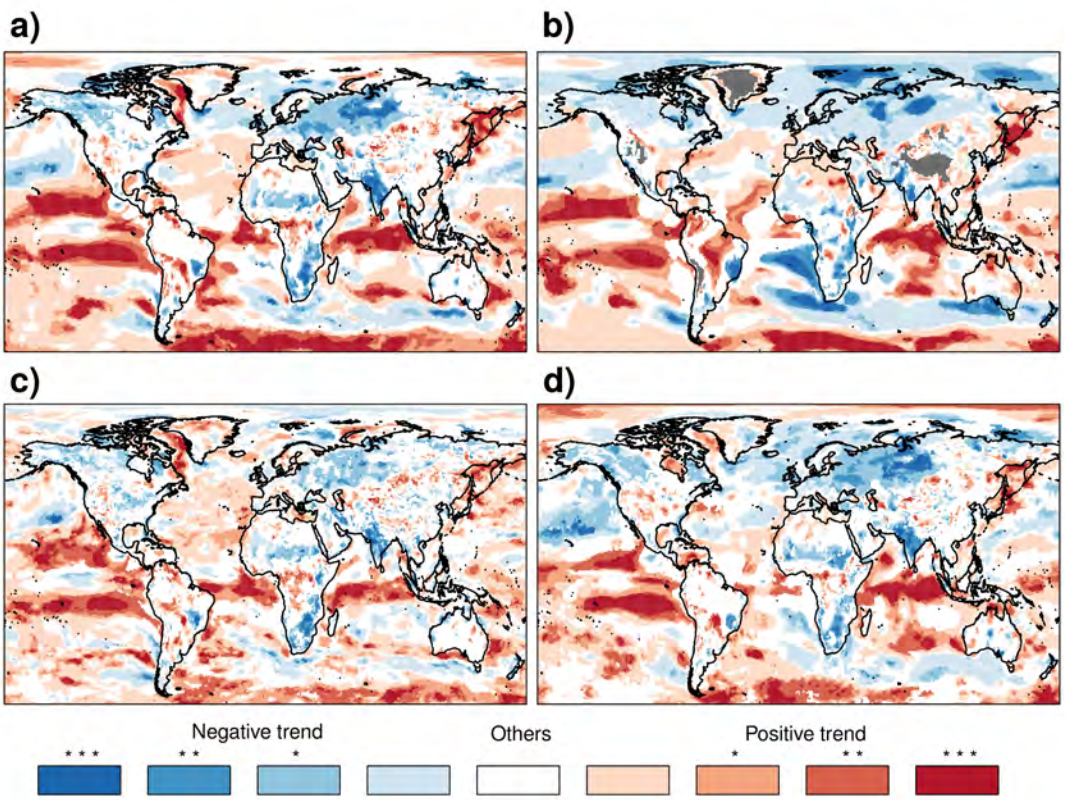

Figure 24 – Coherence maps between the ERA-Interim, JRA-55 and MERRA-2 reanalyses about the a) 10-m and b) 850 hPa c) 10^{th} percentile and d) 90^{th} percentile wind speed trends. Blues (Reds) indicate agreement between the three reanalyses about the negative (positive) trends of 10-m wind speed for DJF in the 1981-2015 period. Asterisk indicates that the trends are significant (t-test at a 95% confidence level): no asterisk indicates that the trends are not significant, (*) only one of the reanalysis has significant trends, (**) that any two reanalyses have significant trends, and (***) that the three reanalyses have significant trends. Grey areas indicate where the surface level is higher than 850 hPa.

trends. These limitations are not affecting the 2-m air temperature, as this variable shows a higher number of coherent regions among the three reanalyses used here (Figure B9) than those illustrated for the 10-m wind speed. This important information is typically not reported in the reanalysis documentation available to wind energy users, who might misuse the reanalysis data to characterise long-term variability of wind speed. The trends of wind speed at 850 hPa for JRA-55 and MERRA-2 (Figure B12) show that the JRA-55 trends at 850 hPa are similar in magnitude to those of both ERA-Interim and MERRA-2, supporting the hypothesis that the overestimation of the JRA-55 trends is a feature due to the treatment of the winds near the surface.

The consistency among the three reanalyses in the representation of the trends for the 10^{th} and 90^{th} percentiles of the wind speed has been shown in Figure 24(c,d). Differences between the 10^{th} and 90^{th} percentiles can be identified over Eurasia where the three reanalyses agree in the negative trends, but for the 10^{th} percentile, these trends are not significant. By contrast for the 90^{th} percentile, the negative trends are significant in the three reanalyses. In most of the regions, coherence maps for the extremes are very similar to that obtained for the 10-m wind speed (Figure 24a), which indicates that the uncertainty affecting the reanalyses is similar for the high and low wind speed to that for the mean wind speed. The analysis of the uncertainty from the different observational sources for the 2-m air temperature trends have been also carried out (Figure B9). The coherence among the renalyses is particularly high over land areas in most of the seasons, but particularly in SON, when the three reanalyses agree in the positive 2-m air temperature trend in most of the regions over land. The discrepancies are mostly over the tropical oceans, particularly in the tropical Atlantic, where the MERRA-2 reanalysis displays positive temperature trends, while in the ERA-Interim and JRA-55 these trends are very low and non-significant. Over land, white areas are identified in South Africa in DJF, MAM and JJA, and also in Australia in DJF and MAM. However, the number of regions where the reanalyses show a disagreement in the temperature trends is lower than for the 10-m wind speed trends.

3.5.4 Trends in the seasonal predictions

The near-surface wind speed trends in the seasonal forecasts from ECMWF System 4 have been estimated for comparison with that based on the reanalyses. This comparison is important from the verification point of view because trend differences in the predictions and observations will impact on the forecast quality estimates. The trends of the wind speed seasonal predictions have been obtained in the same way as in the reanalyses (i.e. as the slope of the linear regression of the 35 values for each season and grid point), but in that case they have been computed based on the ensemble mean of the 51 members.

The seasonal variations of the ECMWF System

4 wind speed trends are illustrated in Figure A3. Variations of the ECMWF System 4 wind speed trends can be observed among the different seasons. For example, in the tropical Pacific positive and significant trends are much more intense in DJF (Figure 25a) and MAM (Figure 25b) than in the other seasons. Over land, most of the trends are negative, except in North America, northeastern Brazil, northern Africa and southwestern Asia, where the trends are positive in the boreal winter and spring (Figure 25a,b). In Australia, positive trends are also identified, particularly in MAM and SON.

The trends of the ECMWF System 4 seasonal forecasts are low compared to that from the

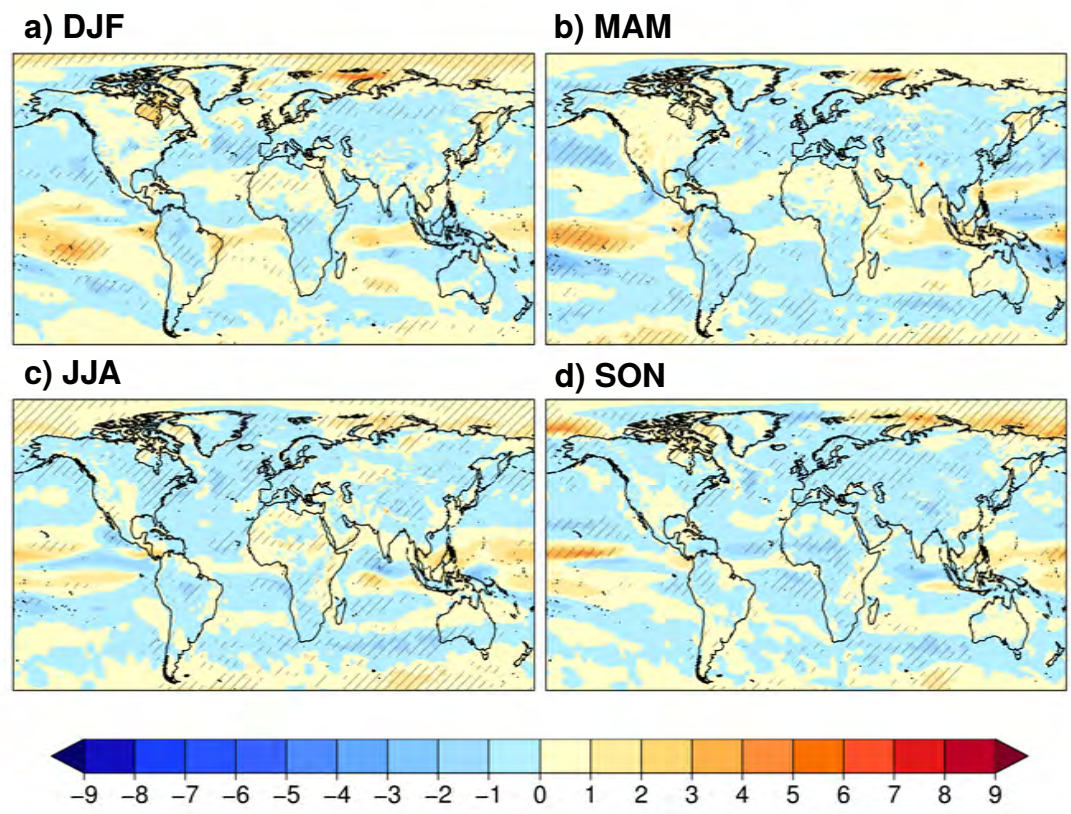

Figure 25 – Normalised linear trend (% per decade) of the ECMWF System 4 seasonal forecasts of 10-m wind speed. They have been calculated as the linear trend of 10-m wind speed seasonal forecasts divided by its seasonal climatology over the period 1981-2015 in a) DJF, b) MAM, c) JJA, and d) SON. ECMWF System 4 seasonal predictions are initialised the 1^{st} day of November, February, May and August respectively. Hatched regions indicate where the trends are significant (t-test at a 95% confidence level).

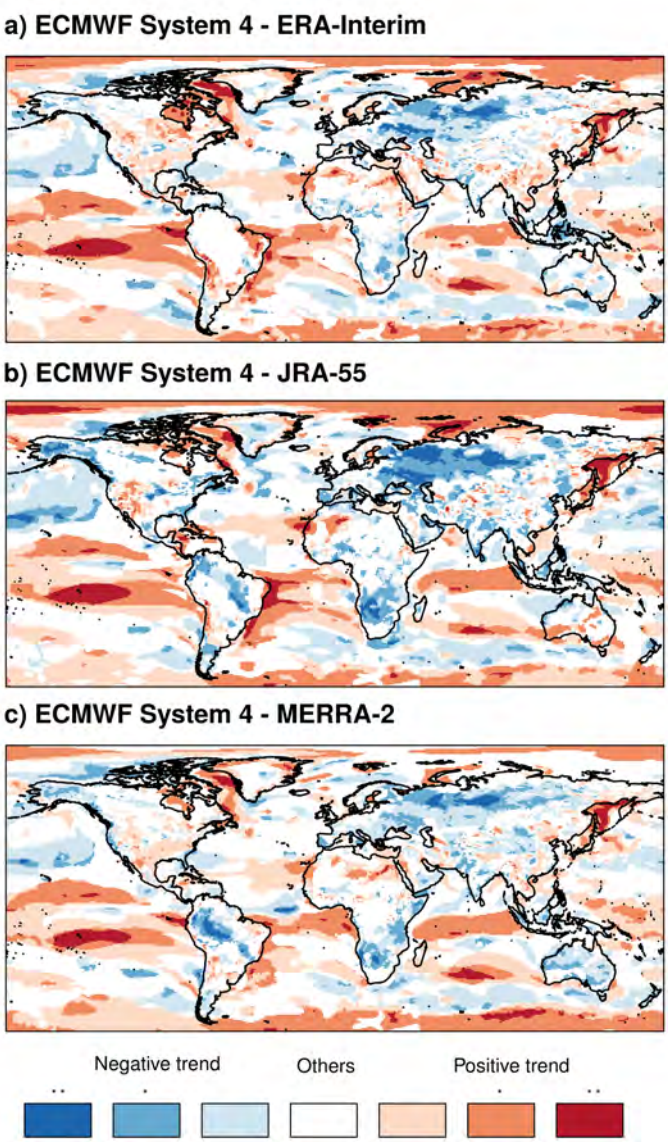

Figure 26 – Coherence maps between the trends of the ECMWF System 4 seasonal forecasts of 10-m wind speed trends and those produced by a) ERA-Interim, b) JRA-55 and c) MERRA-2. Blues (Reds) indicate agreement between the seasonal predictions and the reanalysis about the negative (positive) trends. This corresponds to DJF in the period 1981-2015. Asterisk indicates that the trends are significant (t-test at a 95% confidence level): no asterisk indicates that the trends are not significant neither in ECMWF System 4 nor the reanalysis, (*) either the seasonal predictions or the reanalysis has significant trends, (**) both the seasonal predictions and the reanalysis show significant wind speed trends.

reanalyses, but they are significant in some regions. The 10-m wind speed trends in the seasonal forecasts range between -1 and 1 % per decade in most of the regions, while in the reanalyses they become the 9% per decade (Figure 21). The underestimation of the wind speed trends by ECMWF System 4 is the result of working with the ensemble mean, as the average operation filters the variability.

The trends of the ECMWF System 4 2-m air temperature seasonal predictions have been computed, and the results are included in the Appendix B (Figure B10). The 2-m air temperature trends based on the ECMWF System 4 seasonal predictions are positive in most of the regions and seasons. However, ECMWF System 4 underestimates the intensity of the trends in regions such as the Arctic, where the positive 2-m air temperature trends reach their maximum values. Besides these differences in the intensity, negative trends are displayed over Siberia for the reanalyses, which are positive in the seasonal predictions.

Despite several discrepancies are identified, the differences between the reanalyses and seasonal predictions are less intense for the 2-m air temperature than in the case of wind speed.

To further evaluate the consistency of the trends in predictions and observations, the coherence maps between the predictions and the reanalyses have been displayed in Figure 26 for the DJF season. Over the ocean, the positive wind speed trends in the tropics and the sea of Okhotsk are consistent in the seasonal predictions and in the three reanalyses as indicated by the dark red. Agreement in the negative trends can be also identified in some regions over land, such as Alaska, Eurasia or South Africa, where reanalyses and seasonal predictions show negative wind speed trends.

By contrast, there are several regions where there is no agreement on the trend sign in predictions and observations. For example in northern South America, in the North Atlantic and also in some regions in Africa several white areas are identified. These differences are obtained in the comparison with each reanalysis, however, some dependency with the reanalysis can be also identified. In Australia, negative wind speed trends are displayed by ECMWF System 4 and MERRA-2, while ERA-Interim and JRA-55 only show negative trends in some small regions.

The consistency among the trends in the seasonal predictions and observations has also been explored for the 2-m air temperature (Figure B10). The number of regions for which the consistency among the seasonal predictions and the reanalyses is much higher for temperature than for wind speed, indicating that the uncertainty affecting the temperature trends is lower for this variable than for the near-surface wind speed. Reanalyses and seasonal predictions agree in the positive temperature trends in most of the regions, with only some exceptions such as the decline of the air temperature in DJF in Siberia, which have been reported for different authors (e.g Cohen et al. 2014) and that is not reproduced by ECMWF System 4.

The characterisation of these discrepancies is important for the comparison of the seasonal predictions with an observational reference, as this represents a source of uncertainty affecting the verification process, particularly in those regions where the seasonal predictions and the observational references display opposite trends, which could lead to a reduction of skill.

3.6 Conclusions

In this chapter, a description of the statistical properties of the two most important climate variables used in the wind industry, 10-m wind speed and 2-m air temperature, has been performed. A exploratory assessment of the statistical properties of wind speed and temperature in the ECMWF System 4 seasonal forecast system and three observational references (i.e. ERA-Interim, JRA-55, MERRA-2) has been used to identify some sources of uncertainty affecting the seasonal predictions. This uncertainty leads to the underestimation of the forecast quality, a piece of information that should be provided to the wind energy users, when they employ these predictions for different applications. The identified differences in the statistical parameters of the probability distribution between predictions and observations appear not only in their climatologies. They have been also observed in the standard deviation, skewness, kurtosis and Shapiro-Wilk test. It is suggested that all this information should be taken into account when bias adjustment methods are applied, as some of the standard bias correction approaches only adjust the mean value (Marcos et al. 2018).

Inconsistencies among the wind speed in the different reanalyses have not been reported before in the literature, while they could have an important impact for the wind energy users as they evaluate the climatology and long-term wind speed variability using reanalysis data. But this uncertainty is not affecting only evaluations performed in terms of reanalysis. These differences are also an important factor to be considered in the verification of the seasonal climate predictions. However, recommendations about which dataset offers the best performance cannot be provided. Such information should be used for the evaluation of 10-m wind speed and 2-m air temperature, as observational datasets with global coverage are not currently available. Future analyses will focus on the validation of the reanalyses with observations from different sources in those regions that are the most relevant for the wind industry.

The assessment of the near-surface wind speed trends has revealed that low-frequency wind speed variability is observed in several regions, which when analysed using these linear trends can be attributed to changes in the atmospheric circulation (Torralba et al. 2017a). Nevertheless, the seasonal predictions of 10-m wind speed do not show such intense trends, which when taking into account the unavoidable smoothing effect of using the ensemble mean when estimating the trends in the predictions, could be related to the ECMWF System 4 misrepresentation of some of the forcing those changes in the

atmospheric circulation. This issue requires further investigation, but it is an important result that needs to be considered in the forecast verification process as these differences in the trends could lead to an underestimation of the seasonal forecast quality.

04

Seasonal prediction of wind energy relevant climate indices

04 Summary

Objective

To evaluate the capabilities of seasonal forecast systems to appropriately reproduce large-scale processes such as El Niño Southern Oscillation (ENSO), North Atlantic Oscillation (NAO) and storm tracks. This is essential to understand the overall seasonal forecast quality as systematic errors in seasonal forecasts of these wind energy relevant climate indices based on large-scale phenomena could be responsible for the lack of skill in specific regions.

Methodology

- Wind energy relevant climate indices: Niño-3.4 (average sea surface temperature over the Equatorial Pacific), NAO (leading Principal Component of the sea level pressure (SLP) in the North Atlantic), NPST (North Pacific storm track intensity, 2-10 days bandpass filter of the daily SLP in the North Pacific region) and NAST (North Pacific storm track intensity, 2-10 days bandpass filter of the daily SLP in the North Atlantic region) indices.
- Pearson correlation to assess the ECMWF System 4 predictability of the indices.
- One-point-correlation maps to investigate the ECMWF System 4 systematic errors in the ENSO, NAO and storm tracks teleconnections to wind speed and temperature using both ensemble mean and individual ensemble member approaches.

Results

- The Niño-3.4 and NPST indices exhibit good levels of skill as a consequence of the ability of the ECMWF System 4 to simulate the seasonal variability in both the tropics and those regions where the teleconnections from the tropics are more intense, such as the North Pacific. NAO and NAST indices show low correlations, which is related to a large amount of unpredictable internal variability dominating the North Atlantic region.
- Positive biases in the intensity of the storm tracks are identified in the four seasons and they reach maximum values over the oceans. In the northern North Pacific, the ECMWF System 4 is predicting a faster alternation between cyclones and anticyclones and/or more intense cyclones and anticyclones than in the observational reference. These biases are established very early into the forecast period as they appear for all the forecast months. In the North Atlantic, the systematic errors for the storm tracks are smaller than over the North Pacific but have a marked dependency with the lead time.

- One-point-correlation maps between the index and the spatial variable using the ensemble mean show larger values than the one-point correlation maps obtained with the observational reference. This happens because the ensemble averaging smooths out some of the inter-annual variability, enhancing the relationship between the climate driver and the climate variable. In fact, when the one-point correlation maps are computed using all ensemble members instead of the ensemble mean the values are of a similar order as in the observational reference.

- ENSO shows a high influence on climate conditions at the global scale, but this influence is more intense for 2-m air temperature than for 10-m wind speed. Furthermore, the ENSO teleconnections to wind speed in ECMWF System 4 show some discrepancies when compared to ERA-Interim which are not obtained for the air temperature. These discrepancies can be related to the difficulties of the model to reproduce local processes such as those identified in northern North America, although there are examples in the literature where errors in the teleconnections are linked to a misrepresentation of the Rossby wave propagation.

- Despite the low skill obtained for the NAO index, the regional impact of the NAO on both wind speed and air temperature are generally well reproduced by ECMWF System 4.

- The influence of the NAST and NPST indices on wind speed and temperature is comparable in both ECMWF System 4 and in ERA-Interim in the North Atlantic and North Pacific regions, respectively. Beyond their corresponding region of influence, the NAST and NPST teleconnections have important errors. These errors might be the consequence of the biases in either the storm tracks or the wind speed and air temperature, or both.

Conclusions

- The positive and significant skill obtained for the Niño-3.4 and NPST indices indicate that these indices could be used to improve the skill in the seasonal predictions of wind speed and air temperature in those regions where the teleconnections are not correctly reproduced by the predictions, such as northern North America.

- ECMWF System 4 displays biases in its representation of the storm tracks in the northern North Pacific. This result has not been previously documented and its causes require further investigation. These biases should be considered when storm tracks are used to diagnose and improve seasonal predictions of wind speed and temperature.

- One-point-correlation maps based on the ensemble mean show a larger sensitivity to the forecast time than in the case the maps are estimated using individual members. This should be used as a warning in the interpretation of one-point correlation maps in ensemble systems.

- Generally, the teleconnections from ENSO, NAO and storm track activity with air temperature have been widely investigated, but their assessment for wind speed has been only done for specific regions. Besides, they have rarely been studied in a seasonal forecast context. Therefore, the characterisation of the teleconnections for wind energy relevant indices can be particularly relevant for both wind energy users and the research community.

04

Seasonal prediction of wind energy relevant climate indices

The quality of the seasonal forecasts is related to the seasonal forecast systems' capacity to simulate large-scale processes (Stockdale et al. 2011). If the seasonal prediction systems are able to reproduce the large-scale phenomena and their related climate conditions, this could increase user confidence in their representation of the most relevant climate variables such as air temperature, wind speed and precipitation (Sillmann et al. 2017).

The ability of seasonal forecasts to simulate inter-annual modes of variability has been characterised generally using the ENSO and the NAO phenomena[1]. The ENSO is the main mode of variability in the tropical Pacific. It is usually described as a coupled ocean-atmosphere phenomenon with a frequency of occurrence between 2 and 7 years (Philander 1990; Trenberth 1997). The remote influence of a large-scale climate pattern, such as ENSO, is widely known as teleconnection. The NAO is the leading mode of variability at in the North Atlantic region (Hurrell and Deser 2010). Particularly, wind speed and air temperature conditions over Europe are strongly related to the NAO (Hurrell 1995). Hence, the predictability of the phenomena some months in advance could benefit wind energy activities (Jerez et al. 2013).

There are several studies in which seasonal forecasts of ENSO and NAO teleconnections to temperature and precipitation have been described (e.g. Kim et al. 2012; Molteni et al. 2015), but the impact on wind speed variability at the global scale has been less explored.

[1] The main characteristics of ENSO and NAO have been described in chapter 1.

To complement the characterisation of the remote influence of inter-annual variability phenomena beyond ENSO and NAO, the capacity of the seasonal forecast systems to simulate intra-seasonal storm track intensity and their associated impacts has been also explored (Yang et al. 2015). Storm tracks are the preferred paths followed by storm systems in tropical and extra-tropical regions. Storms tend to form where surface temperature gradients are large, and the jet stream influences (and receives the feedback) their speed and direction of travel. These routes are more prevalent over the oceans than over land due to the smaller surface roughness and the strong temperature gradients. The intensity and location of the storm tracks vary seasonally and in response to climate variations, such as changes in tropical SST (Shaw et al. 2016). Storms are a source of extreme events such as high winds and extreme precipitation, which can lead to windstorm damage, flooding, and coastal storm surge (Della-Marta et al. 2010). Consequently, storm tracks can have significant impacts on both economy and society. The dynamical processes involved in shifts in the location of the storm tracks as a response to climate change have been extensively studied in the literature (e.g. Chang et al. 2002; Yin 2005). However, only a limited number of studies (Compo and Sardeshmukh 2004; Yang et al. 2015) have explored to which extent the state-of-the-art seasonal forecast systems are able to reproduce the variability of the storm track intensity and their remote impact.

The analysis of wind energy relevant teleconnections (i.e ENSO, NAO and storm tracks) aims to identify limitations in the current seasonal forecast systems to reproduce the main drivers of the climate variability at seasonal timescales. Furthermore, large-scale teleconnections are more predictable than smaller scale anomalies. As a consequence, quantifying and understanding the response of 10-m wind speed and 2-m air temperature to these patterns may help to predict anomalous fluctuations in wind energy resources (Brayshaw et al. 2011; Couto et al. 2015).

This chapter is organised as follows. The description of the indices and the metrics used in the evaluation are described in section 4.1. The predictability of the ENSO and NAO indices is evaluated in section 4.2. Section 4.3 includes a description of the systematic errors affecting the storm track intensity and predictability. Finally, the relationship between wind energy relevant indices with 10-m wind speed and 2-m air temperature is discussed in section 4.4.

4.1 Methodology

4.1.1 ENSO and NAO indices

The time evolution of the ENSO and NAO has been characterised by two widely used indices: Niño-3.4 index and NAO index. These indices have been computed for the ECMWF System 4 and for ERA-Interim. In the case of the seasonal predictions, they have been obtained separately for the different forecast months.

The definition of the indices used to characterise the time variability of the ENSO and NAO indices and the definition of the storm tracks in ECMWF System 4 and ERA-Interim is provided below. The analysis has been performed for all the seasons and start dates available, therefore 15 ensemble members have been selected to ensure the consistency of the results for each start date. The different metrics used for the study of the teleconnections of these indices to wind speed and temperature are also described. In this chapter the ERA-Interim reanalysis has been selected as a reference, but the same analyses could be performed for JRA-55 or MERRA-2.

Niño-3.4 index (Trenberth 1997) is computed as the average of the seasonal seasurface temperature SST anomalies in the Equatorial Pacific region [5° S- 5° N, 120°-170° W]. An example of this index has been illustrated in Figure 27 for the boreal winter (December-January-February, DJF) and ERA-Interim reanalysis. However, the index has been also computed for every season: March-April-May (MAM), June-July-August (JJA) and September-October-November (SON). To illustrate the typical spatial structure of ENSO, the linear regression of SST anomalies onto the standardised Niño-3.4 index is shown in

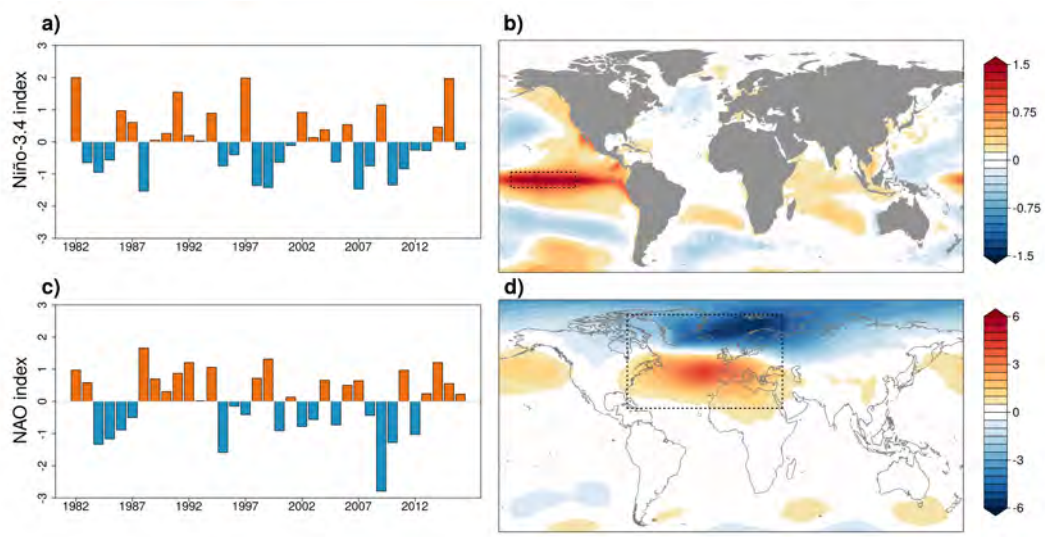

Figure 27 – Niño 3.4 and NAO indices and spatial patterns. a) Niño-3.4 index computed as the average of the SST anomalies in the Equatorial Pacific region [5° S-5° N, 120°-170° W], b) regression map (°C/std) of the SST anomalies onto the Niño-3.4 index, c) NAO index obtained as the standarised principal component corresponding to the leading mode of the SLP anomalies in the North Atlantic region [20°-80° N, 80° W-40° E], d) regression map (hPa/std) of the SLP anomalies onto the NAO index. Both Indices and regression maps have been computed from the ERA-Interim reanalysis for December to February (DJF) in the 1982-2016 period.

Figure 27b. Figure 27b shows the typical ENSO characteristics with intense warm SST anomalies over the central-eastern tropical Pacific surrounded by negative SST anomalies in the El Niño phase.

NAO index (Hurrell et al. 2003) has been computed as the standardised leading principal component (PC) resulting from the principal component analysis (PCA) (Wilks 2011) of the sea level pressure (SLP) anomalies over the North Atlantic region [20°-80° N, 80° W - 40° E]. For the seasonal predictions, the PCA has been applied over all individual members simultaneously. An example of the NAO index and its associated spatial pattern has been included in Figure 27(c,d). The regression of the SLP anomalies onto the NAO index (Figure 27d) depicts a dipole structure with a centre of negative sea level pressure over Greenland and an anomalous anticyclonic structure over the Azores in its positive phase.

4.1.2 Storm track definition

Storm tracks have been computed as the standard deviation of the bandpass filtered[2] daily-mean SLP anomalies (Chang and Fu 2002; Yang et al. 2015) with cut-off periods between two and ten days, which allows for retaining extra-tropical cyclone variability. This analysis has been performed for each season and grid point individually. In the predictions, storm tracks have been computed for each member and forecast time separately.

Although the storm tracks can be computed from the 500 hPa geopotential height (Blackmon 1976), other variables such as SLP have been also widely used for their estimation (Ulbrich et al. 2008; Yang et al. 2015). In this analysis, SLP has been preferred instead of the geopotential height to enable the characterisation of the storm tracks at surface level.

Maps of the storm tracks are displayed for the extra-tropical region [20°-90° N] in the Northern Hemisphere, where they play a more dominant role in the atmospheric variability. In the Southern Hemisphere, storm track activity is more persistent throughout the year in both location and intensity than in the Northern Hemisphere (Trenberth 1991). This difference is mainly related to the predominance of the oceans in the Southern Hemisphere, which stabilises and strengthens the circulation and prevents the circulation to be slowed down by the orography (Chang et al. 2002).

The impacts of the storm track intensity on 10-m wind speed and 2-m air temperature have been explored by two storm track indices, the North Atlantic storm track intensity (NAST index) and the North Pacific storm track intensity (NPST index):

NAST index has been computed as the spatial average storm track intensity in the North Atlantic [35°-60° N, 280°-300° E].

[2] The Butterworth' bandpass filter included in the R-package "signal" (Ligges et al. 2015) has been employed. The resulting storm tracks are equivalent to those obtained from the application of 24-hours filter (e.g Chang and Fu 2002), which has been used to assess the robustness of the analysis (not shown).

NPST index is the equivalent index for the North Pacific [35°-60° N, 140°-220° W] region.

4.1.3 Metrics

The predictability of the wind energy user relevant indices from ECMWF System 4 has been quantified in terms of the Pearson correlation (described in Appendix A.1.1). The Pearson correlation is computed with the ensemble mean of the index and the corresponding index in the observational reference.

The impact of these indices on wind speed and air temperature conditions at grid point level has been evaluated through one-point correlation maps. One-point correlation maps are computed by correlating the wind energy relevant indices with the anomalies of the impact variables (wind speed and air temperature). The methodology to investigate the teleconnections in the ECMWF System 4 seasonal predictions and in the reference dataset has been summarised in Figure 28.

In the seasonal forecasts, two options for the estimation of the one-point correlation maps have been explored. In one of them, the correlation has been computed between the ensemble mean (ens.mean) of both the teleconnection indices and the impact variables. The other option uses the one-point correlation map using all the ensemble members

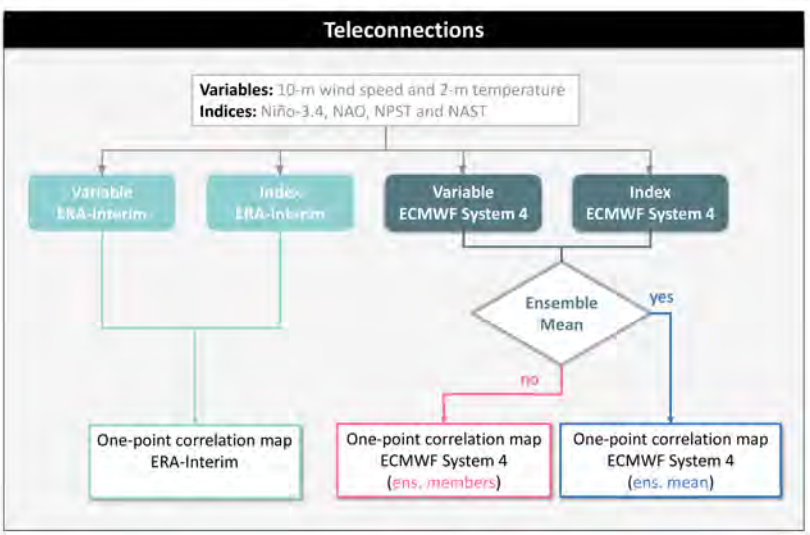

Figure 28 – Summary of the methodology used to explore the teleconnections in the ERA-Interim reanalysis and ECMWF System 4 seasonal predictions. The indices used to represent variability of the climate drivers and the impact variables are specified at the bottom of the figure.

simultaneously (ens.members in Figure 28).

The two methods give different results because the ensemble averaging of the former reduces the inter-annual variability of the variables used in the correlation.

4.2 Seasonal predictability of wind energy relevant climate indices

The predictability of the ECMWF System 4 to simulate the inter-annual variability of the Niño-3.4 and NAO indices has been computed for the four seasons and the five months of lead time that can be obtained with a seven-month forecast (Figure 29).

The Niño-3.4 index displays correlation values above 0.7 for all the seasons and forecast months (Figure 29a) indicating that the ECMWF System 4 correctly simulates the year-to-year variations of this index. The high correlation values for the seasonal forecasts of the Niño-3.4 index are related to the ability of the seasonal forecast system to skilfully predict the SST in the tropical Pacific some months in advance (Doblas-Reyes et al. 2013b; Chen et al. 2016). The better performance is obtained in DJF and MAM when correlations are above 0.9 in most of the lead times. The lowest Niño-3.4 correlations (0.7-0.8) are obtained in the boreal summer. These seasonal variations are related to the so-called "spring predictability barrier" for which most of the ENSO predictions (measured by the Niño-3.4 index here) show a skill decline for the boreal spring start dates (Duan and Hu 2016).

Seasonal predictions of the NAO index (Figure 29b) show lower correlation values than the Niño-3.4 index in all seasons and lead times. The positive and significant correlations of the NAO index are restricted to the DJF and MAM forecasts initialised in December and March respectively. Previous studies have suggested that seasonal forecast systems show limited levels of predictability in the North Atlantic due to the dominant role of the unpredictable natural internal variability in that region (Kushnir et al. 2006; Kim et al. 2012). However, recently some seasonal forecast systems have shown higher predictability levels of the NAO (Athanasiadis et al. 2017; Baker et al. 2018).

4.3 Evaluation of the extra-tropical storm tracks

To illustrate the seasonal characteristics of the storm tracks, the average of the storm tracks from ERA-Interim in the period 1982-2016 (i.e. climatology) are displayed for each individual season (Figure 30). These climatologies show a marked annual cycle with the maximum intensity in DJF (Figure 30a), followed by SON (Figure 30d), MAM (Figure 30b) and JJA (Figure 30c). The spatial distribution of the climatological storm tracks is the consequence of the meridional temperature gradient combined with the specific distribution of continents and oceans (Chang and Fu 2002). In the Northern Hemisphere, the maximum intensity of the storm tracks is found in the North-Western Atlantic for DJF. Another region of high activity is in the North Pacific

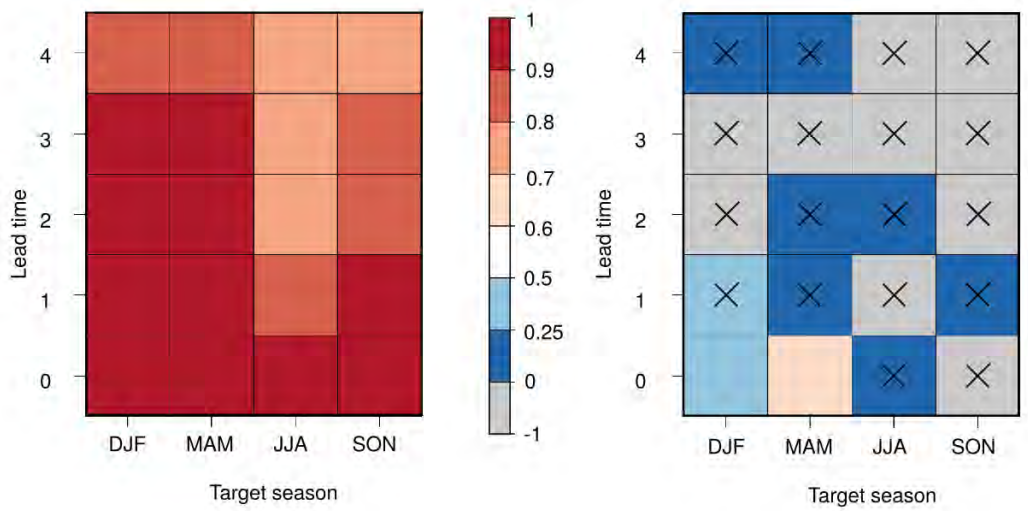

Figure 29 – Pearson correlation coefficient between the ECMWF System 4 ensemble mean of the a) Niño-3.4 and b) NAO indices and the corresponding indices from the ERA-Interim reanalysis. The indices correspond to the 1982-2016 period. Pearson correlations are shown as a function of the target season (x-axis) and lead time (y-axis). Crosses denote non-significant correlation values (one-tailed t-test at a 95% confidence level)

(Figure 30). These maxima are obtained for the four seasons, although they are twice lower in boreal summer than in winter. In summer the storm tracks maxima are shifted poleward, and from summer to autumn they are shifted to the southeast following the equatorward migration of the meridional temperature gradient (Eichler and Higgins 2006).

To compare storm track intensity from ERA-Interim and from ECMWF System 4, the spatial patterns of the storm track climatology in DJF have been illustrated in Figure 31. These maps show a similar spatial distribution of maximum and minimum values in ERA-Interim (Figure 31a) and in the ECMWF System 4 (Figure 31b), but the seasonal forecasts systematically overestimate the magnitude of the ERA-Interim storm track intensity in most regions, particularly in the North Atlantic and North Pacific.

To further explore the storm track intensity in these regions, the NAST and NPST indices have been used (defined in section 4.1.2). A positive bias can be observed for both NAST and NPST indices, but it is larger in the NPST index, as indicated by the ECMWF System 4 overestimation every year. To

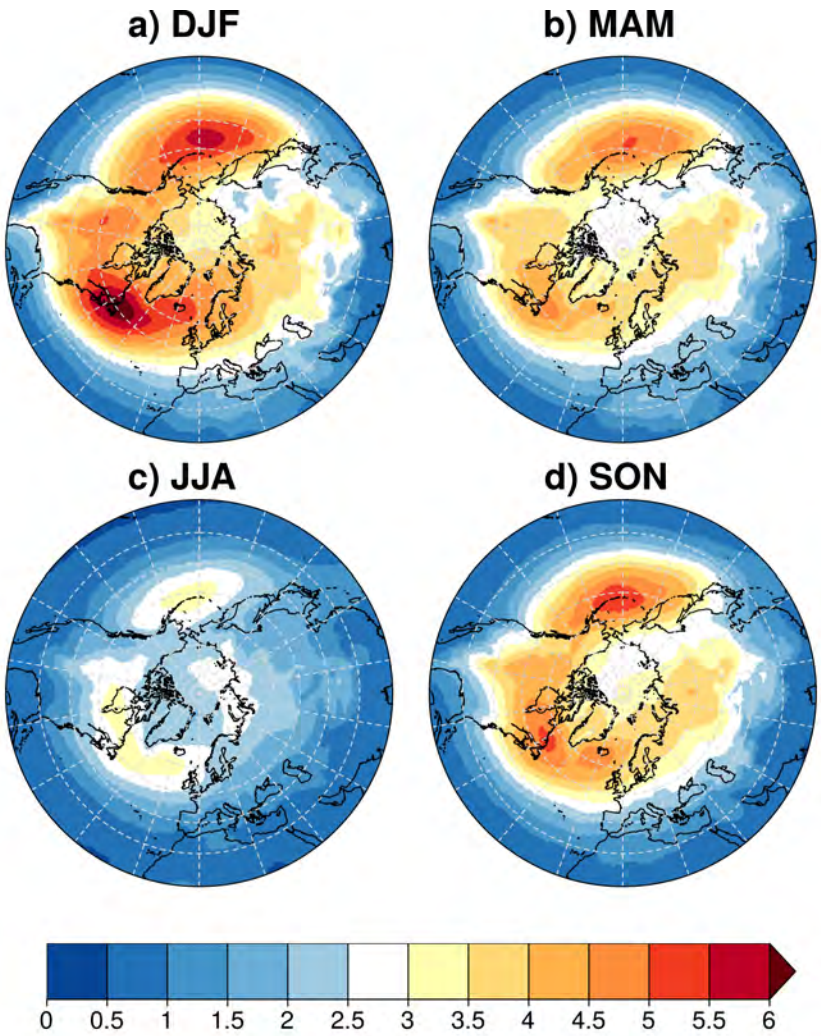

Figure 30 – ERA-Interim climatological storm track intensity. Storm tracks are measured by the standard deviation of the band-pass (2-to-10 days frequencies) filtered anomalies of sea level pressure (hPa) in the 1982-2016 period. Storm tracks have been computed for the following seasons a) DJF, b) MAM), c) JJA and d) SON.

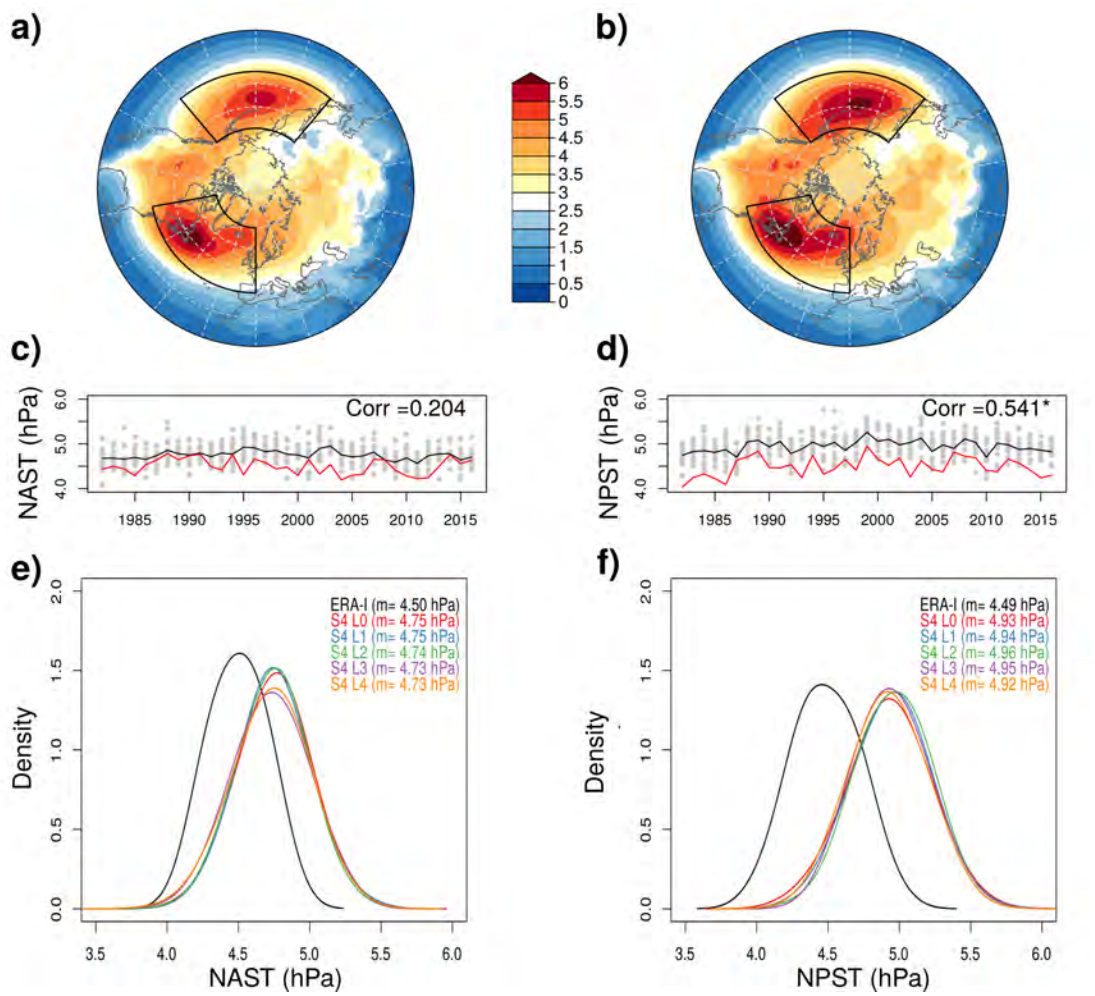

Figure 31 – Comparison of the climatological storm track intensity (hPa) of a) ERA-Interim and b) ECMWF System 4. Storm tracks correspond to the DJF season in the in the 1982-2016 period. ECMWF System 4 seasonal forecasts initialised the 1^{st} of November have been used. NAST and NPST indices obtained as the time series of the averaged c) North Atlantic [35°-60° N, 280°-300° E] and d) North Pacific [35°-60°N, 140°-220° W] storm track intensity. Indices are represented for ERA-Interim (red line) and ECMWF System 4 (grey dots as ensemble members and black line as ensemble mean). Pearson correlation for the NAST and NPST indices between the ensemble mean predictions and the reanalysis are shown in the top-right corners (asterisk indicates that the correlations are significant at a 95% confidence level). The probability density function of the storm tracks in the e) North Atlantic and f) North Pacific indices computed with the data corresponding to the 36 values, and in the case of the predictions also with the 15 members.

investigate if the seasonal forecast system is able to reproduce the year-to-year variability of the storm track intensity, Pearson correlations have been computed for the NAST and NPST indices (top-right corners in Figures 31c,d). The correlations are 0.2 and 0.5, respectively indicating that the NPST index shows higher predictability than the NAST index. The significant correlation obtained for the NPST index could be related to the influence of the ENSO on the storm tracks in the North Pacific (Eichler and Higgins 2006; Seager et al. 2010), which is in agreement with ECMWF System 4's positive skill in the ENSO predictions (discussed in the previous section). This positive and significant correlation in the NPST index suggests that the ECMWF System 4 predictions could have good performance in the predictions of those variables driven by the storm tracks variability (e.g. sea level pressure, 2-m air temperature or 10-m wind speed). By contrast, the limitations of ECMWF System 4 to predict the variability in the North Atlantic region (Kim et al. 2012) lead to a non-significant correlation value for the seasonal forecasts of the NAST index. This result fits well with the results in the previous section where ENSO has much more predictability than the NAO.

To investigate the evolution of the systematic errors in the storm track intensity with the forecast time, the NAST and NPST probability density functions (PDFs) have been illustrated for the different lead months (Figures 31e,d respectively). The NAST PDFs (Figure 31e) display discrepancies with the corresponding PDF for ERA-Interim in both the mean value and variability. Nevertheless, the NPST PDFs of the seasonal forecasts are very consistent in all the lead months, with a similar shape to the NPST PDF from ERA-Interim (Figure 31f), but always with a positive bias.

The spatial distribution of the biases affecting the storm track intensity in the ECMWF System 4 predictions, as well as their dependency on the different seasons and forecast times, are illustrated in Figures 32 and 33. The four seasons show a consistent positive bias, but season-to-season variations in the spatial distribution of these systematic errors, and changes in their intensity can be observed (Figure 32). The maximum bias is found in winter over the North Pacific region where the differences between predictions and observations reach values over 0.9 hPa. These biases are found not only over the ocean; western North America and northeastern Asia show values over 0.5 hPa. This overestimation of the storm tracks suggests that either ECMWF System 4 predicts a faster alternation between cyclones and anticyclones than ERA-Interim or that the system reproduces more intense cyclones and anticyclones than those observed or both. The seasonal cycle in the bias is consistent with the storm track seasonal cycle, with the lowest values obtained for JJA (Figure 32c). These values become negative in some regions of the North Pacific, and North Atlantic, although they are rather weak (values between -0.1 and -0.3 hPa). In MAM and SON (Figure 32b,c) the overestimation of the storm tracks is less intense, particularly over North

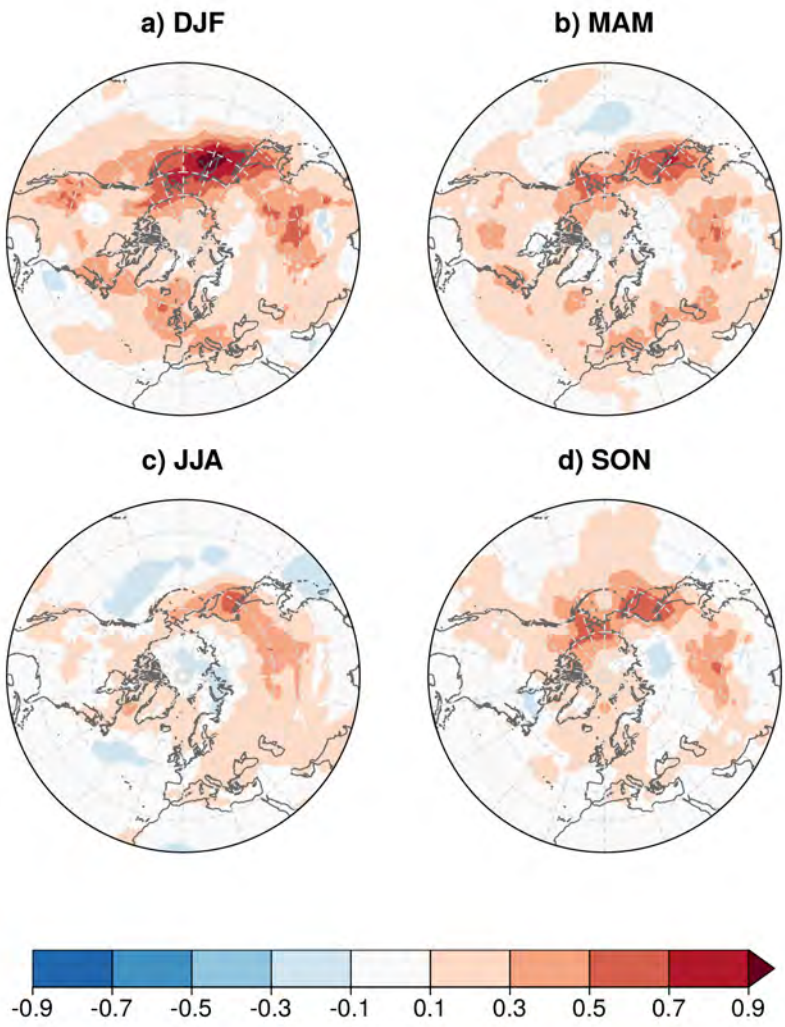

Figure 32 – Bias (hPa) between the storm tracks predicted by the ECMWF System 4 and the ERA-Interim reanalysis. Storm tracks correspond to the period 1982-2016 and the seasons. Storm track intensity has been computed for the following seasons a) DJF, b) MAM), c) JJA and d) SON. ECMWF System 4 seasonal forecasts initialised one month ahead have been used.

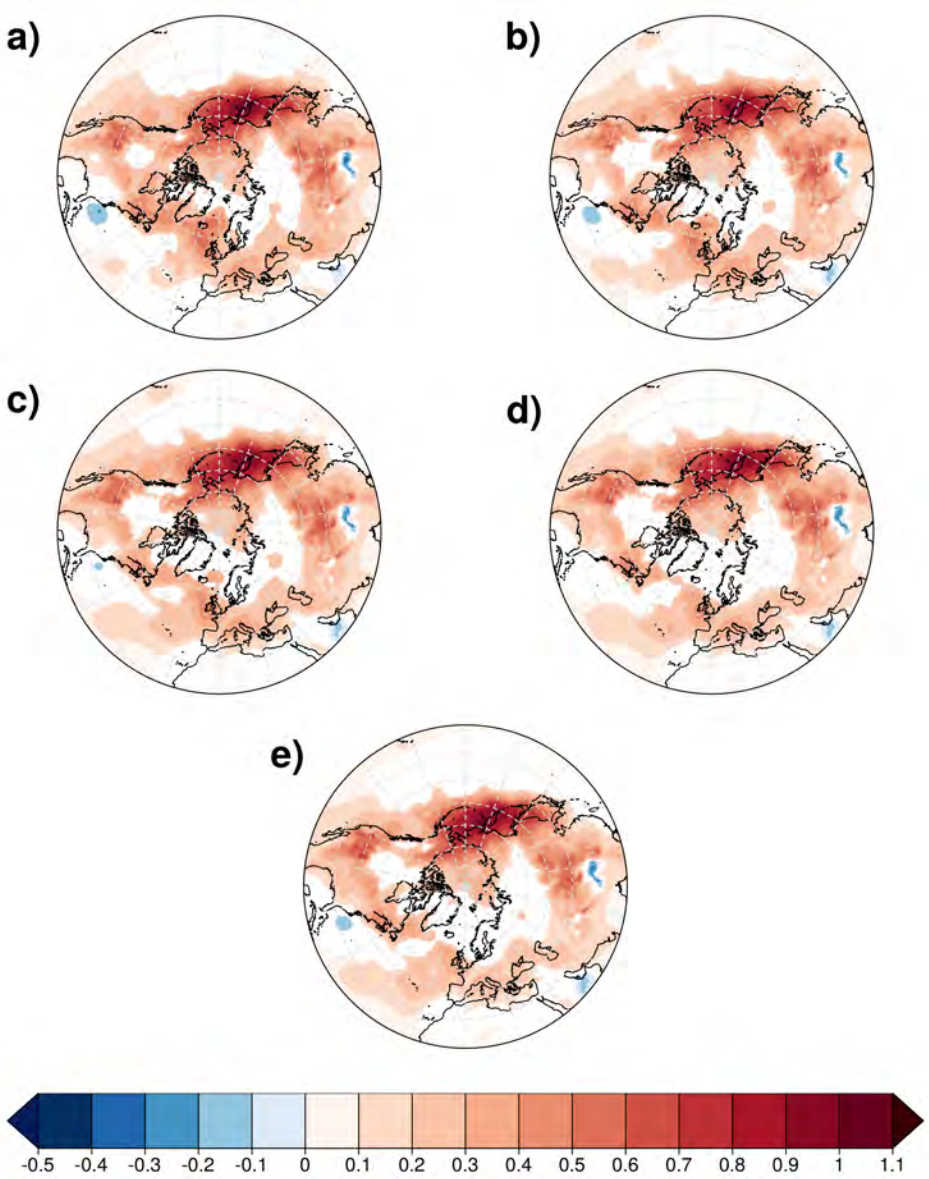

Figure 33 – Bias (hPa) between the storm tracks predicted by the ECMWF System 4 and the ERA-Interim reanalysis for different lead months. Storm tracks correspond to the DJF season in the in the 1982-2016 period. ECMWF System 4 seasonal forecasts initialised the 1^{st} of a) December, b) November, c) October, d) September and e) August have been used. White areas denote regions where the bias is not significant at a 95% confidence level.

America where the values range between 0.1 and 0.3 hPa.

The biases in the storm tracks are displayed for the forecasts of the boreal winter with different lead times in Figure 33. Biases are very similar for the all forecasts times in both location and magnitude, particularly in the most problematic region in the North Pacific. This can be interpreted as the systematic error of the storm tracks being established very early into the forecast period, probably after just a few days. However, the positive biases of the boreal winter storm tracks over the Atlantic basin extend towards the equator as the lead time increases.

4.4 Teleconnections of wind energy relevant climate indices

After the comparison of Niño-3.4, NAO, NPST and NAST indices in ECMWF System 4 and ERA-Interim, the systematic errors affecting their teleconnections to the 10-m wind speed and 2-m temperature are explored. This evaluation has been performed by comparing the one-point correlation maps for ERA-Interim with the corresponding maps for ECMWF System 4.

4.4.1 ENSO impact on wind speed and temperature

The relationship between the Niño-3.4 index and wind speed and air temperature from ERA-Interim reanalysis is shown in Figure 34 (top row) for DJF. This season has been selected for illustrative purposes because this is the season when the Niño-3.4 index shows the highest forecast skill. The results for other seasons have been included in the Appendix (Figure B16).

The strength of the ENSO teleconnections to the wind speed and temperature is particularly high over the oceans where the highest correlations are found (Figure 34, top-left panel). The maximum correlations are in the tropical Pacific, but the variability of wind speed and temperature also shows a linear correspondence with the Niño-3.4 index in other basins and remote regions. This global influence is produced by the atmospheric circulation response to the SST anomalies in the equatorial Pacific when an ENSO event occurs (Trenberth et al. 1998; Alexander et al. 2002). Despite the widespread influence of ENSO on wind speed and temperature, there are some regions for which this phenomenon is not playing a dominant role. One example of this is Europe, where low and non-significant correlation values between the Niño-3.4 index and the wind speed and temperature are obtained for the DJF season. Although it has been demonstrated that ENSO can affect the European climate, its impact is difficult to isolate because the ENSO signal is attenuated by non-linear modulations in that region (Brönnimann 2007; Rodríguez-Fonseca et al. 2016). In addition, the impact of ENSO on the climate conditions in the European climate tend to be higher during late fall than in the winter season discussed here (e.g. King et al. 2018).

Wind speed conditions are driven by ENSO

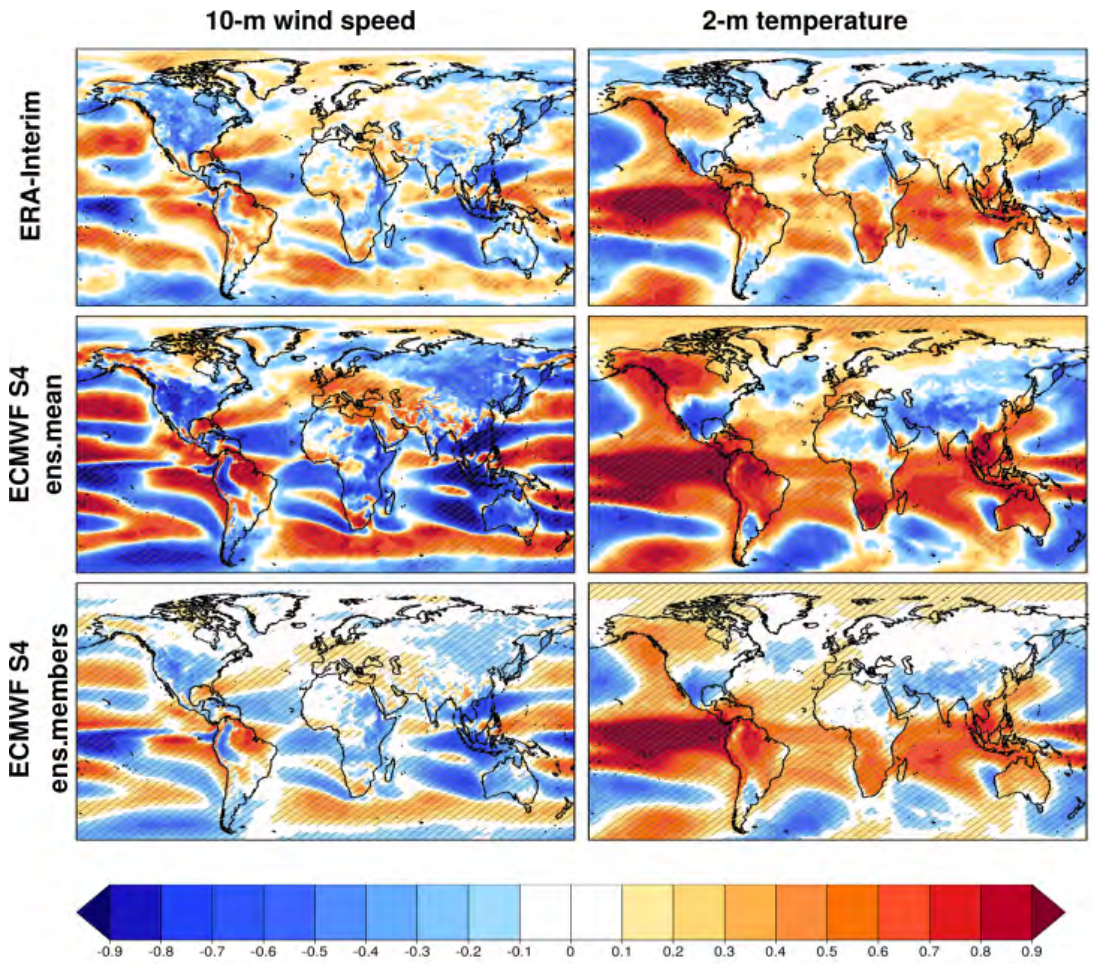

Figure 34 – One-point correlation maps between the 10-m wind speed (left column) and 2-m air temperature (right column) with the Niño-3.4 index. Correlations have been computed for the ERA-Interim reanalysis (top row) and for the ECMWF System 4 seasonal forecasts in DJF for the 1982-2016 period. The correlations in the seasonal forecasts have been computed for the ensemble mean (middle row) and for the concatenated ensemble members (bottom row). ECMWF System 4 seasonal forecasts initialised the 1^{st} of November have been used. Hatching denotes regions with significant correlation values (two-tailed t-test at a 95% confidence level).

in several regions over land. Negative and significant correlations between the Niño-3.4 index and wind speed from ERA-Interim (Figure 34, top-left panel) are obtained in North America for the DJF season. By contrast, positive correlations appear in South America (except in the northwestern part where negative correlations are shown). Eastern Africa, the Arabian Peninsula or Indonesia are other regions for which a linear relationship, which is indicated by high and significant correlations, between the wind speed variability and the Niño-3.4 index is found. In other seasons (Figure B16), ENSO shows influence on the wind conditions in different regions. For instance, significant correlations are also identified in western Russia in JJA or Australia in MAM.

One-point correlation maps between the Niño-3.4 index and 2-m air temperature from ERA-Interim (Figure 34, top-right) show more intense correlations than with the wind speed. Over land, similar results to those presented in Yang and DelSole (2012) with positive and significant correlations between the 2-m air temperature and the Niño-3.4 index in northern North America, South America, South Africa and southern Asia have been obtained. These results also show variations with the season (Figure B16). For example, the relationship between the Niño-3.4 index and the 2-m air temperature in North America is more intense in DJF than in other seasons and significant correlations displayed for most of the African continent are only observed for DJF and MAM.

To investigate how ECMWF System 4 simulates the ENSO teleconnections to wind speed and temperature, one-point correlation maps have been computed. These maps have been obtained by correlating the ensemble mean of the Niño-3.4 index and the ensemble mean of either 10-m wind speed or 2-m air temperature one-point correlation (Figures 34, central row). The maps show strong correlations in most regions, which indicates that ENSO dominates the predictable part of the variability. However, there are regions such as in the North Atlantic where these correlations are not significant, indicating a weak statistical relationship between the predictable component of ENSO and the climate conditions in that region, as explained above. An interesting feature of these maps is that they show more intense correlations than the corresponding correlations from ERA-Interim. This is the consequence of the ensemble mean operation filtering part of the variability.

When the individual ensemble members are used to compute the one-point correlation maps (Figures 34, bottom row), the results show higher resemblance to those obtained for the observational reference, but with slightly weaker correlation values. Despite this similarity, some exceptions have been found. For example, the positive correlations between the Niño-3.4 index and the 2-m air temperature obtained for the ERA-Interim in Asia are negative for the ECMWF System 4 (Figures 34, bottom-left panel). In northern North America, the linear relationship between the Niño-3.4 index and the wind speed obtained for ERA-Interim is not reproduced by ECMWF System 4, which

shows correlations that are virtually zero. These differences can be interpreted as systematic errors of the forecast system.

The comparison of the one-point correlation maps of the second and third row of Figure 34 reveals that it is important to estimate the teleconnections using the individual ensemble members. The reason to prefer the estimates using the individual ensemble members instead of the ensemble is that the individual members realistically simulate the physical relationship between the index and the physical variable, in this case, wind speed and temperature.

As explained above, systematic errors in the ECMWF System 4 representation of the ENSO teleconnections have been identified. These errors suggest that the influence of ENSO on wind speed and temperature can be affected by local processes, which are more of a challenge for global climate simulations. They can also be the cause of a misrepresentation of large-scale processes such as the source and the propagation of the Rossby waves typically involved in the ENSO teleconnections (Trenberth et al. 1998).

Systematic errors in the ECMWF System 4 representation of the ENSO teleconnections are a function of the forecast time. Differences in the one-point correlation maps between the Niño-3.4 index and 10-m wind speed from ECMWF System 4 and ERA-Interim in DJF for the predictions initialised in December (lead 0), November (lead 1), October (lead 2), September (lead 3) and August (lead 4) are shown in Figure 35. Regions such as northern North America, the North Atlantic, the Mediterranean or southwestern Asia show important variations of the ENSO teleconnections to the 10-m wind speed for the different lead times. The differences when using the ensemble mean with the equivalent maps in ERA-Interim (Figure 35, left column) reach maximum values for the DJF predictions initialised in August. Similar results are obtained for temperature (Figure 36, left column). For example, over South America, South Africa, Australia or the North Pacific, low and non-significant correlation differences between the Niño-3.4 index and the 2-m air temperature are identified for the DJF predictions initialised in December, but they become high and significant for the predictions initialised in August.

By contrast, the differences for the one-point correlations computed by concatenating the individual ensemble members (Figure 35 and 36, left column) do not show such a strong variation with the forecast time. One exception is found in northern North America, which is a key region for wind energy activities (Vaillancourt et al. 2014). In that particular area, ECMWF System 4 shows correlation values close to zero, while in the observational reference the ENSO show a linear response in the wind speed. The ECMWF System 4 misrepresentation of the ENSO influence on the wind speed can be translated into low levels of skill in that region. Only significant differences over some regions in the tropical Pacific, and in northern North America can be identified for the correlations between the Niño-3.4 index and the wind speed.

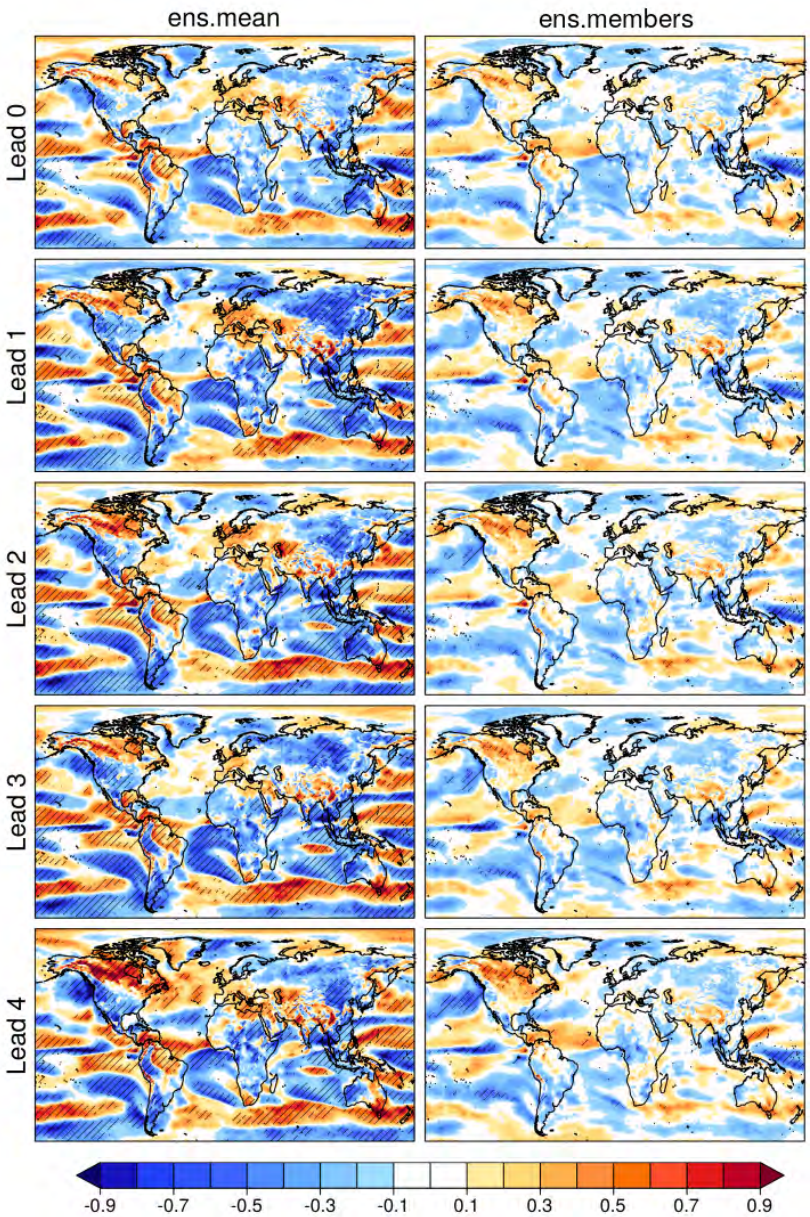

Figure 35 – Lead time dependency of the DJF differences between the ECMWF System 4 seasonal forecasts and ERA-Interim in the one-point correlation maps of the 10-m wind speed and the Niño-3.4 index. Differences are obtained for the ECMWF System 4 one correlation maps based on the ensemble mean (left column) and concatenated ensemble members (right column). Correlations have been computed for the 1982-2016 period. ECMWF System 4 seasonal forecasts initialised the 1^{st} of December (lead 0), November (lead 1), October (lead 2), September (lead 3) and August (lead 4) have been used. Hatching denotes regions with significant correlation differences (two-tailed Fisher test at a 95% confidence level).

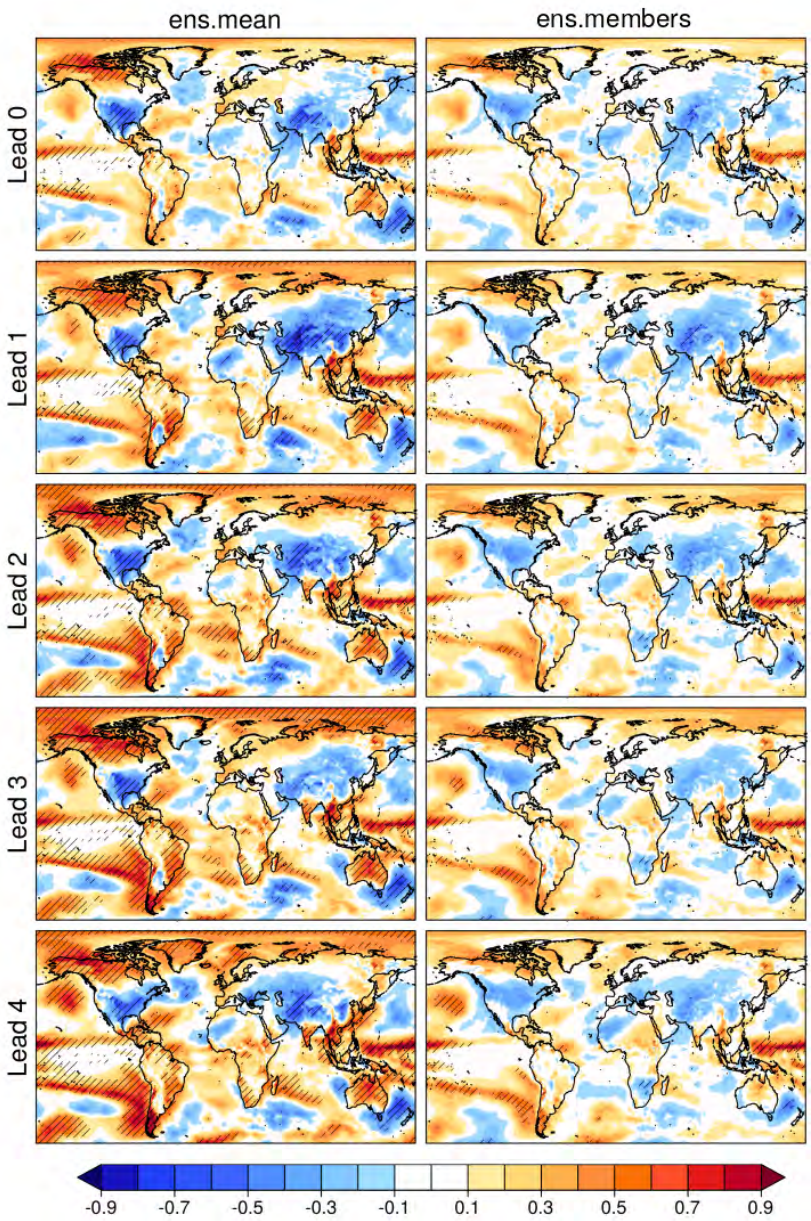

Figure 36 – Lead time dependency of the DJF differences between the ECMWF System 4 seasonal forecasts and ERA-Interim in the one-point correlation maps of the 2-m air temperature and the Niño-3.4 index. Differences are obtained for the ECMWF System 4 one correlation maps based on the ensemble mean (left column) and concatenated ensemble members (right column). Correlations have been computed for the 1982-2016 period. ECMWF System 4 seasonal forecasts initialised the 1^{st} of December (lead 0), November (lead 1), October (lead 2), September (lead 3) and August (lead 4) have been used. Hatching denotes regions with significant correlation differences (two-tailed Fisher test at a 95% confidence level).

In the case of temperature, significant differences are restricted to the western equatorial Pacific, eastern Pacific, some regions in southern South America and South Africa.

The decrease of the correlations computed with the ensemble means for long forecast times is related to the reduction of the inter-annual variability as a consequence of the averaging over all the ensemble members. Such a decrease with forecast time is not obvious when the correlations are computed using all ensemble members because the physical relationship between ENSO and the climate variables in the seasonal forecast system is well represented by the individual members regardless of the forecast time. For this reason, it is recommended to always estimate the teleconnections using the full ensemble instead of the ensemble mean.

4.4.2 NAO impact on wind speed and temperature

The role of the NAO on the variability of wind speed and temperature at seasonal timescales has also been examined (Figure 37). The results included here correspond to the MAM season, as this season the ECMWF System 4 shows the maximum skill for the seasonal forecasts of the NAO index (Figure 29b). One-point correlation maps between the NAO index with the 10-m wind speed and 2-m air temperature from ERA-Interim have been included in the Appendix B (Figure B17) for the four seasons. In DJF, the NAO index shows the highest correlation values with wind speed and air temperature. However, the NAO teleconnections to wind speed over Europe are significant in the four seasons. This is not the case for the air temperature, for which the NAO index only displays significant correlations with the 2-m air temperature in Europe for DJF and MAM. Negative and significant one-point correlation values between the NAO index and 2-m temperature are also obtained for South America (in JJA and SON) and northwestern Africa.

The influence of the NAO in the boreal spring is mostly concentrated over the North Atlantic, where the NAO index shows the highest correlations with wind speed and temperature (Figure 37, top row). In the northern North Atlantic, a spatial structure with positive-negative-positive correlations appears as a wind speed response to the NAO (e.g Zubiate et al. 2017). This indicates that the positive phase of the NAO leads to an increase of the wind speed in northeastern North America, northern Europe and over the tropical Atlantic and a reduction of wind speed over the United States, southwestern Europe and the Mediterranean. In the case of the air temperature, negative correlations with the NAO index in MAM are shown for the northwestern Atlantic whereas positive and significant correlations can be found in Europe and the United States (Figure 37, top-left panel). Significant correlations are also found for northern Africa, where a positive phase of the NAO leads to an increase in wind speed and a reduction of the air temperature.

Beyond North America and Europe, some regions affected by the NAO can be also found.

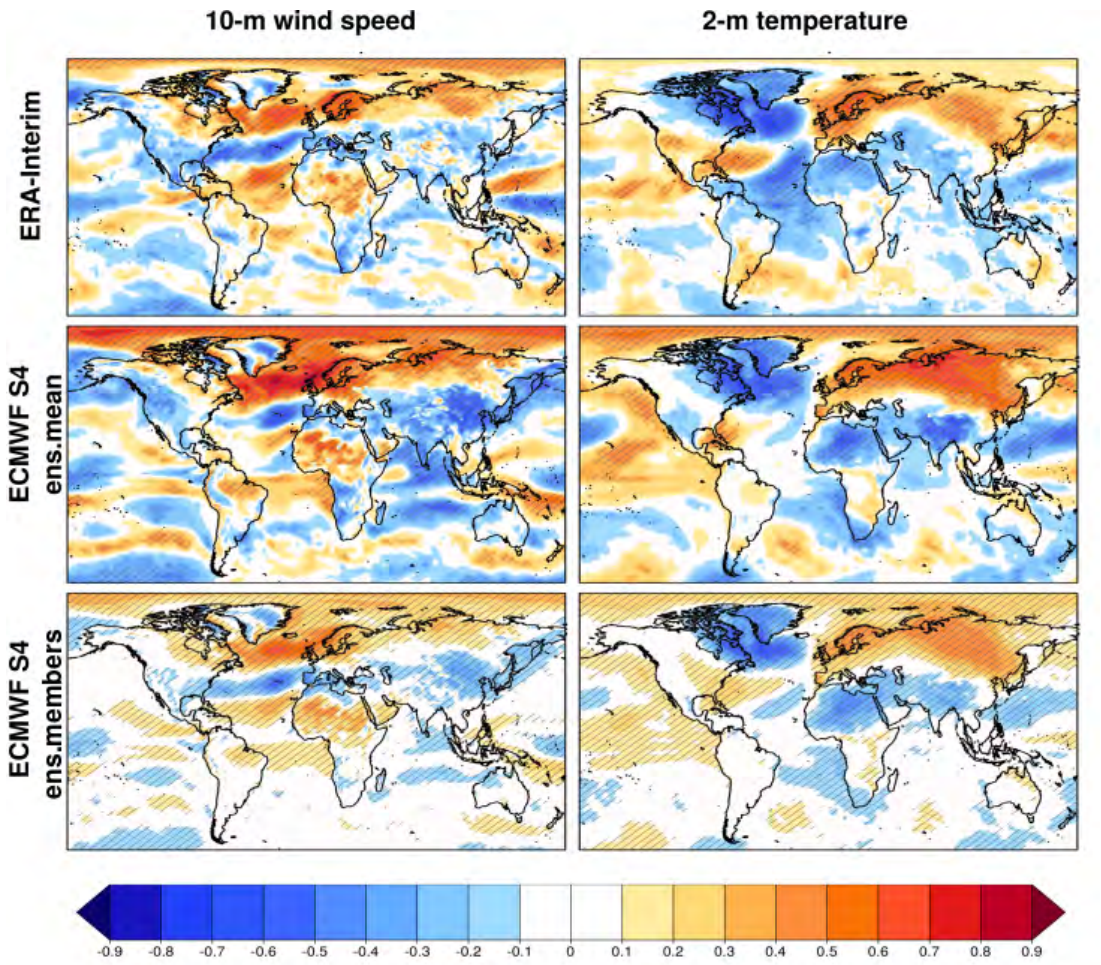

Figure 37 – One-point correlation maps between the 10-m wind speed (left column) and 2-m air temperature (right column) with the NAO index. Correlations have been computed for the ERA-Interim reanalysis (top row) and for the ECMWF System 4 seasonal forecasts in MAM for the 1982-2016 period. The correlations in the seasonal forecasts have been computed for the ensemble mean (middle row) and the concatenated ensemble members (bottom row). ECMWF System 4 seasonal forecasts initialised the 1^{st} of February have been used. Hatching denotes regions with significant correlation values (two-tailed t-test at a 95% confidence level).

For example, positive correlations between the NAO index and the wind speed and temperature from ERA-Interim are identified in northeastern Asia. This illustrates the linear relationship between the NAO and the wind speed and temperature in that region, which has been suggested to be the expression of the Atlantic variability impact on East Asia (Bollasina and Messori 2018).

One-point correlation maps between the seasonal forecasts of the NAO index and the climate variables are very similar to those obtained for ERA-Interim. Nevertheless, some discrepancies are found in North America. Correlations of the NAO index based on the ensemble mean exhibit larger amplitudes than those computed with the individual ensemble members, which is similar to what was obtained for the Niño-3.4 index. The high resemblance between the one-point correlation maps in the seasonal forecasts and the observational reference indicates that although the ECMWF System 4 has a limited skill to predict the NAO index, it is able to correctly reproduce the physical mechanism that connects the NAO signal to wind speed and temperature anomalies in different regions of the globe.

Differences between the one-point correlation maps based on the seasonal forecasts and the corresponding from the observational reference for the NAO index and the wind speed and temperature can be found in the Appendix B (Figures B18 and B19). The results are very similar to those obtained for ENSO with a strong dependency of the differences with the forecast time in the one-point correlation maps based on the ensemble mean. However, when the individual ensemble members are used for the computation of the one-point correlation maps for the NAO index there is no region over land where the discrepancies between ECMWF System 4 and ERA-Interim in their representation of the NAO teleconnections can be singled out.

4.4.3 Storm tracks impact on wind speed and temperature

To explore if ECMWF System 4 is able to simulate the impact of the storm tracks on wind speed and temperature, the NAST and NPST storm track indices defined in section 4.3 are employed. As in the previous cases, the NAST and NPST teleconnections to wind speed (Figure 38) and air temperature (Figure 39) have been evaluated through one-point correlation maps obtained by correlating the index and the local climate variable with the individual ensemble members. The results based on the ensemble mean predictions can be found in the Appendix (Figures B20 and B21).

Wind speeds show positive correlations with the NAST over the North Atlantic region (Figure 38, top row) which illustrates the linear relationship between the near-surface wind speed with the North Atlantic storm tracks. These positive correlations are obtained in both ERA-Interim and ECMWF System 4 in DJF for all the lead times. However, some discrepancies can be found between the seasonal forecasts and the reanalysis. For example, the negative and

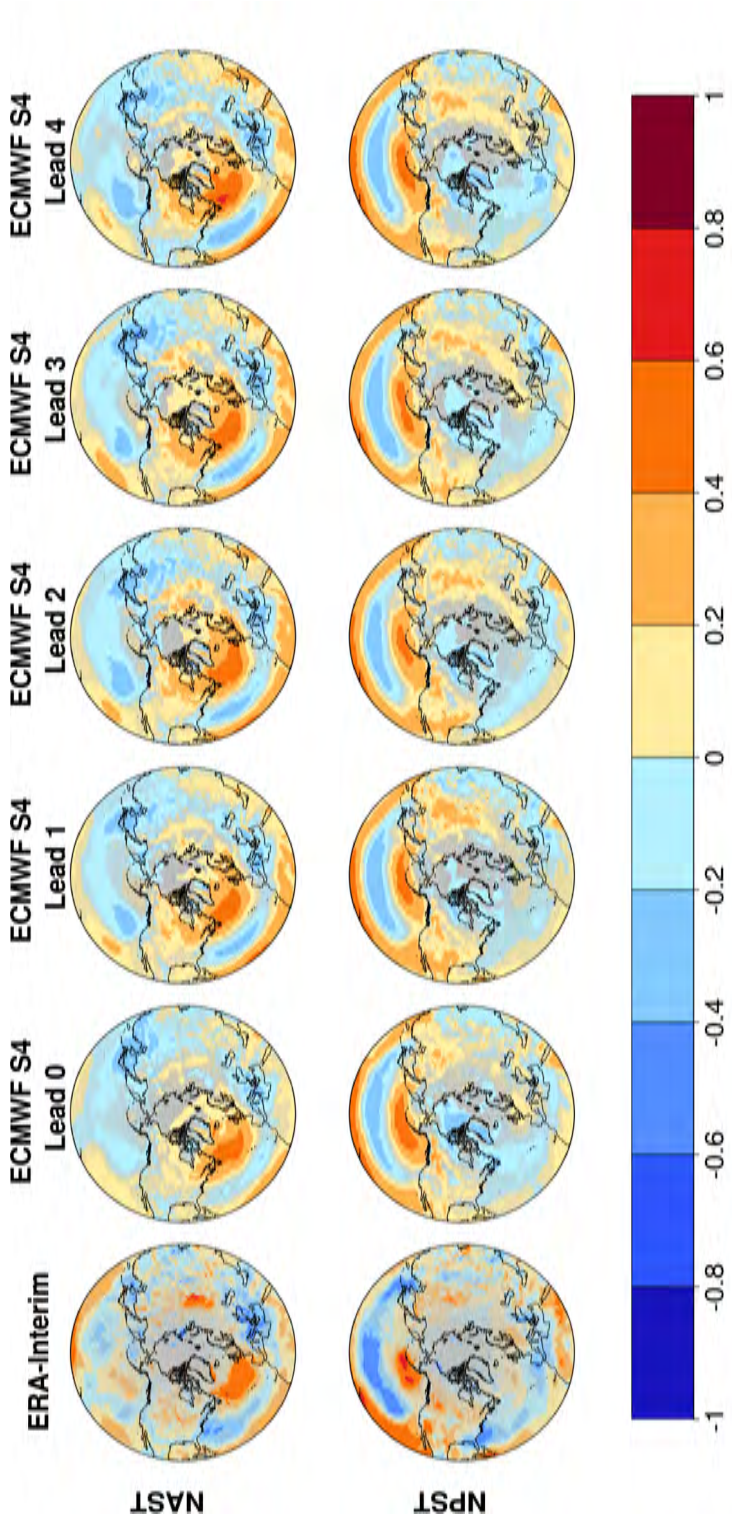

Figure 38 – One-point correlation map between the NAST (top row) and NPST (bottom row) indices and 10-m wind speed. The maps are based on the ERA-Interim reanalysis (first column) and ECMWF System 4 seasonal forecasts for DJF in the period 1982-2016. ECMWF System 4 seasonal forecasts initialised in December (lead 0), November (lead 1), October (lead 2), September (lead 3) and August (lead 4) have been used. Regions with non-significant correlation values (two-tailed t-test at a 95% confidence level) are masked.

Figure 39 – One-point correlation map between the NAST (top row) and NPST (bottom row) indices and 2-m air temperature. The maps are based on the ERA-Interim reanalysis (first column) and ECMWF System 4 seasonal forecasts for DJF in the period 1982-2016. ECMWF System 4 seasonal forecasts initialised the 1^{st} of December (lead 0), November (lead 1), October (lead 2), September (lead 3) and August (lead 4) have been used. Regions with non-significant correlation values (two-tailed t-test at a 95% confidence level) are masked.

significant correlations between the NAST index and the wind speeds in the southeastern North America coast, which extend towards Africa and the Mediterranean, are weaker in the seasonal predictions than in the reanalysis. In the North Pacific, ECMWF System 4 does not show the positive (but non-significant) correlations between the NAST index and the wind speed obtained for ERA-Interim. This result is in agreement with the bias in the storm tracks obtained for that region (section 4.3), which is translated into a different representation of the NAST teleconnections to the wind speeds in the seasonal forecasts and in the reanalysis. Over land, the NAST index positive teleconnections to wind speed (Figure 38, top row) are obtained for western France and the United Kingdom for all the lead months. However, these correlations are not significant in ERA-Interim illustrating a systematic error in the ECMWF System 4 representation of the NAST index teleconnections to wind speed.

The strong association between the NPST index (Figure 38, bottom row) with the wind speed variability in the North Pacific is shown by a correlation pattern with a dipole of positive and negative values in winter. The same structure is obtained in the ECMWF System 4 for all the lead months, although the correlations are slightly weaker and more zonally extended than for ERA-Interim (for which the positive correlations in the northern North Pacific are more restricted to North America). Over land, the NPST index displays negative correlations with the southern Europe wind speeds and positive with the northern Europe wind speeds, but none of them is significant.

ECMWF System 4 shows limitations in its representation of the influence of NAST and NPST over wind speeds in Asia and southern North America, where the system shows positive and significant correlations not present in the ERA-Interim results. These discrepancies increase with the lead time.

The impact of the storm tracks on the 2-m temperature has been depicted in Figure 39. Generally, the storm tracks influence on temperature is well represented by the ECMWF System 4, but the main differences between the predictions and the observational reference appear in the magnitude of the one-point correlation maps. For instance, the positive correlations between the NAST index and the air temperature in Asia are much more widespread in the seasonal forecasts than in the reanalysis. This indicates that ECMWF System 4 overestimates the relationship between the 2-m air temperature and the NAST index.

ECMWF System 4 also shows more areas with significant correlations than those obtained for ERA-Interim. For example, the NPST index has positive correlations with the air temperature in North America, but in ERA-Interim these correlations are not significant. This result is the consequence of the sensitivity of the significance test to the sample size (discussed in chapter 3), which is 15 times (as 15 ensemble members have been used) larger in the seasonal forecasts than in the observational reference.

These results indicate that ECMWF System 4 shows important discrepancies with the results obtained for ERA-Interim. The discrepancies could be linked to the mean biases affecting the storm tracks and the underlying sea level pressure, but also to the biases of the wind speed and air temperature due to other phenomena.

4.5 Conclusions

There is a large number of processes responsible for the climate variability, but ENSO, NAO and storm tracks are some of the most relevant phenomena for the wind energy sector, as they have variability at both inter-annual and intra-seasonal timescales. The skilful prediction of these wind energy relevant indices is one of the key challenges for the state-of-the-art seasonal forecast systems because the correct simualation of the variability in these indices could lead to a good representation of the variability of wind speed and air temperature.

To evaluate the potential skill in the seasonal predictions of the wind energy relevant indices (Niño-3.4, NAO, NPST and NAST) the Pearson correlation has been used. High correlations for the Niño-3.4 index have been obtained for all seasons and forecast times. The NPST index also has shown positive and significant correlation values, in spite of the strong bias that should be further analysed. The significant correlations of the NPST index might be related to the skill in the Niño-3.4 index because ENSO is one of the mechanisms modulating the storm track variability in the North Pacific. These results reveal that either the Niño-3.4 index or the NPST index could be used as predictors in a hybrid empirical-dynamical prediction model aimed at improving the skill of climate variables such as wind speed or temperature. This could be achieved by combining the empirical relationship between the index and the climate variables from the observational reference with the skilful seasonal forecasts of the indices.

Seasonal forecasts of the NAO index and the NAST index show low correlation. This might be related to the limitations of the ECMWF System 4 in the North Atlantic region, which is dominated by internal variability harder to predict. However, some recent advances have shown that the influence of ENSO, the stratosphere or sea ice in the North Atlantic region could enhance the predictability in extra-tropical areas (e.g. Scaife et al. 2014). Hence, if new seasonal forecast systems introduce some improvement in the representation of these sources of predictability, useful levels of skill could be achieved in the future for this region.

The teleconnections of the wind energy relevant indices to wind speed and air temperature have been explored by one-point correlation maps. For the seasonal forecasts, one-point correlation maps between the index and the climate variable have been computed with the ensemble mean predictions but also with the individual ensemble members. These maps have been compared to the corresponding one-point correlation maps from ERA-Interim to characterise the systematic errors in the teleconnections. The differences between the one-point teleconnection maps in

predictions and observations are larger when the ensemble mean is used, because the inter-annual variability of the ensemble mean decreases for long leads, as a consequence of the averaging operation (Stockdale et al. 2011). However, one-point correlation maps based on the individual ensemble members are comparable to the correspondent maps from the observational reference. Systematic errors in the ENSO teleconnections to wind speed have been identified in regions such as North America in DJF, where the negative correlations of the Niño-3.4 index and wind speed obtained for ECMWF System 4 are not obtained in ERA-Interim. These systematic errors become maximum for the DJF seasonal forecasts initialised in August. By contrast, the NAO teleconnections to wind speed and temperature show a strong similarity between the seasonal predictions and the reanalysis, indicating that the ECMWF System 4 is able to reproduce the physical mechanisms involved in the NAO teleconnections, even if the system is not providing skilful predictions of the NAO index.

ECMWF System 4 is also able to reproduce the inter-annual variations of the storm tracks, especially over the North Pacific where positive and significant correlations are obtained. The influence of the NAST and NPST indices on the wind speed from ERA-Interim is more intense over the ocean and only some regions over land. The linkage between the storm tracks and the temperature shows better agreement between the seasonal forecasts and the observational reference than the links obtained for the wind speed. However, in some regions such as western Europe, the seasonal forecast system is not able to correctly reproduce the influence of the storm tracks intensity on temperature variability. These differences are the combination of the biases affecting the storm tracks and the underlying sea level pressure together with the biases of wind speed and temperature (shown in chapter 3).

Despite the teleconnections from ENSO, NAO and storm track activity with air temperature having been widely investigated, the ability of the seasonal predictions to reproduce these teleconnections to wind speed has not been looked at. When assessing the teleconnections of the wind energy relevant indices in the ECMWF System 4 to the 10-m wind speed, they show larger errors than for the 2-m air temperature. This is an important aspect that will be relevant for both wind energy users and the research community.

05

Euro-Atlantic weather regimes for wind energy applications

05 Summary

Objective

To investigate the usefulness of a weather regime (WR) classification for each month of the year in the context of the wind energy applications. The main goal is to understand the fraction of wind speed and air temperature variability that can be explained in terms of weather regimes in the Euro-Atlantic region, and in which regions these WRs play a dominant role. In addition, the seasonal predictability of the WRs in ECMWF System 4 will be explored.

Methodology

- Four regimes for each month of the year based on sea level pressure (SLP) have been obtained.
    - ERA-Interim: k-means (KM) clustering approach
    - ECMWF System 4: KM clustering approach and an assignation approach using the minimum root mean square distance (RMSD).
- Metrics: composite maps, spatial correlation, monthly frequencies of occurrence, Pearson correlation
- Method to reconstruct climate variables (10-m wind speed and 2-m air temperature) from the WR monthly frequencies of occurrence.

Results

- Typically WR classifications use data for a whole season. The definition of a set with four clusters computed separately for each month of the year allows relating specific wind speed and temperature anomalies with the most recurrent atmospheric circulation structures in each month. The classification for each separate month produces WRs that can be substantially different to those obtained in the seasonal classifications.
- There are several regions in Europe, particularly those surrounding the North Sea where the variability of wind speed and temperature can be reconstructed by the monthly frequencies of occurrence of WRs. This effect is particularly important in December, January and February when the inter-annual variability of the reconstructed wind speed and air temperature shows a very good agreement with the original wind speed and temperature.

- WRs obtained from the application of the KM analysis to the seasonal forecasts show different patterns to those based on the observational reference. This reflects the influence of the systematic errors affecting this kind of predictions. However, the application of the RMSD method produces WRs with similar spatial patterns to the WRs obtained from the observational reference. This makes possible to assess the predictability of these regimes, and consequently to generate a forecast product that can be used by wind energy users for decision-making.
- ECMWF System 4 accurately predicts the monthly frequencies of occurrence of the WRs only for lead time 0. The fact of not finding predictability beyond lead time 0 reflects the difficulties to predict the seasonal climate in the North Atlantic region.

Conclusions

- The WR obtained for each calendar month could be employed to explain the atmospheric variability and their influence on anomalous wind speed and air temperature. This application can be exploited to provide wind energy users with information in those regions for which the WRs dominate the climate variability, such as the North Sea in winter.
- The comparison of the two methodologies employed for the computation of WRs from seasonal forecasts has demonstrated that the two approaches are complementary. The KM analysis is a useful diagnostic tool to identify systematic errors in seasonal predictions. However, to generate a product based on seasonal predictions of WRs in an operational context, the RMSD method is most suitable to perform an effective verification, which is essential to distribute climate information tailored to specific users' needs.
- Despite the limited forecast quality of the ECMWF System 4 WRs, this work can be employed as a benchmark for future analysis in regions for which seasonal prediction systems show good levels of skill, such as North America.

Publications

This chapter discusses the contributions of the author of this thesis to:

- Cortesi, N., **V. Torralba**, N. Gonzalez-Reviriego, A. Soret, F.J. Doblas-Reyes, under review: Characterization of European wind speed variability using weather regimes. *Climate Dynamics*.

05

Euro-Atlantic weather regimes for wind energy applications

Weather regimes (WRs) can be defined as the most recurrent large-scale atmospheric circulation structures that allow the characterisation of the complex atmospheric dynamics in a particular region (Vautard 1990; Michelangeli et al. 1995). They have been extensively used to investigate the atmospheric variability at the mid-latitudes, as these regimes are associated with extreme weather events such as heat waves or droughts (Yiou et al. 2008; Quesada et al. 2012).

Wind energy users need to properly characterise the climate variability in a wide range of timescales because this variability can affect the balance between wind energy production and demand (Brayshaw et al. 2011). The strong association between the weather regimes and the wind power production has indicated that WRs can be used to understand the atmospheric variability and to improve the current forecasting approaches in the wind industry (Couto et al. 2015). For this reason, wind energy users have shown interest in the WRs as a tool to understand the atmospheric variability. In particular, the identification of regions where the WRs have a great influence on the wind energy resources can help to guide new deployment strategies that minimise the risk related to the variations in wind energy outputs (Grams et al. 2017).

However, the potential of WRs for wind energy applications has not been exploited yet. One of the problems is that most of the WR studies focus mainly on the winter season (e.g. Cassou 2008; Dawson et al. 2012; Stryhal and Huth 2017) and these seasonal classifications are not sufficiently detailed to fully understand the variability in

wind energy conditions (Grams et al. 2017). To overcome this limitation and to satisfy the users' needs a weather regime classification for each individual month of the year is proposed (Cortesi et al. 2019). The goal is to describe the month-by-month variations of the most recurrent circulation structures and also to investigate to which extent WRs can be used to describe the variability of impact variables such as wind speed and temperature in a specific month.

Besides of the WR application to improve wind energy activities, WRs can also be used as a diagnostic tool to investigate the performance of the climate forecast systems (Fil and Dubus 2005; Dawson et al. 2012; Ferranti et al. 2015; Matsueda and Palmer 2018). WRs tend to persist in quasi-stationary states typically on timescales of a few weeks with subsequent transitions between regimes. Seasonal forecasts do not seek to predict the time of occurrence of such transitions, but rather to estimate which regimes are the most likely to be prevalent over the coming month or season (Palmer and Anderson 1994). Those forecast systems that are not able to reproduce the spatial patterns and monthly frequency of occurrence of the WRs could fail to simulate the climate variability and its long-term changes (Hannachi et al. 2017). Hence, the assessment of WRs can help to better understand climate predictability on intra-seasonal and inter-annual timescales.

In this chapter, a set of WRs for each month of the year is defined. The potential of those WRs to understand wind speed and air temperature variability is explored. Furthermore the seasonal predictability of the WRs is evaluated. The results have been systematically compared with those obtained with the WRs estimated using all the data available for a specific season. The details on the data processing and methodology have been included in section 5.1. The description of the WRs (spatial patterns and monthly frequency of occurrence) and their impact on wind speed and air temperature are provided in section 5.2. The monthly frequency of occurrence of the WRs has been used to reconstruct the 10-m wind speed and 2-m air temperature and the results are discussed in section 5.3. Then, the ability of the ECMWF System 4 seasonal forecast system to reproduce observed WRs is explored in section 5.4. As there is not standard procedure available in the literature to define WRs based on seasonal predictions, two different approaches have been used. The opportunities and limitations of these methodologies and their relevance to provide wind energy users with climate information based on WRs have been discussed in section 5.5.

5.1 Methodology

5.1.1 Data processing

This analysis is based on daily means of sea level pressure (SLP) in the period 1982-2016 (35 years) for the Euro-Atlantic region [27°- 81° N, 85.5° W - 45° E]. The seasonal predictions of the ECMWF System 4 have been employed and ERA-Interim has been used as a

reference dataset. The sensitivity of the WRs classification to the choice of the reanalysis has been explored in Cortesi et al. (2019) and it is demonstrated that different reanalyses produce equivalent WR classifications. As this analysis has been performed for each individual month of the year, 15 members have been used to obtain consistent results among the months. Although geopotential height at 500 hPa has been widely used in the literature to obtain weather regimes (Cassou 2008; Dawson et al. 2012; Ferranti et al. 2015), this assessment is based on SLP (Fereday et al. 2008; Neal et al. 2016; Stryhal and Huth 2017). This choice is justified because SLP is less affected by global warming than the geopotential height and can provide more information about the impact of WRs on those surface variables, which is the most relevant for wind energy applications.

Weather regimes have been obtained from the daily SLP anomalies. These anomalies have been computed as deviations from the daily climatologies of the SLP in that region. The daily climatologies have been previously smoothed out by a Loess filter (Cleveland and Devlin 1988) to remove the short-term variability and retain the annual cycle (Mahlstein et al. 2015). To take into account the dependency of the grid box size, the anomalies have been weighted by the cosine of the latitude.

For the assessment of the WRs impact on wind energy users' relevant variables, the 10-m wind speed and 2-m air temperature anomalies have been used. In the case of the wind speed, the anomalies have been normalised by the climatological mean wind speed and expressed as a percentage of the mean. This transformation has been performed because wind speed shows strong regional gradients, with much higher wind speeds occurring over the oceans than over land, and with large spatial variations over the continents. Therefore, the normalisation of the anomalies is helpful for the interpretation of the wind speed variations associated with a specific weather regime. Although the WRs have been obtained over the Euro-Atlantic region, the representation of their impact on wind speed and air temperature is restricted to the European region [27°–81° N, 25.3° W – 45° E] where wind farms are installed.

5.1.2 Weather regime computation

WRs have been derived from SLP daily anomalies of the ERA-Interim reanalysis and ECMWF System 4 as illustrated in Figure 40. Two methodologies have been employed, the k-means algorithm and the minimum root-mean-square distance, which has been used only for the predictions.

Method 1 – k-means classification (KM): is one of the most common methods used in climate research for the classification of WRs is the k-means algorithm (Hartigan and Wong 1979). This clustering method produces a partition of all states in a predefined number of clusters (R), which maximises the ratio of the variance between the cluster centroids and the average intra-cluster variance. The objective of this choice is that the points in the clusters are

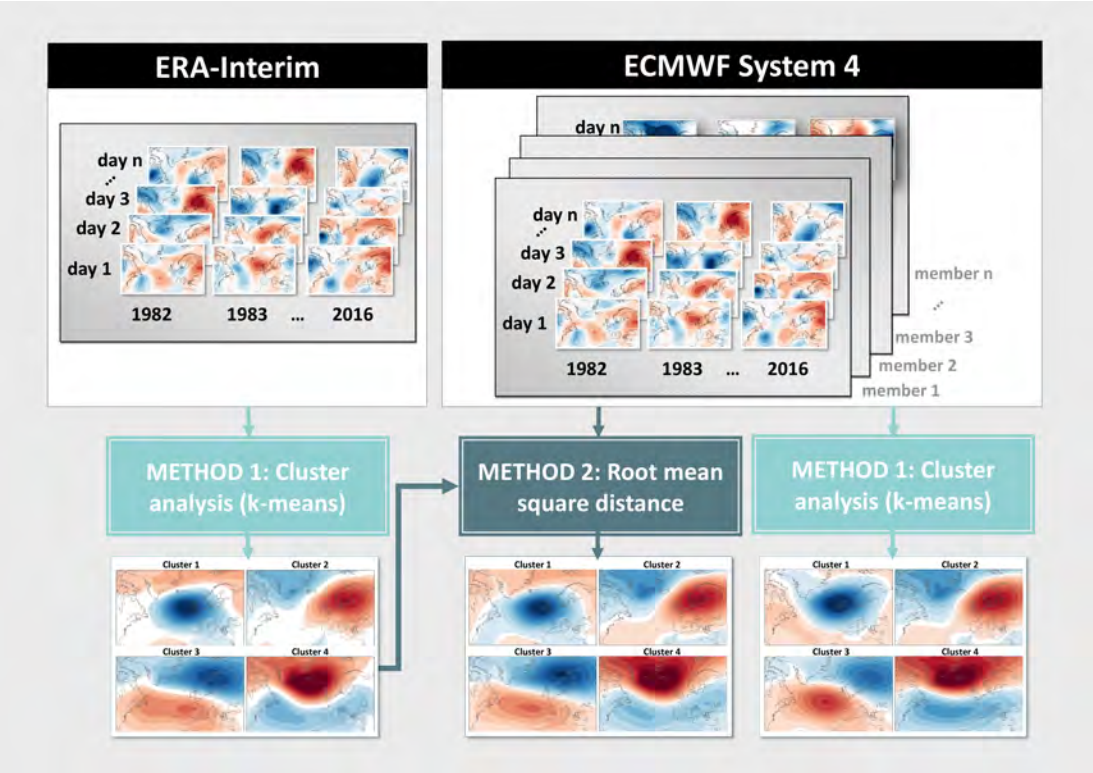

Figure 40 – Workflow used to perform weather regime classifications for each month of the year from daily sea level pressure anomalies. The k-means (KM) method has been applied over the ERA-Interim daily anomalies to obtain a reference classification. Then two different classifications have been obtained for the seasonal forecasts from the ECMWF System 4 forecast system. The KM clustering technique has been applied directly on the seasonal forecasts to produce one classification (light green, right). The second classification is obtained by the minimum root-mean-square distance (RMSD, dark green) between the anomalies from the ECMWF System 4 and the KM classification from ERA-Interim. A detailed description of these methods can be found in the text.

as close as possible to their cluster centroid. The cluster partitions are obtained from an iterative process, and the centroid coordinates are those leading to the maximum variance ratio. In this work cluster partitions have been generated from 100 iterations with 30 different initial centroids. This iterative process is the reason that the average monthly frequency of occurrence associated with each regime can vary when the cluster analysis is repeated. Although typically the centroid coordinates are obtained by projecting the anomaly field onto empirical orthogonal functions, here the KM method has been directly applied over the area weighted (by the cosine of the latitude) daily SLP anomalies to take into account extreme SLP values. The

main difficulty of the KM methodology is how to choose the optimal number of clusters (R). In this work, four clusters (R=4) are selected, because it is the value traditionally employed in the literature for the WR assessment (e.g. Fil and Dubus 2005; Dawson and Palmer 2015).

Method 2 – root-mean-square distance (RMSD): is based on the sum of squares differences between the SLP daily anomaly maps from ECMWF System 4 (corresponding to each day, member and forecast time) and a set of clusters employed as a reference. In this work, the reference is the four clusters obtained from the ERA-Interim reanalysis for each separate month. Then, the particular day is assigned to the cluster for which the RMSD is minimum (Neal et al. 2016). This method guarantees that the predicted WRs have very similar spatial structures to the observed regimes, which is essential for their verification.

Firstly, the monthly WR classification has been obtained for the ERA-Interim reanalysis (Figure 40, left side) by the application of the KM clustering approach. The WR classification has been obtained for all the months of the year and also for the boreal winter season to investigate the differences between the WRs estimated separately for each month and the more traditional WRs estimated for each season. The resulting ERA-Interim WRs have been used to explore the role of the WRs on the wind speed and temperature variability.

To obtain the WRs based on the seasonal forecasts from ECMWF System 4 (Figure 40, right side) two different approaches have been adopted. The first method is the same KM cluster analysis that has been used with the ERA-Interim reanalysis, which is useful to investigate how the seasonal forecast systems simulate the weather regimes. As an alternative approach, a WR classification based on the minimum root-mean-square distance (RMSD) between the predicted SLP daily anomalies and the defined clusters from the ERA-Interim reanalysis has been obtained. Although the fair verification of the WRs computed from seasonal forecasts could require that these regimes would be obtained independently from the observational reference, the KM approach presents some limitations when applied to seasonal forecasts. To deal with these limitations, the RMSD methodology is proposed.

5.1.3 Metrics for the weather regime evaluation

Different metrics have been used to evaluate the WR performance in terms of spatial patterns, frequency distribution and also the WR impact on 10-m wind speed and 2-m air temperature. These metrics and the significance tests used are described below.

Composite maps: represent the average of the anomaly maps for all the times that a given condition occurs. In this case, the composite maps have been produced by averaging the maps of the daily anomalies in a specific month (mon) belonging to each specific regime $(r = 1, ..., R)$ in the 1982-2016 period. Therefore, the composite

map has been obtained as follows:

$$CM_{r,mon}(lat,lon) = \frac{1}{N}\sum_{t=1}^{N} z_{r,mon,t}(lat,lon) \quad (5.1)$$

where t^{th} $(t = 1,...,N)$ represents the specific day in the period 1982-2016 belonging to a specific weather regime (r^{th}). These maps have been computed to represent the SLP anomaly maps $(z_{r,mon,t})$ associated with each weather regime, but also to estimate the impact of the WRs on 10-m wind speed and 2-m air temperature.

In the case of the seasonal predictions, the composite maps for each specific regime and month have been computed as:

$$\hat{CM}_{r,mon}(lat,lon) = \frac{1}{N}\frac{1}{M}\sum_{t=1}^{N}\sum_{m=1}^{M} z_{r,mon,t,m}(lat,lon) \quad (5.2)$$

Where the $m^{th}(m = 1,...,M)$ denotes the specific ensemble member.

To evaluate if the composite maps are significant at the 95% confidence level a two-sided t-test under the null hypothesis that the mean of the composite is equal to the mean of the variable has been applied (see Appendix A, section A.3.1a).

Monthly frequency of occurrence: is the percentage of time in a month in which a WR is occurring. This frequency is measured as:

$$freq_{r,mon,yr}(\%) = \frac{ndays_{r,mon,yr}}{ndays_{mon,yr}} \cdot 100 \quad (5.3)$$

where $ndays_{r,mon,yr}$ is the number of days in a month and year belonging to a specific regime and $ndays_{mon,yr}$ is the total number of days in a month. The result is a time series of frequencies per cluster and month.

Spatial correlation: measures the product moment correlation between composite maps from the ECMWF System 4 seasonal forecasts and the corresponding one from the ERA-Interim reanalysis, aggregated over all grid points (Jolliffe and Stephenson 2012). It allows quantifying the potential performance of spatial field forecasts (WRs here). This metric is defined as:

$$SC_{r,mon} = \frac{\sum_{p=1}^{P}\left(\hat{CM}_{r,mon} - \bar{\hat{CM}}_{r,mon}\right)\left(CM_{r,mon} - \bar{CM}_{r,mon}\right)}{P\sigma_{\hat{CM}_{r,mon}}\sigma_{CM_{r,mon}}} \quad (5.4)$$

where P is the number of grid points $(p = 1,...,P)$, $\hat{CM}_{r,mon}$ and $CM_{r,mon}$ are the spatial patterns of the WRs in the seasonal forecasts and observational reference respectively. The $\bar{\hat{CM}}_{r,mon}$ and $\bar{CM}_{r,mon}$ are the averages of the WR maps over the P grid points. The $\sigma_{\hat{CM}_{r,mon}}$ and $\sigma_{CM_{r,mon}}$ are the standard deviation of the composite maps across the spatial grid. The spatial correlation ranges between -1 and 1. $SC_{r,mon} = 1$ indicates that the variation pattern

of the WR in the forecasts perfectly matches the WR spatial pattern in the observational reference. $SC_{r,mon} = 0$ shows that no matching between the spatial variations of the regimes can be found. If the variation of the WR pattern in the seasonal forecasts is completely reversed to the reference, *SC* takes the value of -1. A one-sided t-test has been applied to evaluate if the spatial correlation values are significant at the 95% confidence level (Appendix A, section A.3.1c).

Pearson correlation: has been defined in Appendix A (section A.1.1). It measures the temporal correspondence between the mean frequency of the WRs in the seasonal forecasts with that in the observational reference has been measured by the Pearson correlation coefficient (ρ). For the seasonal predictions, the monthly frequencies have been averaged over the 15 ensemble members. The Pearson correlation is analogous to the spatial correlation previously defined and it ranges between -1 and 1. If there is a perfect association between the ensemble mean of the frequencies and the frequencies of the observational reference $\rho = 1$. When $\rho = 0$ indicates that there is no association between them, and the negative values ($\rho < 0$) indicate that the ensemble mean prediction of the frequencies does not provide added value compared to the climatological frequency. A one-sided t-test has been applied to evaluate if the Pearson correlation values are significant at the 95% confidence level.

Reconstruction of the climate variables: WRs frequencies ($freq_{r,mon,yr}$) and the composite maps resulting from the projection of wind speed and temperature onto the WR frequencies have been used to assess the effectiveness of the WRs in reproducing the variability of these climate variables. The reconstructed climate variable (*varRecon*) are obtained by the following equation:

$$varRecon_{mon,yr}(lat,lon) = \sum_{r=1}^{R} CM_{r,mon}(lat,lon) \cdot freq_{r,mon,yr} \quad (5.5)$$

where $freq_{r,mon,yr}$ is the percentage of days in a month and year assigned to a specific cluster and $CM_{r,mon}(lat,lon)$ is the composite map of the variable to be reconstructed for each WR in a particular month. The reconstruction has been applied in leave-one-out cross-validation, which means that the anomalies corresponding to the year to be reconstructed are excluded for the computation of the composite maps.

5.2 Weather regimes in ERA-Interim

To characterise the differences between the traditionally defined seasonal weather regimes (December-January-February) with those obtained for the individual months (December, January and February) WR spatial patterns are shown in Figure 41.

Clusters 1 and 4 (Figure 41, first and fourth rows) in DJF are similar to the positive and negative phases of the North Atlantic Oscillation (NAO) (Hurrell et al. 2003). However, there are some differences between these clusters

and the spatial pattern of the NAO computed as the leading principal component of the SLP in the North Atlantic (shown in chapter 4). The principal component analysis produces modes of variability that are symmetric (i.e. the positive and negative phases present the same spatial distribution of their centres of action, but with opposite signs). Nevertheless, the KM cluster analysis seeks the most steady states in the atmosphere, which allows identifying independent positive and negative phases (Barrier et al. 2014). It has been demonstrated that the positive and negative phases of the NAO are not symmetric (Cassou et al. 2004; Luo et al. 2018), which is consistent with the results displayed in Figure 41, where Cluster 1 shows centres of action closest to Europe than Cluster 4. Hence, the cluster analysis can be more adequate to describe the atmospheric conditions and their impact on user relevant variables than the principal components analysis.

The monthly-defined WRs for Clusters 1 and 4 are very similar to the DJF spatial patterns. The only exception is found in January, when Cluster 1 shows a centre of negative SLP anomalies over the British Isles instead of the dipole-like pattern shown in the rest of the months. The WR characterised by Cluster 1 leads to different wind speed and temperature responses in January with stronger-than-average wind speed and temperatures in France, the Iberian Peninsula and the North Atlantic (Figures 42 and 43). This result illustrates how a monthly classification allows to better discern the month-by-month variability, an aspect that can be very relevant from a user point of view. For example, positive wind speed anomalies over south-western Europe can be produced by the occurrence of an atmospheric pattern similar to Cluster 1.

The Cluster 2 (Figure 41, second row) in the boreal winter season shows a centre of positive SLP anomalies over Scandinavia covering most of European region. This anomalous anticyclonic circulation is known as Blocking (Vautard 1990) and it leads to a strong reduction of wind speed over most of the European continent (Figure 42). In this atmospheric configuration, the westerlies are not able to reach the European continent as they are shifted to either northern Scandinavia or the Mediterranean region. For that reason, positive wind speed anomalies (Figure 42, second row) appear in both regions and an increase in temperature (Figure 43, second row) appears in northern Europe. The spatial pattern obtained as Cluster 2 in the DJF classification is similarly obtained in December, January and February and their frequencies of occurrence exceed 25%, which illustrates that this weather regime plays a dominant role in the Euro-Atlantic climate in winter. The reduction of wind speed and temperatures associated with Cluster 2 over central Europe can have consequences for the wind energy sector as it can produce economic losses related to the increase of energy demand and the reduction of wind energy supply. Consequently, the anticipation of these events could be very helpful to mitigate the risks related

to these atmospheric conditions.

The Cluster 3 (Figure 41, third row) pattern resembles the Atlantic Ridge, which has also been obtained in seasonal WRs classifications (Fil and Dubus 2005; Cassou 2008; Ferranti et al. 2015). This cluster is characterised by a dipole with positive anomalies over the North Atlantic and the southwestern European countries, and negative anomalies over Scandinavia. The anticyclonic anomaly over central North Atlantic brings cold air from Greenland to the Iberian Peninsula, as shown by the negative temperature anomalies in that area (Figure 43). However in most of the European continent, an increase of wind speed (Figure 42, third row) and temperature (Figure 43, third row) appear as a response to the cyclonic anomalies covering most of the European region. In the classifications obtained for December, January and February this pattern shows slightly different structures. While in December, the Cluster 3 is shifted to the south in comparison with that in DJF, in January a north-south SLP gradient together with an increase of the temperature and wind speed in eastern Europe much more intense than for the rest of the months can be identified.

The ERA-Interim WRs from March to November have been included in the Appendix B (Figures B22, B23 and B24). The KM cluster analysis has been applied over each month individually which results in WRs with spatial patterns for some specific months which do not have any correspondence with those regimes obtained for the previous or the following month. One example of this can be observed in April (Figure B22) for which the Cluster 1 cannot be identified in March or May. Besides, the spatial patterns of the WRs show an annual cycle, with the anomalies of the regimes in the winter months being much more intense than those for summer (Figure B23). This reduction of the WR anomalies is found for the summer months because is in this season when the atmospheric circulation depends more on local processes (Beck et al. 2007).

Despite the randomness of the KM classification that can lead to differences in the frequencies of occurrence of each cluster every time the cluster analysis is performed, some general properties of the frequency of occurrence can be highlighted. Cluster 1 is the most frequent pattern in DJF and February and Cluster 2 is the most frequent in December and January. This shows that in December and January the most recurrent circulation pattern is the one characterised by the anticyclone over Scandinavia, while in February a north-south dipole of sea level pressure anomalies over the Euro-Atlantic region, similar to the positive phase of the NAO, is the most frequent pattern. Cluster 4 is the pattern with the lowest frequency in DJF, December and January, however, in February, the lowest frequency corresponds to Cluster 3. These discrepancies between the frequencies of each cluster for the different months and the seasonal classification evidence the importance of considering intra-seasonal information in the atmospheric classification.

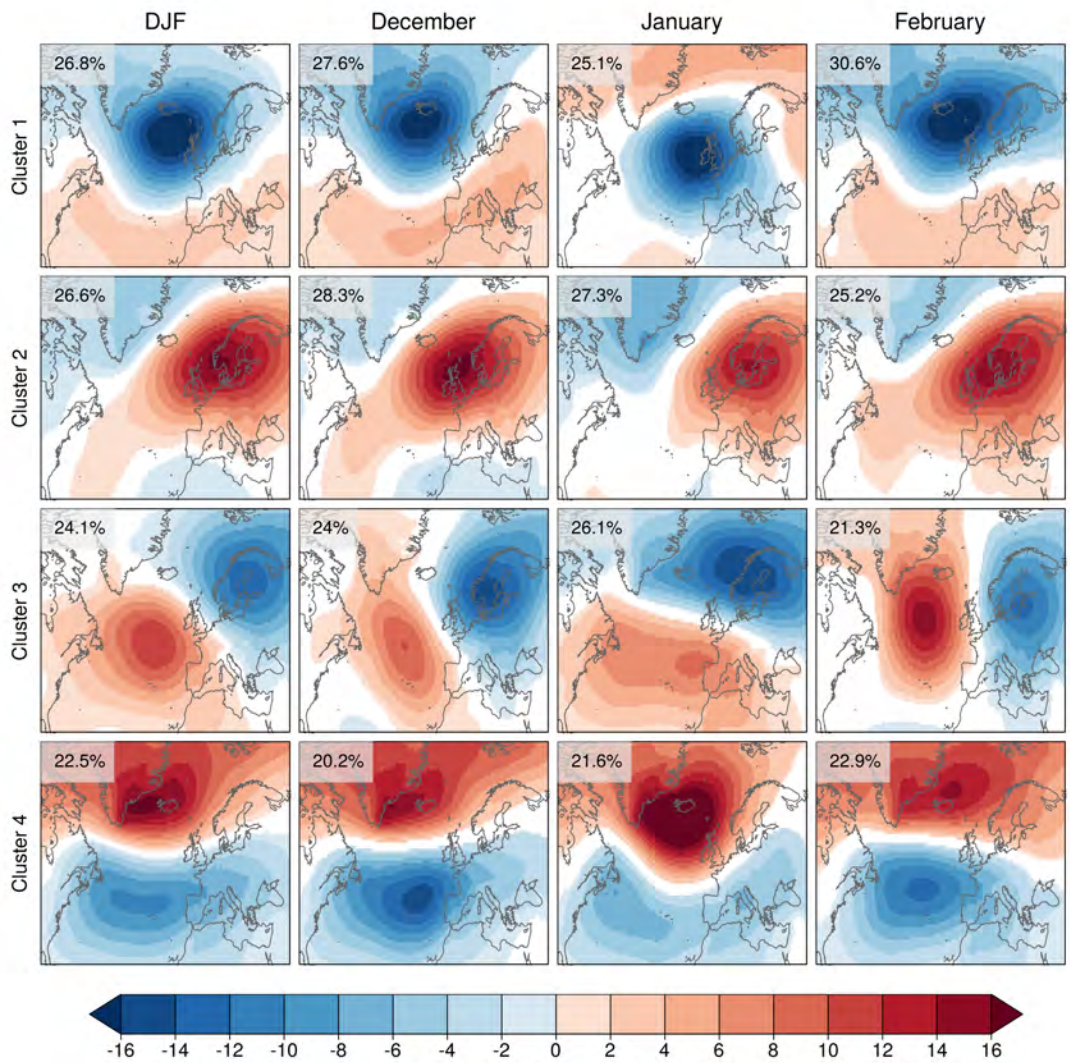

Figure 41 – Composites of the averaged sea level pressure anomalies (hPa), belonging to each one of the clusters obtained by the KM classification in December-January-February (first column), December (second column), January (third column) and February (fourth column). The climatological frequency of each cluster (displayed in the top-left corner) indicates the percentage of days in the 1982-2016 period assigned to each cluster. White areas correspond to regions where the anomalies are not significantly different from zero.

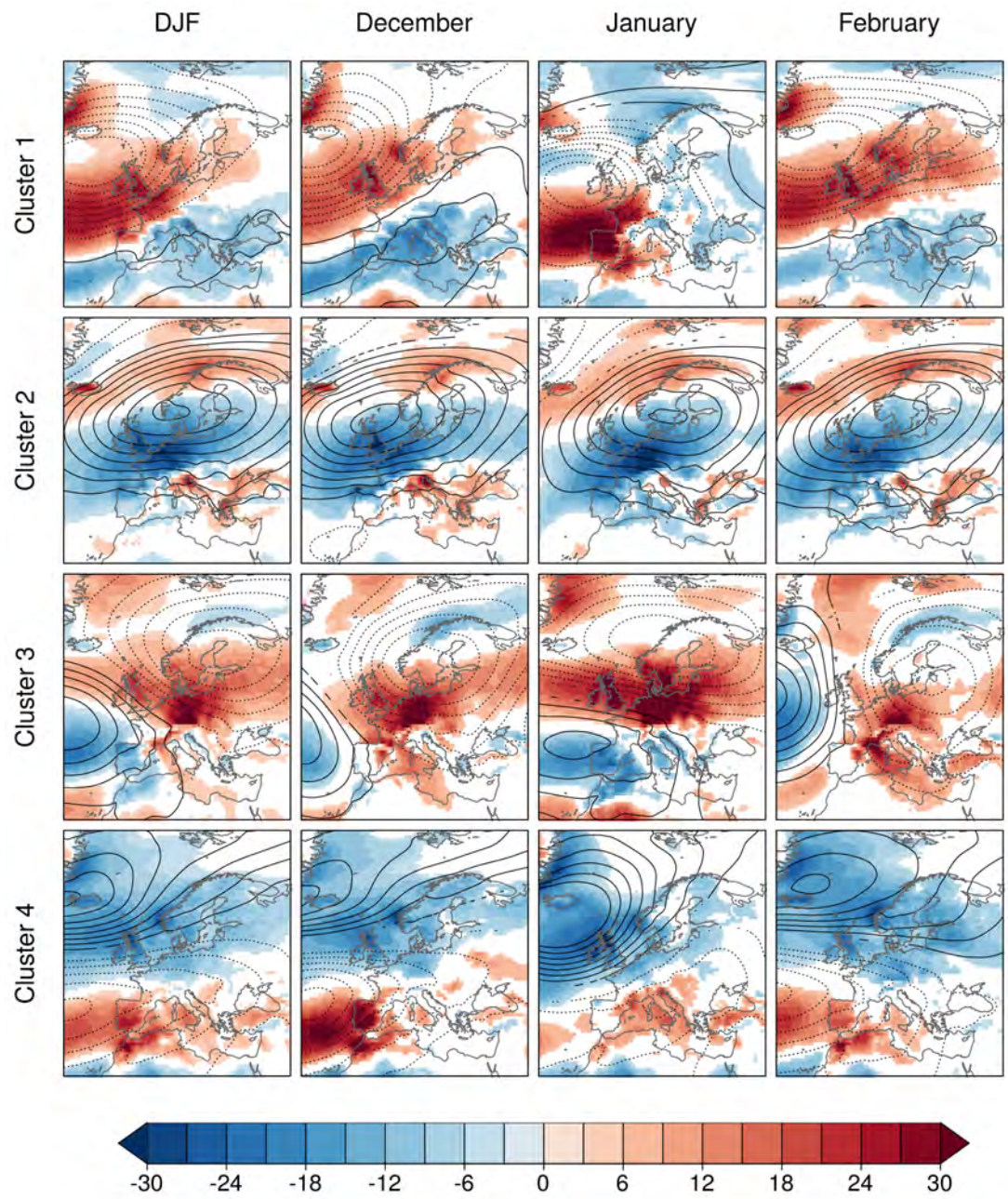

Figure 42 – Composites of the 10-m wind speed (m/s) computed from the daily anomalies occurring in each weather regime for December-January-February (first column), December (second column), January (third column) and February (fourth column) classifications. White areas denote regions where the anomalies are not significantly different from zero (t-test at a 95% confidence level).

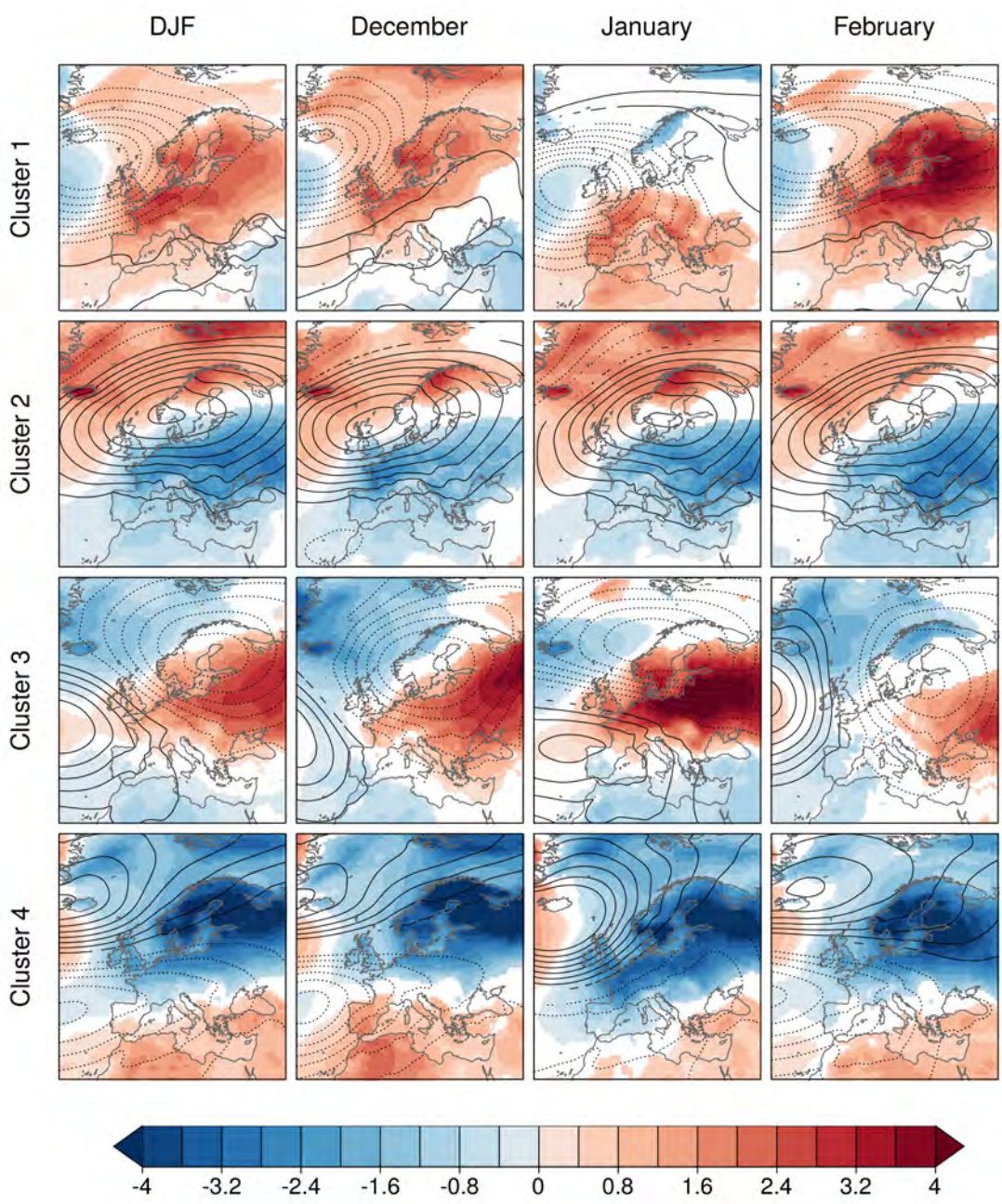

Figure 43 – Composites of the averaged 2-m air temperature (K) computed from the daily anomalies occurring in each WRs for December-January-February (first column), December (second column), January (third column) and February (fourth column) classifications. White areas denote regions where the anomalies are not significantly different from zero (t-test at a 95% confidence level).

5.3 Reconstructing impact variables with WRs

There are several studies in which a certain type of circulation or regime is related to a specific extreme event, such as the heat waves (Cassou et al. 2005; Quesada et al. 2012; Alvarez-Castro et al. 2018). However, the combined effect of the WRs in a particular region and variable has not been quantified yet. To understand the amount of wind speed and temperature variability that can be explained in terms of changes in the frequency of occurrence of weather regimes, these variables have been reconstructed as described in section 5.1.3. The comparison between the reconstructed and original variables enables the identification of regions where the weather regimes are a good approximation to describe the impact of the atmospheric circulation on the variability of wind speed and temperature. This is very interesting for wind energy applications as the anomalies in relevant climate variables could be understood in terms of specific regimes.

The performance of the method to reconstruct the air temperature and wind speed using the WR frequencies is estimated by the Pearson correlation (Figure 44). This metric is used to investigate if the inter-annual variability of the wind speed and air temperature can be recreated by the reconstructed variables and also to identify in which months and regions WRs are dominating their variability. Figure 44 shows the results of these correlations for the winter months, but the results for all the months of the year can be found in the Appendix B (Figures B25 and B26).

There are some regions in northern Europe, such as the British Isles, northern France, Germany, Denmark and also southern Scandinavia where high correlations are found. This reveals that in adjacent regions to the North Sea, WRs play a dominant role on the wind speed and air temperature variability. However, there are month-by-month variations in the strength of this relationship. For example, in December and February positive and significant correlations are found for the reconstructed wind speed (Figure 44, top row) over Iceland, but in January these correlations drop to 0. This reflects that either the WRs are not dominating the wind speed variability in that specific month or that the classification obtained is not representative for that region. A similar result is obtained for the Iberian Peninsula in February. Southeastern Europe is the region where the correlations are negative for the different months showing the poorest influence of the WRs on the wind speed.

In the case of temperature (Figure 44, bottom row), most of the European countries show positive and significant correlations in the winter months, which evidences that changes in the frequency of occurrence of the WRs drive the temperature variability. In December and January the correlations are near zero over Italy, and something similar occurs in northern Scandinavia in January. This suggests that there are additional factors to the WRs affecting the 2-m air temperature in those regions.

These results suggest that there are several regions in Europe where the variability of wind speed and temperature can be reconstructed by the monthly frequencies of occurrence of WRs in winter. Although it is important to mention that this conclusion cannot be extended to other months of the year (Figures B25 and B26) for which the WRs are less efficient to explain the surface variability, as illustrated by the reduction of the correlation values between the reconstructed and the original variables. Nevertheless, the identification of regions where WRs are dominating the variability of wind energy resources is crucial as future changes in the atmospheric circulation could lead to changes in the wind speed and air temperature and consequently in the energy resources.

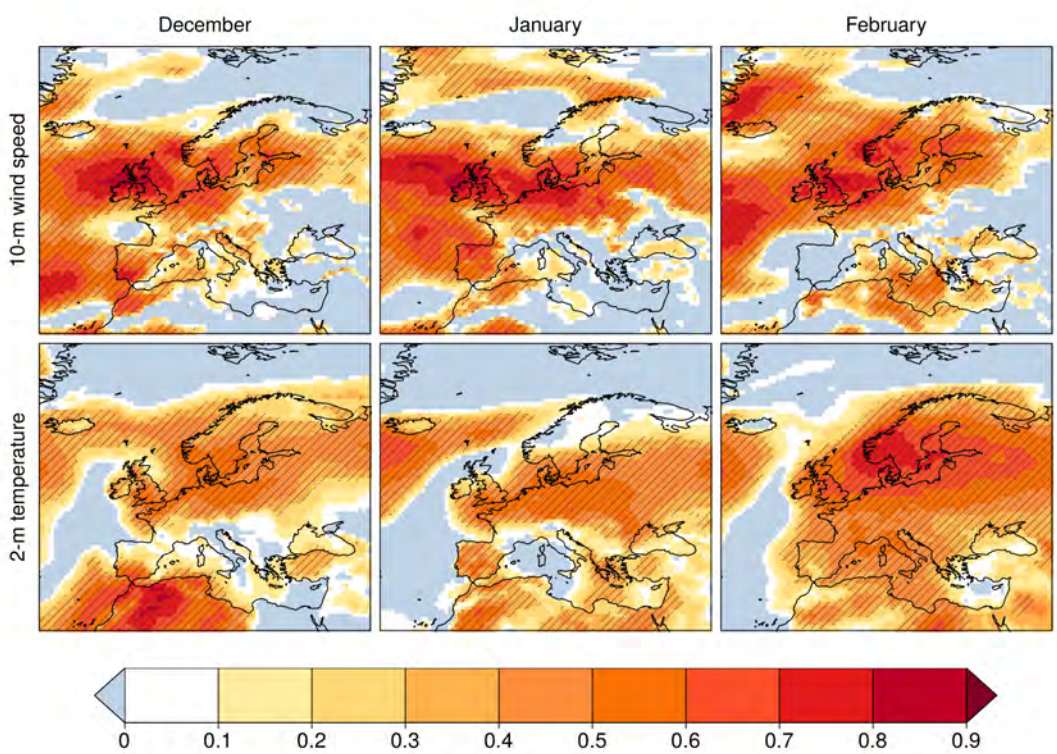

Figure 44 – Pearson correlation between the reconstructed 10-m wind speed (first row) and 2-m temperature (second row) based on weather regimes and the original variables from ERA-Interim. These results have been obtained for the individual months: December, January and February. Hatched areas denote regions where the correlations are significantly different from zero (one-sided t-test at a 95% confidence level).

5.4 Seasonal forecast verification of weather regimes

The limited number of studies about WRs based on seasonal predictions have employed different approaches to classify the simulations. For example in Fil and Dubus (2005) WRs are computed by the application of the KM method (detailed in section 5.1.2), but in Neal et al. (2016) the seasonal predictions of WRs have been obtained with the RMSD assignation method (described in section 5.1.2). The WR spatial structures and the associated spatial patterns of wind speed and air temperature resulting from the two methods have been compared. The linear correspondence between the frequencies of the WRs in the seasonal forecasts and in the observational reference, which can be interpreted as a measure of the WR potential skill, has been evaluated.

5.4.1 Spatial patterns

The capacity of the KM and RMSD methods to produce similar spatial patterns to those observed has been quantified in terms of spatial correlations (metric described in Section 5.1.3) between the WRs based on ECMWF System 4 seasonal forecasts and the corresponding WRs from ERA-Interim for all the months and lead times available (Figure 45).

The spatial patterns of the WRs computed from the seasonal forecasts with the KM method (Figure 45a) have some differences with the ERA-Interim WRs, as indicated by the negative and non-significant spatial correlations in certain months and leads. For example, Cluster 1 displays negative and non-significant correlations with the ERA-Interim Cluster 1 for most of the lead times in April. Figure B27 illustrates the important differences in the spatial patterns of the WRs for April from ECMWF System 4 and ERA-Interim. The ERA-Interim Cluster 1 (Figure B27) consists of a centre with negative anomalies over the North Atlantic and positive anomalies in northern Scandinavia and North Africa. This structure is not found in any of the clusters from ECMWF System 4. Only Cluster 4 shows some similar features for some lead months, although the anomalous cyclonic circulation is shifted to the south-western North Atlantic, and the positive anomalies cover most of the European continent.

The difficulties in matching the WRs from the seasonal predictions with those from the observational reference occur also in months other than April. This is the case in May, August and October for Cluster 3 (Figure 45a) and in December for Cluster 1 for lead months 1 and 5. These results illustrate that the spatial patterns (WRs) derived from the seasonal predictions with the KM method cannot be automatically identified in the observational reference, preventing the verification of the forecasts of the WRs. As verification is a crucial step in the development of climate information to guide decision-making processes, the WRs obtained from the KM methodology are not a suitable product to be integrated into a climate service tailored to the wind energy sector.

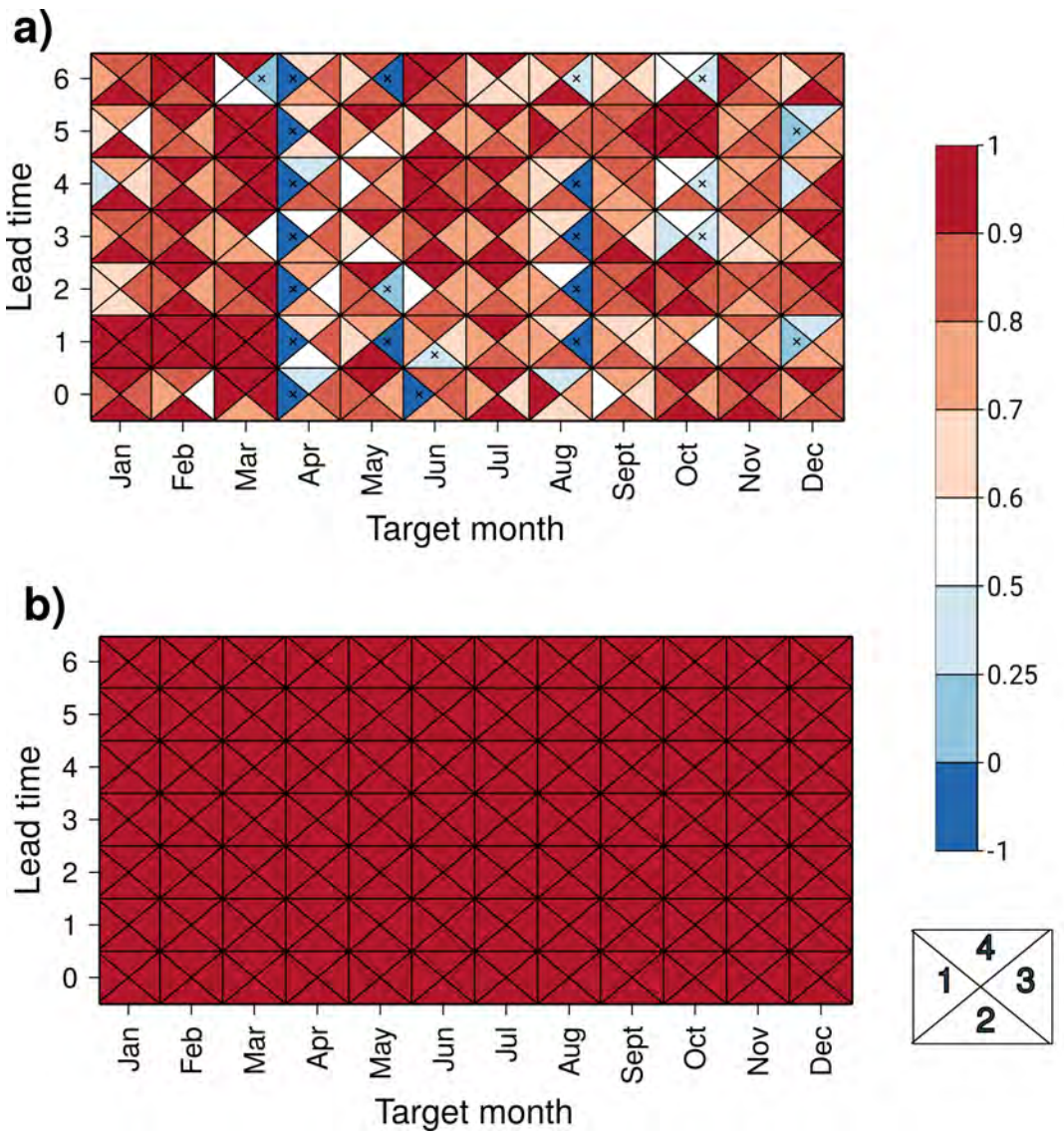

Figure 45 – Spatial correlation between the ECMWF System 4 seasonal predictions and ERA-Interim reanalysis monthly weather regimes patterns obtained by the a) KM and b) RMSD methods. The classifications have been performed with daily sea level pressure anomalies in the 1982-2016 period. Each triangle represents the correlations for each of the four clusters as indicated in the bottom right legend. The spatial correlations are shown as a function of the target month (x-axis) and lead time (y-axis). Crosses denote non-significant correlation values (two-tailed t-test at a 95% confidence level).

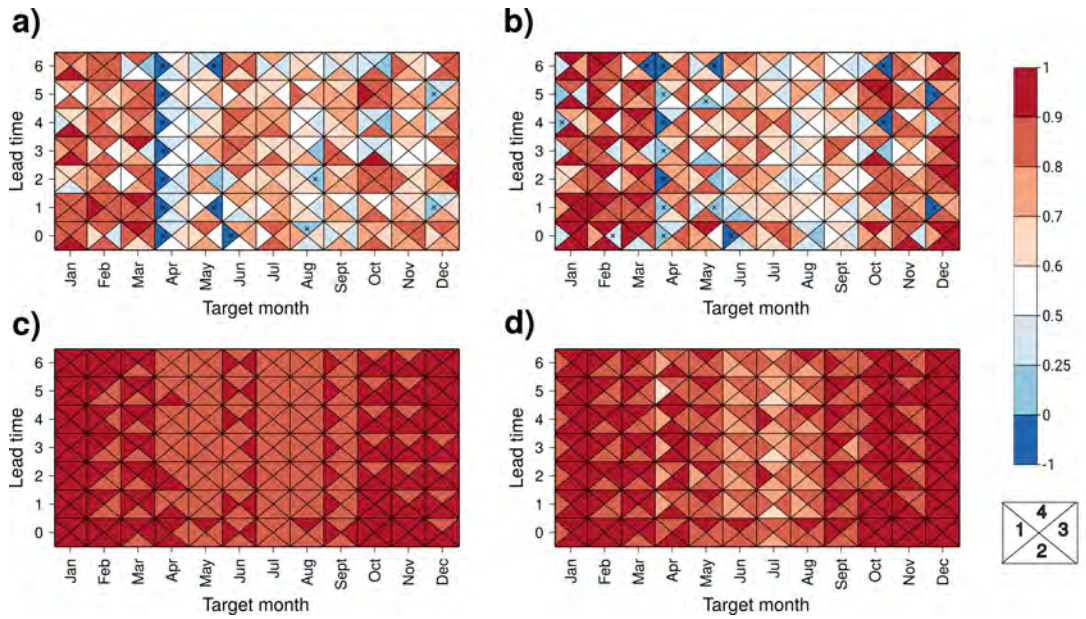

Figure 46 – Spatial correlation between the ECMWF System 4 seasonal predictions and ERA-Interim reanalysis composites of the (a,c) 10-m wind speed and (b,d) 2-m temperature with monthly WRs obtained by the (a,b)KM and (c,d) RMSD methods. The classifications have been performed with daily sea level pressure anomalies in the 1982-2016 period. Each triangle represents the correlations of the composites for each of the four clusters as indicated in the bottom right legend. The spatial correlations are shown as a function of the target month (x-axis) and lead time (y-axis). Crosses denote non-significant correlation values (two-tailed t-test at a 95% confidence level).

The WR classification obtained or the seasonal forecasts by the RMSD method (Figure 45b) shows spatial patterns very consistent with the ERA-Interim WRs for all months and lead times, with spatial correlations above 0.9. This occurs because the RMSD approach seeks to group simulated daily SLP anomalies similar to those from the ERA-Interim reanalysis. Consequently, it is expected that WR maps obtained for the predictions show a high resemblance to those in the observational reference. As an example of the spatial patterns provided by RMSD method, the spatial patterns corresponding to April have been included in the Appendix (Figure B28). In this case, the spatial patterns of the WRS corresponding to the predictions can be clearly identified in the observations.

Spatial correlations have also been used to quantify the correspondence between the composite maps of wind speed and temperature obtained for the monthly WR classification in each month (Figure 46). The results show that the impact of those WRs obtained for the seasonal forecasts from the RMSD method (Figure 46, c and d respectively) show higher

resemblance to the wind speed and temperature composites obtained for ERA-Interim (as their spatial correlations are above 0.7 for all months and lead times) than those obtained by the KM method (Figure 46, c and d, respectively).

Spatial correlations of the composite maps for wind speed and temperature (Figure 46), are lower than for sea level pressure (Figure 45), regardless of the method employed to derive the weather regime classification. This is related to the application of the clustering using the SLP, which leads to robust spatial patterns of SLP for which the intra-cluster variance is maximised. This effect is attenuated in the case of wind speed and temperature, as the classification is performed with SLP, and consequently, the local factors that affect the wind speed and temperature spatial distributions are not taken into account. Besides, the systematic errors of the seasonal forecasts of wind speed and temperature also could lead to differences in the spatial correlations of their composite maps.

The comparison of the KM and RMSD approaches to obtain WRs from the seasonal predictions reveals that the assignation based on the minimum distance (RMSD) provides spatial patterns that can be identified also in the ERA-Interim WRs. This is an essential requirement for the verification of the WRs based on the predictions, and consequently to provide a weather regime product to the users. However, the application of the KM to derive a WR classification is interesting for the modellers, as it is useful to identify the critical months for which the WRs are very different from those in the observational reference. This result highlights an important type of systematic error in the atmospheric circulation that needs to be addressed.

5.4.2 Skill of the predicted weather regimes

To investigate the correspondence between the monthly frequency of occurrence of the clusters obtained from the seasonal predictions and those from the observational reference, both bias and Pearson correlation have been estimated. The results for the biases have been included in the Appendix B (Figure B29). Biases are higher for those frequencies corresponding to the WR classification obtained with KM than with RMSD, although most of them are not statistically significant.

Figure 47 shows that RMSD method provides better correlations than the KM method for all target months and clusters (Figure 47). Nevertheless, positive and significant correlations are mostly restricted to lead 0 for all the target months. In particular, the KM method only shows positive and significant correlations for the frequencies of all clusters in January, October, November and December (Figure 47a). The monthly frequencies obtained by RMSD (Figure 47b) have positive and significant correlations for lead 0, except in May, July and September when these correlations are positive but non-significant. Beyond lead 0, the ability of the seasonal forecast system to reproduce the monthly frequencies of the WRs drops, and only positive correlations are found for the

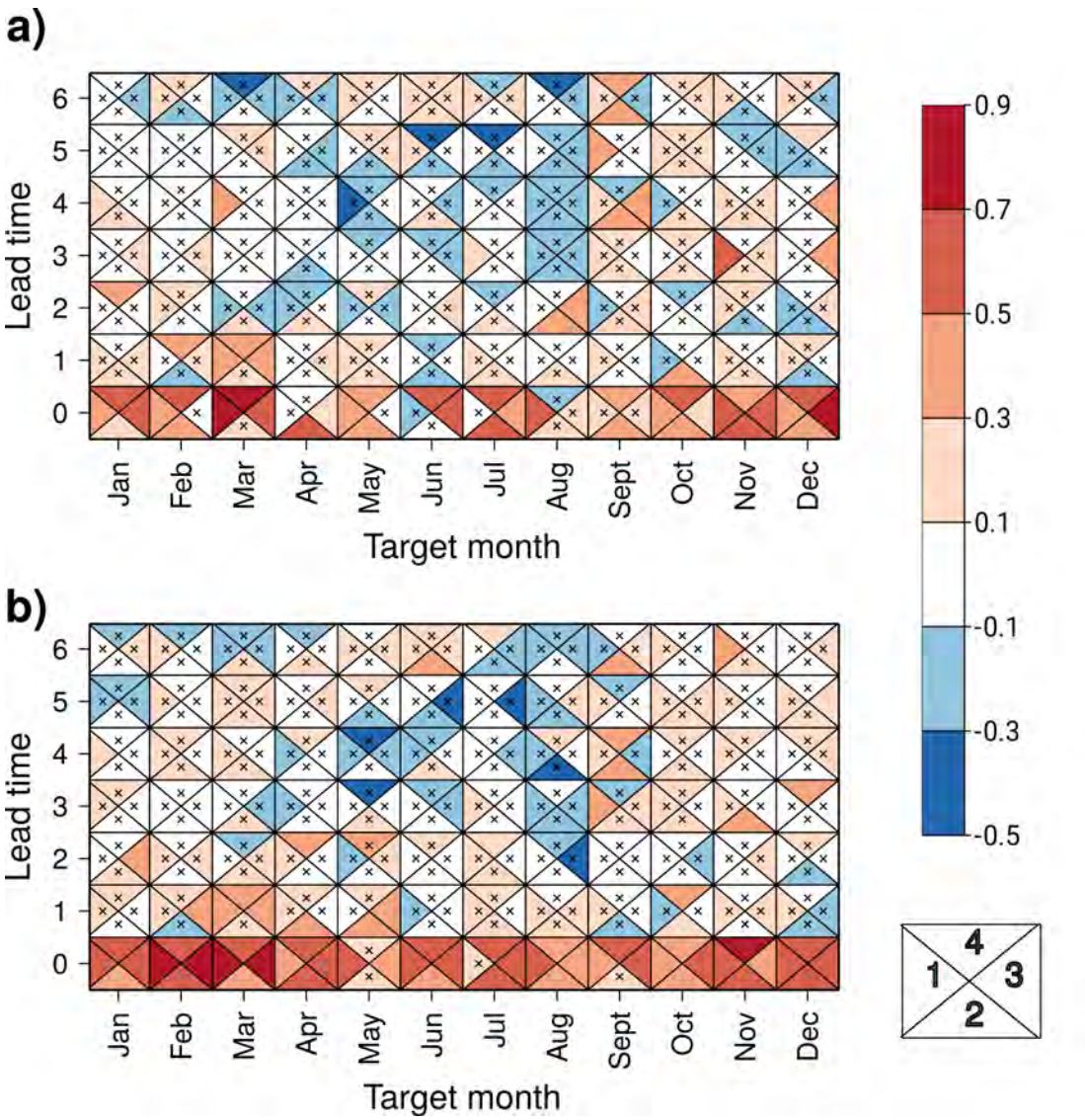

Figure 47 – Pearson correlation between the ECMWF System 4 seasonal predictions and ERA-Interim reanalysis monthly frequencies of occurrence corresponding to the WRs obtained by the (a) KM method and (b) RMSD methods. The classifications have been performed with daily sea level pressure anomalies in the 1982-2016 period. Each triangle represents the correlations for a specific cluster as indicated in the bottom right legend. The spatial correlations are shown as a function of the target month (x-axis) and the lead time (y-axis). Crosses denote non-significant correlation values (two-tailed t-test at a 95% confidence level).

frequencies of some clusters for some leads in what looks like a random distribution. However, one exception can be found in March, when the WRs obtained by the two different methods show positive correlations for Clusters 1, 3 and 4 for the predictions initialised in February (1 lead month).

Despite the fact that the frequencies associated with the WRs obtained by RMSD provide slightly better correlations than those obtained with the KM method, the differences are low. This demonstrates that the limited potential skill of the WRs in the seasonal forecast system is not a result of the approach used to perform the classification. The difficulties of the seasonal forecast system to reproduce the monthly frequencies of occurrence of the WRs can be related to the lack of predictability of the sea level pressure at seasonal timescales in the North Atlantic region (e.g. Kim et al. 2012). Further work is clearly needed to improve the capability to predict the WRs in this area.

5.5 Conclusions

WR classifications have been performed for each season and each month of the year. The differences between the monthly and seasonal WR classifications illustrate that there is intra-seasonal variability in the most recurrent atmospheric circulation, and this affects the description of the WR impact on surface variables such as wind speed and air temperature. This is particularly the case during the equinoctial seasons. The set of WRs obtained for each month is more suitable to explore the role of changes in the atmospheric circulation to drive the climate events that occur at specific months such as wind droughts affecting the Euro-Atlantic region, which can have several implications for the renewable energy sector (Raynaud et al. 2018).

Wind speed and temperature variability can be efficiently reconstructed by employing WRs in several regions over Europe. However, this technique has limitations because it only works in areas and times of the year when WRs play a dominant role on the climate conditions at the surface. It is only in those cases when WRs can be confidently exploited to produce useful information for the wind energy sector. Although the reconstruction has been applied to the wind speed and temperature, it can be used to reconstruct different indicators tailored to specific user needs. For example, the reconstruction of the 95^{th} percentile of the wind speed, which is an indicator of the highest wind speed values in a month, could be useful to explore the role of the WRs in representing the variability of the high wind speed values. The ability of ECMWF System 4 to predict monthly WRs for the different months and lead times has been explored to investigate the potential of the seasonal forecasts to anticipate changes in the atmospheric circulation and their impacts. Two different approaches to derive the monthly WR classification based on seasonal forecasts have been compared. The results reveal that the classification obtained with the RMSD method displays a higher resemblance

(in terms of their spatial structures) to the ERA-Interim classification than those obtained with the KM method. This suggests that in the case a monthly WR classification for seasonal forecasts is performed, the RMSD method is recommended because it produces spatial patterns that can be easily found in the reference WRs, which is essential for their verification.

Nevertheless, the evaluation of the inter-annual variations of the monthly frequencies of occurrence in the WRs obtained with the KM and RMSD methods yields similar results for both approaches. The potential skill of the WRs is restricted to lead 0. These results show that WRs computed for ECMWF System 4 have limited skill to simulate the monthly frequencies of occurrence of WRs, which can be the consequence of the limited predictability of the ECMWF System 4 in the SLP over Europe and that it is shown in the Appendix (Figure B30). To further explore this issue, future research will focus on the assessment of the sensitivity of these results to the different assumptions used in this work such as the variable used to define the WR, the spatial domain or the number of clusters. In addition this analysis could be repeated for those seasonal forecast systems that have demonstrated good levels of skill in the North Atlantic (Athanasiadis et al. 2017; Baker et al. 2018) and for different regions with higher seasonal forecast quality in the sea level pressure than Europe such as North America (Figure B30), which, at the same time, is also a key region for the wind industry.

06

Bias adjustment and verification for wind energy applications

06 Summary

Objective

To develop tailored products that facilitate the widespread use of seasonal forecasts by the wind energy sector through an effective climate service. These products should have two main properties: they need to have adjusted the pervasive forecast bias and provide an estimate of the expected forecast quality. Therefore, the suitability of bias adjustment and reconstruction methodologies to generate seasonal predictions of wind speed usable for wind energy applications are explored. Furthermore, a comprehensive forecast quality assessment that investigates the potential of seasonal forecasts of the mean and extreme wind speed in a season.

Methodology

- Three different bias adjustment approaches: simple bias adjustment, calibration and quantile mapping.
- Linear-regression method to estimate a dynamical-empirical prediction based on the seasonal predictions Niño-3.4 index and the empirical relationship of the 10-m wind speed from the Niño-3.4 index from ERA-Interim.
- Four extreme indices have been defined: 10^{th}(q10) and 90^{th} (q90) percentiles and the fraction of time below/above the $10^{th}/90^{th}$ climatological percentile in a season ($fbq10_{clim}/faq90_{clim}$).
- Deterministic and probabilistic verification metrics (defined in Appendix A)

Results

- Seasonal forecasts of near-surface wind speed from ECMWF System 4 have skill in several regions where there is substantial installed wind power. Besides, after the application of bias adjustment, these predictions are reliable for their use in decision-making.
- Bias adjustment approaches lead to a reduction of the Pearson correlation due to the degeneracy of the information caused by the application of these methods in cross-validation. However, the use of cross-validation is unavoidable with small samples typically available in seasonal climate prediction.
- Probabilistic forecasts improve when bias adjustment is applied due to the sensitivity of the corresponding forecast quality metrics to the systematic errors in the mean, variance and spread. Particularly, the calibration method provides marginally more reliable predictions than the simple bias adjustment and quantile mapping techniques.
- The hybrid empirical-dynamical reconstruction method improves the potential skill of the 10-m wind

speed in Canada and northern Argentina, which are regions for which ECMWF System 4 does not reproduce the ENSO teleconnections of wind speed found in the observational reference. This improvement is particularly important for long lead times.

- Extreme wind speed indicators based on climatological thresholds ($ftaq90_{clim}$ and $ftbq10_{clim}$) do not require a bias adjustment stage because these indices are computed from the climatological percentiles defined in the forecasts and observational reference separately. However, the absolute wind speed extreme indices (q10 and q90) present systematic errors that need to be adjusted when these indicators are used for wind energy applications.

- The Pearson correlation of the extreme wind speed indicators is similar to those of seasonal mean wind speed, which suggests that the predictability of the extreme events arises largely from the forecast system capacity to predict the mean value.

Conclusions

- Seasonal climate predictions of 10-m wind speed can be used by the wind industry in decision-making processes to replace the current naive climatological information in a number of regions.

- Bias adjustment is indispensable for the predictions to be usable, as the energy models require seasonal predictions with similar statistical properties as the observational references. In particular, the calibration approach allows to also improve the reliability, a crucial aspect when probabilistic information is provided to the users.

- The combination of the dynamical and empirical information in the reconstruction approach is a good option to produce information for the wind energy users in regions such as Canada, where the dynamical seasonal forecast systems do not show correct ENSO teleconnections to 10-m wind speed.

- Extreme wind speed indicators can be more informative than the mean wind speed for some wind energy applications. Thus, the similar levels of forecast quality to the mean wind speed is an encouraging result.

- A bias adjustment strategy should be defined in the case of the forecasts for the 10^{th} and 90^{th} percentiles as these indicators are affected by systematic errors. However, the $ftaq90_{clim}$ and $ftbq10_{clim}$ indices do not present those biases and could be directly integrated into a climate service that inform in wind energy decision-making processes.

Publications

Some of the results included in this chapter have been published in :

- **Torralba, V.**, F. J. Doblas-Reyes, D. MacLeod, I. Christel, and M. Davis, 2017: Seasonal climate prediction: A new source of information for the management of wind energy resources. *Journal of Applied Meteorology and Climatology*, 56 (5), 1231–1247, doi: 10.1175/JAMC-D-16-0204.1.

06

Bias adjustment and verification for wind energy applications

One of the main limitations for the integration of the seasonal predictions in wind energy decision-making processes has been the systematic errors affecting these predictions. As it has been mentioned in previous chapters, these errors result from the inability of the climate models to numerically reproduce all the relevant processes responsible of climate variability, but also from the initialization and the limited model resolution (Doblas-Reyes et al. 2013b). Apart from the biases in the mean and other moments of the distribution, for probabilistic forecasts, additional difficulties appear such as the lack of forecast reliability (Pinson 2012). Hence, seasonal predictions require a bias adjustment stage to statistically resemble the observational reference, minimise forecast errors and formulate reliable probabilities.

The bias adjustment of the seasonal predictions of wind speed has been identified as a requirement of the wind energy sector to fulfil acceptable reliability requirements to include these predictions in their decision-making processes. Nevertheless, the application of these methods on seasonal forecasts of wind speed remains as a challenge (Torralba et al. 2017b). Bias adjustment approaches have been already used at several time-scales, and they are starting to gain relevance for the adjustment of systematic errors of seasonal forecasts (Crochemore et al. 2016; Ogutu et al. 2017; Zhao et al. 2017). However, their application has been restricted to temperature and precipitation. In this chapter three bias adjustment methods are employed to correct ECMWF System 4 seasonal predictions of 10-

m wind speed: simple bias adjustment (Leung et al. 1999), quantile mapping (Themeßl et al. 2011) and calibration (Doblas-Reyes et al. 2005). The impact of these adjustments on the forecast quality has been explored with several verification metrics, which have been fully described in Appendix A.

The forecast quality assessment has been used to evaluate the performance of the ECMWF System 4 seasonal prediction system as well as the impact of the bias adjustment techniques on wind speed seasonal forecasts. The goal is to offer the most general and, a priori, relevant information for a user in the wind energy sector instead of the traditional view offered by climate scientists where the information provided to the users is mainly based on the correlation. Correlation is a very useful metric but gives only a small part of the information the user needs.

There are several regions for which the seasonal prediction skill is very limited. This represents a crucial problem for the users who want to employ this information for different applications. One example of the limited skill has been illustrated in chapter 4, where ENSO teleconnections to wind speed are not correctly simulated by the ECMWF System 4 in northern North America. To address this problem a reconstruction method has been applied to derive seasonal predictions of 10-m wind speed with improved forecast quality. Particularly, the reconstruction of 10-m wind speed from the seasonal predictions of the Niño-3.4 index and the empirical relationship between Niño-3.4 index and 10-m wind speed has been performed to explore the benefits of the reconstruction in comparison with the seasonal predictions directly obtained from a state-of-the-art climate forecast system (Jia et al. 2015; Wang et al. 2017a).

Wind energy users are not only interested in the seasonal prediction of the mean wind speed in a season. They also require information about wind speed values in the high and low ends of the distribution. Wind speed extremes are usually defined by the wind energy sector on timescales from minutes to hours because the synoptic wind speed variability could produce damages that affect wind turbines (Kezunovic et al. 2008). Nevertheless, extreme values at seasonal timescales can provide extra information for wind energy applications aimed to minimise the financial risk, related to windstorms or wind droughts (Della-Marta et al. 2010; Walz et al. 2018). To describe the extreme wind speed values in a season four indicators have been defined: 10^{th} and 90^{th} percentiles and the fraction of time in a season below/above the 10^{th}/90^{th} climatological percentiles. It should be borne in mind that the highest and lowest wind speed values might not be relevant to the energy production process because the wind speed range at which turbines function is limited. However, the analysis of the seasonal predictions of these indicators is particularly relevant in the case of the wind speed because, as it has already been detailed in chapter 3, the wind speed distribution presents some deviations from normality. Besides, these discrepancies with a normal distribution are different in the seasonal

forecasts and in the observational reference, which suggests that the forecast quality of the mean wind speed could not be representative of that for higher moments of the wind speed distribution. Therefore, to investigate the potential added value of the seasonal forecasts of extreme wind speed indicators, both biases and forecast quality have been explored.

This chapter raises the limits associated with the ECMWF System 4 seasonal forecast system when its predictions are tailored to satisfy specific users' needs. The analysis focuses on the boreal winter (DJF) because it is the season with higher wind speed variability in the Northern Hemisphere. Consequently, the variability in the supply of wind power is more pronounced in this season. Nevertheless, the potential skill of the seasonal forecasts of 10-m wind speed in different seasons is included in the Appendix (Figure B31) where a strong season-to-season variability is shown. In this chapter the seasonal predictions issued on the 1^{st} of November (one month lead) are used, but the predictability of the seasonal forecasts of wind speed at different lead times is shown in the Appendix (Figure B32). The ERA-Interim reanalysis has been used as the reference dataset for illustration, but the choice of reanalysis dataset is arbitrary as the conclusions are equally valid when using other reanalyses.

This chapter is organised as follows. In section 6.1 the methods used to produce tailored climate predictions of 10-m wind speed are described. Then the suitability of state-of-the-art bias adjustment techniques for the adjustment of wind speed seasonal forecasts is discussed in section 6.2. Then the forecast quality improvements of reconstructed seasonal predictions of 10-m wind speed using the ENSO index with respect to the seasonal predictions of the 10-m wind speed have been explored in section 6.3. Finally, the description and evaluation of wind speed extreme indices are provided in section 6.4. Some of the results discussed in this chapter have been also included in Torralba et al. (2017b).

6.1 Methodology

Most of the analyses performed in this chapter are based on the seasonal forecasts in the 1981-2012 period, which is the shortest period used in this thesis. This part of the work was performed some time ago when the forecast in that period were the only data available. However, the validity of the conclusions has been carefully checked and some of the analyses been replicated. For instance, Figure B33 shows the comparison of the Pearson correlation of the 10-m wind speed for 1981-2012 and for a slightly longer one ending in 2016.

6.1.1 Bias adjustment and reconstruction methods

Three different bias adjustment approaches have been applied to the seasonal (three-month average) forecasts of wind speed: simple bias adjustment, quantile mapping and the calibration method. These methods address different aspects

of the forecast error and produce seasonal forecasts with similar statistical properties to the reference dataset. The reconstruction method based on the linear regression between the 10-m wind speed and the Niño-3.4 index produces seasonal forecasts of the 10-m wind speed from the ECMWF System 4 seasonal forecasts of the Niño-3.4 index. Bias adjustment and reconstruction approaches have been applied in leave one-year out cross-validation (described in chapter 2, section 2.4.2) to mimic as closely as possible an operational context in which new coefficients might be estimated to predict each year. As a result, the correlation of the bias adjusted forecasts decreases compared to the correlation computed directly with the raw forecasts. This is due to the cross-validation leading to an implicit leakage of information from the training data to the verification sample, which results in the degeneracy of the skill (Barnston and van den Dool 1993). However, there is no comparable procedure that allows for the use of the same data to perform the bias adjustment and to evaluate the skill (Barnston et al. 2012).

Simple bias adjustment: this method is based on the assumption that both the reference and predicted distributions of the seasonal wind speed are well approximated by a Gaussian (normal) distribution. The adjustment, when performed without cross-validation, creates predictions with the same mean and standard deviation as the reference dataset (Leung et al. 1999). The Gaussian assumption is a limitation of the approach because the monthly and seasonal wind speed distribution can be, at times, slightly non-gaussian as it has been already discussed in chapter 3.

The simple bias correction scheme can be summarised in this way:

$$y'_{i,m} = (y_{i,m} - \bar{y})\frac{\sigma_x}{\sigma_y} + \bar{x} \tag{6.1}$$

Seasonal forecasts of wind speed ($y_{i,m}$) for each particular year (i^{th}) and ensemble member (m^{th}) are transformed into anomalies by subtracting the ensemble mean of the seasonal averages ($\bar{y}$) in the climatological period. A new seasonal mean ($y'_{i,m}$) is calculated by multiplying the seasonal mean anomaly by the ratio of the standard deviation of the reference data set (σ_x) to the inter-annual standard deviation of the ensemble members (σ_y) also computed for the forecasts and reference datasets in the training period. Then, the climatology of the reference data set ($\bar{x}$) is added. This is applied for each grid cell separately, resulting in a new wind speed forecast ensemble.

Calibration method: can be considered as a way of obtaining predictions with inter-annual variance equivalent to that of a reference dataset in a similar way to the bias adjustment method, but at the same time ensuring increased reliability of the probability forecasts. In particular, the variance inflation technique (Von Storch 1999; Doblas-Reyes et al. 2005) has been applied. This calibration strategy has been selected because inflation of the ensemble spread is required to obtain reliable probabilities and it

is applied as in Doblas-Reyes et al. (2005).

If $\hat{y}_i$ is the ensemble mean prediction for any grid point at year (i^{th}) and $y_{i,m}$ is the seasonal forecast of the 10-m wind speed for the same year and the ensemble member (m^{th}); then the calibrated estimate ($y'_{i,m}$) can be expressed as:

$$y'_{i,m} = \alpha\hat{y}_i + \beta(y_{i,m} - \hat{y}_i) + \bar{x} \tag{6.2}$$

The coefficients α and β are defined as follows:

$$\alpha = abs(\rho)\frac{\sigma_x}{\sigma_{\hat{y}}} \tag{6.3}$$

$$\beta = \sqrt{1-\rho^2}\frac{\sigma_x}{\sigma_e} \tag{6.4}$$

The $\sigma_{\hat{y}}$ is the standard deviation of the ensemble mean, σ_e is the standard deviation of the anomalies of all ensemble members calculated with respect to the corresponding (i.e. of the same start date and lead time) ensemble mean ($y_{i,m} - \hat{y}_i$), σ_x is the standard deviation of the reference and ρ is the correlation between the ensemble mean forecasts and the reference dataset. The α and β coefficients are found under two constraints. The first one is that the standard deviation of the inflated prediction is the same as that for the reference and the second one is that the predictable signal after the inflation is made equal to the correlation of the ensemble mean with the reference dataset.

This procedure has been applied to the seasonal prediction anomalies. Then, the climatology of the reference dataset ($\bar{x}$) has been added to provide users with seasonal forecasts of wind speed instead of only departures from the mean value.

Quantile mapping: this approach (Themeßl et al. 2011) has been applied to correct all moments of the wind speed probability distribution function. This method employs the probability density function (PDF) of the reference dataset and the PDF of the seasonal forecasts in the reference period and integrates them into cumulative density functions (CDF). These two CDFs are used for the development of a transfer function that is defined as follows:

$$y'_{i,m} = F_x^{-1}\left(F_y(y_{i,m})\right) \tag{6.5}$$

with $y'_{i,m}$ as the adjusted seasonal prediction of the m^{th} member in the target year i^{ih}, $y_{i,m}$ is the original seasonal prediction, F_x^{-1} is the inverse CDF (i.e. quantile function) of the reference dataset and F_y is the CDF of the seasonal forecasts. The probability of observing a determined value in the seasonal forecasts is thus transferred to the quantile of the observed CDF, matching exactly this probability. After the adjustment, the CDF of the seasonal forecasts is equal to the observed one (when applied without cross-validation). For those values that are under the lowest percentile and above the highest percentile a constant extrapolation has been applied (i.e. the values in the predictions under/over the minimum/maximum of the reference dataset will be adjusted with the lowest/highest percentile).

Reconstruction method: The simple procedure to reconstruct the 10-m wind speed predictions is based on linear regression with the Niño-3.4 index. For each grid point, there are N-pairs of Niño-3.4 index and 10-m wind speed $(w_i, w_i' : i = 1, ..., N)$, each representing the predictand (w') and predictor (w). Then, the linear regression can be written as:

$$w' = a + bw \tag{6.6}$$

The coefficients of this regression have been obtained from the 10-m wind speed values and the Niño-3.4 index from ERA-Interim for each particular season and grid point by following these equations:

$$a = \bar{w'} + b\bar{w} \tag{6.7}$$

$$B = \frac{\sum_{i=1}^{N} (w_i - \bar{w}) \left(w_i' - \bar{w'}\right)}{\sum_{i=1}^{N} (w_i - \bar{w})^2} \tag{6.8}$$

where $\bar{w}$ and $\bar{w'}$ are the climatologies of the Niño-3.4 index and the wind speed respectively over the 1982-2016 period used for the reconstruction. Once the coefficients are computed from the ERA-Interim data, they are introduced in the equation 6.6 together with the seasonal predictions of the Niño-3.4 index. This reconstruction has been performed in leave-one-out cross-validation (described in chapter 2, section 2.4.2), which means that the year to be reconstructed is not used for the estimation of the a and b coefficients. The reconstruction has been also performed 'in sample' (without cross-validation) just to explore the impact of the cross-validation on the results.

6.2 Bias adjustment impact on the wind speed forecast quality

To investigate the performance of the seasonal predictions of wind speed, a region in Canada [49.5°-53.0° N, 248.9°-250.3° E] has been selected. This country is an important player in terms of energy resources (Vaillancourt et al. 2014) and a global leader in the sustainable development of wind energy. This region had an exceptional year in 2014 for wind energy development, ranking seventh globally in terms of new installed capacity (CWEA 2015) that year. For the election of the region, two factors have been taken into account. The former is the potential skill available in such region (Figure B31) and the latter is its relevance for the wind energy sector. Two more regions have been considered: central United States and northern Scandinavia and their corresponding results have been included in the Appendix (Figures B34, B35, B36 and Table B1).

The time series have been obtained by spatially averaging the predictions over the grid points in the region of Canada before the bias adjustment is applied. The time series of the raw seasonal forecasts of wind speed (Figure 48a) is compared to the time series bias adjusted with different methods: simple bias adjustment (Figure 48b), calibration (Figure 48c) and quantile mapping (Figure 48d). The effect of the bias adjustment over the predictions is that when the adjustments are applied, the hindcasts (grey dots) show similar mean and variance to the reference dataset (black dots). After the bias adjustment

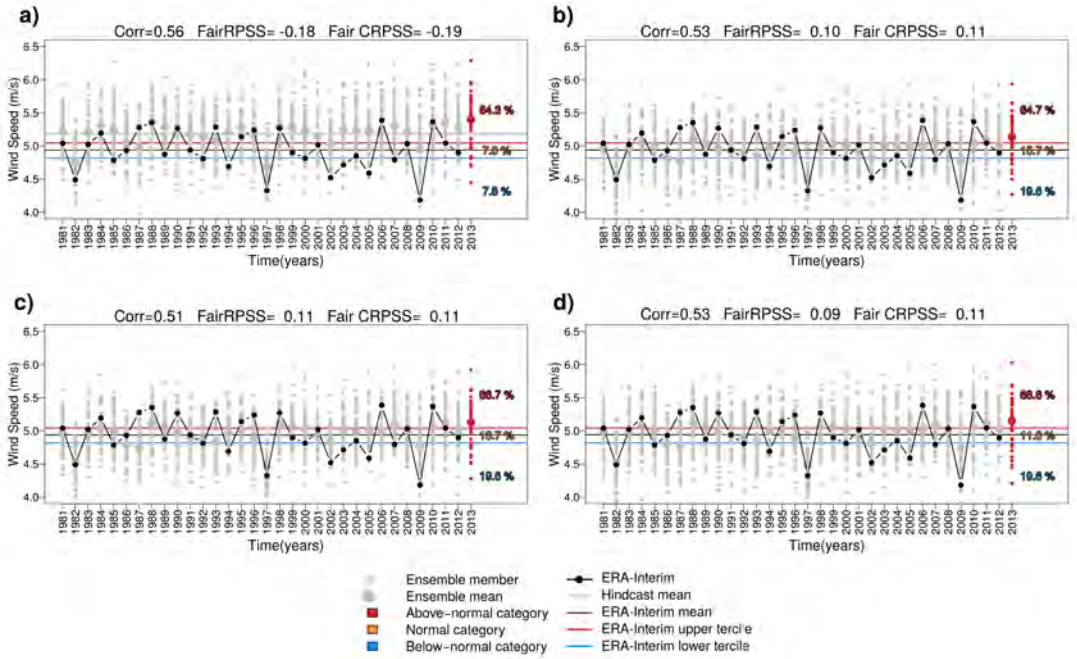

Figure 48 – Time series of 10-m wind speed from ECMWF System 4 and ERA-Interim reanalysis in winter (DJF) for a region in Canada [49.5°-53.0° N, 248.9°-250.3° E]. These predictions have been initialised on the 1^{st} of November for the period of 1981-2013 and they have been bias adjusted with different methods: a) none, b) simple bias adjustment, c) calibration and d) quantile mapping. The grey/black horizontal lines show the mean of the hindcasts/observations over the 1981-2012 period. The ensemble members of the forecast year (2013) are represented as red dots. The percentages indicate the fraction of members in each category, which are limited by the terciles of the reference dataset. Correlation, FRPSS and FCRPSS are shown in the upper part of each panel and they have been computed for the period 1981-2012.

(Figure 48 b,c and d), the probabilities in each category differ as a result of the changes in the ensemble distribution. The skill changes according to the bias adjustment, showing a decrease in the correlation and an increase in the probabilistic skill scores. The decrease of the correlation is due to the cross-validation, which leads to an implicit leakage of information and degeneracy in this measure of potential skill (Barnston and van den Dool 1993; Barnston et al. 2012). The improvement of the fair RPSS (FRPSS) and the fair CRPSS (FCRPSS) (metrics defined in Appendix, section A.1.2) are associated with the reduction of the systematic errors. This result is also obtained for the other two regions considered (Figure B34) which also show the enhancement of the probabilistic skill scores when the three bias adjustment

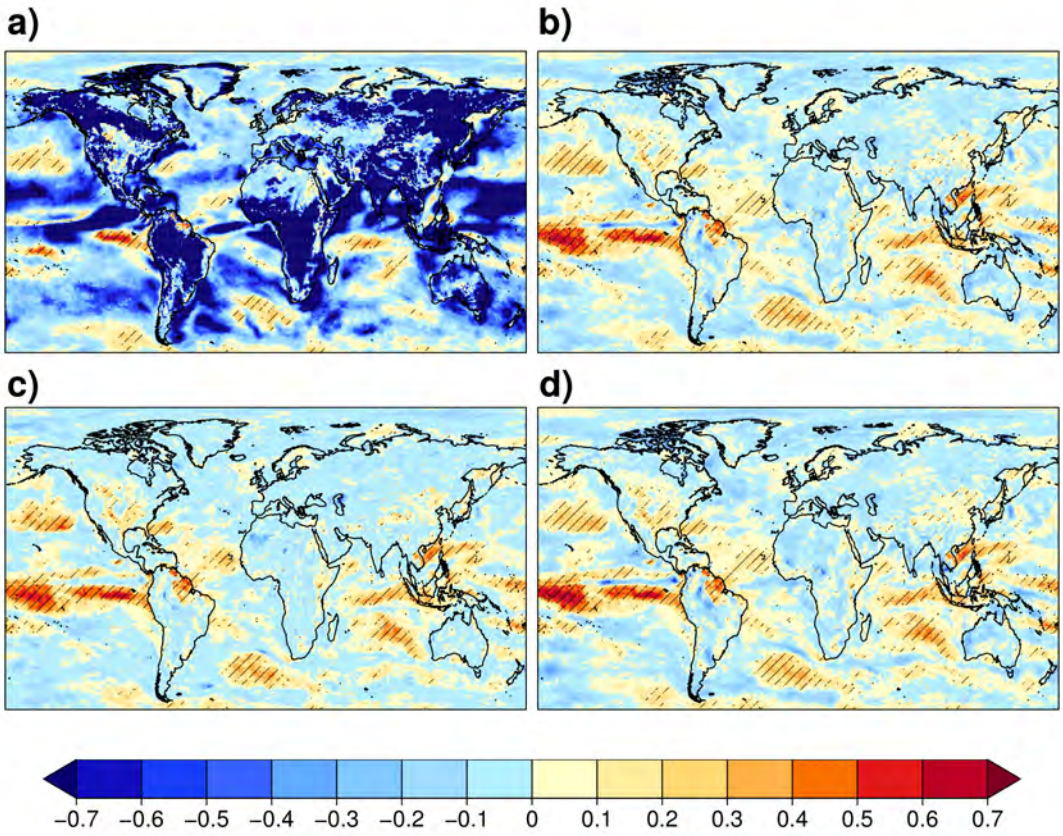

Figure 49 – Fair ranked probability skill score (FRPSS) for tercile events of 10-m wind speed forecasts from ECMWF System 4 and ERA-Interim reanalysis in winter (DJF). The predictions have been initialised on the 1^{st} of November for the period of 1981-2012. These seasonal forecasts have been bias adjusted with different methods: a) none, b) simple bias adjustment, c) calibration and d) quantile mapping. Hatched regions indicate FRPSS significantly (95% confidence level) larger than zero.

approaches are applied. Contrary to the correlation, the FRPSS and the FCRPSS are both sensitive to the systematic differences in the statistical properties (mean, variance) of the predicted variables with respect to those in the observations as well as to the inadequacy of the ensemble dispersion to act as a prediction of the forecast error (the lack of reliability). This is a useful example of the importance of using more than one forecast quality measure, in particular when dealing with user-relevant variables.

The seasonal forecast system considered allows estimating the global forecast quality of the different sets of predictions. The FRPSS maps for the raw, simple bias adjusted, quantile

mapping adjusted and calibrated wind speed are shown in Figure 49, but the corresponding results for the Pearson correlation and FCRPSS have been included in the Appendix B (Figures B37 and B38). It is noticeable that the spatial distribution of the correlation (Figure B37c) for the calibrated predictions is noisier than in the other three types of forecasts considered. This noise is due to the coefficients estimated in the calibration having a smaller spatial decorrelation length and being less robust than the mean and variance used in the simple bias adjustment.

The raw predictions (Figure 49a) display very low scores all around the world. These widespread negative values are the result of the systematic errors, as the probabilities used to compute the FRPSS are estimated from the two terciles defined in ERA-Interim. The highest values are found in tropical regions, in particular in some regions of northeast South America and northwestern Africa. This maximum can be explained because the largest predictability at seasonal timescales is attributed to anomalies in the tropical sea surface temperatures (SST) resulting from coupled ocean-atmosphere phenomena, in particular, those related to ENSO events (Kirtman and Pirani 2009) that mainly affect the regions mentioned above.

Figure 49 (b,c and d) shows that the FRPSS increases globally when bias adjustment is applied reconstructing their maximum values in the tropics. Although the skill is relatively low at extra-tropical latitudes, some positive skill is found in some regions in Europe as the North Sea or Scandinavia, which display positive values. Wind speed predictions show the highest skill in northern Europe, while in southern Europe negative RPSS values are found. This is in agreement with previous work (e.g. Weisheimer et al. 2011) indicating that seasonal dynamical predictions have limited forecast quality over Europe.

The skill improvement is also present in southeastern Asia, the central United States or northeastern South America where positive values appear when the three bias adjustment techniques are applied. The bias adjustment allows the skill in those regions associated with ENSO teleconnections (Quan et al. 2006; Hamlington et al. 2015), as well as with other sources of seasonal to inter-annual predictability, such as the persistence of the North Pacific decadal oscillation (Gershunov and Cayan 2003) to emerge. Wind speed with positive skill in North America has important implications for the wind energy sector in this economically active region.

Making sure that the forecast ensemble has reliable probabilities is a critical aspect for the user because it suggests that the ensemble predictions represent the forecast error, within statistical sampling, and it can be trusted in specific applications that have been developed using observational references.

To analyse the impact of the bias adjustments on reliability, reliability diagrams (Figure 50) have been used. They allow the comparison between the observed frequencies with forecast

probabilities (obtained from the ensemble forecasts) for binary events. This type of diagram has been fully described in Appendix A (section A.2.2). For illustration purposes, the events are defined by the thresholds of the lower and upper terciles, although other thresholds can be defined. If the forecast system is reliable, then a good agreement should exist between forecast probabilities and observed relative frequencies and the graph should be close to the diagonal.

The reliability curve for the below-normal category (i.e. the category defined by the events that verify when the value is below the lower tercile; blue line) corresponding to the raw data (Figure 50a) has a positive slope. This means that as the forecast probability of the event occurring increases, so does the chance of observing the event and, therefore, the forecasts have a certain degree of reliability. However, if a steeper slope than the diagonal appears, the probability forecasts are considered as under-confident because the events are forecast with probabilities less extreme than they should. For this category the reliability curve is above the diagonal line, indicating that the predicted probabilities are always lower than the observed frequencies. This illustrates the systematic errors inherent to the raw predictions. The below-normal curve flattens when the forecast probability is above 0.6, which means that if the forecast probability is higher than 0.6 then no relationship exists between the forecast probabilities and the frequency of the observed below-normal wind speeds. The reliability curves for the raw predictions of the above-normal and normal categories (red and orange lines) are almost horizontal suggesting that the forecasts are over-confident. This means that the predictions show poor resolution, meaning that for most of the predicted probabilities, the observed frequencies take often the climatological value (0.33 in this case). Particularly, the normal category shows only a narrow set of forecast probabilities issued, with values ranging from 0.1 to 0.7. The frequency of the forecast probabilities is also shown in the sharpness diagrams which are displayed on the right part of the reliability diagrams. The sharpness diagrams indicate if the seasonal forecast system is able to predict different levels of predictability (i.e. the frequencies in the sharpness diagram are uniformly distributed). For example, in the below-normal category, the most populated rank in the sharpness diagram is the first one, which evidences the bias in the probabilities of the below-normal wind speeds in the Canadian region.

The bias adjusted predictions (Figure 50 b,c and d) have reliability diagrams with their points lying closer to the diagonal than found for the raw predictions. This corresponds to a better agreement between the forecast probabilities and the frequency of the observed event than in the raw predictions. This effect is also shown for the Scandinavian and central United States regions B35. This result suggests that the systematic errors have been adjusted making the probabilities more reliable.

The over-confidence showed for the above-

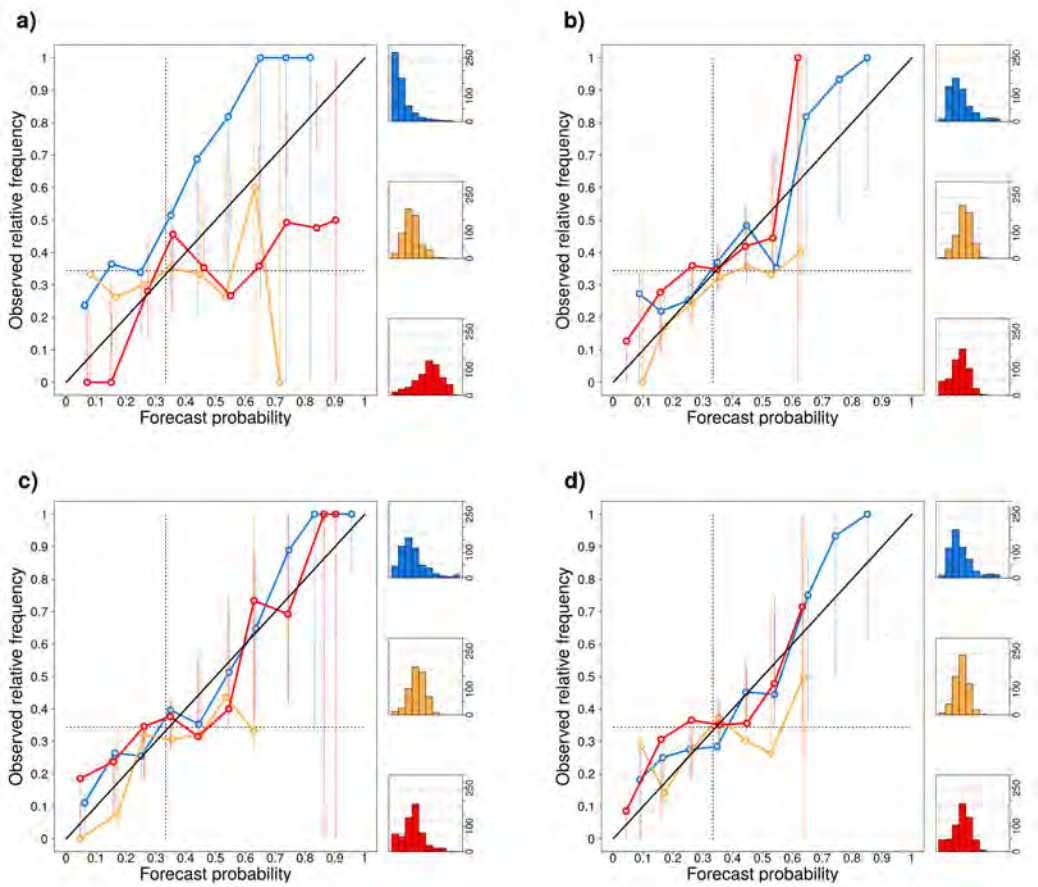

Figure 50 – Reliability diagrams of 10-m wind speed forecasts from ECMWF System 4 and ERA-Interim reanalysis in winter (DJF) for a region in Canada [248.9°-250.3° E, 49.5°-53.0° N]. The grid points in that region are pooled together. The predictions have been initialised on the 1^{st} of November for the period of 1981-2012 and they have been bias adjusted with different methods: a) none, b) simple bias adjustment, c) calibration and d) quantile mapping. Results for three categories are represented: above-normal (red line), normal (orange) and below-normal wind speeds (blue). Right panels show the sharpness diagrams with the distribution of samples for each forecast probability bin and each event. The consistency bars have been represented as vertical lines to illustrate how likely the observed relative frequencies are under the assumption that predicted probabilities are reliable.

normal event and the under-confidence affecting the predicted probabilities of the below-normal category in the raw predictions is not present in the bias adjusted predictions. However, the above-normal event (red curve) of the predictions adjusted with the simple bias adjustment and quantile mapping methods (Figure 50 b,d respectively) only reach forecast

probability values around 0.65, while for the calibrated predictions values over 0.9 can be found. This makes the calibration method slightly superior to the other two.

The slope of the curve for the normal category (orange line) becomes horizontal for forecast probabilities over 0.2 for the predictions adjusted with the simple bias adjustment (Figure 50b) and quantile mapping (Figure 50d) methods and over 0.3 for those predictions adjusted with the calibration method (Figure 50c). This result demonstrates that the system cannot discriminate between predictable and unpredictable normal wind speeds for this category in this region, which is not surprising because normal events might not have strong forcing signals, which are those associated with the predictability of the system (Van Den Dool and Toth 1991).

Furthermore, for the calibrated predictions of below-normal and above-normal wind speeds, sharpness diagrams (Figure 50 c) show more homogeneously populated bins. This means that the forecast system is able to predict those events with a larger range of forecast probability values. Conversely, the raw and the bias adjusted predictions with the simple and quantile mapping methods display their frequency peaks near the climatological frequency, so that they predict often the event with a climatological probability. These results show, again, the improvement in the reliability of the predictions obtained when calibration is applied, improvements that are particularly relevant to the users.

To extend the reliability analysis, the rank histograms for seasonal wind speed predictions in the same Canadian region [49.5°-53.0° N, 248.9°-250.3° E] have been computed (Figure 51). The description of the rank histograms is provided in Appendix A (section A.2.1). For the raw predictions (Figure 51a), the overpopulated lower ranks and the negative slope in the rank histogram illustrate that a positive unconditional bias is present in the data with most of the observations exceeded by the majority of the ensemble members, leaving the highest rank categories less populated. The bias adjusted forecasts show more homogeneously populated ranks (Figure 51 b,c and d) indicating that the reliability of the ensemble improves when the bias adjustment is applied. However, the deviation from flatness of these rank histograms could be the result of some forecast deficiencies still remaining after the bias adjustment. For instance, for the simple bias adjusted forecasts (Figure 51b), one rank shows small values that might indicate that the ensemble underestimates the true uncertainty range. These low values for one particular rank are also obtained for the calibrated forecasts in northern Scandinavia (Figure B36f) and for the forecasts adjusted with the quantile mapping in central United States (Figure B36g).

To assess if the deviations from flatness of the rank histograms are attributed to either chance or deficiencies in the forecasts, goodness-of-fit test statistics (Jolliffe and Primo 2008) have been applied. The three statistical tests, the Pearson χ^2, the JP slope and JP convex, allow

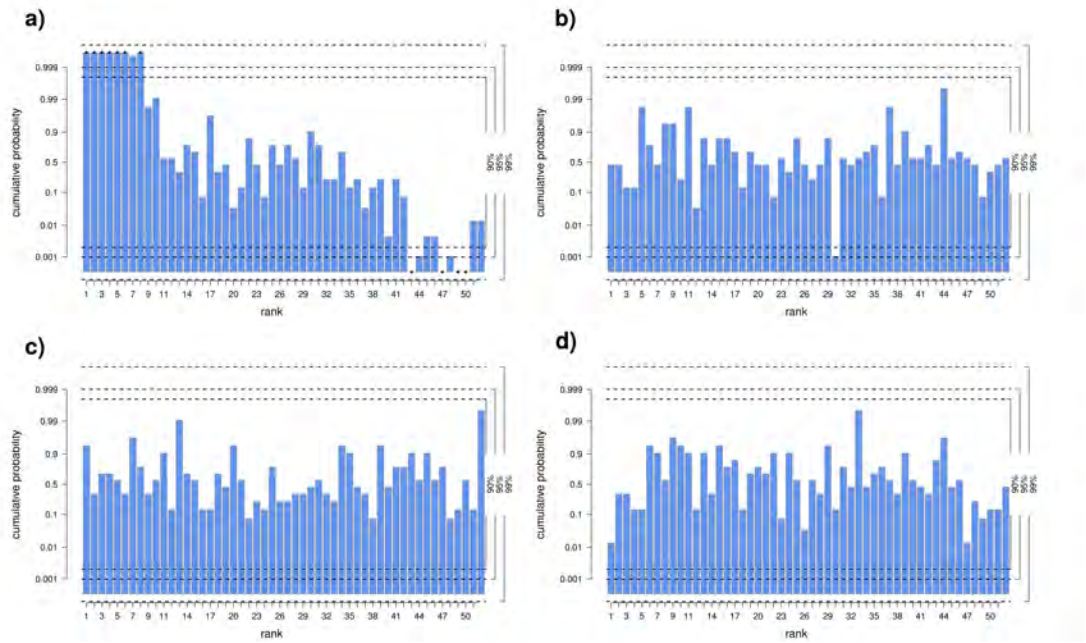

Figure 51 – Rank histograms of 10-m wind speeds forecasts from ECMWF System 4 and ERA-Interim reanalysis in winter (DJF) for a region in Canada [49.5°-53.0° N, 248.9°-250.3° E]. The predictions have been initialised on the 1^{st} of November for the period of 1981-2012. The seasonal forecasts have been bias adjusted with different methods: a) none, b) simple bias adjustment, c) calibration and d) quantile mapping.

Table 3 – Goodness-of-fit tests: Pearson χ^2, JP-slope and JP-convex statistics formulated by Jolliffe and Primo (2008) and their p-values in brackets. They have been computed from the rank histograms (Figure 51) of 10-m wind speed forecasts from ECMWF System 4 in winter (DJF) for the period 1981-2012.

	Pearson χ^2	JP slope	JP convex
Uncorrected	311.61 (8.6×10^{-39})	217.89 (2.6×10^{-49})	18.57 (1.6×10^{-5})
Simple bias corrected	57.21 (0.30)	0.06 (0.80)	0.01 (0.92)
Calibrated	54.86 (0.33)	0.04 (0.84)	2.75 (0.10)
Quantile mapping corrected	64.97 (0.09)	1.23 (0.27)	6.98 (0.01)

identifying if the forecasts are biased or whether the ensemble has over or under-confidence. The null hypothesis is that the rank histogram is uniform, and the results are included in Table 3.

Table 3 displays that departures from flatness exist for the raw forecasts since the tests take high values, showing that the ensemble is affected by biases and over or under-confidence, as evidenced by the high JP slope and JP convex tests. The results are statistically significant, with the p-values being virtually zero. The tests applied to the bias adjusted forecasts indicate that the deviation from flatness is minimised when these methods are applied. The Pearson χ^2 for the calibrated data has lower values than the bias adjusted with the simple and quantile mapping methods. The JP tests provide no evidence of departures from flatness with p-values higher than 0.10 for the simple bias adjusted and calibrated predictions. Consequently, these results and the reliability diagrams show that the biases and the over or under-confidence in the raw ensemble are adjusted when the calibration is applied.

The quantile mapping method produces adjusted forecasts that are not affected by biases, although they show under-confidence, as indicated by a JP-convex p-value of 0.01 that shows that the null-hypothesis of flatness can be rejected at a 95% confidence level. The low values in the JP-convex p-value for the quantile mapping are also shown in the seasonal forecasts of 10-m wind speed in northern Scandinavia and central United States (Table B1). This is in agreement with the results shown in Zhao et al. (2017) that demonstrate that the quantile mapping method cannot ensure the reliability and consistency of the adjusted forecasts.

6.3 Reconstruction of the 10-m wind speed from the Niño-3.4 index

As it has been shown in the previous section, there are several extra-tropical regions where the seasonal forecasts of the 10-m wind speed show limited skill. This can prevent wind energy users interested in those regions to employ this climate information for their decision-making. To improve the current level of skill in that relevant region for the wind industry, a reconstruction method based on ENSO has been applied. The reconstruction method combines the skilful seasonal forecasts of the Niño-3.4 index (from ECMWF System 4) index with the relationship of this index with the 10-m wind speed in the ERA-Interim reanalysis.

The comparison between the 10-m wind speed predictions obtained from the ECMWF System 4 (raw) and those obtained by reconstruction has been carried out in terms of correlation maps. The goal is to identify if the predictions (raw or reconstructed) can provide some added value with respect to those predictions based on climatology, which represent the benchmark currently employed by the wind energy users. When the correlation is positive, the forecast system provides additional information with respect to a reference consisting of a constant (climatological) or random forecast. In any other case, the reference is not beaten by the forecast

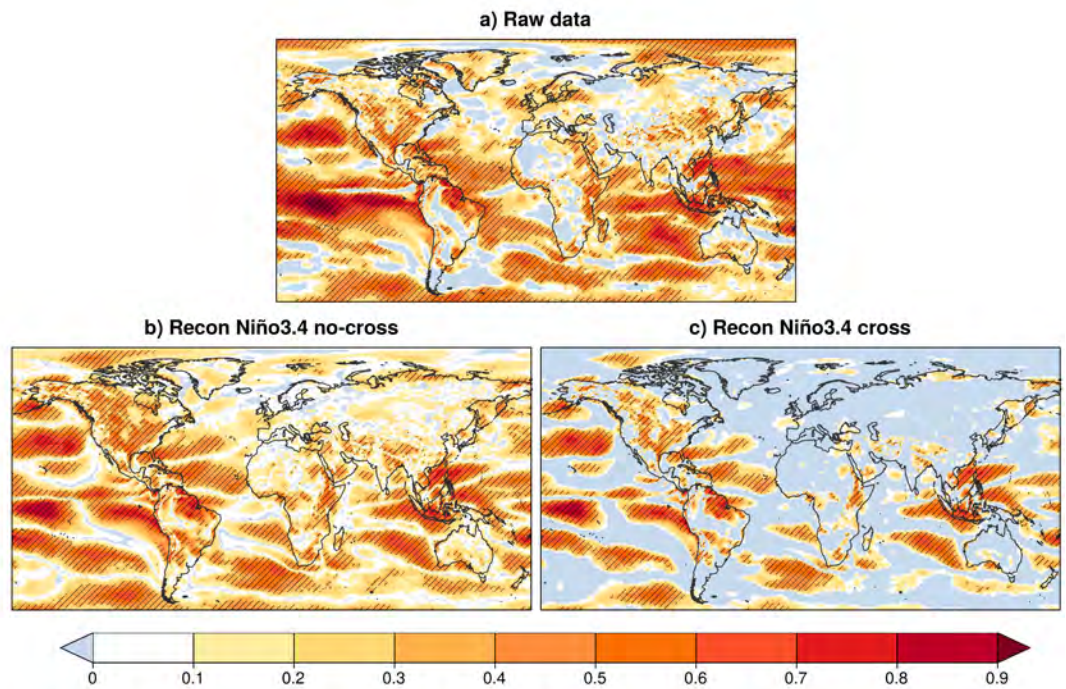

Figure 52 – Pearson correlation between the ERA-Interim data and the seasonal forecasts of 10-m wind speed from a) ECMWF System 4 b) reconstruction from the Niño-3.4 index "in sample" and c) reconstruction from the Niño-3.4 index in cross-validation in DJF. These seasonal forecasts have been initialised the 1^{st} of November over the 1982-2016 period. Hatched regions indicate correlation significantly (one-tailed t-test at the 95% confidence level) larger than zero.

system.

Figure 52a shows the correlation maps for the raw 10-m wind speed seasonal predictions. There are regions for which correlation values are high and significant. Although most of those regions are located over the oceans, some examples such as the United States, northeastern South America, western Africa, northern Europe or central Asia are found over land. By contrast, there are regions for which the seasonal predictions of 10-m wind speed from the ECMWF System 4 cannot provide extra information compared to a climatological or random reference. The regions for which the potential skill of wind speed is limited can benefit from the reconstruction based on the Niño-3.4 index. This index has been selected because it characterises the time evolution of ENSO, which is one of the main sources of predictability at seasonal timescales. In addition, it has been shown in chapter 4 that ECMWF System 4 predicts this index with high skill.

The effect of the application of the reconstruction method in cross-validation is shown in Figure 52. The comparison of the Figure 52b ("in sample") and Figure 52c shows a strong reduction of the correlation for the reconstructed 10-m wind speed in cross-validation. This is an important comparison because other studies (e.g. Scaife et al. 2014) consider the predictability of key climate indices without considering the toll to be paid by an out-of-sample validation.

Results of the reconstruction when cross-validation is not applied (Figure 52b) show a general improvement of the correlation values in comparison with those obtained for the raw data in those regions where negative correlations were obtained like South America or western Africa. However, there are also regions for which the correlations of the reconstructed 10-m wind speed are lower than for the raw data. For example, in the British Isles and southern Scandinavia, correlations are positive and significant in the raw data but they become negative for the reconstructed predictions.

There are several regions over the oceans where the reconstructed seasonal forecasts of 10-m wind speed in cross-validation (Figure 52c) show positive and significant correlations. This suggests that in those regions the predictability is mainly related to ENSO. There are also some examples like over North America, some regions in South America, eastern Africa or Indonesia that can be found over land.

Cross-validation must be applied to emulate as closely as possible an operational context in which the coefficients of the regression are estimated using past predictions. However, the comparison with the reconstructed predictions for which cross-validation has not been applied (Figure 52b) illustrates the challenge posed by the limited sample sizes available in the current state-of-the-art seasonal predictions systems.

To assess the performance of the reconstruction for different lead times, the correlations for the 10-m wind speed from ECMWF System 4 and those predictions obtained from the reconstruction applied in cross-validation are shown (Figure 53). To quantify the correlation improvement from the reconstruction, the differences between the two maps have been plotted.

Wind speed taken directly from ECMWF System 4 (Figure 53) shows high correlation values in most of the regions over the oceans. However, the high number of regions with negative correlation over land suggests that there is not potential skill in the seasonal predictions of wind speed in those regions. The number of regions for which the correlation drops as the lead time increases become higher for lead four (DJF predictions initialised in August). Examples of these regions with negative correlations are northern North America, southern South America, southern Europe, western Africa, and also in northern Asia.

The 10-m wind speed reconstructed from the Niño-3.4 index shows positive correlation values in less regions than those 10-m wind speed

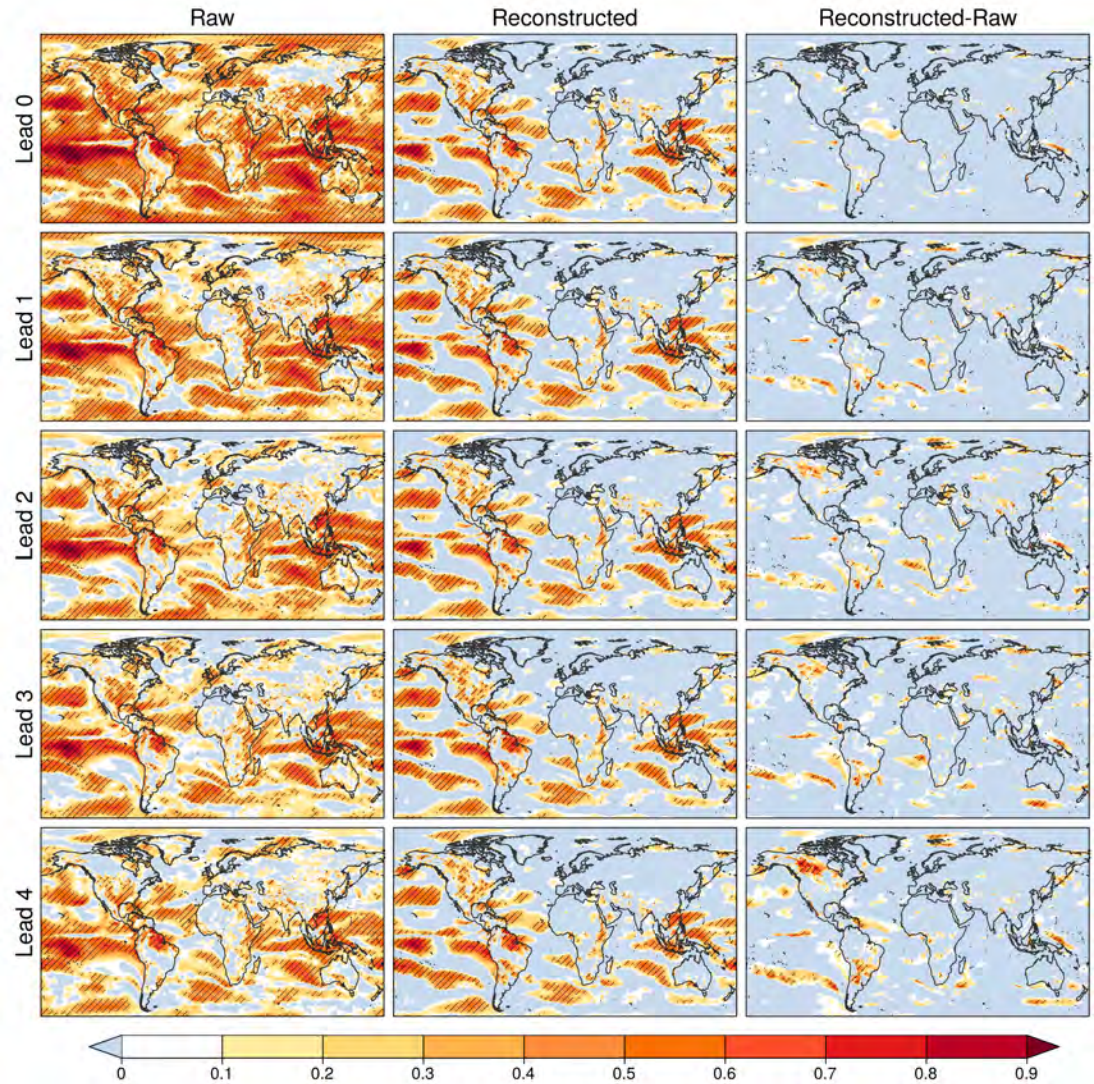

Figure 53 – Correlation between the 10-m wind speed from ECMWF System 4 (left column), the reconstructed 10-m wind speed predictions from the Niño-3.4 index (middle column) and the differences between them (right column). ERA-Interim has been used as a reference dataset. Predictions for DJF in the 1982-2016 period have been used. Each row corresponds to a different initialisation date: December (lead 0), November (lead 1), October (lead 2), September (lead 3) and August (lead 4). Hatched regions indicate correlation significantly (one-tailed t-test at the 95% confidence level) larger than zero.

predictions taken directly from ECMWF System 4, but there are some regions for which ENSO is playing a dominant role on the predictability of 10-m wind speed. Although these regions are mostly over the ocean, some areas over land such as North America, northeastern South America, western Africa, or Indonesia show positive and significant skill when the seasonal forecasts of 10-m wind speed are reconstructed from the Niño-3.4 index.

Only two of these regions, Canada and northern Argentina do not exhibit positive correlation values when they are taken directly from the seasonal forecast system. Consequently, the seasonal predictions of wind speed in those regions could be improved by their reconstruction based on the Niño-3.4 index. In these two regions ENSO teleconnections to 10-m wind speed are not well reproduced by ECMWF System 4 (chapter 4), so the combination of the

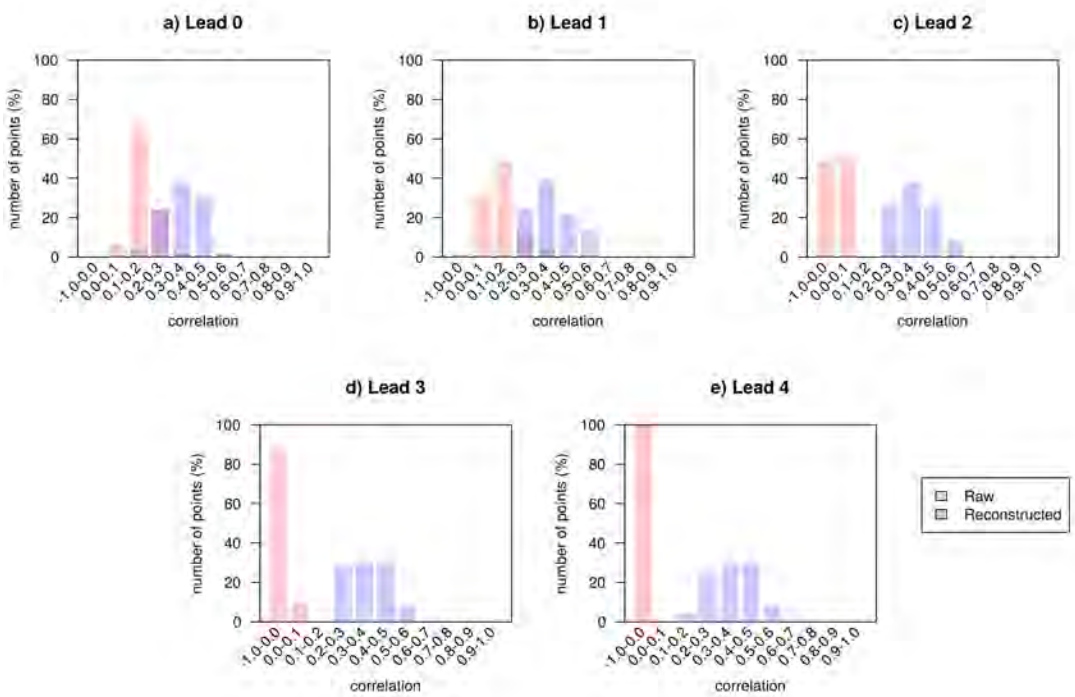

Figure 54 – Percentage of points in Canadian region [55.8-58.6 ^{o}N and 253.8-259.5 ^{o}E, 45 grid points] with different correlation ranks in the 10-m wind speed seasonal predictions from ECMWF System 4 (red) and those reconstructed from the Niño-3.4 index (blue). ERA-Interim has been used as the reference dataset. Predictions for DJF in the 1982-2016 period have been used with different initialisation dates: a) December (lead 0), b) November (lead 1), c) October (lead 2), d) September (lead 3) and e) August (lead 4).

observed relationship between wind speed and the Niño-3.4 index with the skilful prediction of the Niño-3.4 index results in improved correlation values. This effect is more significant as the lead time increases, as shown by the high values of the differences in these two areas for the DJF predictions initialised in August.

To further illustrate this result the correlation values have been classified in one small region over Canada [55.8°-58.6° N, 253.8°-259.5° E] for which the reconstructed predictions show an improved correlation in comparison with the raw data (Figure 54). In this figure it can be appreciated that the raw predictions in that area show most of the correlation values around 0.1 and 0.2 for lead 0 and lead 1, but at lead 2 more than a 40% of the grid points have negative correlation values which become the 100% in lead 4. This effect is not observed for the reconstructed predictions, which display positive correlation values with most of the points between 0.2 and 0.5 in all the lead times.

The correlation values for the reconstructed fields remain constant as the lead time increases, while the seasonal predictions from ECMWF System 4 show a decreasing skill with the lead time. This is due to the Niño-3.4 index being skilful along the lead time, which is a feature successfully exploited by the reconstruction.

6.4 Seasonal predictions of extreme wind speeds

The wind energy sector is particularly vulnerable to extreme wind speed events (Sinden 2007; Pryor and Barthelmie 2013). For that reason, the protection against wind energy risks associated with wind storms or prolonged periods of low wind power generation requires the seasonal forecasts of unusual winds.

Wind energy users currently define wind extremes as those instantaneous values outside of the turbine operation range (i.e. the minimum wind speed required for the activation of the turbine and the wind speed value for which the turbine braking system is applied to slow down or stop it from spinning, to protect mechanical equipment from damage). As the wind speed distribution based on high-frequency instantaneous values is very different from the distribution of the six-hourly winds of the seasonal predictions, wind speed indices based on percentiles have been defined instead of the fix thresholds used by the industry.

6.4.1 Definition of wind extreme indices

The definition of the wind speed extreme indices has been performed by following the methodology proposed in previous works (Hamilton et al. 2012; Pepler et al. 2015; Prodhomme et al. 2016) for the estimation of temperature and precipitation extreme events at seasonal timescales.

Two indices have been used to characterise the low wind speeds, an absolute index, the monthly 10^{th} percentile ($q10$) and a relative index, the fraction of time in a season with wind speed values under the 10^{th} percentile ($fbq10_{clim}$). High values of wind speed

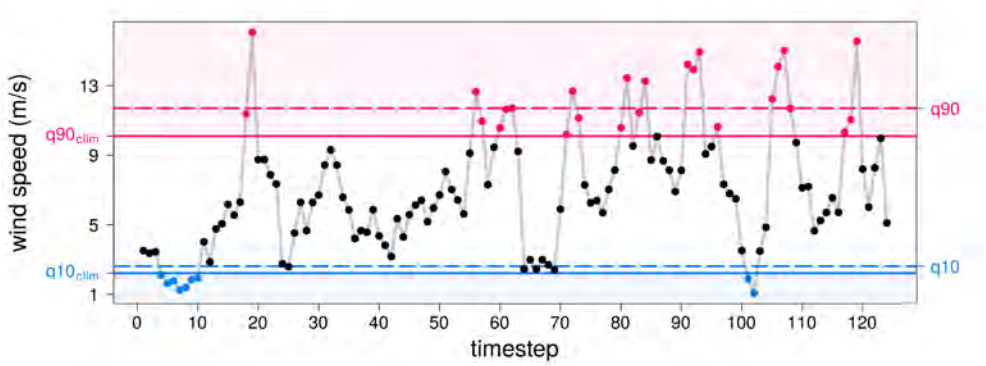

Figure 55 – Illustration of the methodology used to compute extreme wind speed indicators. The time series of the ERA-Interim wind speed values in a month is represented for the 124 timesteps (31 days, and 4 values per day [00,06,12,18 UTC]) in an arbitrary grid point. The *dashed blue/pink lines* mark the $10^{th}/90^{th}$ percentiles in the target month. The *blue/pink solid lines* show the monthly $10^{th}/90^{th}$ climatological percentiles based on the 1981-2012 period. The fraction of time in the month under/over the $10^{th}/90^{th}$ climatological percentile ($fbq10_{clim}/faq90_{clim}$) is computed as the number of wind speed values in the month non-exceeding/exceeding the $10^{th}/90^{th}$ climatological percentile (*blue/pink dots*) divided by the total amount of wind speed values in the month (i.e. $fbq10_{clim} = 9/124$ and $faq90_{clim} = 21/124$).

have been characterised with the monthly 90^{th} percentile ($q90$) and the fraction of time in a season with wind speeds values over the climatological 90^{th} percentile ($faq90_{clim}$), respectively. To illustrate the methodology used to define these indices the six-hourly wind speed values for a particular month and grid point have been represented in Figure 55.

The indices are described in more detail below:

$\boldsymbol{q10}$: is the threshold under which the 10% of the wind speed values in a month are found (Figure 55, *blue solid line*). It can be expressed as:

$$q10 = F^{-1}(p) \tag{6.9}$$

where F^{-1} is the inverse empirical cumulative distribution function (i.e. quantile function) of the wind speed values and $p = 10$.

$\boldsymbol{q90}$: is the threshold under which the 90% of the wind speed values in a month are found (Figure 55, *pink solid line*). It is computed as:

$$q90 = F^{-1}(p) \tag{6.10}$$

where F^{-1} is the inverse empirical cumulative distribution function (i.e. quantile function) of the wind speed values and $p = 90$.

$\boldsymbol{fbq10_{clim}}$: is the fraction of time in a month/season with wind speeds (z_i)lower than the climatological 10^{th} percentile. It is defined

as:

$$fbq10_{clim} = \frac{1}{N}\sum_{i=1}^{N} t_i \quad \text{and}$$
$$t_i = \begin{cases} 1 & z_i \leq q10_{clim} \\ 0 & z_i > q10_{clim} \end{cases} \quad (6.11)$$

where N is the number of wind speed values in a month. In the example shown in Figure 55 $N = 124$ (31 days x 4 values per day). The variable t_i is equal to zero if the i^{th} wind speed value (z_i) is higher than $q10_{clim}$ (*dashed blue line*) and equal to one when z_i is lower than $q10_{clim}$ (Figure 55, *blue dots*).

$\boldsymbol{faq90}_{clim}$: is the fraction of time in a season with wind speeds (z_i) exceeding the climatological 90^{th} percentile ($q90$).

$$faq90_{clim} = \frac{1}{n}\sum_{i=1}^{N} t_i \quad \text{and}$$
$$t_i = \begin{cases} 0 & z_i < q90_{clim} \\ 1 & z_i \geq q90_{clim} \end{cases} \quad (6.12)$$

where N is the number of wind speed values in a month. In the example shown in Figure 55 ($N = 124$). The variable t_i is equal to zero if the i^{th} wind speed value (z_i) is lower than $q90_{clim}$ (*dashed pink line*) and equal to one when z_i is higher than $q90_{clim}$ (Figure 55, *pink dots*).

These indices have been computed from the six-hourly 10-m wind speed values from ERA-Interim reanalysis and the ECMWF System 4 seasonal predictions. They have been computed for each individual month and then averaged across the season (three months) to take into account the intra-seasonal variability of the wind speed thresholds. The seasonal forecasts of the extreme indices have been obtained for each ensemble member and grid point individually.

6.4.2 Systematic errors in the seasonal forecasts of extreme winds

The biases of the seasonal forecasts of the wind speed extreme indices are shown in Figure 56. The systematic errors mostly affect the q10 and q90 percentiles (Figure 56a,b). This is because these indices are absolute thresholds, which have been computed for the observations and the predictions individually. Therefore they show analogous systematic errors to those obtained for the seasonal mean wind speed (chapter 3). However, some differences between the two tails of the wind speed distribution are found. The higher values for the 90^{th} (Figure 56b) than for the 10^{th} percentile (Figure 56a) evidence the different degree of asymmetry (skewness) of the predicted and observed six-hourly wind speed distributions.

The biases are positive in most of the regions suggesting that the seasonal forecast system overestimates both low and high wind speed values. The bias of the $q90$ index (Figure 56 b) is superior to the $q10$ index, particularly over the tropics where the bias for the $q90$ is higher than 1.8 m/s while the $q10$ biases only reach values between 1-1.4 m/s. The spatial structure of the biases in $q10$ and $q90$ also shows some differences. For instance, the low wind speed values show a positive bias in northern Europe (Figure 56a) that is negative for the

$q90$ percentile. This indicates that the six-hourly observed wind speed distribution is wider than the predicted distribution in that particular region.

These discrepancies between the biases found for the high and low wind speed values indicate that bias adjustment methods tailored to correct the full probability distribution should be applied to correct those wind speed values before the extreme indices are derived (i.e. to correct the six-hourly wind speed distribution).

The $fbq10_{clim}$ and $faq90_{clim}$ (Figure 56c,d) biases are very low (0.2% as maximum). This lack of systematic errors appears as a consequence of the way in which these indices have been defined. This is because they are relative indices based on the climatological percentiles in the observations and the predictions.

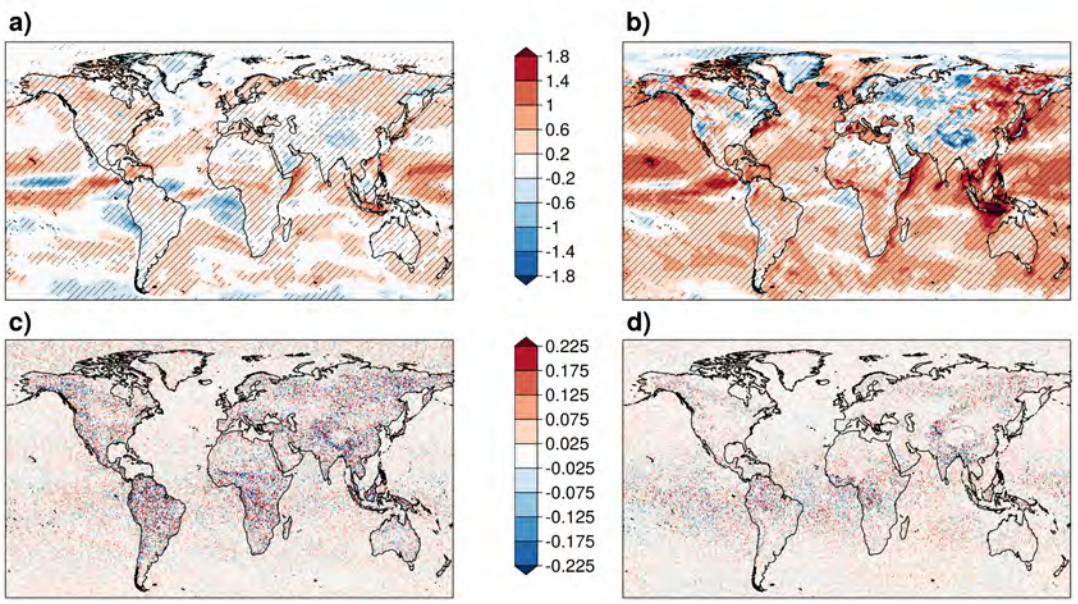

Figure 56 – Bias of the ECMWF System 4 seasonal forecasts of the 10-m wind speed extreme indicators: a) 10^{th} percentile (m/s), b) 90^{th} percentile (m/s), c) fraction of time under the 10^{th} climatological percentile (%) and d) fraction of time above the 90^{th} climatological percentile (%). The bias is related to the ERA-Interim reanalysis in winter (DJF). The predictions have been initialised on the 1^{st} of November for the period of 1981-2012. Hatched areas correspond to regions where the bias is significant at the 95% confidence level (two-tailed t-test).

6.4.3 Predictability of the wind speed seasonal extremes

The comparison of the correlations obtained for the extreme indices characterising the low wind speed values (q10 and $fbq10_{clim}$) and those for the high wind speed values (q90 and $faq90_{clim}$) shows that the former produce noisier correlation maps than those extreme indices for the higher wind speed values. The differences between these two different sets of indices are evidence of the asymmetry in the predictability of the climatological wind speed distribution relative to the six-hourly wind speed values. The 10^{th} and 90^{th} climatological percentiles that have been used for the creation of $fbq10_{clim}$ and $faq90_{clim}$ do not match the probability density function of ERA-Interim and this translates into differences in their associated indices.

The extreme indices considered exhibit similar positive and significant correlation in both oceanic and tropical regions over land such as northern South America, northeastern Brazil, western Africa and southeastern Asia. Extra-tropical regions also show positive and significant correlation, as it has been found for North America. The four extreme indicators show similar correlation to the mean wind speed, although they are generally smaller for the extremes than for the mean wind speed. Some exceptions are found in the tropical Atlantic and central South America where the $q10$ and $fbq10_{clim}$ show higher correlations than the seasonal mean and also in northeastern Brazil where $q90$ and $faq90_{clim}$ display higher correlations than the mean wind. This result is in agreement with previous studies (Hamilton et al. 2012; Pepler et al. 2015; Bhend et al. 2017) that have shown that the predictability of the extreme indices derived from the seasonal forecasts is a consequence of the inherent potential skill of the mean.

6.5 Conclusions

Seasonal forecasts tailored to the wind energy sector represent an innovation in the use of climate information to better manage the future variability of wind energy resources. The minimum level of quality required for climate predictions will highly depend on the decision to be made, the vulnerability of the sector at a particular time and location, and the variability of the wind resource. Wind energy users have traditionally employed a simple approach that is based on an estimate of retrospective climatological information. Instead, seasonal forecasts can better support the balance between wind energy demand and supply. Here it has been shown that the ECMWF System 4 seasonal forecasts of near-surface wind speed have skill in several regions where there is substantial installed wind power. Although the most skilful regions are concentrated in the tropics, there are some extra-tropical areas where the seasonal predictions could provide an added value to the reference climatology.

The relative merits of different techniques for the statistical bias adjustment of ensemble forecasts to address different aspects of the

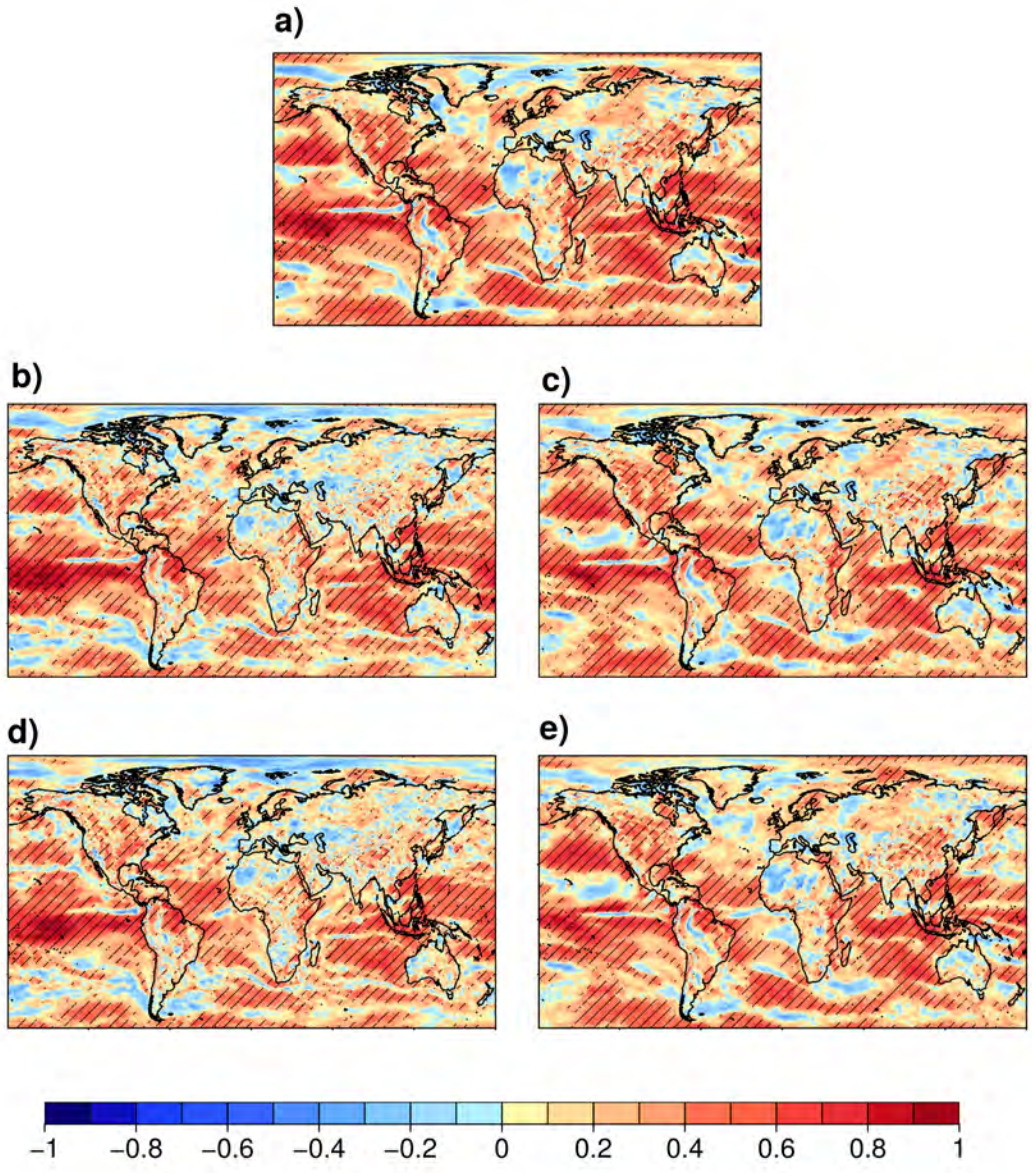

Figure 57 – Pearson correlation of the 10-m wind speed forecasts of a) mean wind speed value, b) 10^{th} percentile, c) 90^{th} percentile, d) fraction of time under the 10^{th} climatological percentile and e) fraction of time above the 90^{th} climatological percentile from ECMWF System 4 and ERA-Interim reanalysis in winter (DJF). The predictions have been initialised the 1^{st} of November for the period of 1981-2012. Hatched regions indicate correlation significantly (one-tailed t-test at the 95% confidence level) larger than zero.

forecast error have been illustrated. The most important gain in forecast quality for seasonal predictions comes through the increase in their skill and reliability, the latter being a critical aspect of the forecasts from the user perspective because it guarantees the trustworthiness of the probabilistic predictions. This work reveals that calibration is necessary because it produces an improvement in both skill and reliability, making this technique essential for seasonal predictions to be usable.

However, bias adjustment methods are not able to improve the misrepresentation of the physical mechanisms leading to low levels of skill. For that reason, a reconstruction approach based on empirical and dynamical forecasts has been applied. As it has been illustrated in chapter 4, ENSO teleconnections with wind speed are different in the seasonal predictions and in the observations for northern North America. When the seasonal predictions of 10-m wind speed are reconstructed from the empirical relationship between the Niño-3.4 index with the 10-m wind speed combined with the seasonal predictions of the Niño-3.4 index, an improvement of the correlation values in comparison with that for the raw predictions is found. This result indicates that the misrepresentation of the ENSO teleconnections to the 10-m wind speed is responsible for the low skill in that region. Hence, in the case that wind energy users are interested in the seasonal predictions of 10-m wind speed in that area, the reconstruction methodology generates more useful information than that produced directly from the seasonal forecast system.

Future work will be based on the combination of bias adjustment approaches with reconstruction methodologies, which take into account information of the large-scale circulation, to improve the skill of the seasonal forecasts of wind speed in relevant regions for the wind industry. The combination of bias adjustment methods with large scale circulation patterns such as ENSO is referred to as process-conditioned bias adjustment, and it has been recently used by Manzanas and Gutiérrez (2018) to adjust the systematic errors affecting the ECMWF System 4 seasonal forecasts of precipitation in northwestern Peru.

The description of the current capabilities of the seasonal prediction systems to produce accurate wind speed seasonal forecasts requires that the information about the mean wind speed predictability is complemented with information about the tails of its distribution (i.e. low and high wind speed values in a season). The potential skill of the extreme wind speed indicators is very similar to that illustrated for the mean wind speed, which shows that the predictability of the wind speed is mainly related to the seasonal forecast systems capacity to reproduce the variability of the mean wind speed. Bias adjustment is not essential for the wind speed indices based on climatological thresholds ($faq90_{clim}$ and $fbq10_{clim}$) because these indices are defined from the 10^{th} and 90^{th} climatological percentiles computed from the predicted and reference distributions separately. However, the wind speed extreme indices based on

absolute thresholds ($q10$ and $q90$) require a bias adjustment stage to reduce the systematic errors. Two different strategies could be followed to overcome this problem. On one hand, the application of a bias adjustment approach such as the quantile mapping, which corrects the full wind speed six-hourly probability distribution, and then to compute the 10^{th} and 90^{th} percentiles based on the bias adjusted wind speed. On the other hand, the implementation of bias adjustment over the wind speed extreme indices, although this approach has the problem that the consistency between the 10^{th} and 90^{th} percentiles derived from the six-hourly wind speed distribution cannot be guaranteed. These considerations should be taken into account in the case the seasonal predictions of these indicators have to be delivered in an operational way, and they should be further explored in the future.

07 Conclusions and perspectives

07 Conclusions and perspectives

Seasonal climate forecasts have the potential to become an important planning tool for energy traders, energy producers, plant operators and plant investors. Seasonal forecasts can lead to better and timely management of climate variability related risks. However, this source of climate information comes with a new set of challenges for end users. For instance, the information produced is complex and often hard to understand or apply in a decision-making context. These limitations have prevented the penetration of the seasonal predictions in wind energy decision-making processes.

This PhD thesis provides a comprehensive description of the opportunities and limitations of an operational seasonal forecast system for wind energy applications. The analysis, which takes into account the limitations mentioned above, has two main objectives:

1. The characterisation of the systematic errors **(chapter 3)** affecting seasonal predictions of the near-surface wind speed and temperature and sources of predictability **(chapter 4)** using the state-of-the-art ECMWF System 4 seasonal forecast system.

2. The development of pioneering products tailored to the specific needs of the wind energy sector based on seasonal forecasts. These products include the use of weather regimes as a tool to characterize the variability of wind speed and temperature over the Euro-Atlantic region **(chapter 5)** and the assessment of bias correction methods to produce high-quality seasonal forecasts **(chapter 6)**.

This chapter summarizes the main novel contributions of this thesis and discusses their relevance in section 7.1. During the development of this work, new research lines related to the generation of climate services for the wind energy sector have emerged. Those research lines (section 7.2) will be implemented in the near-future. Finally, the implications of this thesis for the development of an effective climate service are discussed in section 7.3.

7.1 Conclusions

The achievements of this thesis have resulted in the generation of methodologies and knowledge that is valuable in different research fields (e.g. climate prediction, climate services, wind energy, ...). Besides, some of these contributions could be transposed into the development of climate services for different sectors such as agriculture or water management. The most relevant scientific contributions of are described below.

1. Characterisation of the wind speed and temperature systematic errors in seasonal forecasts

The mean biases in seasonal forecasts are usually estimated as the difference between the mean climatology in predictions and observations. These mean biases show a high sensitivity to the dataset used as the observational reference, with a higher uncertainty for wind speed than for temperature. The high sensitivity of the mean biases to the observational reference is an important result that illustrates the need to systematically include several observational references in the evaluation of the seasonal forecasts. This is particularly the case for the 10-m wind speed. Systematic errors in high-order moments of the climatological distribution have been also explored. The results indicate that the ECMWF System 4 hindcasts represent the distributions of wind speed and temperature with a shape different to the reference one. For instance, important discrepancies have been illustrated for the standard deviation, skewness and kurtosis. To summarise these differences, a goodness-of-fit normality test has been applied, showing deviations from normality that depend on the region and the variable. This information is very relevant for wind energy applications that use these parameters to describe wind speed and air temperature because the different moments of the distribution are often biased in the seasonal forecasts. In that case, the use of the direct model output will lead to incorrect decisions. This justifies the need for bias adjustment of the seasonal forecasts.

2. Description of the uncertainty affecting different observational references

The uncertainty in the observational reference has an impact on different aspects of the seasonal forecasts. For instance, long-term trends of 10-m wind speed and 2-m air temperature are some of the aspects with the largest observational uncertainty. The discrepancies between the different reanalyses can lead to inconsistencies in the evaluation of wind energy resources.

The wind speed trends in different global reanalyses (ERA-Interim, JRA-55 and MERRA-2), considered as observational proxies, agree in the decline of the wind speed in Europe, India and South Africa. This reduction of the wind speed in the last decades could be related to changes in the atmospheric circulation. This is suggested as the main source because some of the factors previously proposed in the scientific literature, such as changes in the land use, are invalidated by an equivalent decrease in wind speed at the 850 hPa level. The inconsistencies in the wind speed trends for regions such as northern South America are particularly relevant to wind energy users who employ reanalyses to estimate the resource in poorly observed areas. The JRA-55 reanalysis should be used with particular care because it underestimates the wind speeds over land, resulting in extremely negative trends. The uncertainty affecting the 2-m air temperature is lower than in the case of the 10-m wind speed, as the three reanalyses show coherent trends in most of the land areas, although the uncertainty level varies with the region.

3. Evaluation of the global wind speed and temperature trends in the seasonal forecasts

The differences between the trends in the observational references and those simulated by the ECMWF System 4 can have an impact on the seasonal forecast quality. This occurs because forecast quality measures are the result of the mean distance between the observational reference and the forecast, and trends can be an important contributor to this distance. However, a description of the trends in seasonal forecasts of both the 10-m wind speed and the 2-m air temperature is still lacking. The comparison of the trends in the ECMWF System 4 seasonal predictions and the reanalyses shows similar results in terms of the sign. The discrepancies are higher for the 10-m wind speed than for the 2-m temperature, which is related to the higher observational uncertainty of the former. Besides, the trends of the seasonal forecasts of 10-m wind speed and 2-m temperature are much less intense than those in the reanalyses, which can be the result of the trends based on the ensemble mean but also the underestimation of the observed trend by the forecast system. This disagreement could be also related to the misrepresentation of those forcings responsible for the changes in the atmospheric circulation which cause wind speed trends.

4. Prediction of wind energy relevant climate indices

There is a number of climate indices relevant to wind energy applications that can be used to understand the predictive capability of seasonal forecast systems. These indices are in some cases linked to large-scale phenomena with substantial seasonal predictability, like ENSO or NAO. Others are linked to extra-tropical climate variability and the occurrence of wind extremes like the storm tracks. The potential skill (measured through the Pearson correlation of the ensemble mean prediction) of ECMWF System 4 to simulate the Niño-3.4 index for ENSO,

the NAO index and indices of the storm track activity in the North Atlantic (NAST) and North Pacific (NPST) have been explored for different start dates and forecast times. The Niño-3.4 and NPST indices show positive and significant correlations with ERA-Interim, which can be traced back to the large ENSO skill of this system. By contrast, low correlations have been obtained for the NAO and NAST indices. This might be due to a large amount of unpredictable internal variability characteristic of the North Atlantic region. Although ENSO and NAO skill assessments are common in seasonal forecasting, the prediction of the storm track activity is more innovative. For that reason, the assessment of the storm tracks has been extended to also characterise the ECMWF System 4 systematic errors for the different seasons and forecast times. The most important error is found in the North Pacific, where the storm track intensity in winter is overestimated for all forecast months. The large bias in the NPST index requires an appropriate bias adjustment approach before it is used in applications. Systematic errors in the North Atlantic storm tracks are smaller but have a marked dependency with the forecast time. The large correlation for the Niño-3.4 and NPST indices suggests that they could be used as predictand in a hybrid empirical-dynamical model to improve the quality of the predictions.

5. Teleconnections of wind energy relevant indices

The ability of the seasonal forecast systems to simulate the teleconnections of wind energy relevant indices with wind speed and temperature is essential to understand the seasonal forecast quality. When the teleconnections are not appropriately reproduced the impact of the indices that determine the variability might be shifted, implying that the variability might be correctly predicted but in the wrong place. Several studies have evaluated the impact of ENSO and NAO on the air temperature at a global scale. However, the teleconnections of both these indices and other wind energy relevant indices with wind speed have rarely been explored. Teleconnections of the Niño-3.4, NAO, NPST and NAST indices with the 10-m wind speed and 2-m temperature have been evaluated using one-point correlation maps. This analysis has been performed for both the seasonal forecasts and the ERA-Interim reanalysis, which has been used as a reference here, separately. Their comparison allows identifying the systematic errors in the teleconnection regional signal. For the seasonal forecasts, one-point correlation maps have been computed employing two different approaches. In the first approach, the ensemble mean of the index is correlated with the ensemble mean of the local variable. These results show a very strong dependency with the forecast time, as the inter-annual variability of the ensemble mean decreases, particularly for long forecast times, as a consequence of averaging over all the members. In the second approach, each individual member of the index is correlated with the corresponding value of the local variable. The resulting one-point correlation maps are

very similar for the different forecast months because the inter-annual variability is not filtered by the ensemble averaging operation. When the observed teleconnections are compared to those in ECMWF System 4, the resemblance of the maps is higher for the teleconnection maps computed using the individual members. This suggests that a validation of the forecast system teleconnections should be performed using the individual members because this approach preserves the forecast inter-annual variability. The ENSO teleconnections are generally well reproduced by ECMWF System 4, although the discrepancies with the observed teleconnections are higher for wind speed than for temperature. For example, the negative and significant correlations between ENSO and wind speed displayed by ERA-Interim in northern North America are not present in the forecast system. It was shown that this systematic error has implications in the seasonal forecast quality of wind speed predictions in that area. The NAO index shows low levels of skill, but its teleconnections to wind speed and temperature are well represented by the seasonal forecast system. The NPST and NAST teleconnections in ECMWF System 4 show good agreement with the reference teleconnections in the North Pacific and North Atlantic sectors, respectively. However, in some remote regions, severe discrepancies between the predicted and reference teleconnections to wind speed and temperature are found. The misrepresentation of the teleconnections in the forecast system evidences the systematic errors that are relevant for the understanding of the forecast quality by both wind energy users and modellers. However, the search for the cause of this systematic error is beyond the scope of this thesis and it is suggested as future work.

6. Weather regime classification to describe local wind speed and temperature variability

An additional way to describe the inter-annual variability in the Euro-Atlantic region is by characterising the daily atmospheric circulation. There are several ways to do this, the analysis of weather regimes (WR) being a popular one. Most of the WR classifications available in the literature have been defined for either the winter and/or summer seasons. However, wind energy users need to understand the impact of the atmospheric variability on wind energy resources throughout the year. To address this specific need, a WR classification for each month of the year has been produced. Four WRs have been obtained from the k-means cluster analysis applied to sea level pressure over the Euro-Atlantic region. The resulting classification describes atmospheric patterns for the equinoctial months that are not identified in the traditional winter/summer classifications. As a result, there are changes in the WR responses in the wind and air temperature that can be easily related to the WRs in a specific month. These variables can be reconstructed from the WR using the frequency for each month. Such reconstruction helps to determine the suitability of the classification to describe the local user variables. The results have revealed that there

are several regions over Europe for which the variability of wind speed and air temperature can be explained by changes in the frequency of occurrence of the monthly WRs. However, the efficiency of the reconstruction and, hence, the ability of the WRs to explain the variability of local wind and air temperature, is highly dependent on the region and month evaluated. Those regions where the WR influence is very high can benefit from the reconstruction of wind speed and temperature. This offers the possibility of improving the seasonal forecasts whenever they show better levels of skill to predict large-scale patterns such as those represented in the WRs. Besides, monthly WRs represent a convenient framework to understand the wind and air temperature changes in most parts of Europe.

7. Seasonal forecast quality of the Euro-Atlantic weather regimes

As explained in the previous point, changes in the atmospheric circulation play a dominant role in the variability of wind and air temperature. The characterisation of the atmospheric circulation with WRs helps to exploit this feature. Hence, the WR prediction some months in advance can be very useful for the wind industry. WRs have been validated in the ECMWF System 4. The WRs of the seasonal predictions have been computed by two different methodologies. First one is a k-means cluster analysis, which has been applied to the seasonal forecast daily data to investigate the degree of similarity of the simulated WRs with the classification obtained for ERA-Interim. This method is useful to characterise the WR systematic errors in the seasonal forecasts. For instance, the cluster analysis produces some simulated WRs whose spatial patterns do not match any pattern in the reference. As a consequence, it is not always possible to map the simulated and reference WRs for a specific month. To overcome this major limitation for the forecast quality assessment of the simulated WRs, an alternative approach to the direct clustering of the hindcast data has been proposed. The alternative approach is based on the classification of the anomalies of each simulated day using the maximum similarity with the reference WRs. In other words, the simulated day was assigned to the WR in the observational reference with which the root mean square distance is minimum. This methodology allows to effectively relate the simulated WRs to the reference weather regimes and is the most suitable for the development of a WR product for the users. The biases in the monthly frequency of occurrence of each regime are low, which indicates that the seasonal predictions provide climatological monthly frequencies of occurrence similar to the corresponding from ERA-Interim. The potential skill of ECMWF System 4 to predict the mean frequency of occurrence of a particular weather regime is restricted to the first forecast month. This result is related to the limitations of ECMWF System 4 to produce skilful monthly-mean predictions of sea level pressure in the North Atlantic region. Future work will apply this methodology to other regions with higher

predictability and still of interest to the wind energy sector like North America.

8. Bias adjustment of wind speed seasonal forecasts

Seasonal forecasts tailored to wind energy decision-making processes need to fulfil two specific requirements to facilitate the integration of these forecasts into energy models: they need to produce reliable probabilities and have similar statistical properties to the observational references. As it has been shown at length in this thesis, seasonal forecasts of wind speed are affected by a wide range of systematic errors. Therefore they need to be bias adjusted to be usable by wind energy applications. Bias-adjustment techniques have been widely applied in the seasonal forecast context. However, their suitability for the 10-m wind speed has not been explored yet. Three different bias adjustment methodologies have been compared here: simple bias correction, quantile mapping and calibration. These methods have been applied in cross-validation to emulate the operational context. Cross-validation leads to the degeneracy of the information that results in a reduction of the correlation of the bias-adjusted forecasts in comparison to the correlation obtained from the raw forecasts (i.e. the original output of ECMWF System 4). However, the bias-adjusted forecasts show an improvement of the probabilistic skill scores (FRPSS and FCRPSS) as a consequence of the seasonal forecasts having the same statistical properties to the observations. The reliability assessment based on reliability diagrams and rank histograms has revealed that the calibration method produces more reliable predictions than the simple bias correction and the quantile mapping. This result indicates that the calibration method could be the most suitable for the development of seasonal forecasts tailored to wind energy applications. Furthermore, the seasonal forecasts of bias-adjusted 10-m wind speed exhibit skill in some extra-tropical regions. These results evidence the added value of the adequately processed seasonal forecasts in comparison with the information currently used (i.e. retrospective climatologies) for wind energy decision-making.

9. Wind speed seasonal forecast improvement using an ENSO index

The limited skill of the seasonal predictions described in the previous point has important implications in some regions where wind farm power installed is substantial. One example of these regions is central Canada, where no skill is found. The ENSO teleconnection analysis for wind speed suggested that the misrepresentation of the teleconnection in that region could be responsible. A way to exploit the significant skill in predicting ENSO to improve the wind speed seasonal forecasts consists in reconstructing the wind field with an ENSO index. The reconstruction method uses the observed empirical relationship between the Niño-3.4 index and the local wind speed. This approach shows that the boreal winter forecasts initialised in August in central Canada, unskilful in the original forecasts, when reconstructed

with the forecast Niño-3.4 index have positive correlation. These results suggest that there is good potential for the development of hybrid empirical-dynamical approaches to produce usable seasonal forecasts.

10. Verification of seasonal forecasts of extreme wind speed indicators

Information about extreme winds can be useful for wind energy users as wind extreme events can produce severe losses through damage to the infrastructure or production reduction. For that reason to complement the seasonal forecast information of the mean 10-m wind speed, four wind extreme indicators have been defined: 10^{th} and 90^{th} percentiles of the local wind speed monthly values and the fraction of time below/above the 10^{th}/90^{th} percentile of the local wind speed climatological distribution in a season. These indices have been computed using six-hourly data and have been evaluated in terms of mean bias and correlation of the ensemble mean to investigate the potential of this kind of indicators for wind energy decision-making. Seasonal forecasts of the fraction of time below/above the climatological 10^{th}/90^{th} percentiles do not require bias adjustment because the climatological percentiles have been computed separately for the predictions and the observational reference. However, the 10^{th} and 90^{th} percentiles might show a mean bias when the reference and simulated variability are different. The correlation between these four extreme indices is very similar to the correlation obtained for the seasonal forecasts of the mean 10-m wind speed. This is an encouraging result because the skill of extreme indicators, which could be more informative for some wind energy applications than the mean 10-m wind speed, may be inferred from the skill of the mean forecast.

7.2 Future work

The development of climate services based on seasonal climate forecasts is a research discipline in its early stages. Such novelty led to innovative research lines during the development of this thesis. It also led to some ideas that deserve further exploration to improve the quality of future operational climate services. Some of these ideas are described below.

The ECMWF System 4 seasonal forecasts have shown difficulties to provide skilful climate information over Europe. The low forecast quality represents a major limitation for the integration of this information in wind energy applications. One option to improve the seasonal forecasts in this region is the combination of seasonal forecasts from different forecast systems in a multi-model ensemble. This combination approach usually provides, on average, better results than the best single forecast system because it takes into account, among other things, their lack of reliability (e.g Weigel et al. 2008). However, due to different operational implementation of each individual system (hindcast length, ensemble size, lagged or burst ensemble generation, spatial resolution, ...), the construction of a coherent multi-model

is a challenging task. Future work will be based on the exploration of methodologies that can optimise the climate information produced by the single seasonal forecast systems included in Copernicus Climate Change Service (C3S, https://climate.copernicus.eu/seasonal-forecasts).
This work will aim at providing wind energy users with the best information currently possible.

Another way to improve the seasonal forecasts of wind speed and air temperature consists in exploiting the predictability of the atmospheric flow. The atmospheric circulation in the Euro-Atlantic region can be characterised in several ways, such as a number of weather regimes or a set of modes of variability. If the seasonal forecasts are able to predict either the weather regimes or the leading modes of climate variability, wind speed and air temperature fields can be reconstructed from them. The atmospheric circulation indices could increase the number of predictors used in the hybrid model developed in chapter 6 and improve the seasonal forecast skill in some regions. However, forecasts of the frequency of the Euro-Atlantic weather regimes are only skilful for the first forecast month. This might not be the case of other forecast systems, and it is an aspect that should be explored. It is expected, though, that the skill of the weather regimes over North America is higher. Hence, seasonal forecasts of North American weather regimes offers an important potential for the wind energy sector. Similar arguments apply to the modes of variability analysed like ENSO, NAO or the storm track intensity and even others not considered in this thesis like the Pacific North American (PNA), the Indian Ocean Dipole (IOD) or the Quasi-biennial Oscillation (QBO).

The large-scale atmospheric circulation indices can also be combined with bias adjustment approaches to improve the seasonal forecast quality. These bias adjustment methodologies are defined as process-conditioned bias adjustments (Manzanas and Gutiérrez 2018). Their main advantage is that they conditionally modify the inter-annual variability of the raw seasonal forecasts to better represent the variability of the reference dataset. The systematic exploration and the development of process-conditioned bias adjustments should offer the possibility to improve seasonal forecasts of wind energy relevant variables.

Seasonal forecasts of either wind speed or air temperature, or both, might not be enough for some wind energy applications. In some cases, users also need to obtain information about the expected wind energy production. Within the wind energy community, several methodologies to estimate short-term forecasts of wind energy production from meteorological forecasts are used. However, these methodologies cannot be directly implemented at seasonal timescales because seasonal forecasts have coarser spatial and temporal resolutions compared to the short-term meteorological forecasts. The coarser grid used implies, for instance, that the model variables are less representative of the local variability, which is the one users are familiar with. Some progress has been made to find

optimal procedures to transform the observed wind speed into wind energy at seasonal timescales (MacLeod et al. 2018). This knowledge will be applied to illustrate if skilful and reliable seasonal forecasts of wind energy production can be produced.

Both seasonal forecast quality assessment and bias adjustment require the use of a reference dataset. The choice of a particular reference dataset and its intrinsic uncertainty (be it either available or not) strongly affects wind speed and forecast quality estimates, as it has shown in this thesis with several reanalyses. Nevertheless, the number of reference datasets employed for that evaluation is typically limited. To complement this information the potential of new datasets such as the ERA-5 reanalysis (https://cds.climate.copernicus.eu/cdsapp#!/home), which is the first reanalysis including estimates of its uncertainty, should be explored. This reanalysis is particularly relevant for wind energy users as it includes wind speed at 100 m. Besides, to increase the robustness and relevance of the climate information distributed among wind energy users, ERA-5 should be compared with in-situ data for specific wind farm locations. This assessment has not been carried out during this thesis because the observational databases containing wind speed measurements are limited. However, in the framework of the INDECIS project (http://www.indecis.eu/) a database of wind mast data is being produced. Observations of wind speed in specific locations and at different heights will be used to further understand the dynamical mechanisms leading to wind speed trends.

Surface wind speed exhibits substantial variability at much smaller spatial scales than the typical resolution of current global climate forecast systems. For this reason, wind energy users usually demand high-resolution information that allows characterising this variability. Increased spatial resolution can be obtained using downscaling approaches, which aim at adapting coarse climate simulations into time series for specific locations. There are several methodologies to perform downscaling on seasonal forecasts and they can be classified in dynamical or statistical methods. Dynamical downscaling usually employ a regional climate model driven by boundary conditions from a global climate model to derive smaller-scale information. Statistical downscaling is based on the empirical relationships between the local climate variables (the predictands) and the large-scale variables (the predictors). Hence, observations in specific wind farms, whenever the time series is long enough, should be used as predictand to investigate the suitability of downscaling methods to produce useful local information for the wind energy sector.

7.3 Final remarks

The main scientific contributions described in section 7.1 represent an innovation in the use of climate information to satisfy the needs of a number of wind energy users. These results can be used as a benchmark for the future generation of seasonal forecast systems and related climate

services initiatives.

This thesis opens the field to the development of a climate service through the creation of tailored products that facilitate the widespread use of seasonal forecasts by the wind energy sector. However, a climate service is more complex than developing seasonal climate information because it should include aspects such as knowledge transfer (informing, documenting, and providing training) or the design of operational online interactive platforms that allow users to easily explore probabilistic predictions.

During this PhD thesis, the scientific work presented has been constantly interacting with knowledge transfer activities and the development of operational online tools. One example of this interaction is the RESILIENCE prototype (http://resilience.bsc.es/), an online decision support tool designed in the framework of the EUPORIAS and CLIM4ENERGY projects that incorporates the bias adjusted seasonal predictions of wind speed described in Chapter 6. This tool is being improved to include more variables and indicators under the on-going S2S4E project (https://s2s4e.eu/). Another example of an online tool is the New European Wind Atlas (NEWA, see online at http://euwindatlas.eu/), which is currently in development. This atlas will provide access to skill evaluation of the seasonal forecasts of wind speed developed in chapter 6.

Seasonal climate information tailored to the wind energy sector is a necessary part for a successful climate service, but it should be informed by efforts to engage with well-identified wind energy users from a social science perspective to ensure the relevance and timeliness of this new source of climate information.

Appendices

A Metrics for the forecast quality assessment

In this PhD thesis two main aspects of the forecast quality have been evaluated, skill and reliability. Skill quantifies the forecast quality against a reference forecast. In this work, the seasonal forecasts have been compared with a climatological forecast, which refers to always forecasting the mean value of the variable over a retrospective period. This choice has been made taking into account the current practices in the wind industry, where the climatology is used as a benchmark. Reliability quantifies the agreement between the forecast probabilities and the observed relative frequencies. The forecast quality assessment has been carried out by employing different skill and reliability metrics (section A.1). The methods employed to evaluate the significance of all the metrics employed in this thesis are explained in section A.2. These metrics have been computed by two R-language-based software packages: s2dverification (Manubens et al. 2018) and SpecsVerification[1].

A.1 Forecast quality metrics

To investigate the skill of the ensemble mean, the deterministic Pearson correlation has been used. However, ensemble forecasts are often issued as probabilities for binary or categorical events. For that reason, different probabilistic forecast quality metrics have been also used. Ranked probability skill score (RPSS) and continuous ranked probability skill score (CRPSS) have

[1] https://cran.r-project.org/web/packages/SpecsVerification/index.html

been selectd because they summarize different forecast attributes such as the skill, resolution or reliability. In particular, the fair version of these skill scores (Ferro 2014), which reward probabilistic predictions with ensemble members that perform as if they have been sampled from the same distribution than the reference dataset, have been used. The rank histogram and the reliability diagram are complementary tools to assess the reliability of the seasonal prediction system. The former assesses the full forecast ensemble and does not require the formulation of forecast probabilities, an aspect that is necessary in the case of the reliability diagram, where the features of both the forecast system and the statistical model that transforms the ensemble into probabilities are assessed.

A.1.1 Deterministic metric: Pearson correlation

The Pearson correlation coefficient (Wilks 2011) between the deterministic ensemble mean and the reference data set has been used as a measure of the linear correspondence between the retrospective forecasts and the observational reference. This can be defined as:

$$\rho = \frac{\sum_{i=1}^{N} (x_i - \bar{x})(\hat{y}_i - \bar{y})}{\sqrt{\sum_{i=1}^{N} (x_i - \bar{x})^2 (\hat{y}_i - \bar{y})^2}} \qquad \text{(A.1)}$$

where x_i and $\hat{y}_i$ are the observational reference and the ensemble mean anomalies values in each season over the $i = 1, 2, ..., N$ years. The $\bar{y}$ and $\bar{x}$ are the average of the ensemble mean and the reference over the N years.

The Pearson correlation ranges between -1 and 1. If $\rho = 1$ there is a perfect association between the ensemble mean and the observational reference. When $\rho = 0$ indicates that there is no association between the ensemble mean and the reference dataset, thus the ensemble mean prediction does not provide added value relative to the retrospective climatology. If the ensemble mean predictions are worse than the past climatology, then $\rho < 0$ and in that case the climatological prediction should be used. Positive correlation is the minimum requirement for forecasts to have some potentially useful information because it depends not only on the potential predictability but also on the precise distribution of the data (Jolliffe and Stephenson 2012). A t-test (defined in section d) has been applied to evaluate if the correlation values are significant at the 95% confidence level.

Pearson correlation is invariant to changes in scale, hence the bias-adjustment of the forecasts does not change the correlation values. However those bias adjustment techniques used in chapter 6 (defined in section 6.2.1) have been applied in leave-one-out cross-validation mode (section 2.5) that causes some deviations in the correlations.

A.1.2 Probabilistic metrics

Skill scores (*SS*) are relative measures of the quality of the forecasting system compared to some baseline forecast (Jolliffe and Stephenson 2012). They are defined as:

$$SS = 1 - \frac{Score}{Score_{bench}} \tag{A.2}$$

where *Score* is a scoring metric for the forecast system under evaluation and the $Score_{bench}$ is the same scoring metric applied to the forecast used as benchmark, which is often built from an observed climatology. While the forecast *Score* ranges between 0 and 1 (with 0 indicating a perfect agreement between the forecast and the reference dataset), SS ranges from $-\infty$ to one, where a negative value of *SS* implies that the forecast is worse than the use of a climatological reference as a forecast, the $SS = 0$ indicates that the forecast provides the same information as the climatological forecast and $SS = 1$ corresponds to a perfect forecast. The skill scores have been computed for two different scoring metrics: the ranked probability score and the continuous ranked probability score. Confidence intervals of these skill scores have been obtained by quantifying the sampling uncertainty (section A.2.2) affecting these estimates when it is possible. Sampling uncertainty estimates allows testing whether the deviations from zero of the skill scores are robust or if they are due to sampling issues.

a) Ranked probability skill score

A comprehensive measure of the predictive skill for the probabilistic seasonal predictions of categorical events is given by the ranked probability score (RPS) (Epstein 1969; Wilks 2011).

The *RPS* is the sum of the squared distance between the cumulative probabilities of the N forecasts and observations pairs for K forecast categories:

$$RPS = \frac{1}{N}\sum_{i=1}^{N}\sum_{l=1}^{K}\left[\left(\sum_{k=1}^{l} p_{i,k}\right) - \left(\sum_{k=1}^{l} e_{i,k}\right)\right]^2 \tag{A.3}$$

where $p_{i,l}$ and $e_{i,l}$ are the predicted and reference probabilities assigned by the i^{th} forecast ($i = 1,...,N$) to the k^{th} category. The $e_{i,l} = 1$ indicates that the reference is in category k^{th}, and $e_{i,l} = 0$ otherwise.

The *RPS* is often expressed as a skill score because it allows assessing the forecast added value compared to the climatological forecasts. The ranked probability skill score (*RPSS*) is given by:

$$RPSS = 1 - \frac{RPS}{RPS_{clim}} \tag{A.4}$$

As any other skill score RPSS ranges from $-\infty$ to one. In this PhD thesis the RPSS has been computed for the evaluation of terciles (three equi-probable categories ($K = 3$) associated with the two terciles of the climatological distribution of the reference). The probabilities have been computed as the fraction of ensemble members in the corresponding category.

b) Continuous ranked probability skill score

The continuous ranked probability skill score (*CRPSS*) is a commonly used probabilistic skill score that allows for the predictive skill

assessment of the full probability distribution (Jolliffe and Stephenson 2012). It is based on the continuous ranked probability score (*CRPS*), a score that reduces to the mean absolute error if a deterministic forecast is used (Wilks 2011). The *CRPS* can be expressed as:

$$CRPS = \int_{-\infty}^{\infty} [F(y) - F_0(y)]^2 \, dy \qquad \text{(A.5)}$$

where $F(y)$ is the cumulative density function of the forecasts and $F_0(y)$ is the cumulative step function that jumps from 0 to 1 at the point where the variable y equals to the observational reference x:

$$F_0 = \begin{cases} 0, y < x \\ 1, y \geq x \end{cases} \qquad \text{(A.6)}$$

The CRPS measures the difference between the predicted and observed cumulative distributions and it can be converted into a skill score (*CRPSS*), measuring the performance of a forecast relative to the climatology:

$$CRPSS = 1 - \frac{CRPS}{CRPS_{clim}} \qquad \text{(A.7)}$$

c) Fair scores

Fair scores to ensemble forecasts have been recently introduced (Fricker et al. 2013; Ferro 2014). A skill score is fair when it favours predictions with ensemble members that perform as if they have been sampled from the same distribution as the reference dataset. The fair version of the RPSS and CRPSS have been used in order to give an estimate of what the skill is when an infinite ensemble size is used (a measure of potential skill).

The differences between the results of the fair and the basic scores are small (0.02 maximum) as they have been illustrated for the CRPSS in Figure A1. These differences are systematic and the fair CRPSS always shows higher values than the CRPSS. The tropics show the lowest differences between the two scores.

d) Rank histograms

Rank histograms (RH) are a simple tool to evaluate the reliability of ensemble forecasting systems (Elmore 2005). They diagnose if the ensemble members and the verifying observation (i.e. observational reference) come from the same probability distribution. If they can be considered as belonging to the same population, the forecasts are statistically consistent and no calibration of the ensemble is needed.

To construct the RH an M member ensemble forecast ($y_i = y_{i,1} + y_{i,2} + ... + y_{i,M}$) and the corresponding observation (x_i) have been considered. The RH is constructed for N forecast-observation pairs ($i = 1, ..., N$). The $M + 1$ possible ranks (bins) are defined by the forecast range and the frequencies of the histogram correspond to the number of observations falling in each rank. When x_i is smaller than all the ensemble members, then the observation is assigned to the first rank, but if it exceeds all the ensemble members then it is placed at the $M + 1$ rank.

If the probabilistic prediction is reliable, then the ensemble members and observations are statistically indistinguishable, and it will be equally probable for the observation to fall in any of the ranks (i.e. the number of counts in each rank is $N/(M+1)$). In this case the RH is flat (as if coming from a uniform distribution).

If the RH is not flat, the particular deviations from flatness could be useful to identify some forecast deficiencies (Hamill 2001). The correspondence between the shape of the RH and the specific problems affecting the ensemble forecasts have been illustrated in Figure A2.

In addition to the over/under-confidence affecting the forecasts or the biases, some deviations from uniformity can appear for reliable forecasts due to randomness or sampling variations. To avoid misinterpretations of the RH, they have been displayed on probability paper (Bröcker 2008). An example of the RH representation on probability paper is shown in Figure A3.

In the y-axis RH represented on probability paper display cumulative probabilities instead of the traditional observed frequencies. This representation indicate how probable that observed frequency would be if the prediction was reliable, which is useful to identify if the deviations from a reliable behavior are systematic or merely random. Furthermore the

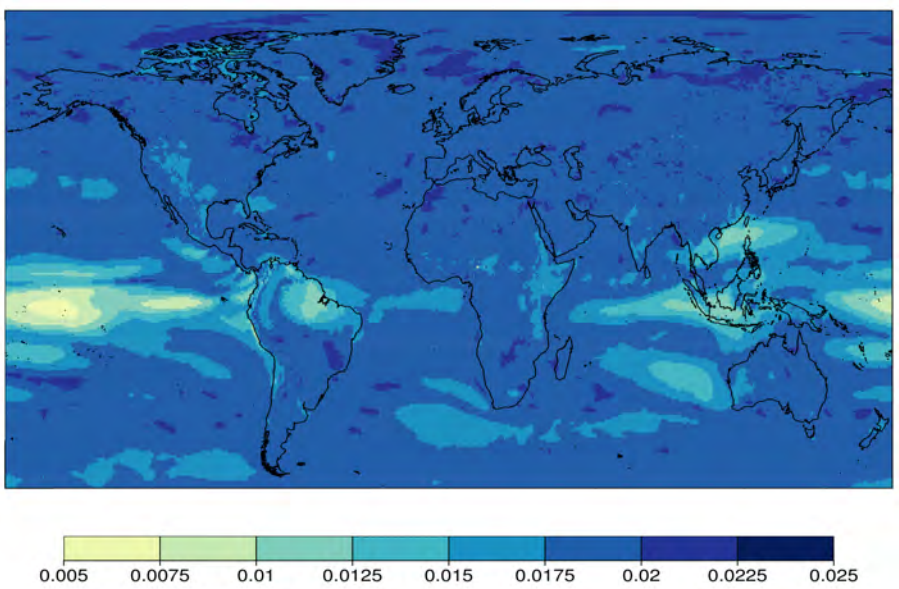

Figure A1 – Differences between the fair continuous ranked probability skill score (FCRPSS) and the continuous ranked probability skill score (CRPSS) for the 10-m wind speed forecasts from ECMWF System 4 and ERA-Interim reanalysis in winter (DJF) for the period 1981-2012. The predictions have been initialized the 1^{st} of November.

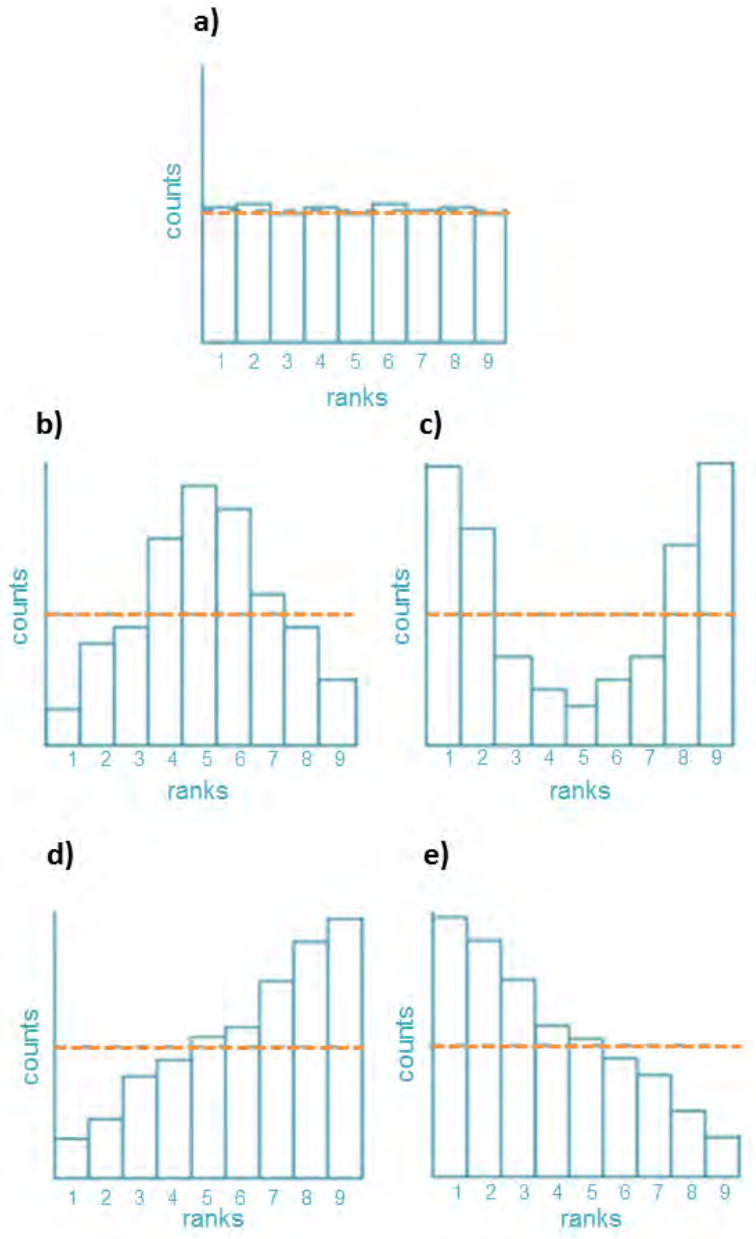

Figure A2 – Illustrative examples of rank histograms for hypothetical ensembles: a) reliable, b) underconfident, c) overconfident, d) negative biased and e) positive biased ensemble forecasts with M=8. Perfect rank uniformity is indicated by the horizontal orange lines (computed as $N/(M+1)$). Adapted from Wilks (2011).

readability of the RH is further improved by scaling the ordinate by a logit-transformation, that has the effect of displaying both small and large probabilities equidistantly. On the right y-axis of the plot the 90, 95, and 99 percent confidence intervals have been represented. If all ranks where equally likely on average, approximately 90% of the ranks histogram would be contained in the 90% confidence interval and approximately 10% of the ranks fall outside this interval.

To complement the visual information provided by the rank histograms, goodness-of-fit test statistics have been also computed: Pearson χ^2, the Jolliffe-Primo test statistic for slope (JP slope) and the Jolliffe-Primo test statistic for convexity (JP convex) (Jolliffe and Primo 2008). The Jolliffe-Primo statistics are obtained from the decomposition of the Pearson χ^2 in components that allow the identification of bias (slope) or under/over-dispersion (convexity) in the forecast ensemble. The detailed mathematical definition of these goodness-of-fit tests can be found in the appendix of Jolliffe and Primo (2008).

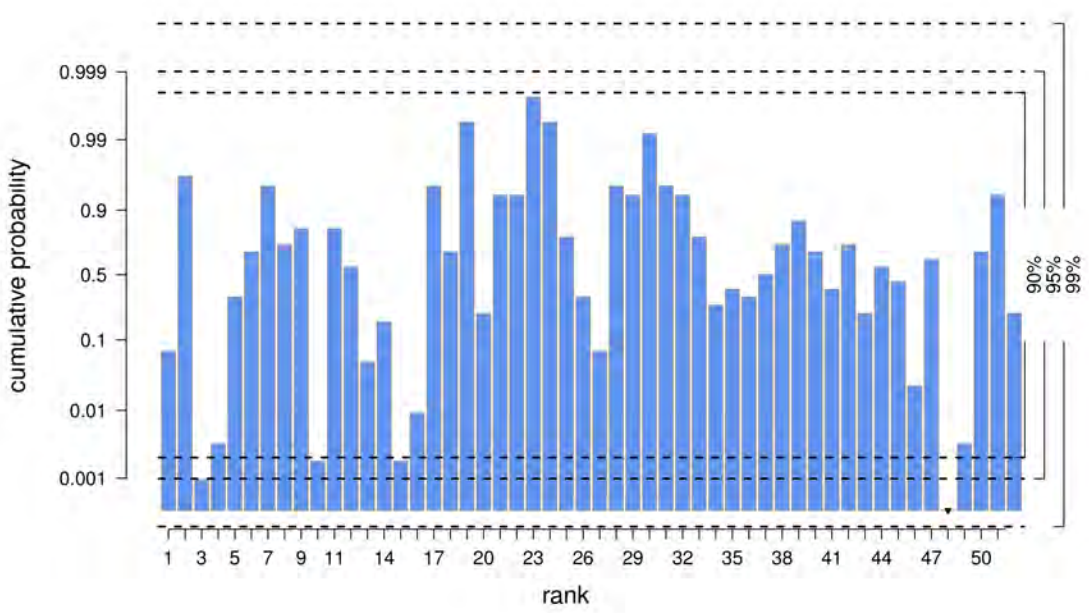

Figure A3 – Example of a rank histogram represented on probability paper (Bröcker 2008) for a forecast with 51 ensemble members. The rank values are represented in the x-axis and the cumulative observed frequencies are displayed in the y-axis which has been scaled on a log-it scale. On the right side of the graph, 90%, 95% and 99% simultaneous confidence intervals are shown.

e) Reliability diagrams

Reliability diagrams are a common diagnostic of probabilistic predictions that assess both reliability and skill. They consist of a plot of the observed relative frequency against the predicted probability of a dichotomous event, providing a quick visual assessment of the impact of tuning probabilistic forecast systems. A perfectly reliable system should draw a line as closely as possible to the diagonal, within a certain measure of uncertainty.

The reliability diagrams have been used to evaluate the three forecast events defined by terciles (Figure A4): below normal (blue), normal (orange) and above normal (red) graphs. To draw a reliability diagram, discretisation and grouping into probability bins of the probability forecasts have to be done. In this work 10 bins

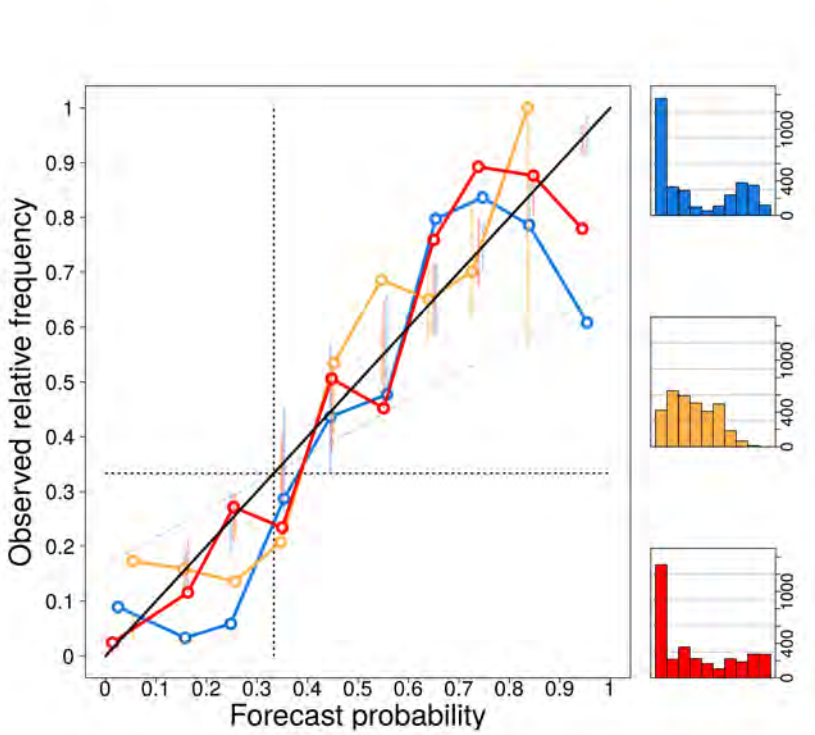

Figure A4 – Example of a reliability diagram for three events: below normal (blue), normal (orange) and above normal (red). Observed frequencies (y-axis) is represented as a function of its forecast probability (x-axis). The diagonal line indicates perfect reliability. The dotted horizontal and vertical lines shows the climatological probabilities (one third). The dotdashed grey line is the no skill line. The consistency bars indicate how likely the observed relative frequencies are under the assumption that predicted probabilities are reliable. Marginal sharpness diagrams show the predicted relative frequencies of the forecast events (y-axis) with different levels of probability (x-axis).

have been used. The climatological forecast probability corresponding to these categories and the long-term frequency of the observed tercile events are one third and they have been displayed as dotted vertical and horizontal lines, respectively. The no skill line has been added as dotted-dashed line. Points falling in the region bounded by the vertical and the no skill lines contribute positively to the forecast skill.

The reliability diagram also includes information about the frequency of the forecast probabilities in each event, which is known as sharpness diagram. Sharpness is a property of the forecasts that gives an indication of the variation in forecast probabilities issued by the forecast system, independently of the observations. They have been represented as a histogram in the right margin of the plot.

The information provided by the reliability diagram should be interpreted with care because even a perfectly reliable forecast system is not expected to have an exactly diagonal reliability diagram due to the limited samples typical of seasonal forecast systems (Jolliffe and Stephenson 2012). To deal with this problem consistency bars are included in these diagrams. They indicate how likely the observed relative frequencies are, under the assumption that predicted probabilities are accurate. These consistency bars are obtained by 500 bootstrap resamples.

A.2 Significance tests

To evaluate if the results obtained in the analyses performed in this thesis are statistically significant, different tests have been applied. This is particularly important in the case of the seasonal predictions as the sample length for evaluation is limited. Consequently, statistical inference is crucial to identify if the results are robust or if they have been obtained by chance (Bröcker and Smith 2007).

A.2.1 Hypothesis testing: t-test

Statistical hypothesis testing uses the information in a sample to decide whether or not to reject the null hypothesis (H_0). A second proposition, the alternative hypothesis (H_1) generally describes the range of possibilities that may be true when H_0 is false. The outcome of this test only has two possibilities: either H_0 is rejected or it is not rejected. The significance level (α) is the probability of rejecting the null hypothesis when it is true. Therefore, the probability of not rejecting the null hypothesis (i.e. confidence level) is $1-\alpha$. The parametric t-test is a statistical hypothesis test in which the statistic follows a t-distribution under the null hypothesis which is partially tabulated in Von Storch and Zwiers (2002, Appendix F). The t-test has been used here for the three different hypothesis tests described below. These definitions are based on Von Storch and Zwiers (2002).

a) Test for difference of means

The t-test has been used to compute the significance of the bias (described in chapter 3). The null hypothesis is that the mean of the ensemble mean predictions ($\bar{y}$) and the mean of the observations ($\bar{x}$) are equal, which can be expressed as:

$H_0 : \bar{y} = \bar{x}$, there is not signifcant difference between the means.

$H_1 : \bar{y} \neq \bar{x}$, there is a signifcant difference between the means.

The test statistic based on the assumption that x and y have unequal variances can be defined as:

$$t = \frac{\bar{y} - \bar{x}}{\sqrt{\frac{{\sigma_y}^2}{N_y} + \frac{{\sigma_x}^2}{N_x}}} \tag{A.8}$$

where σ_x and σ_y are the standard deviations of x and y, respectively. N_x and N_y are the number of ensemble mean predictions and observations used to compute the means ().

The t value will be compared with a tabulated $t_{\alpha/2}$ value for a significance level $\alpha = 0.05$ (95% confidence level). In this two-tailed test, the null hypothesis is rejected when either $t < t_{\alpha/2}$ or $t > t_{(1-\alpha)/2}$.

b) Test for linear trend

To evaluate if the linear trend defined by the equation 3.7 included in chapter 3 (b_1) is statistically significant, the null hypothesis is that the linear trend is zero:

$H_0 : b_1 = 0$, there is no significant trend.

$H_1 : b_1 \neq 0$, there is a significant trend.

In this case the hypothesis is tested by the ratio between the estimated trend and its standard error:

$$t = \frac{b_1}{s_{b_1}} \tag{A.9}$$

Where the standard error is defined as:

$$s_{b1} = \frac{s_e}{\left[\sum_{i=1}^{N} (i - \bar{i})^2\right]^{1/2}} \tag{A.10}$$

and s_e is the variance of the residuals ($e(i) = z(i) - \bar{i}$) about the regression line:

$$s_e^2 = \frac{1}{N-2} \sum_{i=1}^{N} e(i)^2 \tag{A.11}$$

the t value (A.9) will be evaluated through a two-tailed t-test for which the null hypothesis is rejected when either $t < t_{\alpha/2}$ or $t > t_{(1-\alpha)/2}$ and $N-2$ degrees of freedom.

c) Test for linear correlation

The correlation coefficient (ρ) defined in equation A.1 has been employed for different purposes throughout this thesis and their statistical significance has been tested by the following hypothesis:

$H_0 : \rho = 0$, there is no significant correlation.

$H_1 : \rho \neq 0$, there is a significant correlation.

The test used to assess the significance of the

correlation is defined as:

$$t = \frac{\rho\sqrt{N_{eff}-2}}{\sqrt{1-(\rho^2)}} \tag{A.12}$$

Where N_{eff} is the effective sample size that depends on the autocorrelations ($\rho_x, \rho_{\hat{y}}$) of the time series and the number of x and $\hat{y}$ pairs:

$$N_{eff} = N\frac{1-\rho_x\rho_{\hat{y}}}{1+\rho_x\rho_{\hat{y}}} \tag{A.13}$$

In this thesis correlation has been used in two different contexts. The first application is to assess the relationship between the climate variables and the climate indices (one-point correlation maps, chapter 4), and in this case the two-tailed test has been applied (i.e. the null hypothesis is rejected either $t < t_{\alpha/2}$ or $t > t_{(1-\alpha)/2}$ for a significance level $\alpha = 0.05$ and $N-2$ degrees of freedom). However, the correlation has also been employed to assess the association between the seasonal predictions and the observational references (chapters 5 and 6). In this case, a one-tailed t-test (i.e. the null hypothesis is rejected when $t > t_{\alpha}$ value for a significance level $\alpha = 0.05$ and $N-2$ degrees of freedom) has been applied as negative correlations indicate that the seasonal predictions are not providing any added value in comparison to the climatological reference.

d) Test for correlation differences

The statistical significance of the differences between independent one-point correlation maps used in Chapter 4 to explore the association between a particular variable and a climate index in the observational reference (ρ_1) and the seasonal predictions (ρ_2) have been also evaluated by the following hypothesis:

$H_0 : \rho_1 = \rho_2$, There is no significant difference between the correlations.

$H_1 : \rho_1 \neq \rho_2$, There is a significant difference between the correlations.

The first step to evaluate whether the difference between the two correlations are significant is to transform the correlations with the Fisher's z-transform:

$$z_{\rho_1} = \frac{1}{2}ln\left(\frac{1+\rho_1}{1-\rho_1}\right) \tag{A.14}$$

$$z_{\rho_2} = \frac{1}{2}ln\left(\frac{1+\rho_2}{1-\rho_2}\right) \tag{A.15}$$

Then the test obtained from the Fisher's z transformed correlations divided by the standard error of the difference:

$$Z = \frac{\left|z_{\rho_1} - z_{\rho_2}\right|}{\sqrt{\frac{1}{(N_1-3)} + \frac{1}{(N_2-3)}}} \tag{A.16}$$

Where N_1 and N_2 are the number of pairs used to compute (ρ_1) and (ρ_2).

The Z value (A.16) will be compared with the critical $Z_{1-(\alpha/2)}$ value for a significance level $\alpha = 0.05$.

A.2.2 Sampling uncertainty for probabilistic skill scores

Forecast quality metrics are computed with one of many possible samples from a population, therefore they are affected by sampling uncertainty (Jolliffe and Stephenson 2012). The estimation of the sampling uncertainty for a forecast quality metric is used to obtain the confidence intervals of the skill scores (e.g. against a null hypothesis of zero skill) (Wilks 2011).

One approach to assess the sampling uncertainty of forecast quality metrics are the resampling methods (Wilks 2011). These methodologies are computationally very expensive. For that reason, an alternative approach based on the sampling theory has been used here to derive analytical expressions for sampling uncertainty. In this thesis the approach described in Bradley et al. (2008) have been used as it is implemented in the SpecsVerification R-package.

The first step is to compute the standard error of the skill score (defined in equation A.2), which is computed with N pairs of forecasts and observations. The standard error (SE) describes its sampling uncertainty and it is related to the standard deviation of the skill score (σ_{SS}):

$$SE_{SS} = \frac{1}{\sqrt{n}}\sigma_{SS} \tag{A.17}$$

Then the sampling standard deviation of the skill score has been derived from the propagation of uncertainty by a first-order approximation:

$$\begin{aligned}{\sigma_{SS}}^2 = \sigma_{Score}^2 \left(\frac{\partial SS}{\partial Score}\right)^2 + \\ \sigma_{Score_{clim}}^2 \left(\frac{\partial SS}{\partial Score_{clim}}\right)^2 + \\ 2\sigma_{Score}\sigma_{Score_{clim}} \left(\frac{\partial SS}{\partial Score}\right)\left(\frac{\partial SS}{\partial Score_{ref}}\right)\end{aligned} \tag{A.18}$$

Where the partial derivatives can be defined as:

$$\left(\frac{\partial SS}{\partial Score}\right) = \frac{-1}{Score_{clim}} \tag{A.19}$$

$$\left(\frac{\partial SS}{\partial Score_{clim}}\right) = \frac{Score}{Score_{clim}^2} \tag{A.20}$$

If it is suppossed that the SS is normally distributed with unknown variance, the confidence interval for the skill score is then:

$$SS \pm z_{1-\alpha,N-1}\dot{S}E_{SS} \tag{A.21}$$

where $z_{1-\alpha,N-1}$ is the $(1-\alpha)$ quantile of the standard normal distribution. These confidence intervals have been obtained for a 95% confidence level. This approximation can be useful to avoid overinterpretations of the skill scores values (Siegert 2014).

B
Additional figures

This appendix contains the additional figures mentioned along this thesis. The goal of this appendix is to provide supportive information to the different results discussed within the chapters. However, they are presented in an appendix to enhance the thesis readability. The appendix B has been divided in four different sections according to the chapters:

B.1 - Extra figures for chapter 3
B.2 - Extra figures for chapter 4
B.3 - Extra figures for chapter 5
B.4 - Extra figures for chapter 6

The list of figures corresponding to each section are outlined in the subsequent pages.

B.1 Extra figures for chapter 3

Figure B1 – Seasonal mean climatology of the 10-m wind speed (m/s) from ERA-Interim and ECMWF System 4 in the 1981-2015 period 197
Figure B2 – Seasonal mean climatology of the 10-m wind speed (m/s) from JRA-55 and MERRA-2 in the 1981-2015 period 198
Figure B3 – Mean bias of the ECMWF System 4 seasonal predictions of 10-m wind speed (m/s) in DJF for different lead months 199
Figure B4 – Mean bias of the ECMWF System 4 seasonal predictions of 2-m air temperature (K) in DJF for different lead months 200
Figure B5 – Standard deviation ratio of ECMWF System 4 seasonal predictions to ERA-Interim, JRA-55 and MERRA-2 201
Figure B6 – Skewness and kurtosis of the 10-m wind speed from ECMWF System 4, ERA-Interim, JRA-55 and MERRA-2 202
Figure B7 – Skewness and kurtosis of the 2-m air temperature from ECMWF System 4, ERA-Interim, JRA-55 and MERRA-2 203
Figure B8 – P-values of the Shapiro-Wilk goodness-of-fit normality test applied to 10-m wind speed and 2-m air temperature from ECMWF System 4, ERA-Interim, JRA-55 and MERRA-2 204
Figure B9 – Coherence maps between the 2-m air temperature trends produced by ERA-Interim, JRA-55 and MERRA-2 205
Figure B10 –Linear trend of 2-m air temperature (K/decade) from ERA-Interim, JRA-55, MERRA-2 and ECMWF System 4 206
Figure B11 –Normalised linear trend (% per decade) of the 10-m wind speed from JRA-55 and MERRA-2. 207
Figure B12 –Normalised linear trend (% per decade) of the 850 hPa wind speed from JRA-55 and MERRA-2. 208
Figure B13 –Linear trend (m/s per decade) of the 10^{th} (left column) and 90^{th} (right column) of 10-m wind speed from ERA-Interim. 209
Figure B14 –Linear trend (m/s per decade) of the 10^{th} (left column) and 90^{th} (right column) of 10-m wind speed from JRA-55. 210
Figure B15 –Linear trend (m/s per decade) of the 10^{th} (left column) and 90^{th} (right column) of 10-m wind speed from MERRA-2 211

B.2 Extra figures for chapter 4

Figure B16 –One-point-correlation maps between the ERA-Interim 10-m wind speeds and 2-m air temperature with the Niño-3.4 index 212
Figure B17 –One-point-correlation maps between the ERA-Interim 10-m wind speeds and 2-m air temperature with the NAO index 213
Figure B18 –Lead time dependency of the MAM differences between the one-point-correlation maps of the 10-m wind speed and the NAO index in the ECMWF System 4 seasonal forecasts and in ERA-Interim 214
Figure B19 –Lead time dependency of the DJF differences between the one-point-correlation maps of the 2-m air temperatue and the NAO index in the ECMWF System 4 seasonal forecasts and in ERA-Interim 215
Figure B20 –One-point-correlation maps in ECMWF System 4 ensemble mean predictions and the ERA-Interim reanalysis for the NAST and NPST indices and the 10-m wind speed in DJF. 216
Figure B21 –One-point-correlation maps in ECMWF System 4 ensemble mean predictions and the ERA-Interim reanalysis for the NAST and NPST indices and the 2-m air temperature in DJF. 217

B.3 Extra figures for chapter 5

Figure B22 –Weather regime spatial patterns obtained for ERA-Interim by the KM classification method in March, April and May 218
Figure B23 –Weather regime spatial patterns obtained for ERA-Interim by the KM classification method in June, July and August 219
Figure B24 –Weather regime spatial patterns obtained for ERA-Interim by the KM classification method in September, October and November 220
Figure B25 –Pearson correlation between the reconstructed and the original 10-m wind speed from ERA-Interim 221
Figure B26 –Pearson correlation between the reconstructed and the original 2-m air temperature from ERA-Interim 222
Figure B27 –Weather regime spatial patterns obtained for ERA-Interim and ECMWF System 4 by the KM classification method in April 223
Figure B28 –Weather regime spatial patterns obtained for ERA-Interim and ECMWF System 4 by the RMSD classification method in April . . . 224
Figure B29 –Bias between the ECMWF System 4 seasonal predictions and ERA-Interim reanalysis monthly frequencies of occurrence (% days) corresponding to WRs obtained by the a) KM and b) RMSD classification methods 225
Figure B30 –Pearson correlation of the sea level pressure ensemble mean from ECMWF System 4 and the ERA-Interim reanalysis in DJF, MAM, JJA and SON 226

B.4 Extra figures for chapter 6

Figure B31 –Pearson correlation of the 10-m wind speed ensemble mean from ECMWF System 4 and the ERA-Interim reanalysis in DJF, MAM, JJA and SON 227
Figure B32 –Pearson correlation of the 10-m wind speed ensemble mean from ECMWF System 4 and the ERA-Interim reanalysis in DJF for lead times from 0 to 4 months 228
Figure B33 –Pearson correlation of the 10-m wind speed ensemble mean from ECMWF System 4 and the ERA-Interim reanalysis two different periods. 229
Figure B34 –Time series of 10-m wind speed from ECMWF System 4 and ERA-Interim reanalysis in winter (DJF) for a region in Central United States and Northern Scandinavia 230
Figure B35 –Reliability diagrams of 10-m wind speed from ECMWF System 4 and ERA-Interim reanalysis in DJF in Central United States and Northern Scandinavia 231
Figure B36 –Rank histograms of 10-m wind speeds forecasts from ECMWF System 4 and ERA-Interim reanalysis in DJF in Central United States and Northern Scandinavia 232
Figure B37 –Pearson correlation of the ECMWF System 4 ensemble mean and the ERA-Interim reanalysis 10-m wind speed in DJF for different bias adjustments 233
Figure B38 –FCRPSS of the ECMWF System 4 and ERA-Interim reanalysis 10-m wind speed in DJF 235

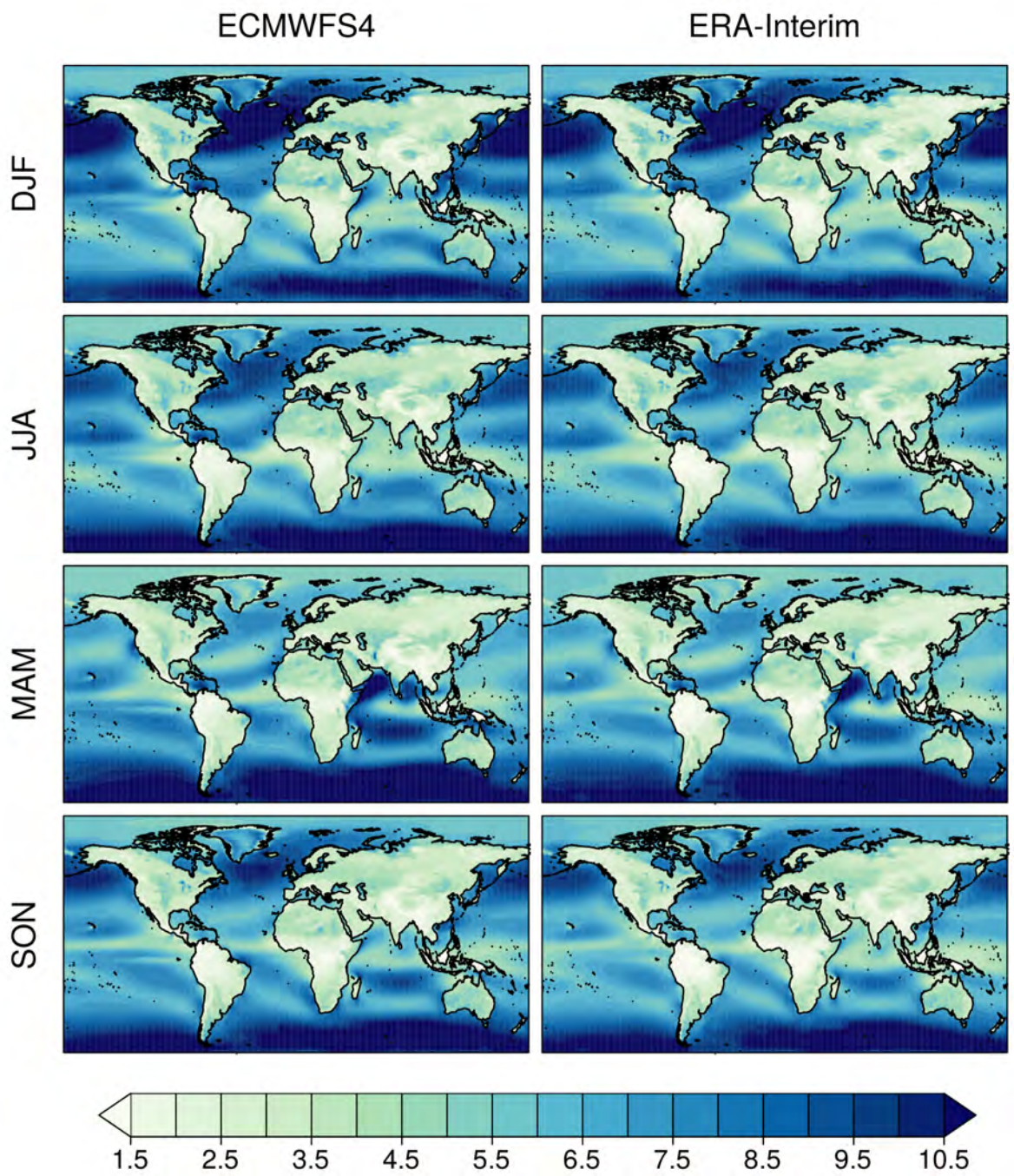

Figure B1 – Seasonal mean climatology of the 10-m wind speed (m/s) from ERA-Interim and ECMWF System 4 in the 1981-2015 period. They correspond to the following seasons: a) DJF, b) MAM, c) JJA and d) SON.

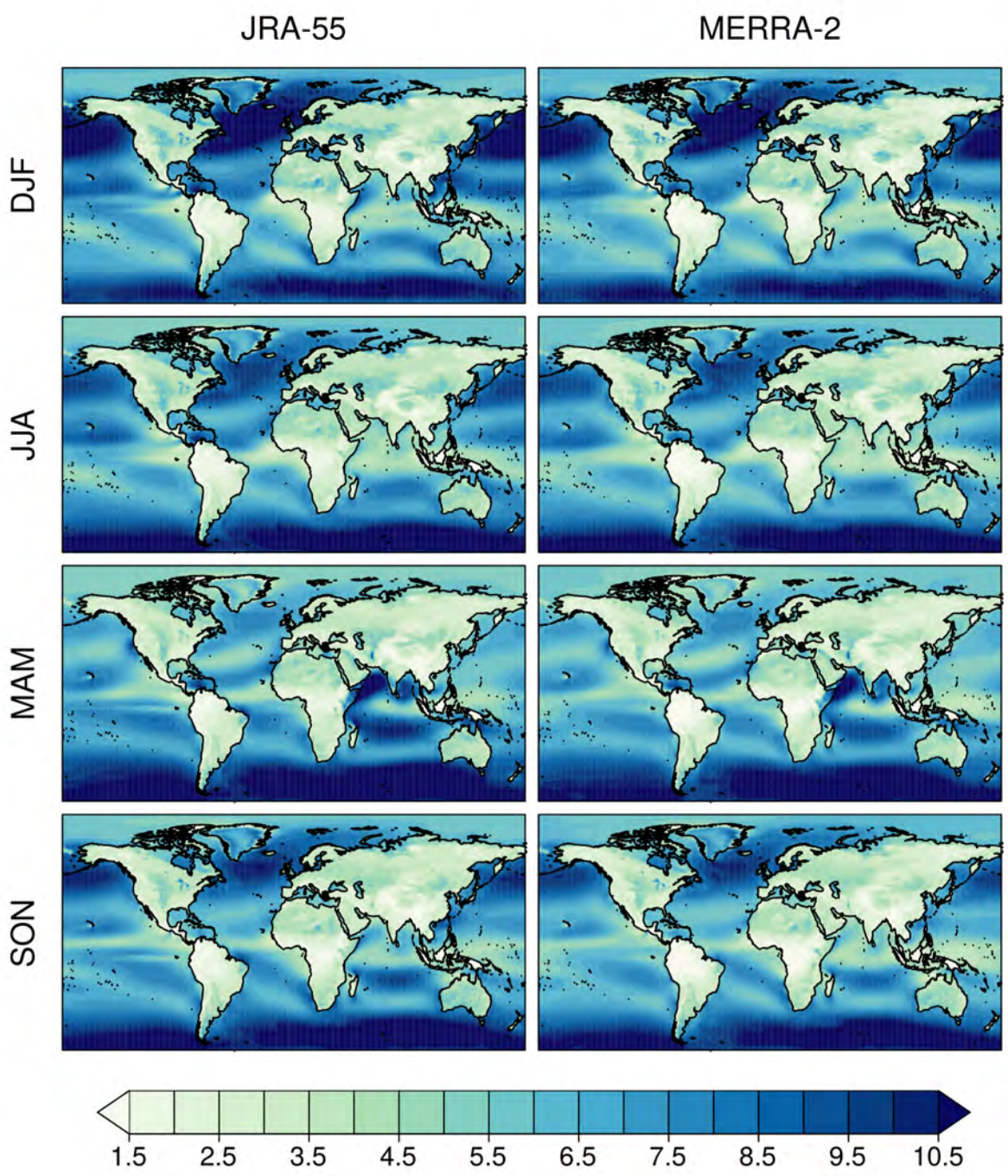

Figure B2 – Seasonal mean climatology of the 10-m wind speed (m/s) from JRA-55 and MERRA-2 in the 1981-2015 period. They correspond to the following seasons: a) DJF, b) MAM, c) JJA and d) SON.

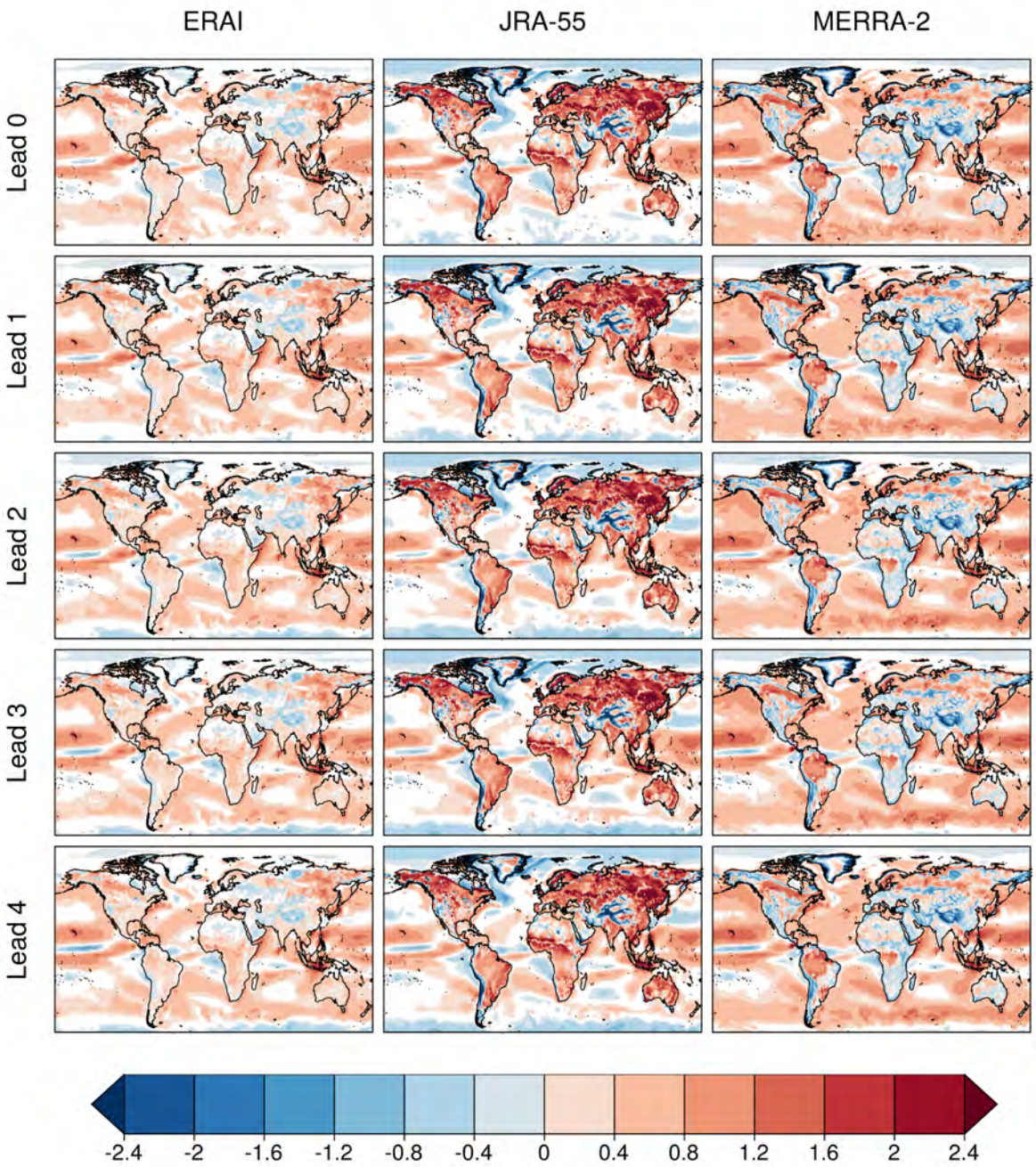

Figure B3 – Mean bias of the ECMWF System 4 seasonal predictions of 10-m wind speed (m/s) in DJF for different lead months. These biases has been computed over the 1981-2015 period. ECMWF System 4 seasonal predictions have been initialised the 1^{st} of December (Lead 0), November (Lead 1), October (Lead 2), September (Lead 3) and August (Lead 4). Three observational references have beeen employed: ERA-Interim, JRA-55 and MERRA-2. White areas deonte non significant biases (t-test at a 95% confidence level).

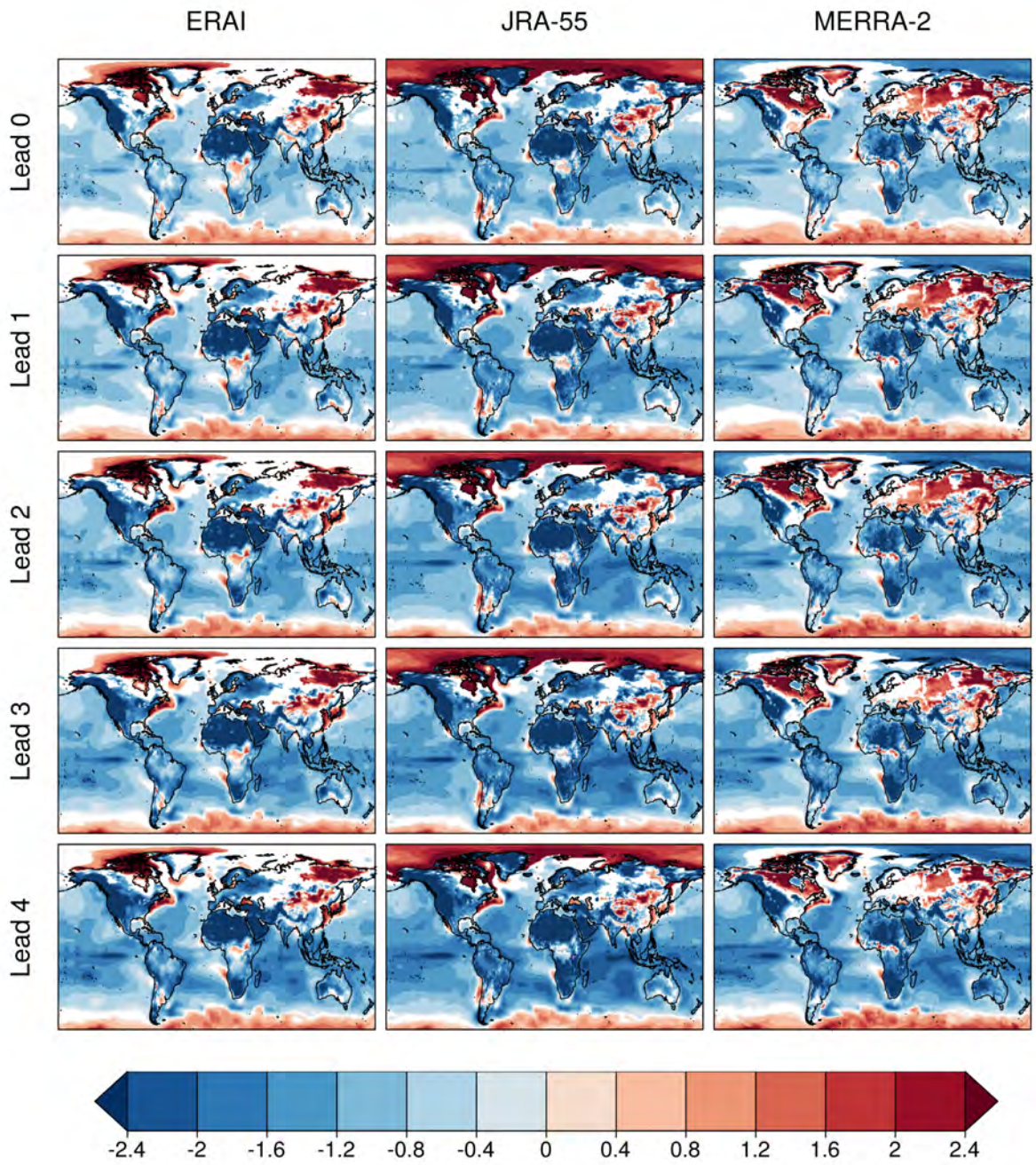

Figure B4 – Mean bias of the ECMWF System 4 seasonal predictions of 2-m air temperature (K) in DJF for different lead months. These biases have been computed over the 1981-2015 period. ECMWF System 4 seasonal predictions have been initialised the 1^{st} of December (Lead 0), November (Lead 1), October (Lead 2), September (Lead 3) and August (Lead 4). Three observational references have beeen employed: ERA-Interim, JRA-55 and MERRA-2. White areas deonte non significant biases (t-test at a 95% confidence level).

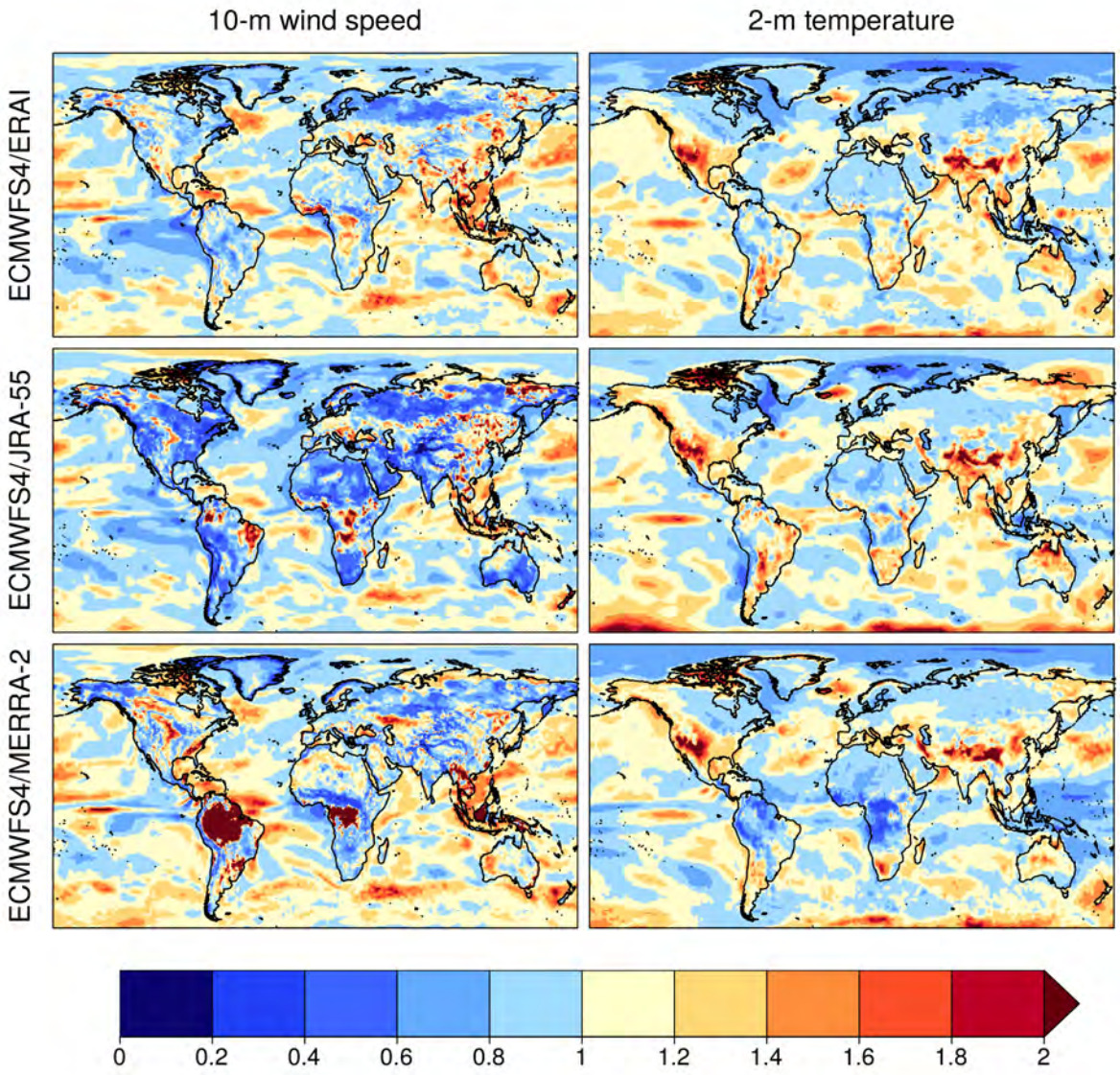

Figure B5 – Standard deviation ratio of ECMWF System 4 seasonal predictions to: ERA-Interim ($\sigma_{S4}/\sigma_{ERA-I}$, first row), JRA-55 ($\sigma_{S4}/\sigma_{JRA-55}$, second row) and MERRA-2 reanalyses ($\sigma_{S4}/\sigma_{MERRA-2}$, third row). This corresponds to the 10-m wind speed (left column) and 2-m air temperature (right column) in DJF over the 1981-2015 period. ECMWF System 4 seasonal predictions have been initialised the 1^{st} of November.

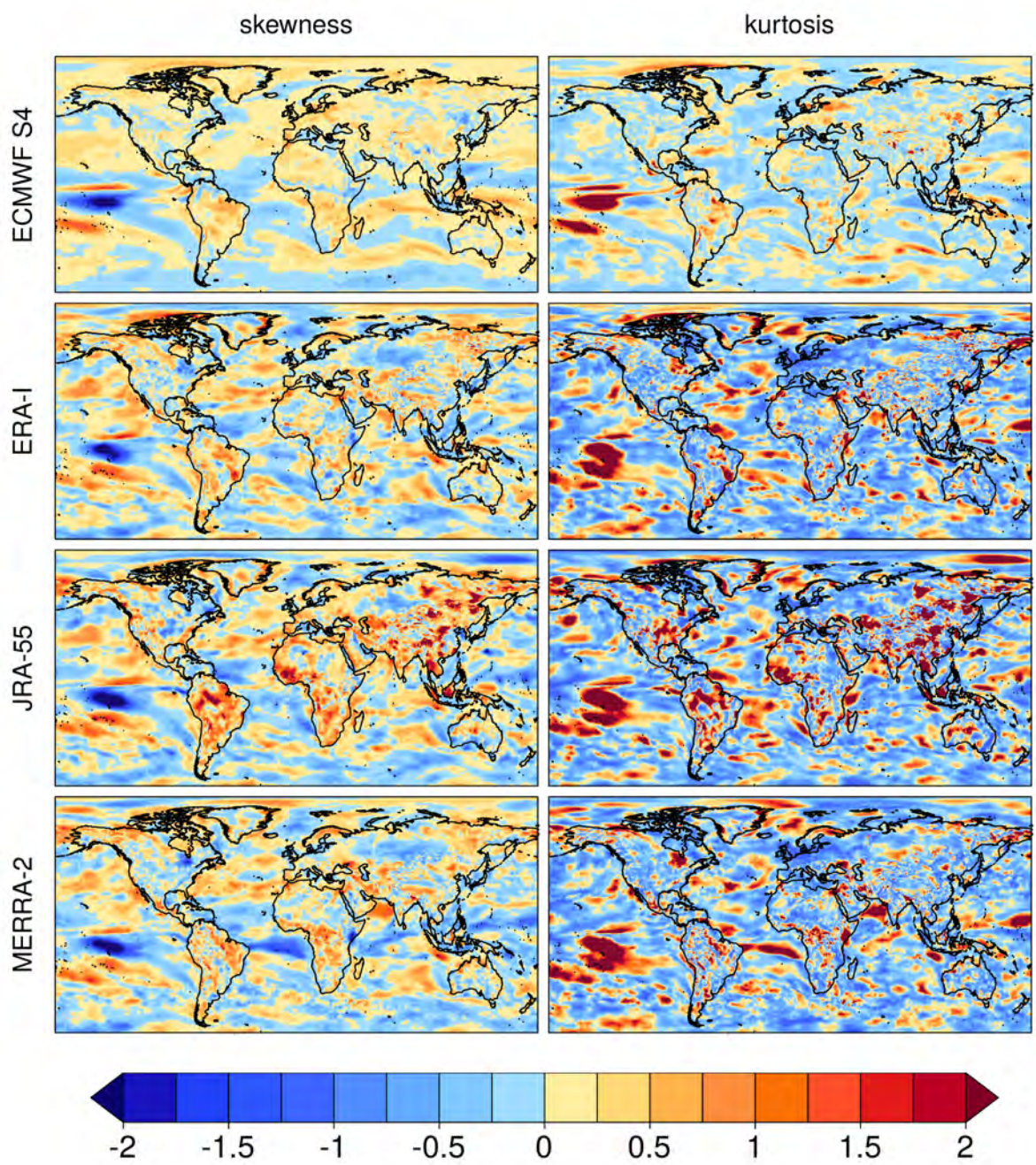

Figure B6 – Skewness and kurtosis of the 10-m wind speed from ECMWF System 4, ERA-Interim, JRA-55 and MERRA-2. This corresponds to the boreal winter (DJF) over the period 1981-2015. ECMWF System 4 seasonal predictions have been initialised the 1^{st} of November.

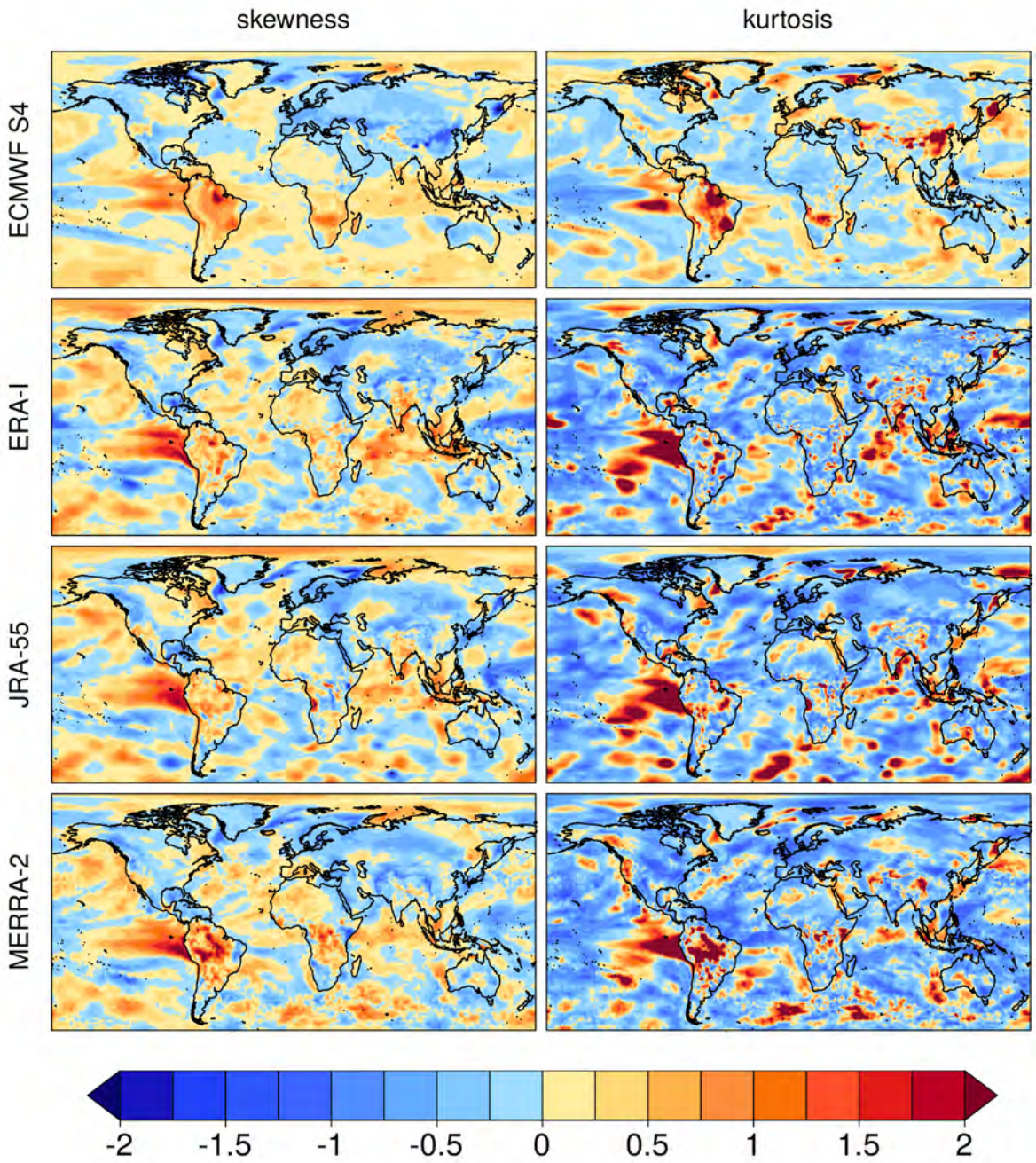

Figure B7 – Skewness and kurtosis of the 2-m air temperature from ECMWF System 4, ERA-Interim, JRA-55 and MERRA-2. This corresponds to the boreal winter (DJF) over the period 1981-2015. ECMWF System 4 seasonal predictions have been initialised the 1^{st} of November.

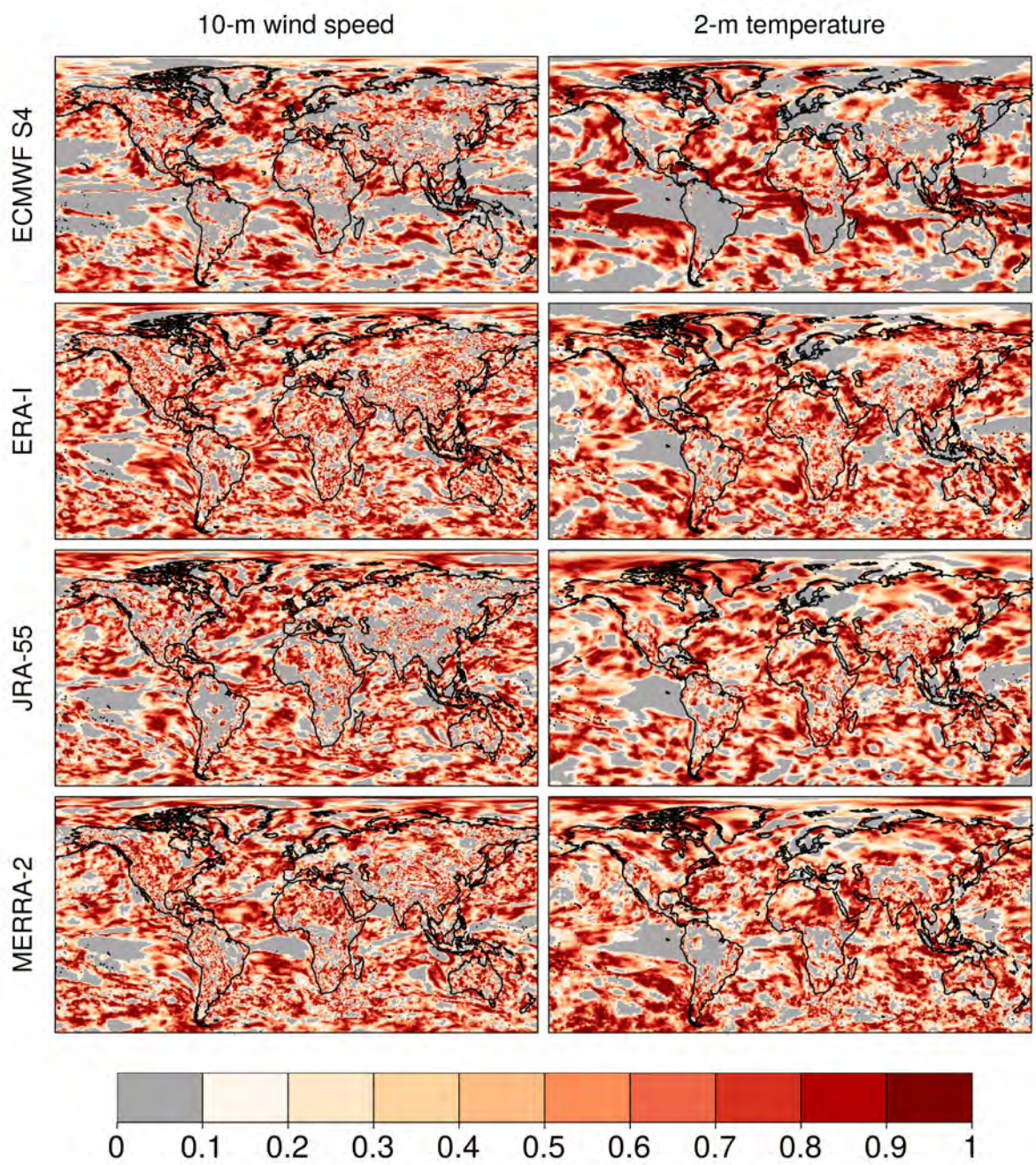

Figure B8 – P-values of the Shapiro-Wilk goodness-of-fit normality test applied to 10-m wind speed and 2-m air temperature from ECMWF System 4, ERA-Interim, JRA-55 and MERRA-2. This corresponds to the boreal winter (DJF) over the period 1981-2015. ECMWF System 4 seasonal predictions have been initialised the 1^{st} of November.

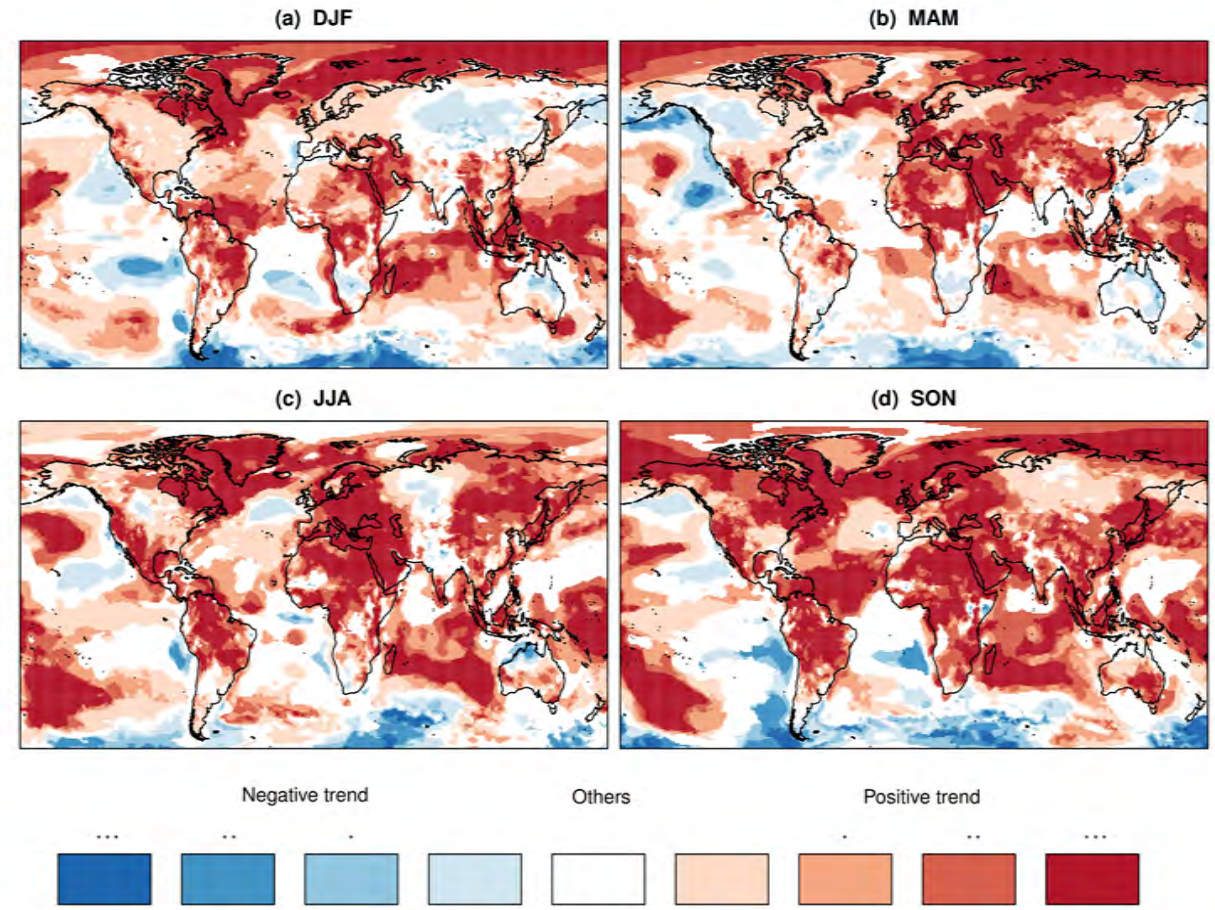

Figure B9 – Coherence maps between the 2-m air temperature trends produced by ERA-Interim, JRA-55 and MERRA-2. Blues (Reds) indicate agreement between the three reanalyses about the negative (positive) trends of 2-m temperature for a)DJF, b) MAM, c) JJA and d) SON in the 1981-2015 period. Asterisk indicates that the trends are significant at the 95% confidence level: no asterisk indicates that the trends are not significant, (*) only one of the reanalysis has significant trends, (**) informs that two reanalyses have significant trends, and (***) indicates that the three reanalyses have significant trends.

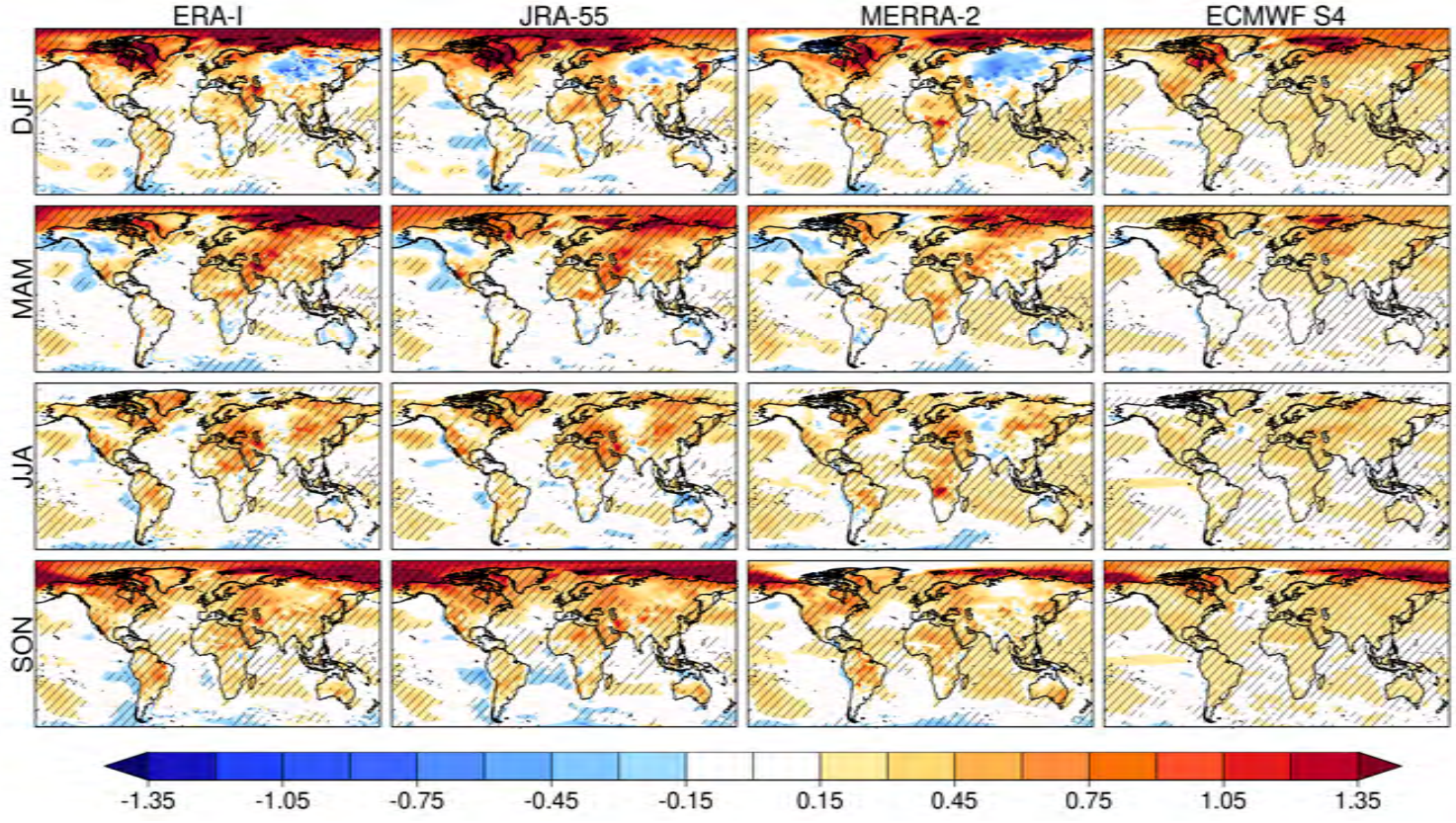

Figure B10 – Linear trend of 2-m air temperature (K/decade) from ERA-Interim, JRA-55, MERRA-2 and ECMWF System 4. They correspond to DJF, MAM, JJA and SON in 1981-2015. ECMWF System 4 seasonal predictions are initialised the 1^{st} of November, February, May and August respectively. Hatched regions indicate where the trends are significant at the 95% confidence level.

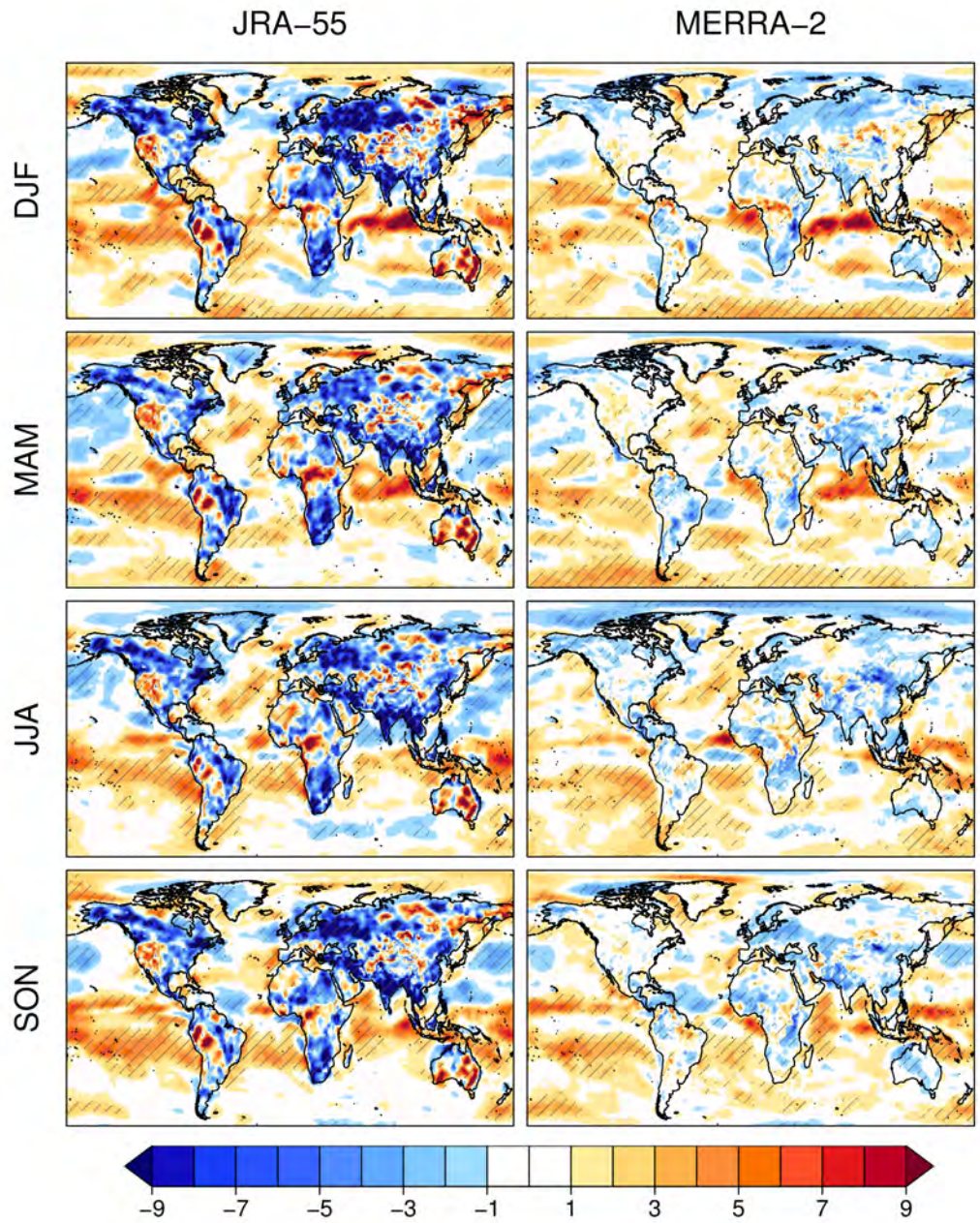

Figure B11 – Normalised linear trend (% per decade) of the 10-m wind speed from JRA-55 and MERRA-2. These normalised trends are calculated as the linear trend of 10-m wind speed divided by its seasonal climatology over the 1981-2015 period in a) DJF, b) MAM, c) JJA and d) SON. Hatched regions show areas where the trends are significant at a 95% confidence level.

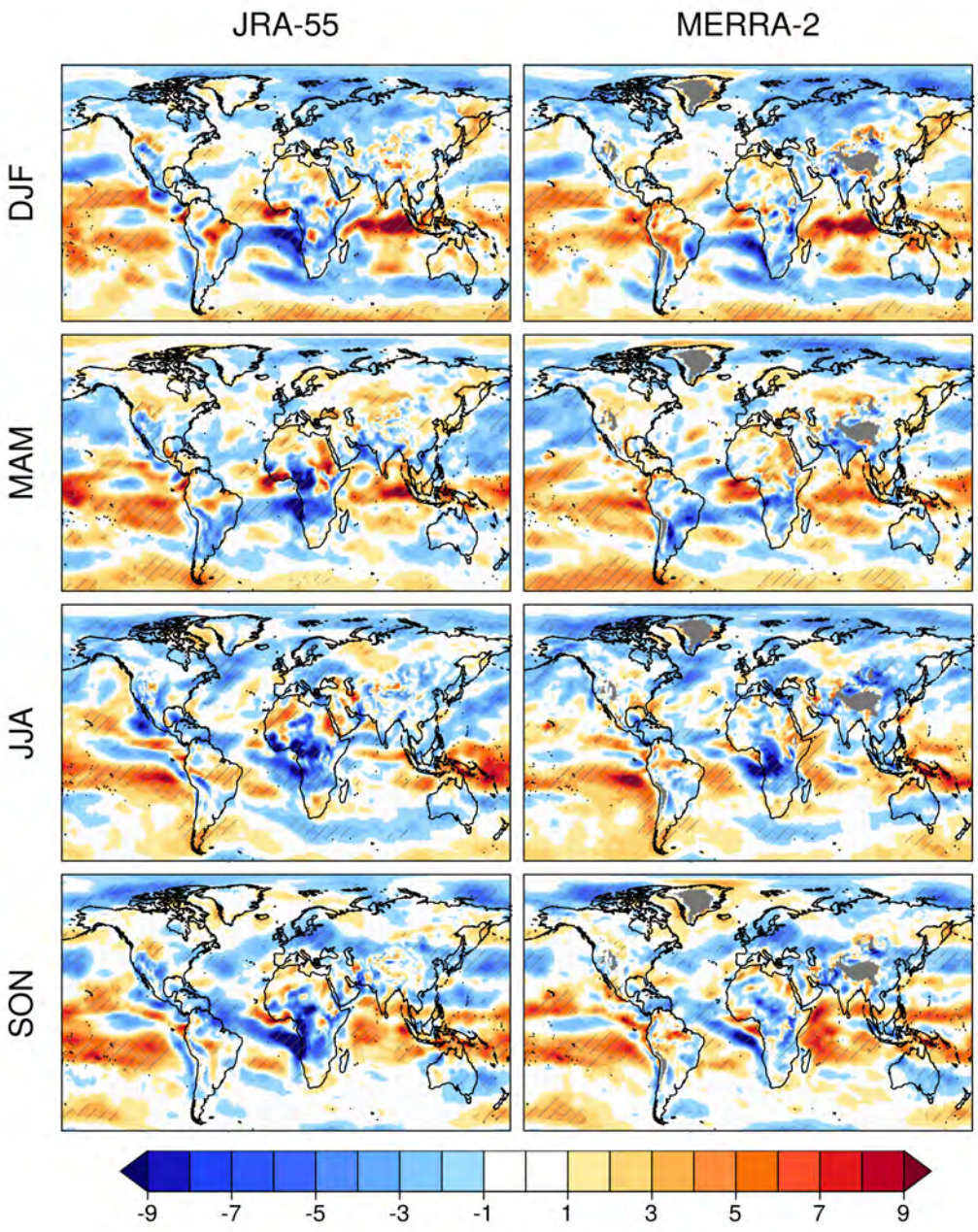

Figure B12 – Normalised linear trend (% per decade) of the 850 hPa wind speed from JRA-55 and MERRA-2. These normalised trends are calculated as the linear trend of 850 hPa wind speed divided by its seasonal climatology over the 1981-2015 period in a) DJF, b) MAM, c) JJA and d) SON. Hatched regions show areas where the trends are significant at the 95% confidence level. Grey areas indicate where the surface level is higher than 850 hPa.

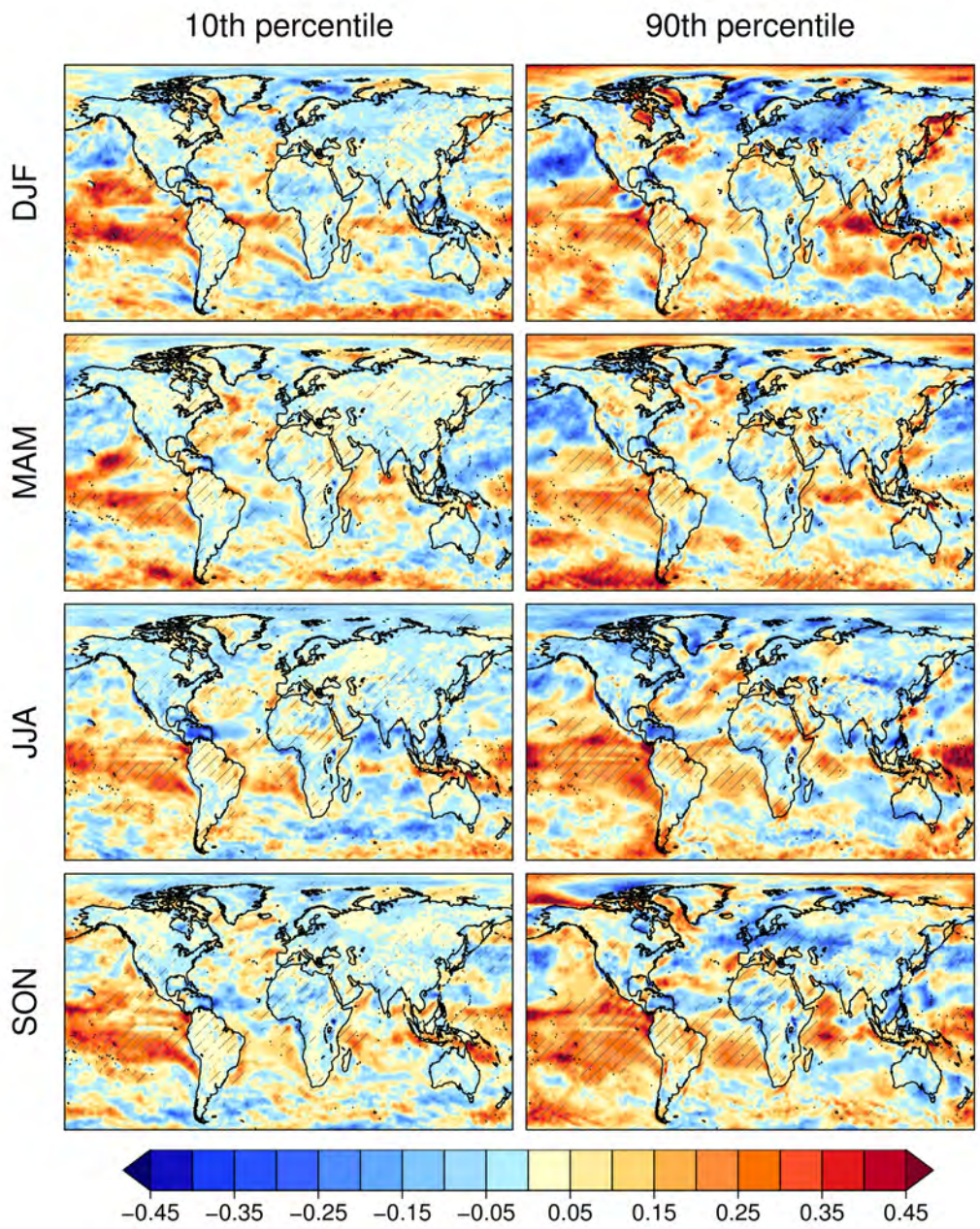

Figure B13 – Linear trend (m/s per decade) of the 10^{th} (left column) and 90^{th} (right column) of 10-m wind speed from ERA-Interim. These trends corresponds to DJF, MAM, JJA and SON in the 1981-2015 period. Hatched regions indicate where the trends are significant at a 95% confidence level.

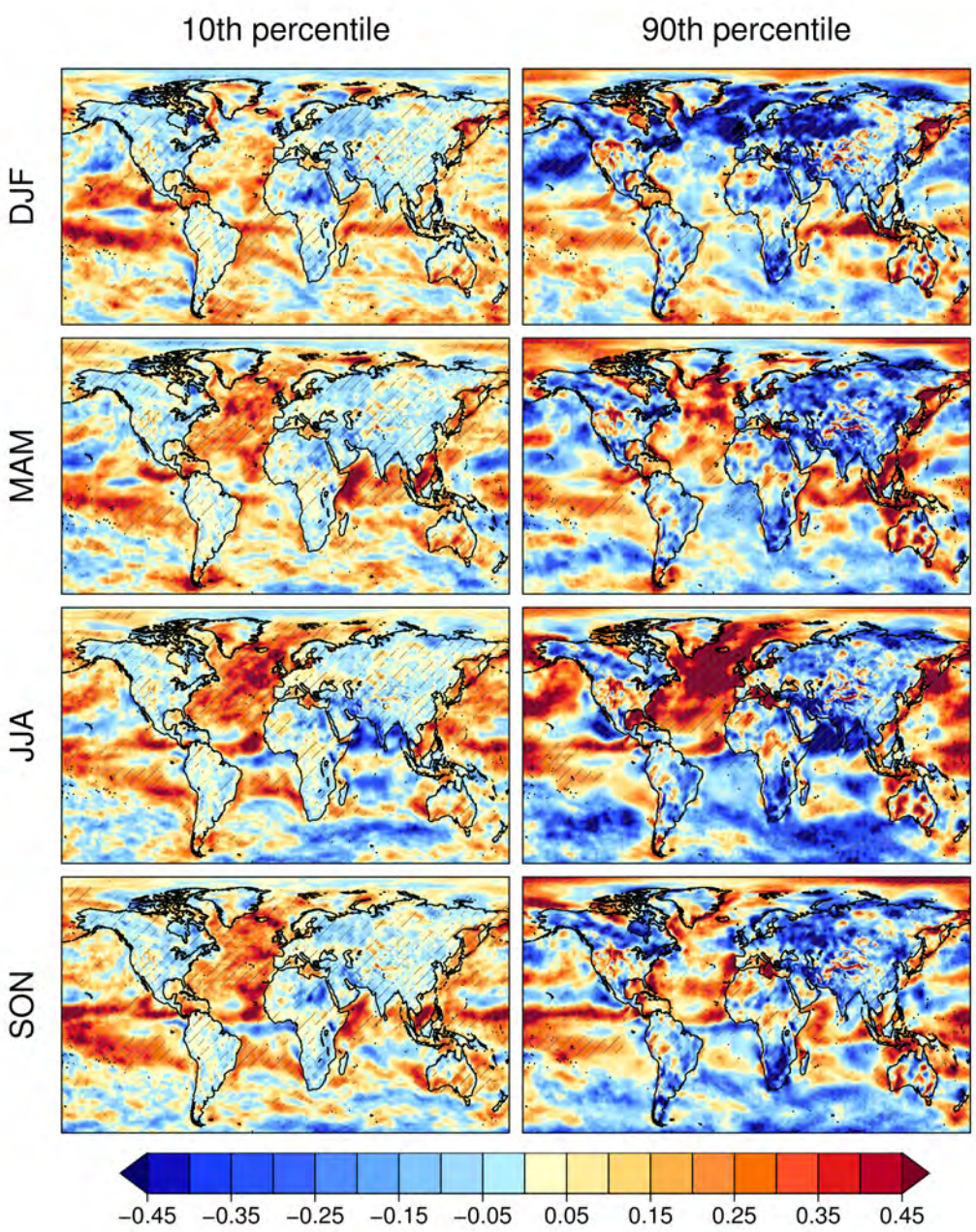

Figure B14 – Linear trend (m/s per decade) of the 10^{th} (left column) and 90^{th} (right column) of 10-m wind speed from JRA-55. These trends corresponds to DJF, MAM, JJA and SON in the 1981-2015 period. Hatched regions indicate where the trends are significant at a 95% confidence level.

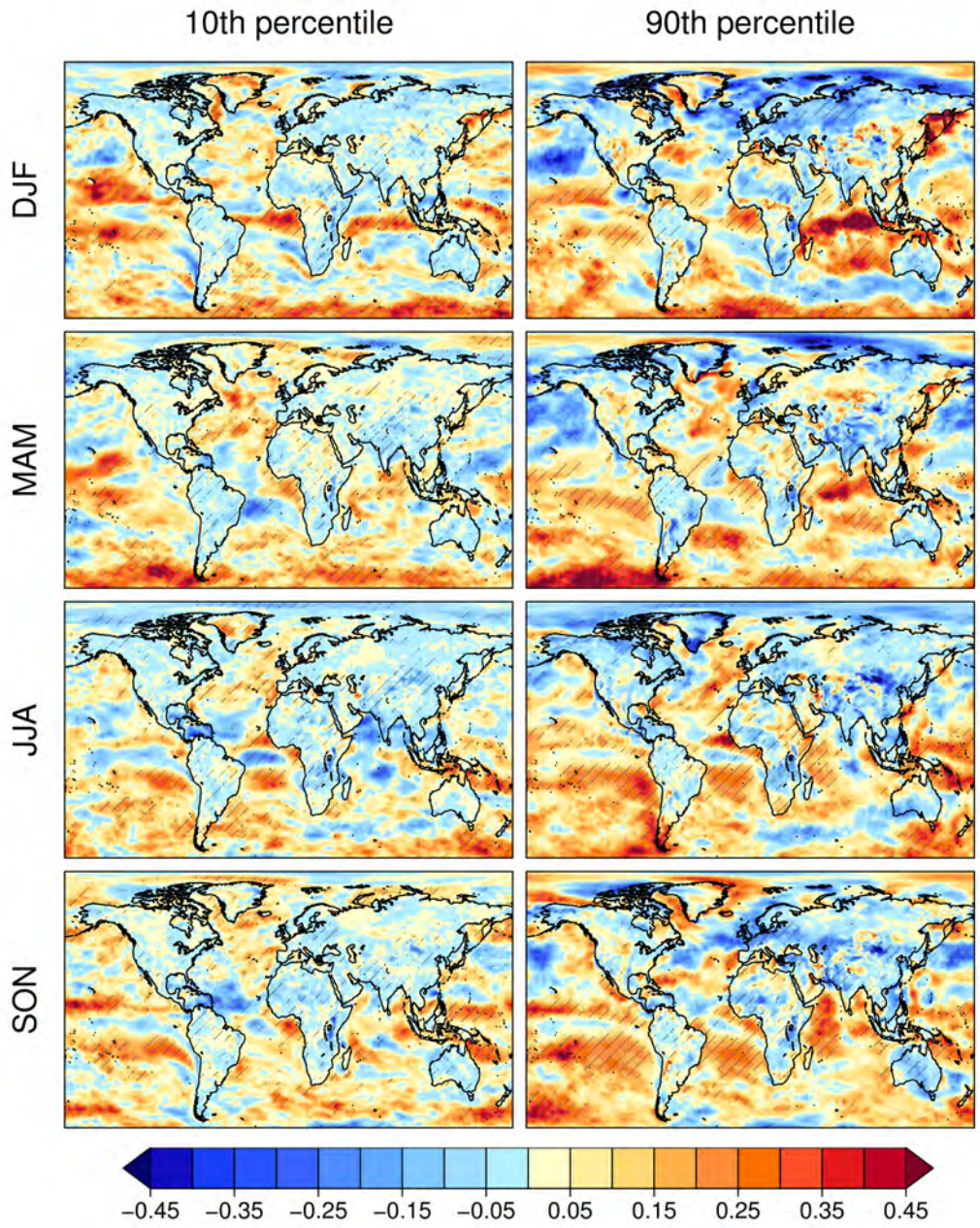

Figure B15 – Linear trend (m/s per decade) of the 10^{th} (left column) and 90^{th} (right column) of 10-m wind speed from MERRA-2. These trends corresponds to DJF, MAM, JJA and SON in the 1981-2015 period. Hatched regions indicate where the trends are significant at a 95% confidence level.

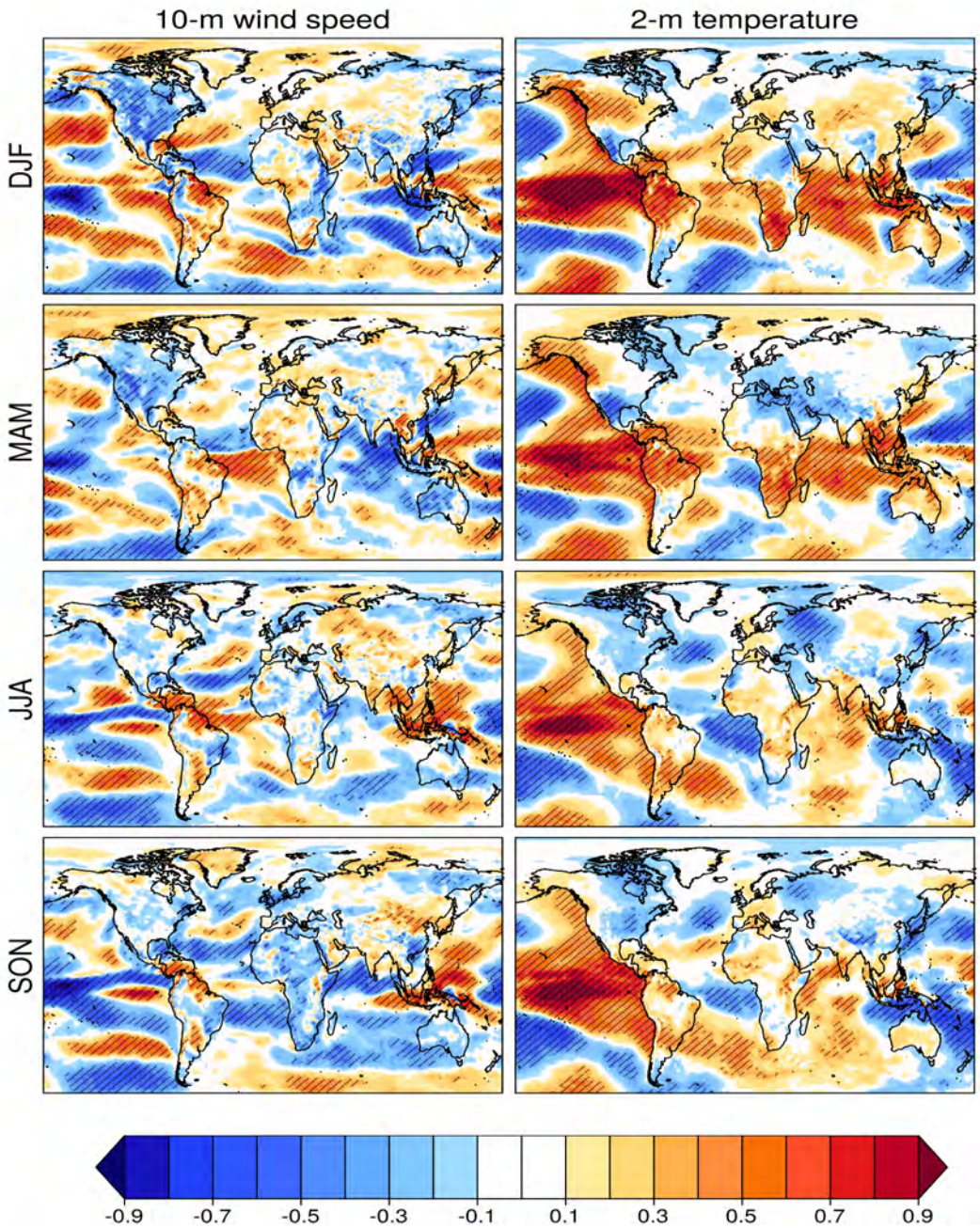

Figure B16 – One-point-correlation maps between the ERA-Interim 10-m wind speed (left column) and 2-m air temperature (right column) with the Niño-3.4 index. Correlations have been computed for DJF, MAM, JJA and SON over the 1982-2016 period. Hatching has been used to denote regions with non-significant correlation values (two-tailed t-test at a 95% confidence level).

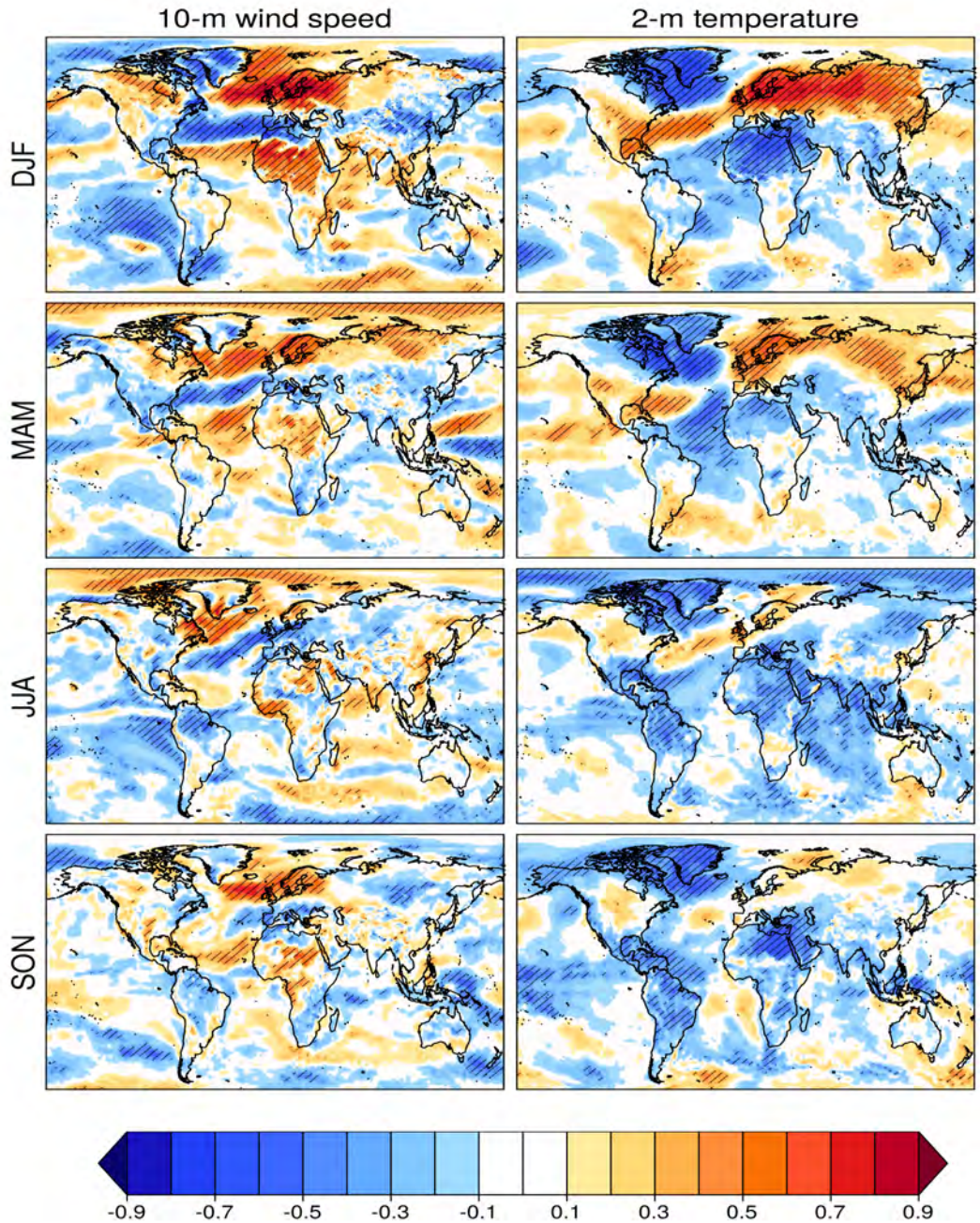

Figure B17 – One-point-correlation maps between the ERA-Interim 10-m wind speed (left column) and 2-m air temperature (right column) with the NAO index. Correlations have been computed for the ERA-Interim reanalysis in DJF, MAM, JJA and SON for the 1982-2016 period. Hatching has been used to denote regions with non-significant correlation values (two-tailed t-test at a 95% confidence level).

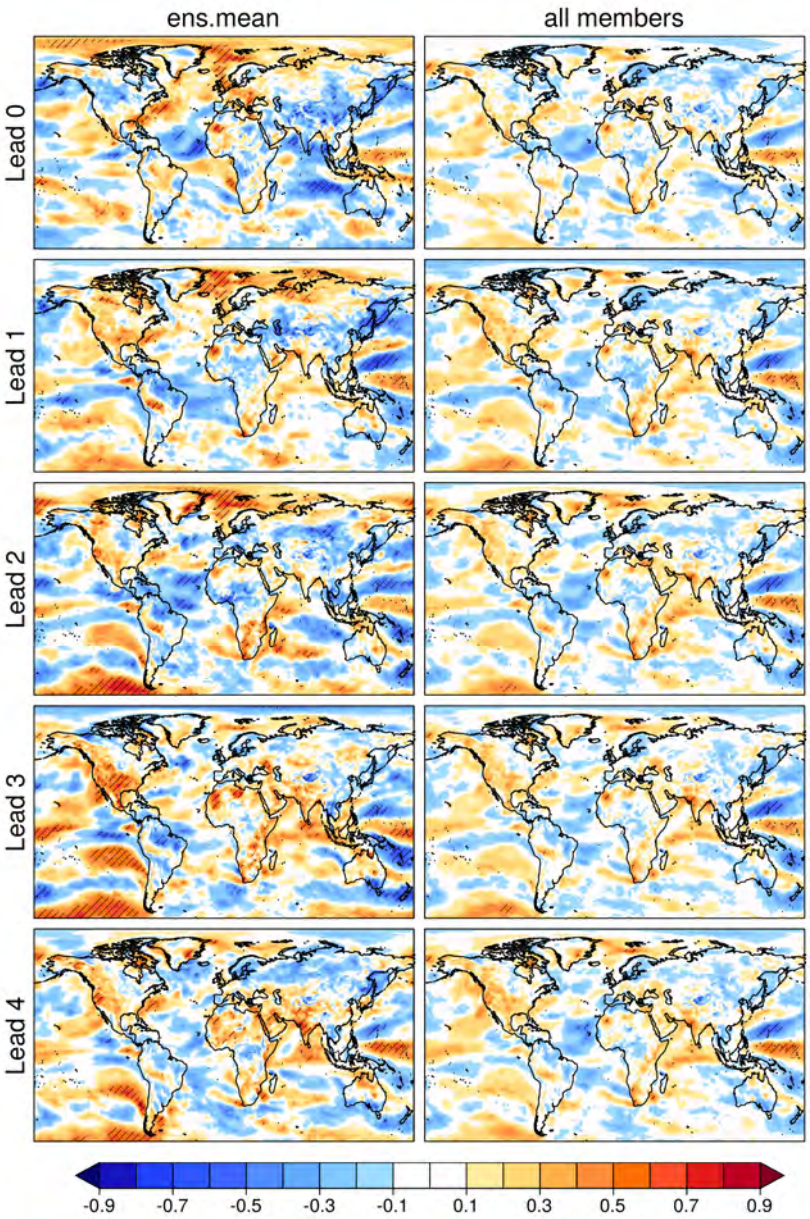

Figure B18 – Lead time dependency of the MAM differences between the one-point-correlation maps of the 10-m wind speeds and the NAO index in the ECMWF System 4 seasonal forecasts and in ERA-Interim. Differences are obtained for the ECMWF System 4 one correlation maps based on the ensemble mean (left column) and concatenated ensemble members (right column). Correlations have been computed for the 1982-2016 period. ECMWF System 4 seasonal forecasts initialised the 1^{st} of December (Lead 0), November (Lead 1), October (Lead 2), September (Lead 3) and August (Lead 4) have been used. Hatching denotes regions with non-significant correlation values (two-tailed Fisher test at a 95% confidence level).

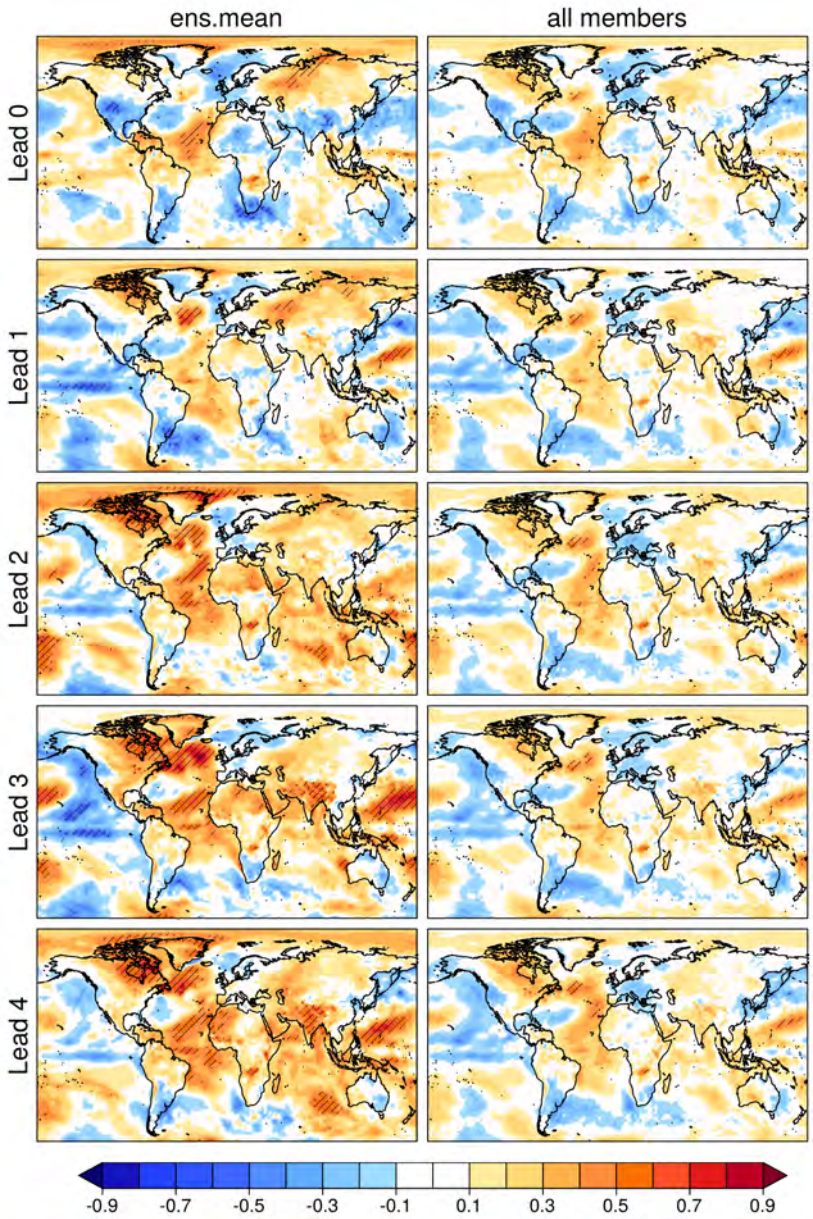

Figure B19 – Lead time dependency of the DJF differences between the one-point-correlation maps of the 2-m air temperatue and the NAO index in the ECMWF System 4 seasonal forecasts and in ERA-Interim. Differences are obtained for the ECMWF System 4 one correlation maps based on the ensemble mean (left column) and concatenated ensemble members (right column). Correlations have been computed for the 1982-2016 period. ECMWF System 4 seasonal forecasts initialised the 1^{st} of December (Lead 0), November (Lead 1), October (Lead 2), September (Lead 3) and August (Lead 4) have been used. Hatching denotes regions with non-significant correlation values (two-tailed Fisher test at a 95% confidence level).

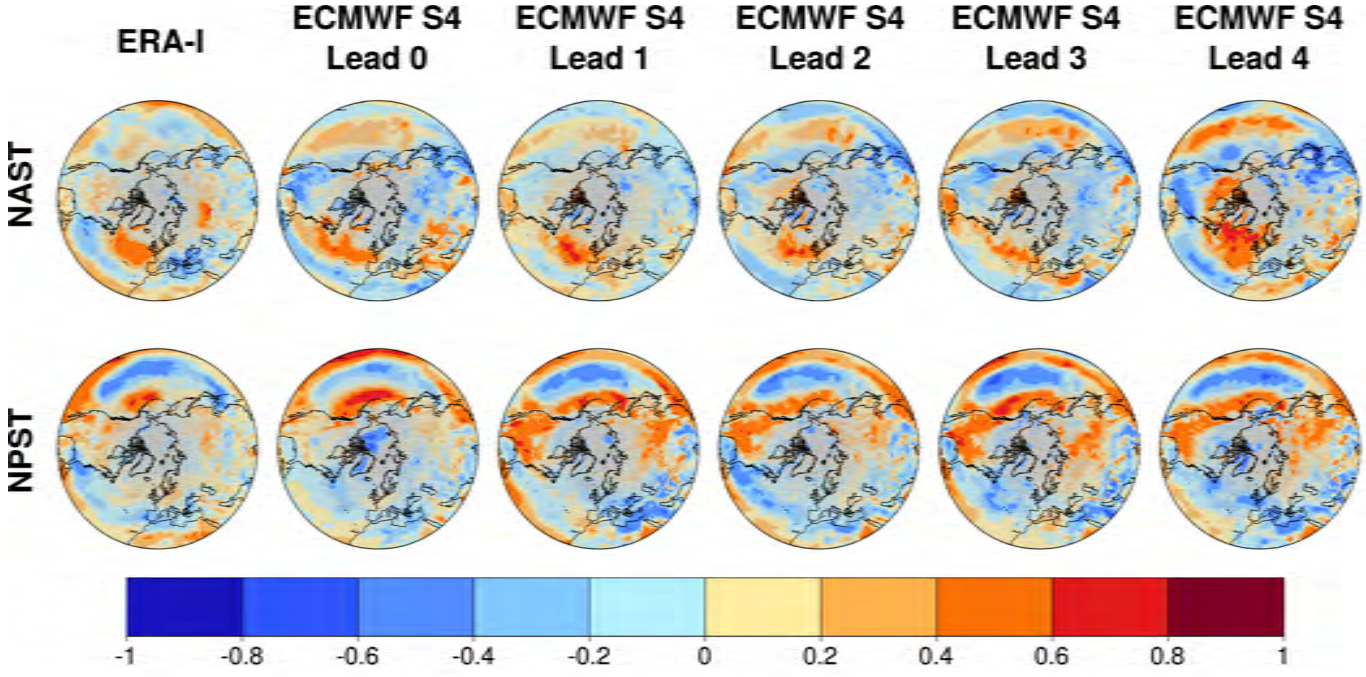

Figure B20 – One-point-correlation maps in ECMWF System 4 ensemble mean predictions and the ERA-Interim reanalysis for the NAST (top row) and NPST (bottom row) indices and the 10-m wind speed. Correlations have been computed for DJF over the 1982-2016 period. The predictions were issued the 1^{st} of November. Regions with non-significant correlation values (two-tailed t-test at a 95% confidence level) are masked.

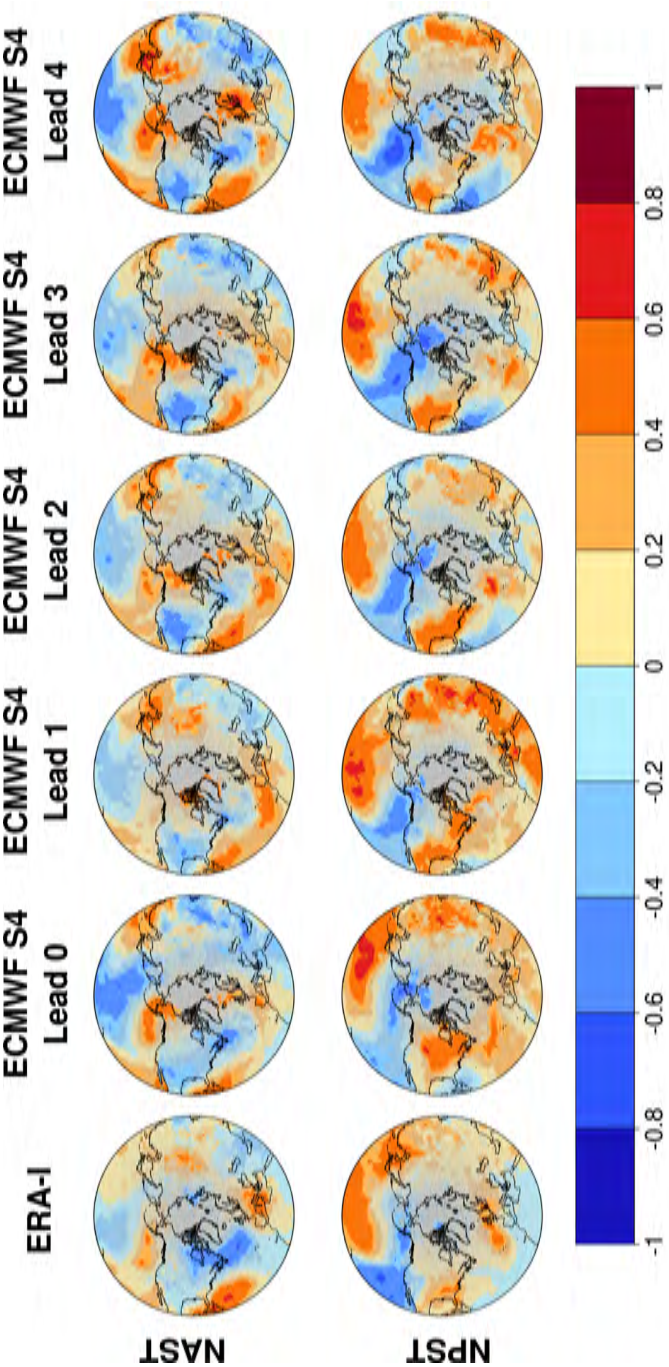

Figure B21 – One-point-correlation maps in ECMWF System 4 ensemble mean predictions and the ERA-Interim reanalysis for the NAST (top row) and NPST (bottom row) indices and the 2-m air temperature. Correlations have been computed for DJF over the 1982-2016 period. The predictions were issued the 1st of November. Regions with non-significant correlation values (two-tailed t-test at a 95% confidence level) are masked.

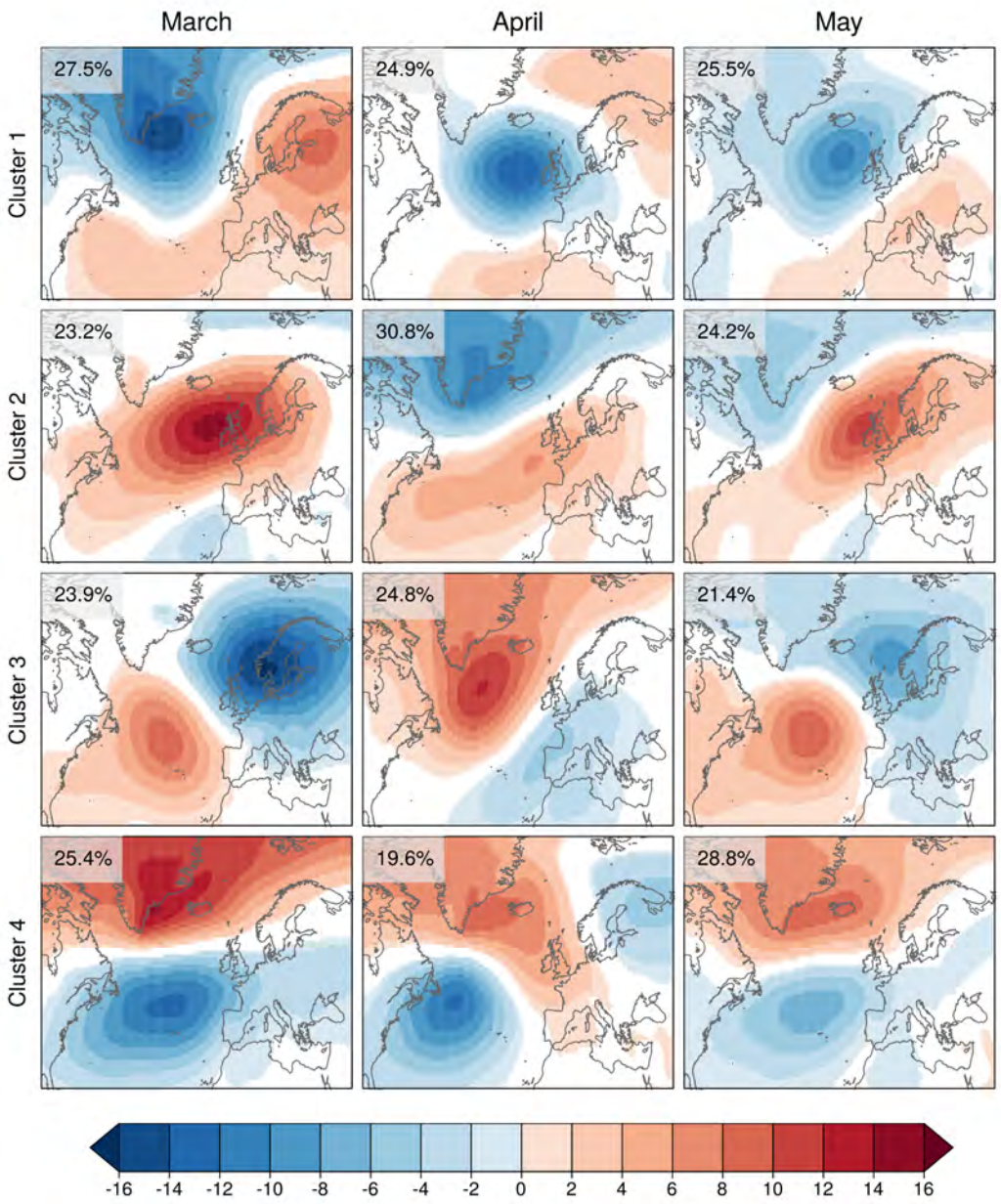

Figure B22 – Weather regime spatial patterns obtained for ERA-Interim by the KM classification method in March, April and May. These maps are the composites of the averaged sea level pressure anomalies (hPa) belonging to each one of the clusters. White areas denote regions where the anomalies are not significantly different from zero (t-test at a 95% confidence level).

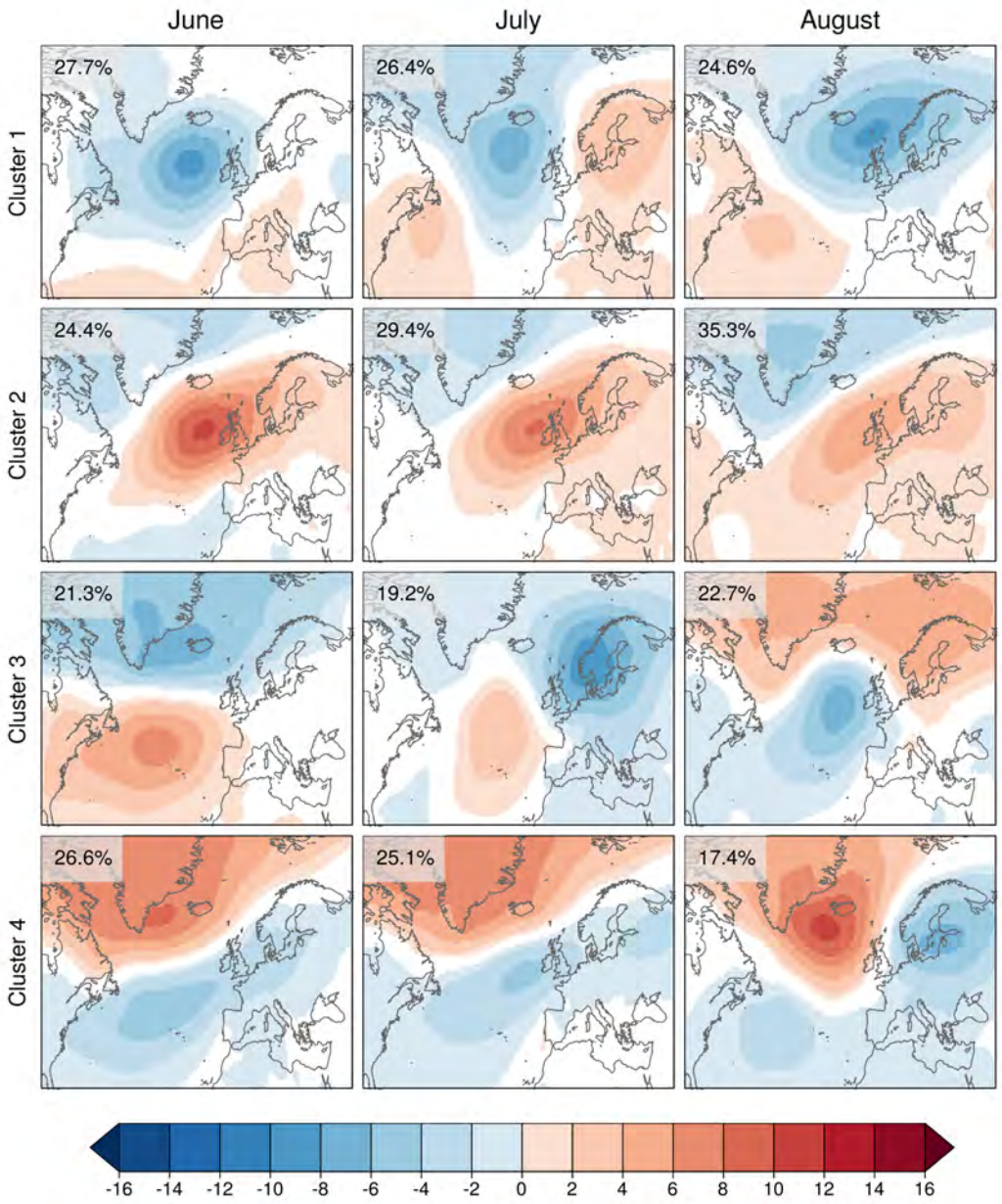

Figure B23 – Weather regime spatial patterns obtained for ERA-Interim by the KM classification method in June, July and August. These maps are the composites of the averaged sea level pressure anomalies (hPa) belonging to each one of the clusters. White areas denote regions where the anomalies are not significantly different from zero (t-test at a 95% confidence level).

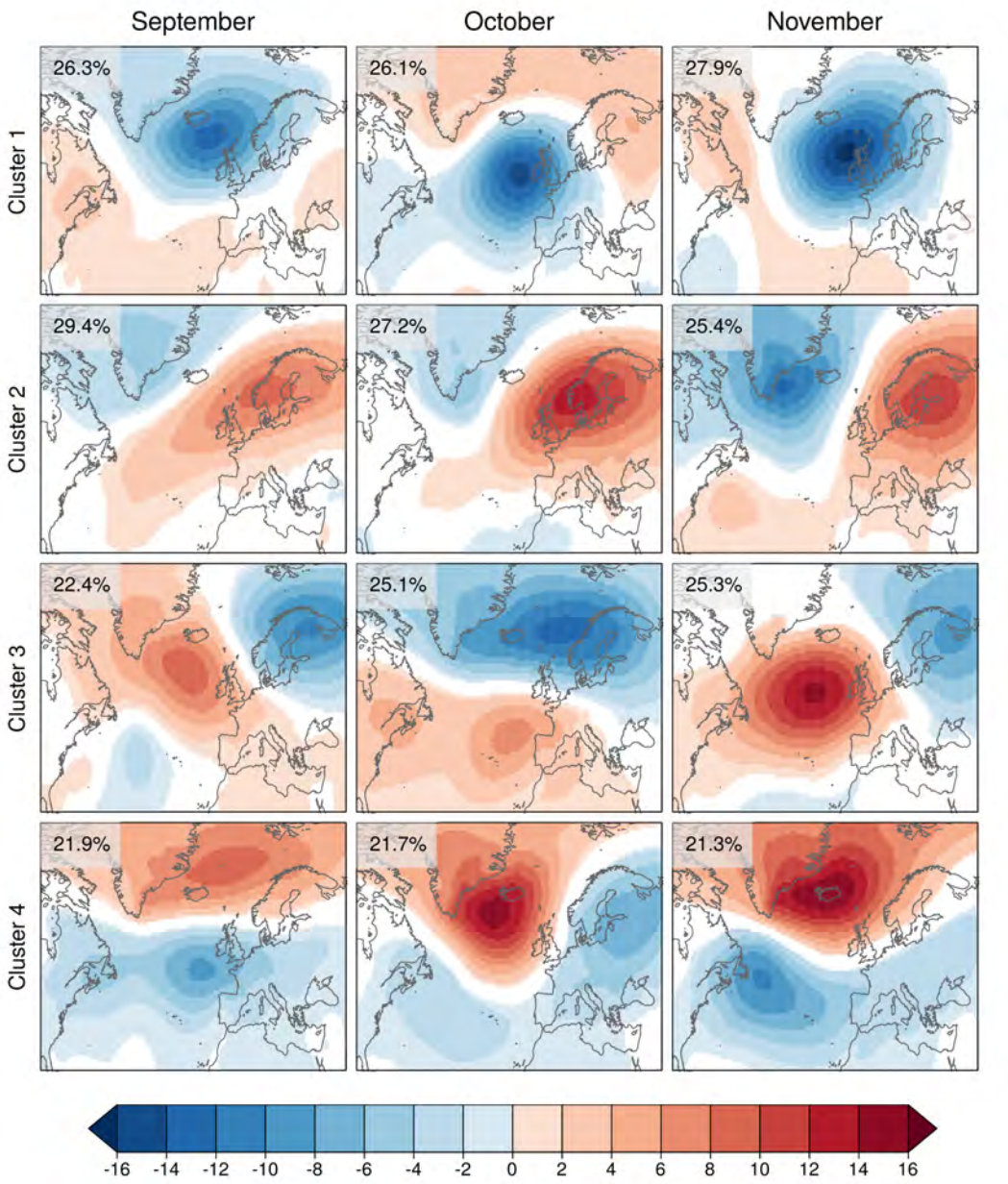

Figure B24 – Weather regime spatial patterns obtained for ERA-Interim by the KM classification method in September, October and November. These maps are the composites of the averaged sea level pressure anomalies (hPa) belonging to each one of the clusters. White areas denote regions where the anomalies are not significantly different from zero (t-test at a 95% confidence level).

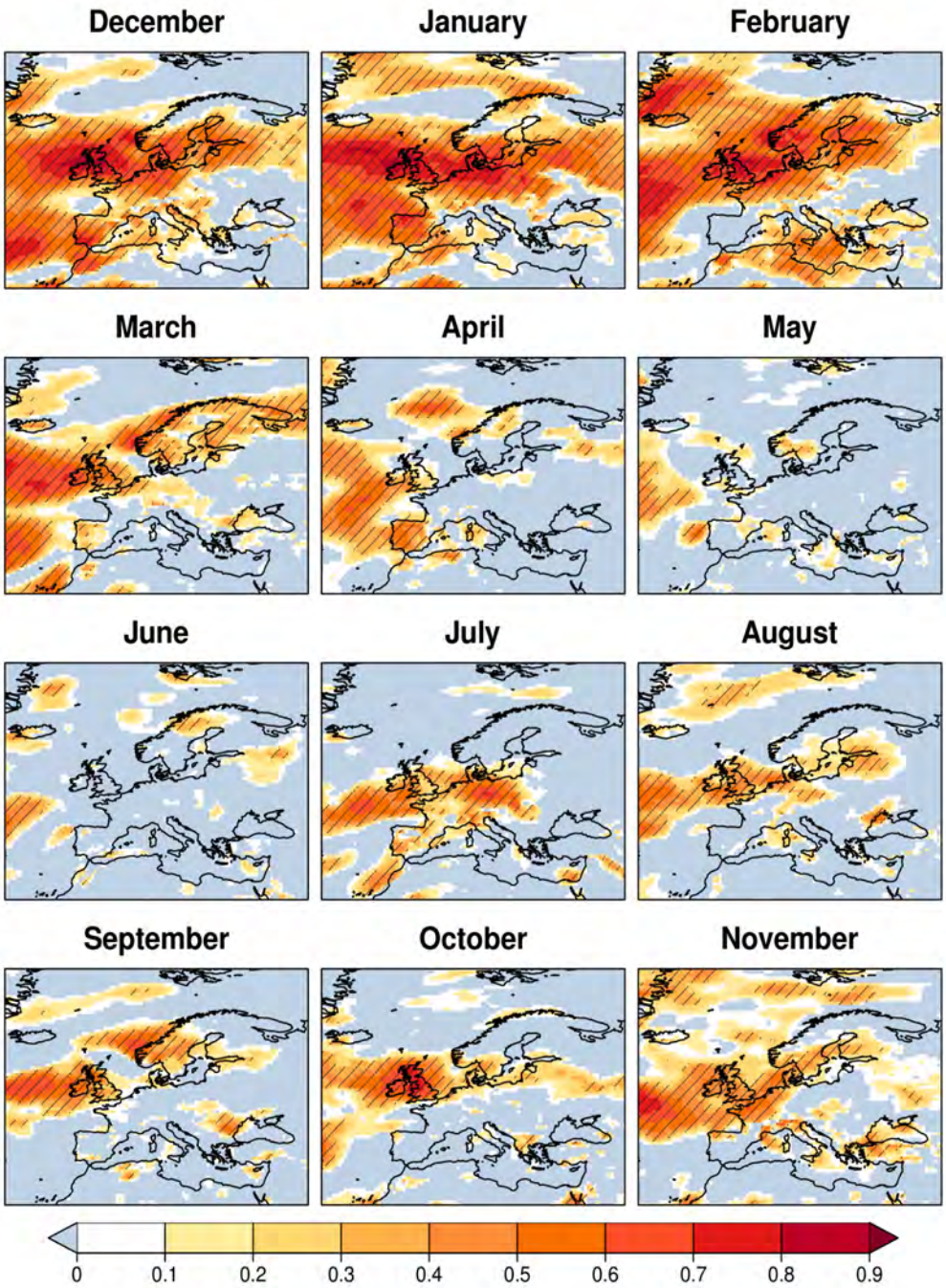

Figure B25 – Pearson correlation between the reconstructed and the original 10-m wind speed from ERA-Interim. The 10-m wind speed has been reconstruced from the weather regime frequency of occurrence in each month. Hatched areas denote regions where the correlations are significantly different from zero (t-test at a 95% confidence level).

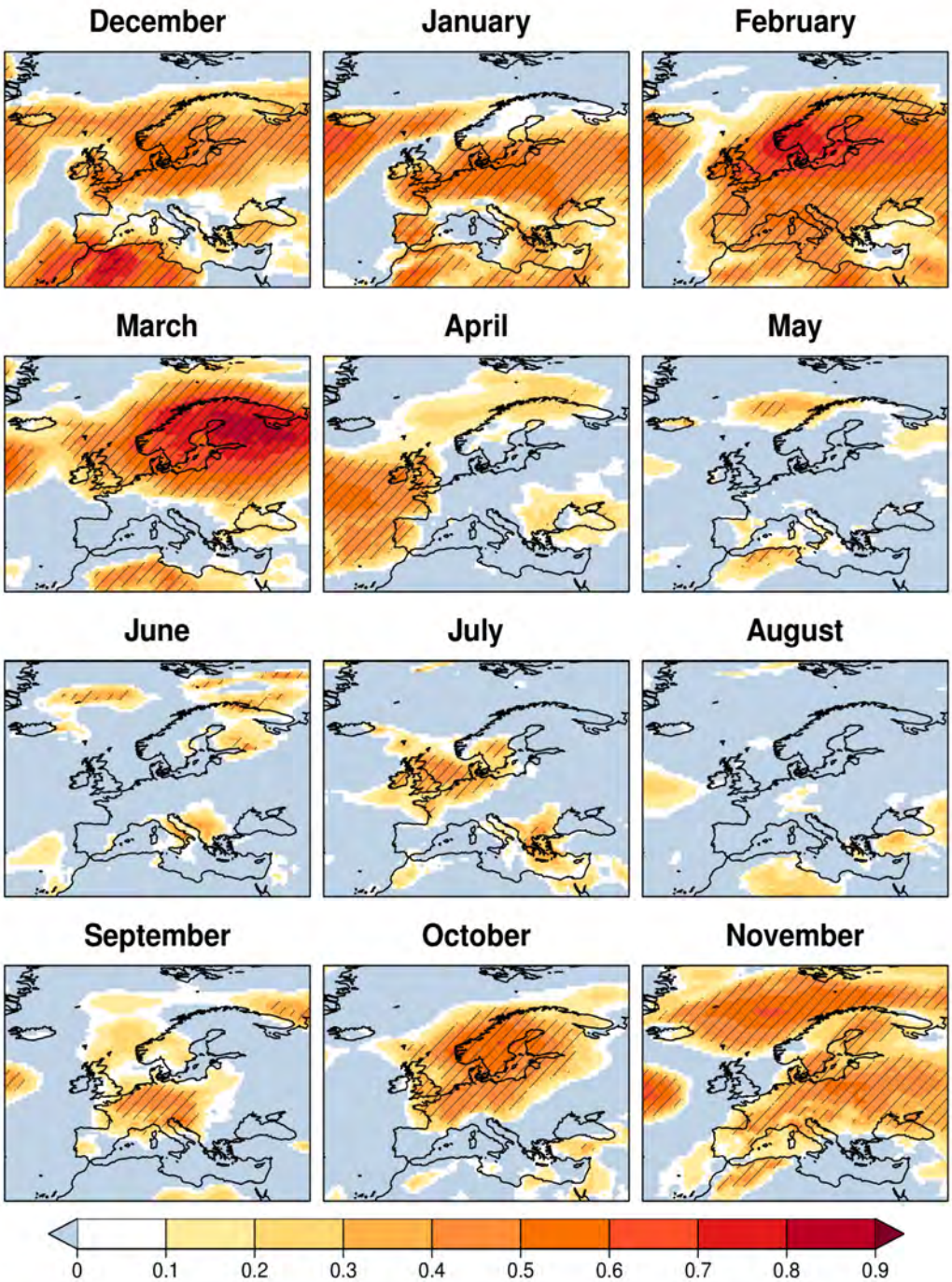

Figure B26 – Pearson correlation between the reconstructed and the original 2-m air temperature from ERA-Interim. The 10-m wind speed has been reconstruced from the weather regime frequency of occurrence in each month. Hatched areas denote regions where the correlations are significantly different from zero (t-test at a 95% confidence level).

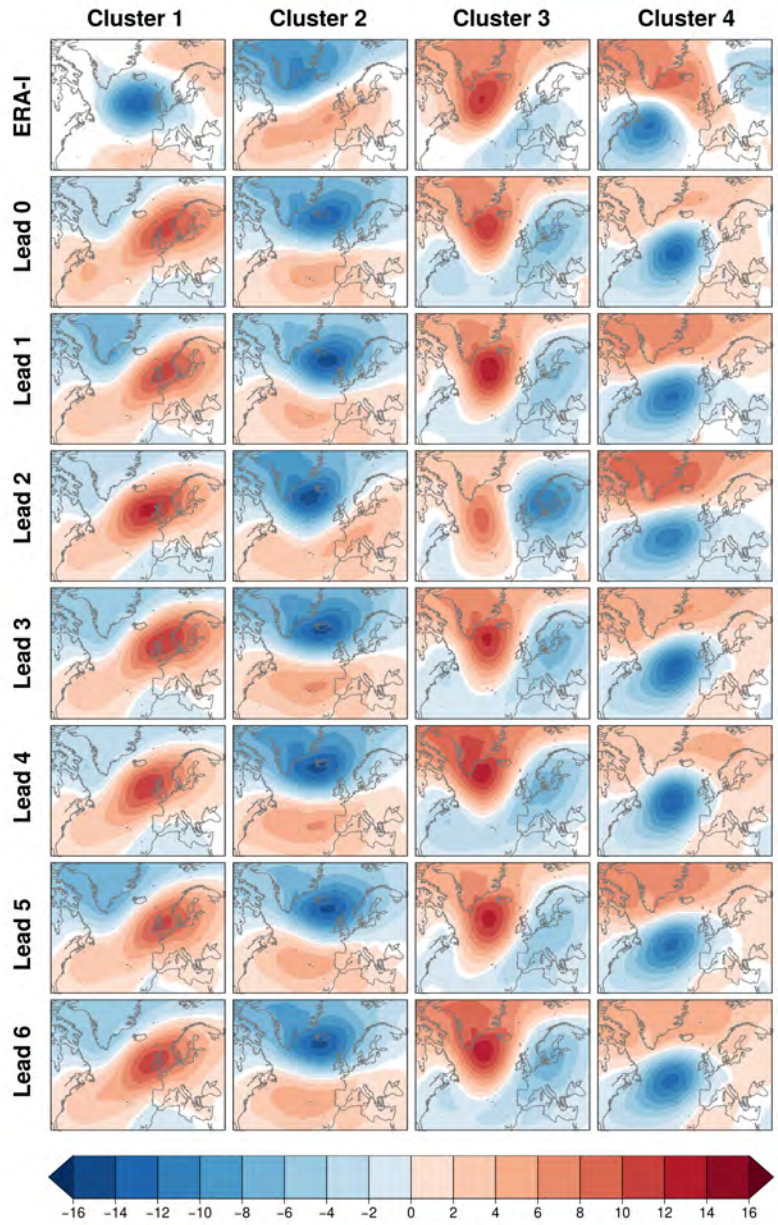

Figure B27 – Weather regime spatial patterns obtained for ERA-Interim and ECMWF System 4 by the KM classification method in April. These maps are the composites of the averaged sea level pressure anomalies (hPa) belonging to each one of the clusters. The classifications have been produced for ERA-Interim (first row) and for the ECMWF System 4 seasonal predictions intialised the 1^{st} of April,March,February,January,December and November (from second to eighth rows). White areas denote regions where the anomalies are not significantly different from zero (t-test at a 95% confidence level).

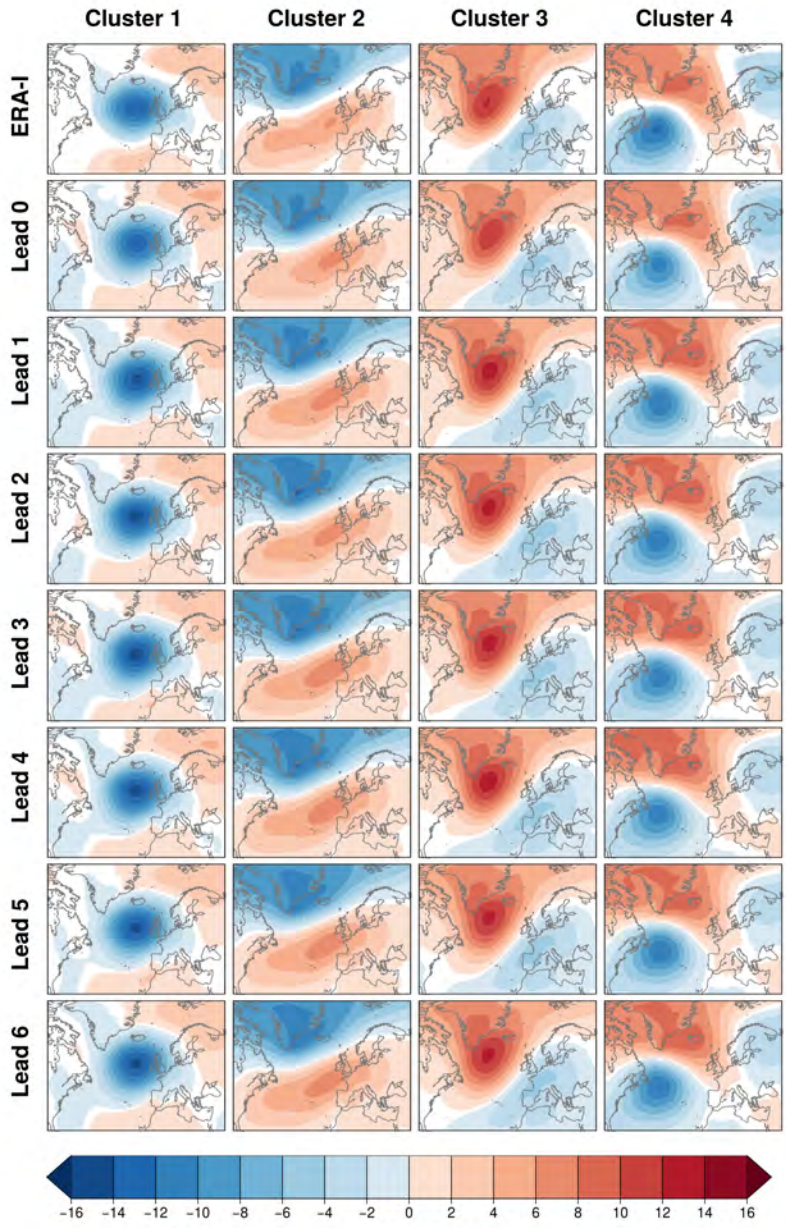

Figure B28 – Weather regime spatial patterns obtained for ERA-Interim and ECMWF System 4 by the RMSD classification method in April. These maps are the composites of the averaged sea level pressure anomalies (hPa) belonging to each one of the clusters. The classifications have been produced for ERA-Interim (first row) and for the ECMWF System 4 seasonal predictions intialised the 1^{st} of April,March,February,January,December and November (from second to eighth rows). White areas denote regions where the anomalies are not significantly different from zero (t-test at a 95% confidence level).

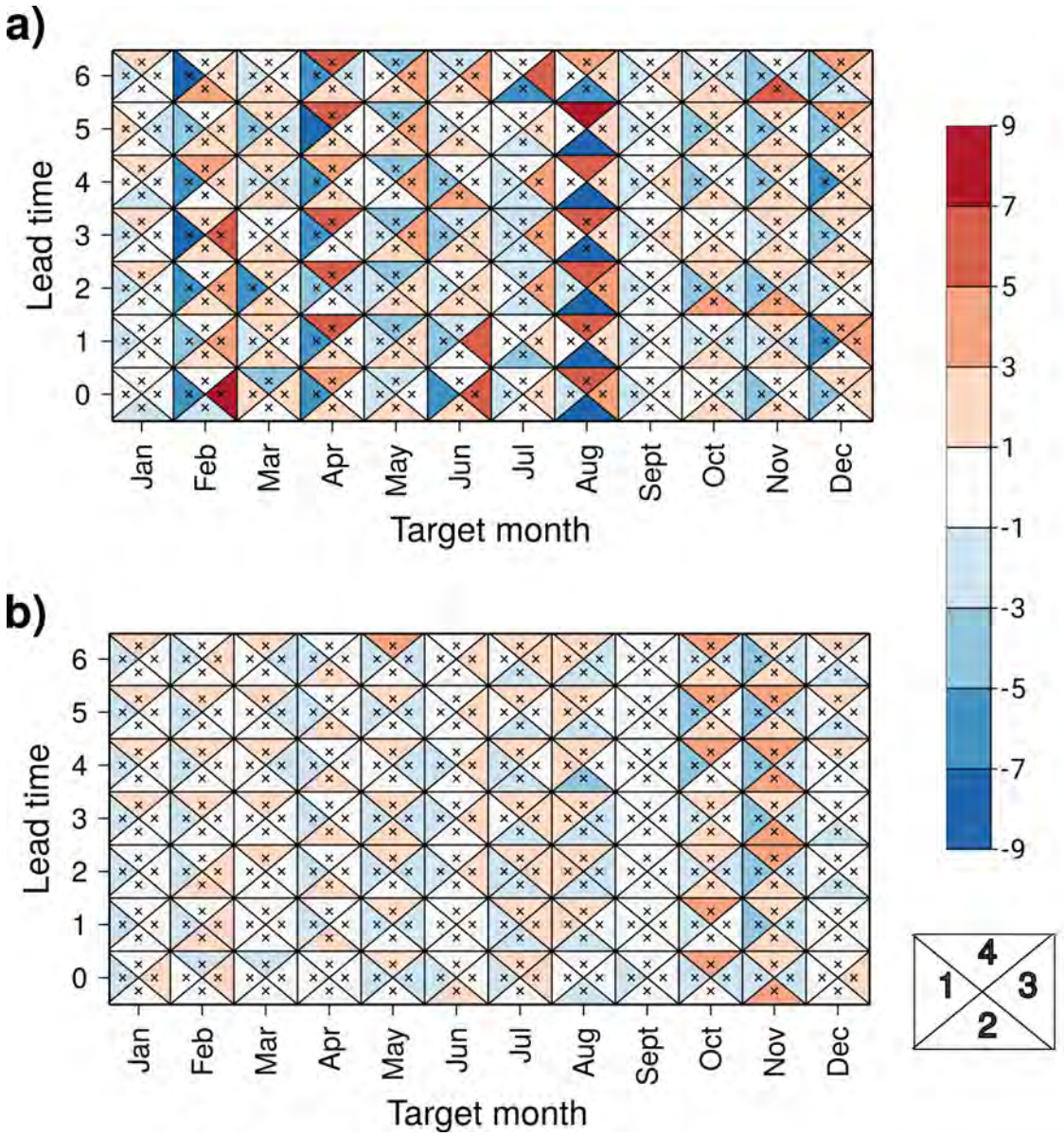

Figure B29 – Bias between the ECMWF System 4 seasonal predictions and ERA-Interim reanalysis monthly frequencies of occurrence (% days) corresponding to WRs obtained by the a) KM and b) RMSD classification methods. The classifications have been performed with daily sea level pressure anomalies in the 1982-2016 period. Each triangle represents the bias in each one of the four clusters as indicated in the bottom right legend. Biases are shown as a function of the target month (x-axis) and the lead time (y-axis). Crosses denote non-significant correlation values (t-test at a 95% confidence level).

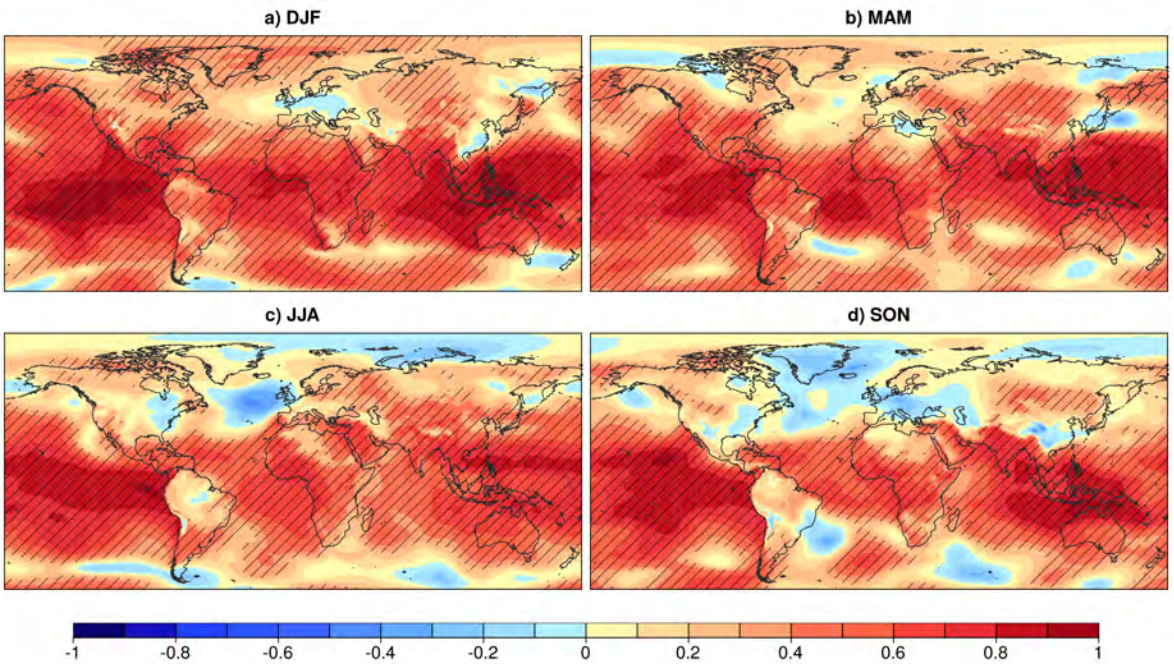

Figure B30 – Pearson correlation of the sea level pressure ensemble mean from ECMWF System 4 and the ERA-Interim reanalysis in a) DJF, b) MAM, c) JJA and d) SON. ECMWF System 4 seasonal predictions have been initialised the 1^{st} of November, February, May and August, respectively (one month lead time) in the 1981-2012 period. Hatched regions indicate correlations significantly higher than zero (t-test 95% confidence level).

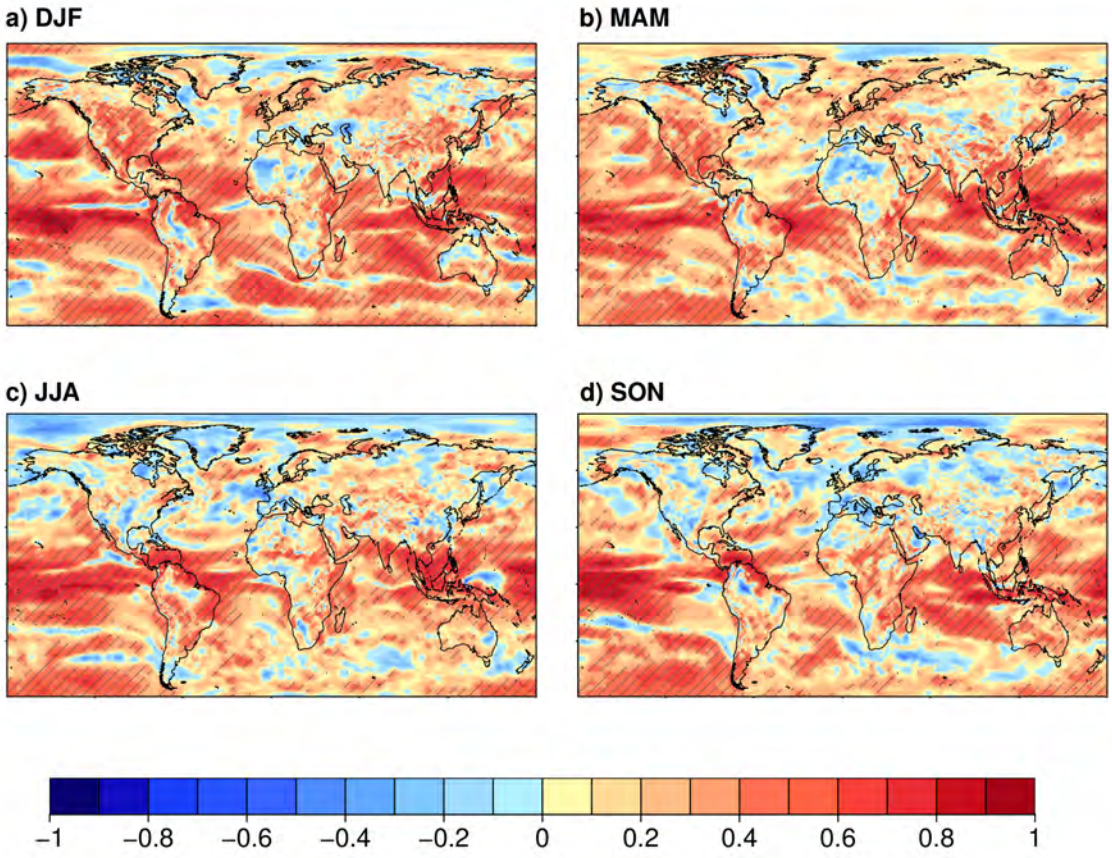

Figure B31 – Pearson correlation of the 10-m wind speed ensemble mean from ECMWF System 4 and the ERA-Interim reanalysis in a) DJF, b) MAM, c) JJA and d) SON. ECMWF System 4 seasonal predictions have been initialised the 1^{st} of November, February, May and August, respectively (one month lead time) in the 1981-2012 period. Hatched regions indicate correlations significantly higher than zero (t-test 95% confidence level).

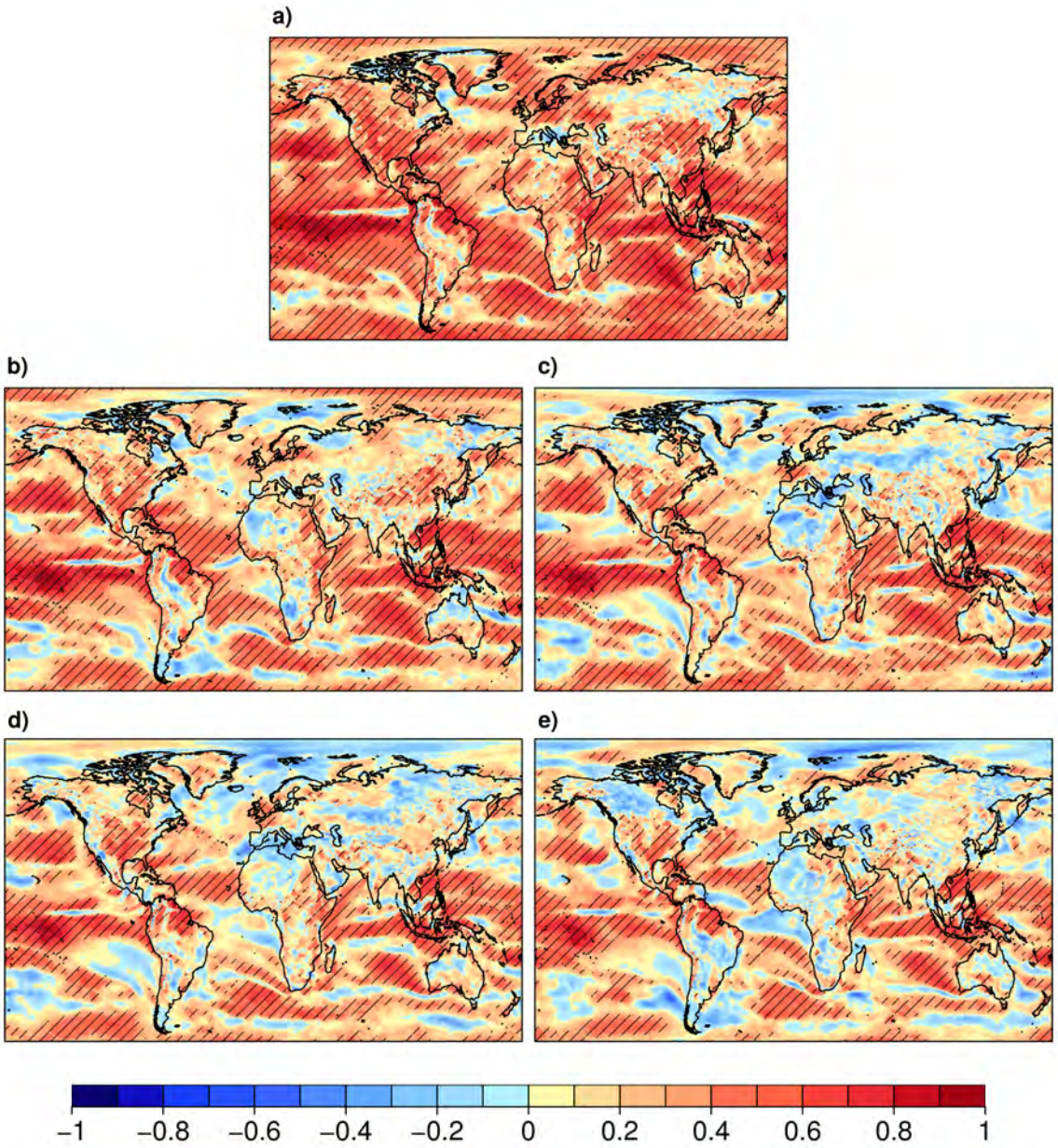

Figure B32 – Pearson correlation of the 10-m wind speed ensemble mean from ECMWF System 4 and the ERA-Interim reanalysis in DJF in the 1981-2012 period. These predictions have been initialised the 1^{st} of December (lead 0), b) November (lead 1), c) October (lead 2), d) September (lead 3) and e) August (lead 4). Hatched regions indicate correlations significantly higher than zero (t-test 95% confidence level).

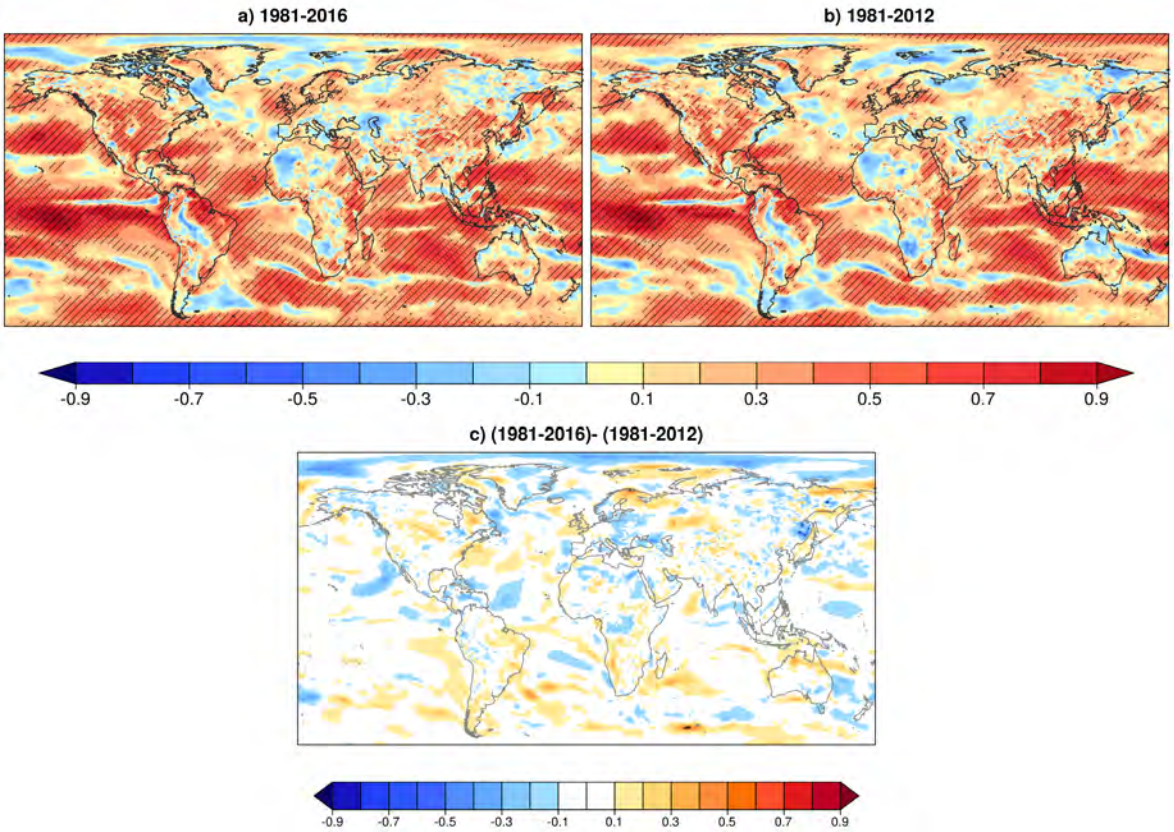

Figure B33 – Pearson correlation of the 10-m wind speed ensemble mean from ECMWF System 4 and the ERA-Interim reanalysis in DJF. These predictions have been initialised the 1^{st} of November in the a)1981-2016, b)1981-2012. c) Differences between the maps shown in panels a and b. Hatched regions indicate significant values at the 95% confidence level (t-test).

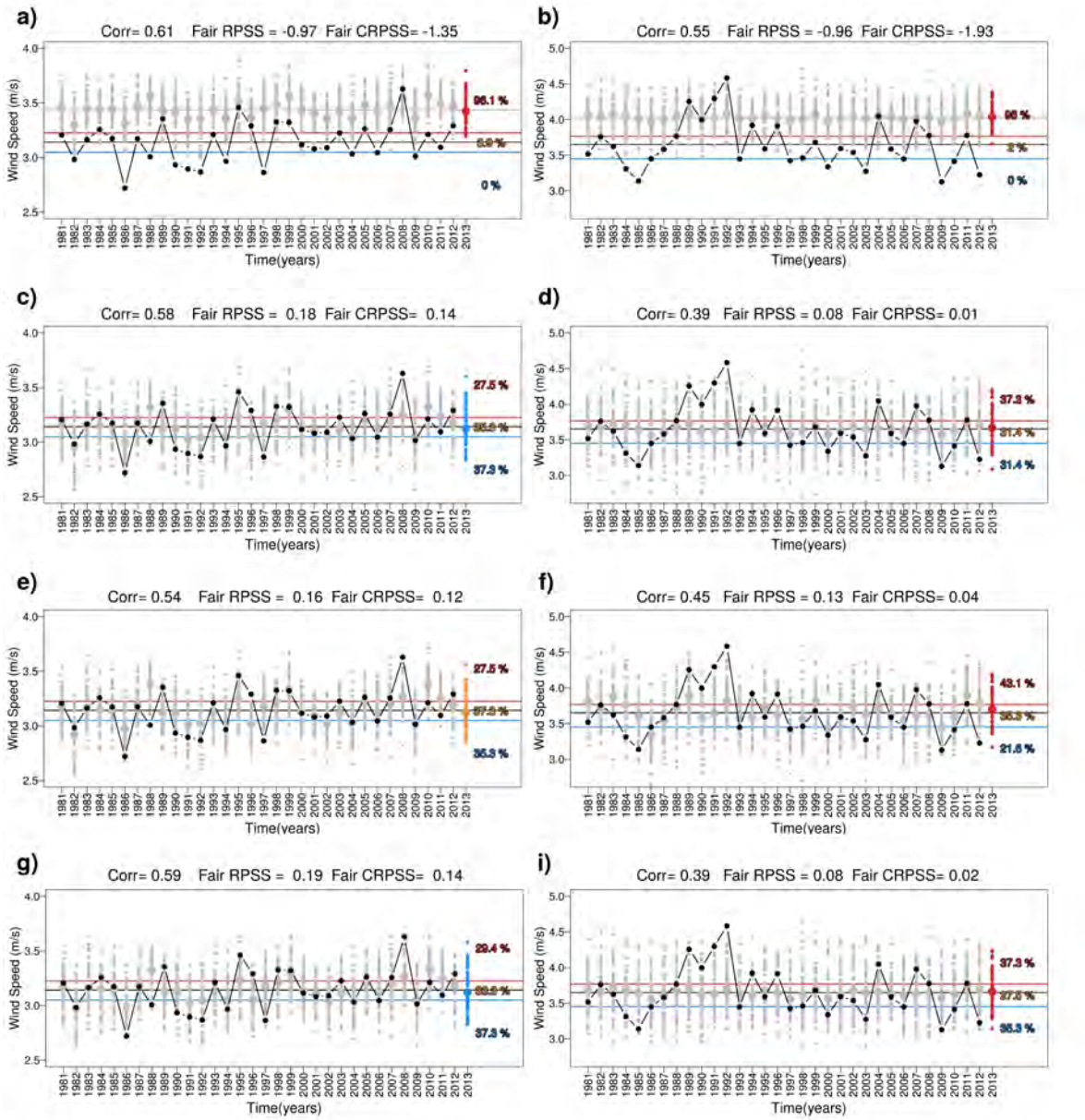

Figure B34 – Time series of 10-m wind speed from ECMWF System 4 and ERA-Interim reanalysis in winter (DJF) for a region in central United States [34°-34.6° N, 264.4°-267.2° E] (right column) and northern Scandinavia [68.4°-69.8° N, 21.1° -23.2° E] (left column). These predictions have been initialised on the 1^{st} of November for the period of 1981-2013 and they have been bias adjusted with different methods: (a,b) none, (c,d) simple bias correction, (e,f) calibration and (g,h) quantile mapping. The grey/black horizontal lines shows the mean of the hindcasts/observations in whole period (1981-2012). The ensemble members of the forecast year (2013) are represented as red dots. The percentages indicate the fraction of members in each category, which are limited by the terciles of the reference dataset. Correlation, fair RPSS and fair CRPSS are shown in the upper part of each panel and they have been computed for the period 1981-2012, excluding the target season.

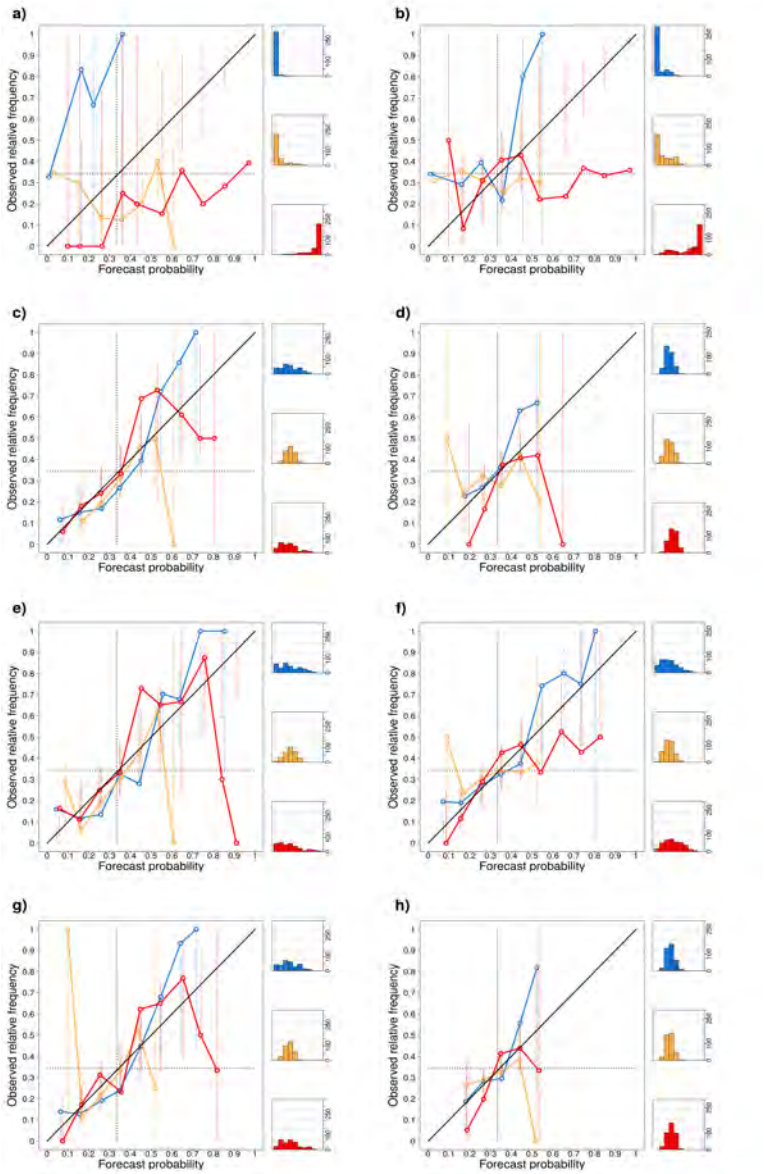

Figure B35 – Reliability Diagrams of 10-m wind speeds forecasts from ECMWF System 4 and ERA-Interim reanalysis in DJF in: central United States [34°-34.6° N, 264.4°-267.2° E] (left column) and northern Scandinavia [68.4°-69.8° N, 21.1°-23.2° E] (right column). The predictions have been initialised on the 1^{st} of November for the period of 1981-2012 an they have been bias adjusted with different methods: (a,d) none, (b,e) simple bias correction, (c,f) calibration and (d,g) quantile mapping. Three events are represented: above-normal wind speeds (red line), normal wind speeds (orange) and below-normal wind speeds (blue). Right panels show the sharpness diagrams with the distribution of samples for each bin and each event. The consistency bars have been represented as vertical lines to illustrate how likely the observed relative frequencies are under the assumption that predicted probabilities are reliable.

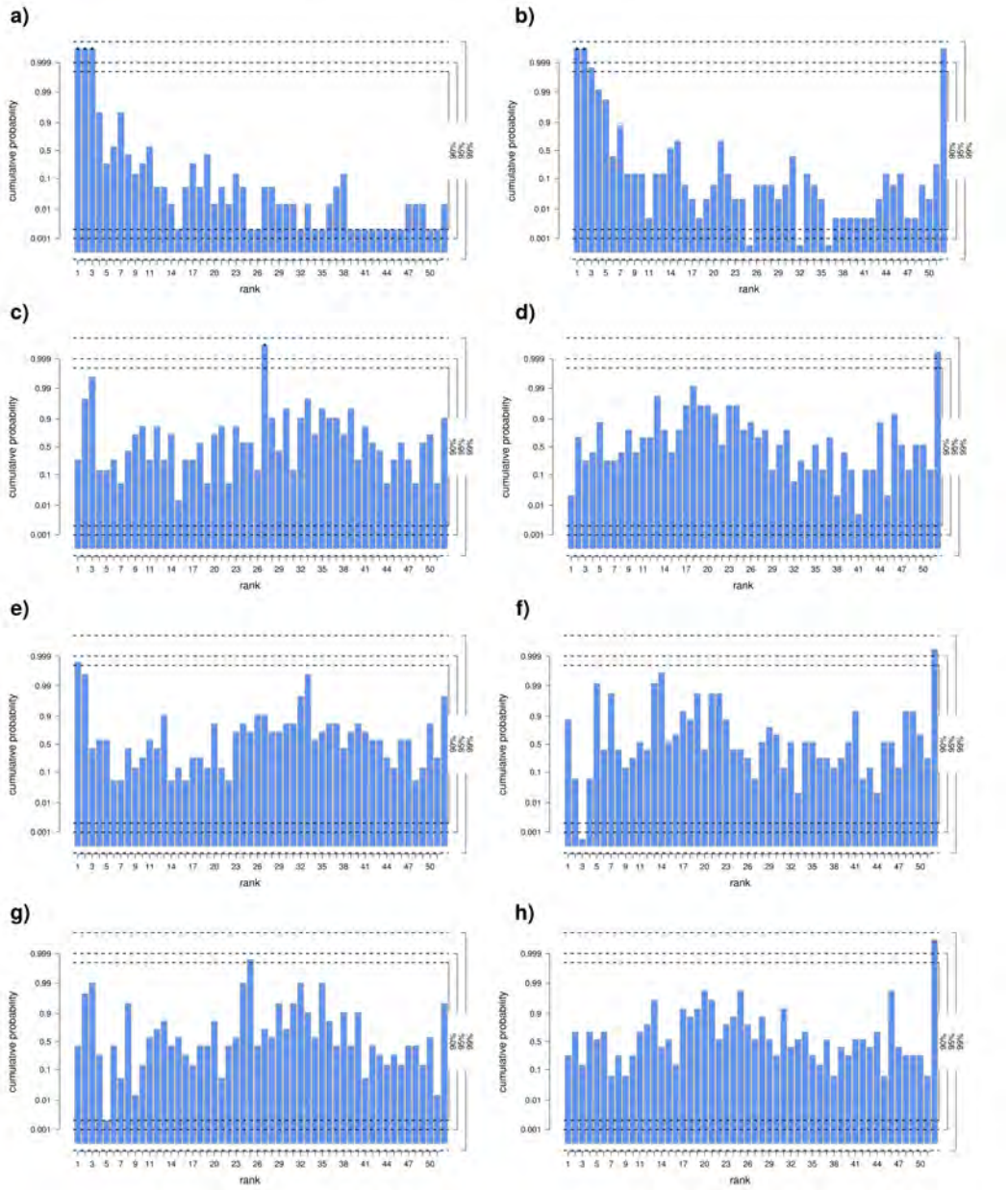

Figure B36 – Rank histograms of 10-m wind speeds forecasts from ECMWF System 4 and ERA-Interim reanalysis in DJF in: central United States [34°-34.6° N, 264.4°-267.2° E] (left column) and northern Scandinavia [68.4°-69.8° N, 21.1°-23.2° E] (right column). The predictions have been initialised on the 1^{st} of November for the period of 1981-2012 an they have been bias adjusted with different methods: (a,d) none, (b,e) simple bias correction, (c,f) calibration and (d,g) quantile mapping.

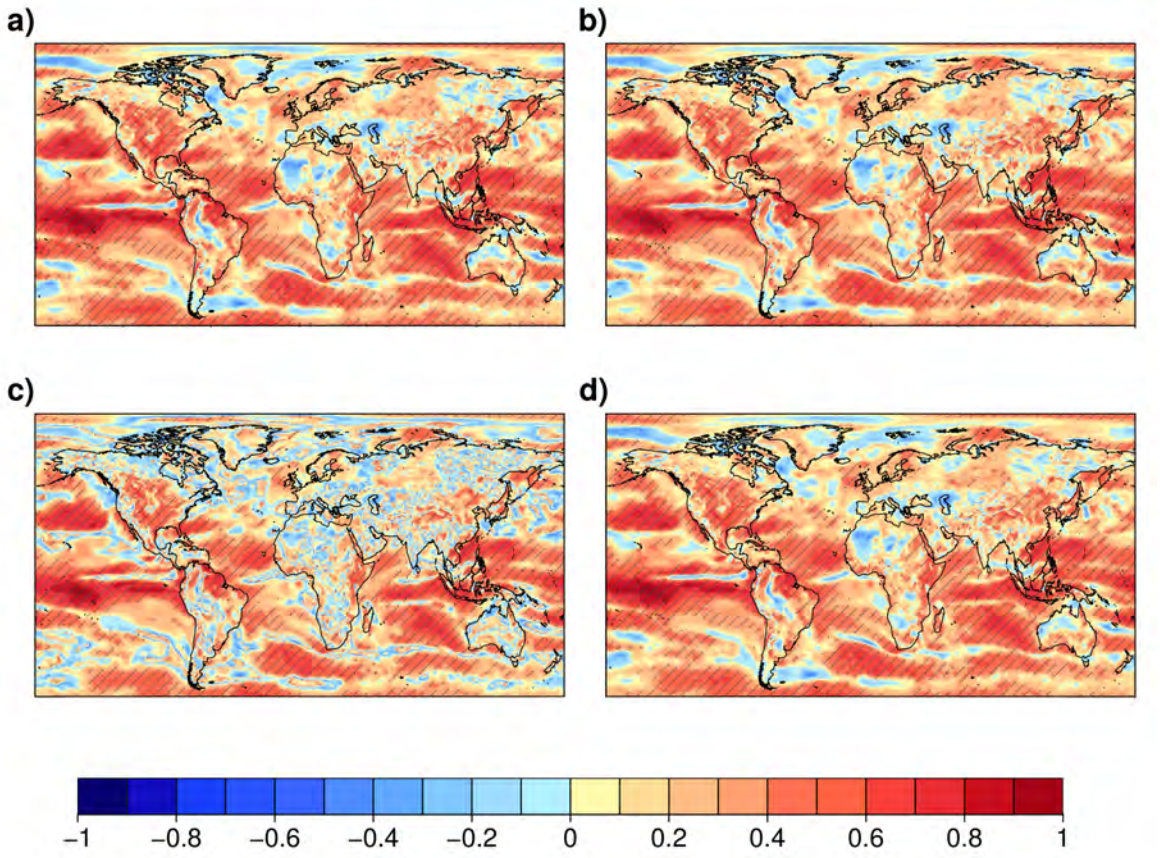

Figure B37 – Pearson correlation of the ensemble mean of 10-m wind speed forecasts from ECMWF System 4 and ERA-Interim reanalysis in DJF. The predictions have been initialised on the 1^{st} of November for the period of 1981-2012 and they have been bias adjusted with different methods: a) none, b) simple bias correction, c) calibration and d) quantile mapping. Hatched regions indicate correlations significantly (t-test 95% confidence level) higher than zero.

Table B1 – Goodness-of-fit tests: Pearson χ^2 , JP-slope and JP-convex statistics formulated by (Jolliffe and Primo 2008) and their p-values in brackets. They have been computed from the rank histograms (Figure B36) of 10-m wind speed forecasts from ECMWF System 4 in winter (DJF) for the period 1981-2012.

		Pearson χ^2	JP slope	JP convex
Central US	**Uncorrected**	4365.53 (0.00)	619.25 (1.1×10^{-136})	691.36 (2.3×10^{-152})
	Simple bias corrected	83.33 (2.8×10^{-3})	0.13 (0.72)	2.10 (0.15)
	Calibrated	73.25 (0.02)	0.30 (0.58)	8.3×10^{-4}) (0.98)
	Quantile mapping corrected	88.53 (8.78)	0.05 (0.83)	5.57 (0.02)
Northern Scandinavia	**Uncorrected**	3231.36 (0.00)	340.00 (6.3710-76)	556.90 (0.04)
	Simple bias corrected	82.65 (3.3×10^{-3})	1.85 (0.17)	2.31 (0.13)
	Calibrated	99.44 (5.7×10^{-5})	0.30 (0.58)	0.03 (0.58)
	Quantile mapping corrected	69.38 (0.04)	6.1×10^{-3} (0.94)	2.88 (0.09)

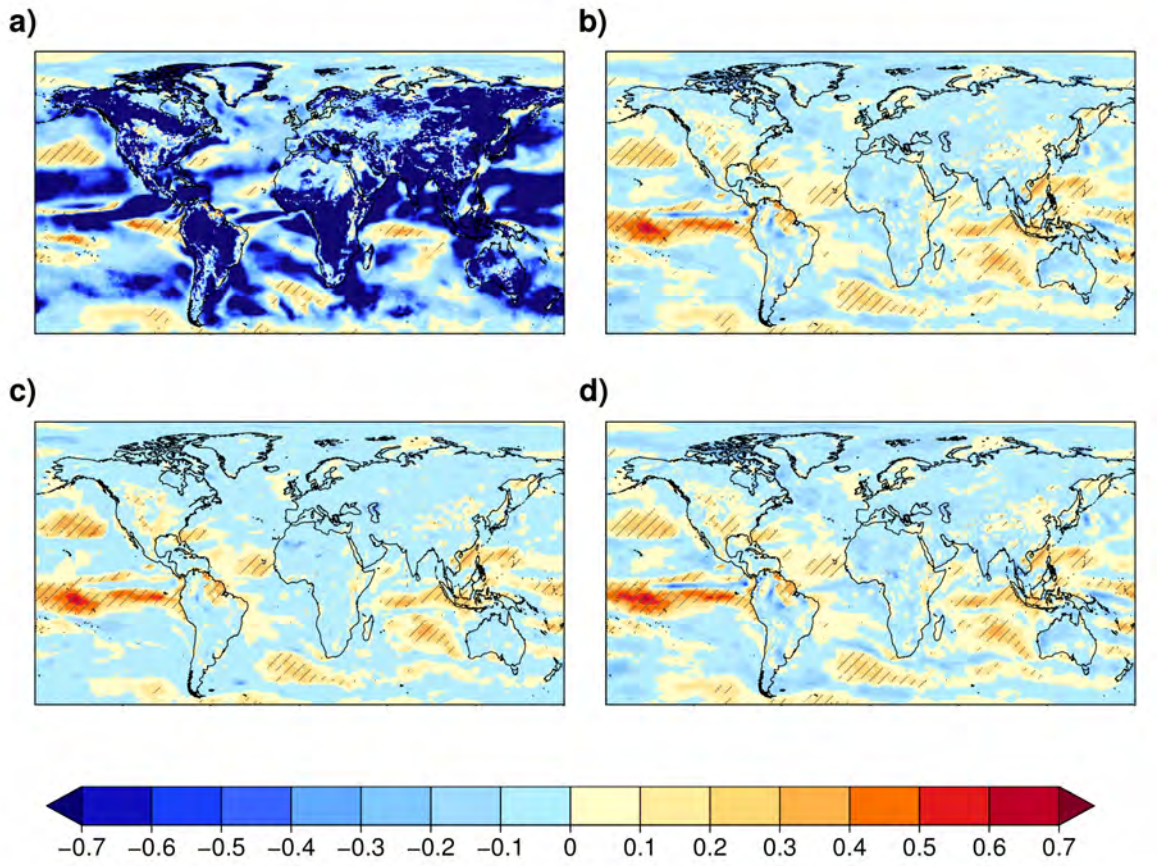

Figure B38 – Fair Continuous Probability Skill Score (FCRPSS) of ECMWF System 4 and ERA-Interim reanalysis 10-m wind speed in DJF. The predictions have been initialised on the 1^{st} of November for the period of 1981-2012 and they have been bias adjusted with different methods: a) none, b) simple bias correction, c) calibration and d) quantile mapping. Hatched regions indicate FCRPSS significantly (95% confidence level) higher than zero.

C List of publications

Publications directly related to this thesis

- **Torralba, V.**, F. J. Doblas-Reyes, and N. Gonzalez-Reviriego, 2017a: Uncertainty in recent near-surface wind speed trends: a global reanalysis intercomparison. *Environmental Research Letters*, **12 (11)**, 114019, doi: 10.1088/1748-9326/aa8a58.

- **Torralba, V.**, F. J. Doblas-Reyes, D. MacLeod, I. Christel, and M. Davis, 2017b: Seasonal climate prediction: A new source of information for the management of wind energy resources. *Journal of Applied Meteorology and Climatology*, **56 (5)**, 1231–1247, doi: 10.1175/JAMC-D-16-0204.1.

- Manubens, N., L.-P. Caron, A. Hunter, O. Bellprat, E. Exarchou, N.S. Fučkar, J. García-Serrano, F. Massonnet, M. Ménégoz, V. Sicardi, L. Batté, C. Prodhomme, **V. Torralba**, N. Cortesi, O. Mula-Valls, K. Serradell, V. Guemas and F.J. Doblas-Reyes, 2018: An R package for climate forecast verification. *Environmental Modelling & Software*, **103**, 29-42, doi:10.1016/j.envsoft.2018.01.018.

- Marcos, R., N. Gonzalez-Reviriego, **V. Torralba**, A. Soret, F.J. Doblas-Reyes, 2018: Characterization of the near surface wind speed distribution at global scale: ERA-Interim reanalysis and ECMWF seasonal forecasting System 4. *Climate Dynamics*, 13, doi:

10.1007/s00382-018-4338-5.

- Cortesi, N., **V. Torralba**, N. Gonzalez-Reviriego, A. Soret, F.J. Doblas-Reyes, under review: Characterization of European wind speed variability using weather regimes. *Climate Dynamics*.

Publications related to this thesis

- MacLeod, D., **V. Torralba**, M. Davis, and F.J. Doblas-Reyes, 2017: Transforming climate model output to forecasts of wind power production: how much resolution is enough?. *Meteorological Applications*, **25(1)**,1-10, doi: 10.1002/met.1660
- Terrado, M., N. Gonzalez-Reviriego N., Ll. Lledó, **V. Torralba**, A. Soret A., F.J. Doblas-Reyes, 2017: Climate services for affordable wind energy. *WMO Bulletin*. 66 (2) URL https://public.wmo.int/en/resources/bulletin/climate-services-affordable-wind-energy.
- Buontempo, C., H. M. Hanlon, M. B. Soares, I. Christel, J. M. Soubeyroux, C. Viel, S. Calmanti, L. Bosi, E. Falloon, J. Palin, E. Vanvyve, **V. Torralba**, N. Gonzalez-Reviriego, F. J. Doblas-Reyes, E. C. D Pope, P. Newton and F. Liggins, 2018: What have we learnt from EUPORIAS climate service prototypes?. *Climate Services*, doi:/10.1016/j.cliser.2017.06.003.
- Manzanas, R., J.M. Gutiérrez, J. Bhend, S. Hemri, F.J. Doblas-Reyes, **V. Torralba**, E. Penabad, A. Brookshaw, 2019 (accepted): Bias adjustment and ensemble recalibration methods for seasonal forecasting: a comprehensive intercomparison using the C3S dataset. *Climate Dynamics*, doi: 10.1007/s00382-019-04640-4.
- Lee, D.Y., F.J. Doblas-Reyes, **V. Torralba**, and N. Gonzalez-Reviriego, 2019: Multi-model seasonal forecasts for the wind energy sector. *Climate Dynamics*, doi: 10.1007/s00382-019-04654-y.
- Lledó, L., **V. Torralba**, A. Soret and F.J. Doblas-Reyes, under review: Advances and gaps in the provision of climate services for the wind power industry: seasonal forecasts of capacity factor. *Renewable energy*.

Other publications

- **Torralba, V.**, B. Rodríguez-Fonseca, E. Mohino, E. and T. Losada, 2015: The non-stationary influence of the Atlantic and Pacific Niños on North Eastern South American rainfall. *Frontiers in Earth Science*, **3**, 55, doi:10.3389/feart.2015.00055.

References

References

A

Acosta Navarro, J., P. Ortega, J. García-Serrano, V. Guemas, E. Tourigny, R. Cruz-García, F. Massonnet, and F. Doblas-Reyes, 2018: December 2016: linking the lowest Arctic sea-ice extent on record with the lowest European precipitation event on record. *Bulletin of the American Meteorological Society*, **99 (12)**, doi: 10.1175/BAMS-D-18-0097.1.

Alessandrini, S., S. Sperati, and P. Pinson, 2013: A comparison between the ECMWF and COSMO Ensemble Prediction Systems applied to short-term wind power forecasting on real data. *Applied Energy*, **107**, 271–280, doi: 10.1016/j.apenergy.2013.02.041.

Alexander, M. A., I. Bladé, M. Newman, J. R. Lanzante, N.-C. Lau, and J. D. Scott, 2002: The atmospheric bridge: The influence of ENSO teleconnections on air–sea interaction over the global oceans. *Journal of Climate*, **15 (16)**, 2205–2231, doi: 10.1175/1520-0442(2002)015<2205:TABTIO>2.0.CO;2.

Alvarez-Castro, M. C., D. Faranda, and P. Yiou, 2018: Atmospheric dynamics leading to West European summer hot temperatures since 1851. *Complexity*, **2018**, doi: 10.1155/2018/2494509.

Ardilouze, C., et al., 2017: Multi-model assessment of the impact of

soil moisture initialization on mid-latitude summer predictability. *Climate Dynamics*, **49 (11-12)**, 3959–3974, doi: 10.1007/s00382-017-3555-7.

Athanasiadis, P. J., et al., 2017: A multisystem view of wintertime NAO seasonal predictions. *Journal of Climate*, **30 (4)**, 1461–1475, doi: 10.1175/JCLI-D-16-0153.1.

Atlas, R., R. N. Hoffman, J. Ardizzone, S. M. Leidner, J. C. Jusem, D. K. Smith, and D. Gombos, 2011: A cross-calibrated, multiplatform ocean surface wind velocity product for meteorological and oceanographic applications. *Bulletin of the American Meteorological Society*, **92 (2)**, 157–174, doi: 10.1175/2010BAMS2946.1.

Auer, I., et al., 2005: A new instrumental precipitation dataset for the greater alpine region for the period 1800–2002. *International Journal of Climatology*, **25 (2)**, 139–166, doi: 10.1002/joc.1135.

B

Baker, L., L. Shaffrey, R. Sutton, A. Weisheimer, and A. Scaife, 2018: An Intercomparison of Skill and Overconfidence/Underconfidence of the Wintertime North Atlantic Oscillation in Multimodel Seasonal Forecasts. *Geophysical Research Letters*, **45 (15)**, 7808–7817, doi: 10.1029/2018GL078838.

Barnes, E. A. and D. L. Hartmann, 2010: Dynamical feedbacks and the persistence of the NAO. *Journal of the Atmospheric Sciences*, **67 (3)**, 851–865, doi: 10.1175/2009JAS3193.1.

Barnston, A. G. and C. F. Ropelewski, 1992: Prediction of ENSO episodes using canonical correlation analysis. *Journal of Climate*, **5 (11)**, 1316–1345, doi: 10.1175/1520-0442(1992)005<1316:POEEUC>2.0.CO;2.

Barnston, A. G., M. K. Tippett, M. L. L'Heureux, S. Li, and D. G. DeWitt, 2012: Skill of real-time seasonal ENSO model predictions during 2002-11: Is our capability increasing? *Bulletin of the American Meteorological Society*, **93 (5)**, 631–651, doi: 10.1175/BAMS-D-11-00111.1.

Barnston, A. G. and H. M. van den Dool, 1993: A degeneracy in cross-validated skill in regression-based forecasts. *Journal of Climate*, **6 (5)**, 963–977, doi: 10.1175/1520-0442(1993)006<0963:ADICVS>2.0.CO;2.

Barrier, N., C. Cassou, J. Deshayes, and A.-M. Treguier, 2014: Response of North Atlantic Ocean circulation to atmospheric weather regimes. *Journal of Physical Oceanography*,

44 (1), 179–201, doi: 10.1175/JPO-D-12-0217.1.

Beck, C., J. Jacobeit, and P. Jones, 2007: Frequency and within-type variations of large-scale circulation types and their effects on low-frequency climate variability in central europe since 1780. *International Journal of Climatology: A Journal of the Royal Meteorological Society*, **27 (4)**, 473–491, doi: 10.1002/joc.1410.

Bengtsson, L., U. Schlese, E. Roeckner, M. Latif, T. P. Barnett, and N. Graham, 1993: A two-tiered approach to long-range climate forecasting. *Science*, **261 (5124)**, 1026–1029, doi: 10.1126/science.261.5124.1026.

Bett, P. E. and H. E. Thornton, 2015: The climatological relationships between wind and solar energy supply in Britain. *Renewable Energy*, **87**, 96–110, doi: 10.1016/j.renene.2015.10.006.

Bhend, J., I. Mahlstein, and M. A. Liniger, 2017: Predictive skill of climate indices compared to mean quantities in seasonal forecasts. *Quarterly Journal of the Royal Meteorological Society*, **143 (702)**, 184–194, doi: 10.1002/qj.2908.

Bichet, A., M. Wild, D. Folini, and C. Schär, 2012: Causes for decadal variations of wind speed over land: Sensitivity studies with a global climate model. *Geophysical Research Letters*, **39 (11)**, doi: 10.1029/2012GL051685.

Blackmon, M. L., 1976: A climatological spectral study of the 500 mb geopotential height of the Northern Hemisphere. *Journal of the Atmospheric Sciences*, **33 (8)**, 1607–1623, doi: 10.1175/1520-0469(1976)033<1607:ACSSOT>2.0.CO;2.

Bloom, S., L. Takacs, A. Da Silva, and D. Ledvina, 1996: Data assimilation using incremental analysis updates. *Monthly Weather Review*, **124 (6)**, 1256–1271, doi: 10.1175/1520-0493(1996)124<1256:DAUIAU>2.0.CO;2.

Boer, G. J., 2009: Climate trends in a seasonal forecasting system. *Atmosphere-Ocean*, **47 (2)**, 123–138, doi: 10.3137/AO1002.2009.

Bollasina, M. A. and G. Messori, 2018: On the link between the subseasonal evolution of the North Atlantic Oscillation and East Asian climate. *Climate Dynamics*, 1–21, doi: 10.1007/s00382-018-4095-5.

Bradley, A. A., S. S. Schwartz, and T. Hashino, 2008: Sampling uncertainty and confidence intervals for the brier score and brier skill

score. *Weather and Forecasting*, **23 (5)**, 992–1006, doi: 10.1175/2007WAF2007049.1.

Brasseur, G. P. and L. Gallardo, 2016: Climate services: Lessons learned and future prospects. *Earth's Future*, **4 (3)**, 79–89, doi: 10.1002/2015EF000338.

Brayshaw, D. J., A. Troccoli, R. Fordham, and J. Methven, 2011: The impact of large scale atmospheric circulation patterns on wind power generation and its potential predictability: A case study over the UK. *Renewable Energy*, **36 (8)**, 2087–2096, doi: 10.1016/j.renene.2014.10.024.

Bröcker, J., 2008: On reliability analysis of multi-categorical forecasts. *Nonlinear Processes in Geophysics*, **15 (4)**, 661–673, doi: 10.5194/npg-15-661-2008.

Bröcker, J. and L. A. Smith, 2007: Scoring probabilistic forecasts: The importance of being proper. *Weather and Forecasting*, **22 (2)**, 382–388, doi: 10.1175/WAF966.1.

Brönnimann, S., 2007: Impact of El Niño-Southern Oscillation on European climate. *Reviews of Geophysics*, **45 (3)**, doi: 10.1029/2006RG000199.

Brooks, M. S., 2013: Accelerating innovation in climate services: The 3 e's for climate service providers. *Bulletin of the American Meteorological Society*, **94 (6)**, 807–819, doi: 10.1175/BAMS-D-12-00087.1.

Brown, M. B., 1975: A method for combining non-independent, one-sided tests of significance. *Biometrics*, **31 (4)**, 987–992, doi: 10.2307/2529826.

Brunet, G., et al., 2010: Collaboration of the weather and climate communities to advance subseasonal-to-seasonal prediction. *Bulletin of the American Meteorological Society*, **91 (10)**, 1397–1406, doi: 10.1175/2010BAMS3013.1.

Buizza, R. and M. Leutbecher, 2015: The forecast skill horizon. *Quarterly Journal of the Royal Meteorological Society*, **141 (693)**, 3366–3382, doi: 10.1002/qj.2619.

Buontempo, C., 2018: *European Climate Services*, 27–40. Springer, doi: 10.1007/978-3-319-68418-5_3.

Buontempo, C., C. D. Hewitt, F. J. Doblas-Reyes, and S. Dessai, 2014: Climate service development, delivery and use in Europe at monthly to inter-annual timescales. *Climate Risk Management*, **6**, 1–5, doi: 10.1016/j.crm.2014.10.002, URL http://dx.doi.org/10.1016/j.crm.2014.10.002.

Buontempo, C., et al., 2018: What have we learnt from euporias climate service prototypes? *Climate Services*, **9**, 21–32, doi: 10.1016/j.cliser.2017.06.003.

C

Cane, M. A., S. E. Zebiak, and S. C. Dolan, 1986: Experimental forecasts of El Niño. *Nature*, **321 (6073)**, 827, doi: 10.1038/321827a0.

Cannon, D., D. Brayshaw, J. Methven, P. Coker, and D. Lenaghan, 2015: Using reanalysis data to quantify extreme wind power generation statistics: A 33 year case study in Great Britain. *Renewable Energy*, **75**, 767–778, doi: 10.1016/j.renene.2014.10.024.

Carta, J. A., P. Ramírez, and S. Velázquez, 2009: A review of wind speed probability distributions used in wind energy analysis. Case studies in the Canary Islands. *Renewable and Sustainable Energy Reviews*, **13 (5)**, 933–955, doi: 10.1016/j.rser.2008.05.005.

Cash, D. W., W. C. Clark, F. Alcock, N. M. Dickson, N. Eckley, D. H. Guston, J. Jäger, and R. B. Mitchell, 2003: Knowledge systems for sustainable development. *Proceedings of the national academy of sciences*, **100 (14)**, 8086–8091, doi: 10.1073/pnas.1231332100.

Cassou, C., 2008: Intraseasonal interaction between the Madden–Julian Oscillation and the North Atlantic Oscillation. *Nature*, **455 (7212)**, 523, doi: 10.1038/nature07286.

Cassou, C., L. Terray, J. W. Hurrell, and C. Deser, 2004: North Atlantic winter climate regimes: Spatial asymmetry, stationarity with time, and oceanic forcing. *Journal of Climate*, **17 (5)**, 1055–1068, doi: 10.1175/1520-0442(2004)017<1055:NAWCRS>2.0.CO;2.

Cassou, C., L. Terray, and A. S. Phillips, 2005: Tropical Atlantic influence on European heat waves. *Journal of Climate*, **18 (15)**, 2805–2811, doi: 10.1175/JCLI3506.1.

Chang, E. K. M. and Y. Fu, 2002: Interdecadal variations in Northern Hemisphere winter storm track intensity. *Journal of Climate*, **15 (6)**, 642–658, doi: 10.1175/1520-0442(2002)015<0642:IVINHW>2.0.CO;2.

Chang, E. K. M., S. Lee, and K. L. Swanson, 2002: Storm track dynamics. *Journal of Climate*, **15 (16)**, 2163–2183, doi: 10.1175/1520-0442(2002)015<02163:STD>2.0.CO;2.

Charney, J. G., J. Shukla, J. Lighthill, and R. P. Pearce, 1981: *Predictability of monsoons*, 99–110. Cambridge University Press.

Chaudhry, N. and L. Hughes, 2012: Forecasting the reliability of wind-energy systems: A new approach using the RL technique. *Applied Energy*, **96**, 422–430, doi: 10.1016/j.apenergy.2012.02.076.

Chen, C., M. A. Cane, N. Henderson, D. E. Lee, D. Chapman, D. Kondrashov, and M. D. Chekroun, 2016: Diversity, nonlinearity, seasonality, and memory effect in ENSO Simulation and Prediction Using Empirical Model Reduction. *Journal of Climate*, **29 (5)**, 1809–1830, doi: 10.1175/JCLI-D-15-0372.1.

Christel, I., D. Hemment, D. Bojovic, F. Cucchietti, L. Calvo, M. Stefaner, and C. Buontempo, 2018: Introducing design in the development of effective climate services. *Climate Services*, **9**, 111–121, doi: 10.1016/j.cliser.2017.06.002.

Clark, R. T., P. E. Bett, H. E. Thornton, and A. A. Scaife, 2017: Skilful seasonal predictions for the European energy industry. *Environmental Research Letters*, **12 (2)**, 24 002, doi: 10.1088/1748-9326/aa57ab.

Cleveland, W. S. and S. J. Devlin, 1988: Locally Weighted Regression: An Approach to Regression Analysis by Local Fitting. *Journal of the American Statistical Association*, **83 (403)**, 596–610, doi: 10.1080/01621459.1988.10478639.

Coelho, C., D. Stephenson, M. Balmaseda, F. Doblas-Reyes, and G. Van Oldenborgh, 2006: Toward an integrated seasonal forecasting system for South America. *Journal of Climate*, **19 (15)**, 3704–3721, doi: 10.1175/JCLI3801.1.

Cohen, J. and C. Fletcher, 2007: Improved skill of northern hemisphere winter surface temperature predictions based on land–atmosphere fall anomalies. *Journal of Climate*, **20 (16)**, 4118–4132, doi: 10.1175/JCLI4241.1.

Cohen, J., et al., 2014: Recent arctic amplification and extreme mid-latitude weather. *Nature geoscience*, **7 (9)**, 627, doi: 10.1038/ngeo2234.

Compo, G. P. and P. D. Sardeshmukh, 2004: Storm track predictability on seasonal and decadal scales. *Journal of Climate*, **17 (19)**, 3701–3720, doi: 10.1175/1520-0442(2004)017<3701:STPOSA>2.0.CO;2.

Cortesi, N., V. Torralba, N. González-Reviriego, A. Soret, and F. J. Doblas-Reyes, 2019: Characterization of european wind speed variability using weather regimes, manuscript submitted for publication in Climate Dynamics.

Couto, A., P. Costa, L. Rodrigues, V. V. Lopes, and A. Estanqueiro, 2015: Impact of weather regimes on the wind power ramp forecast in portugal. *IEEE Transactions on Sustainable Energy*, **6 (3)**, 934–942, doi: 10.1109/TSTE.2014.2334062.

Crane, T. A., C. Roncoli, J. Paz, N. Breuer, K. Broad, K. T. Ingram, and G. Hoogenboom, 2010: Forecast skill and farmers' skills: Seasonal climate forecasts and agricultural risk management in the southeastern united states. *Weather, Climate, and Society*, **2 (1)**, 44–59, doi: 10.1175/2009WCAS1006.1.

Crochemore, L., M.-H. Ramos, and F. Pappenberger, 2016: Bias correcting precipitation forecasts to improve the skill of seasonal streamflow forecasts. *Hydrology and Earth System Sciences*, **20 (9)**, 3601–3618, doi: 10.5194/hess-20-3601-2016.

CWEA, 2015: Installed Capacity. Tech. rep., Canadian Wind Energy Association. URL http://canwea.ca/wind-energy/installed-capacity/.

D

Davis, M., R. Lowe, S. Steffen, F. Doblas-Reyes, and X. Rodó, 2016: *Barriers to using climate information: Challenges in communicating probabilistic forecasts to decision-makers*, 95–113. Springer, doi: 10.1007/978-3-319-20161-0_7.

Davis, R. E., 1978: Predictability of sea level pressure anomalies over the North Pacific Ocean. *Journal of Physical Oceanography*, **8 (2)**, 233–246, doi: 10.1175/1520-0485(1978)008<0233:POSLPA>2.0.CO;2.

Dawson, A. and T. Palmer, 2015: Simulating weather regimes: Impact of model resolution and stochastic parameterization. *Climate Dynamics*, **44 (7-8)**, 2177–2193, doi: 10.1007/s00382-014-2238-x.

Dawson, A., T. N. Palmer, and S. Corti, 2012: Simulating regime structures in weather and climate prediction models. *Geophysical Research Letters*, **39 (21)**, doi: 10.1029/2012GL053284.

De Felice, M., A. Alessandri, and F. Catalano, 2015: Seasonal climate forecasts for medium-term electricity demand forecasting. *Applied Energy*, **137**, 435–444, doi: 10.1016/j.apenergy.2014.10.030.

Decker, M., M. A. Brunke, Z. Wang, K. Sakaguchi, X. Zeng, and M. G. Bosilovich, 2012: Evaluation of the reanalysis products from GSFC, NCEP,

and ECMWF using flux tower observations. *Journal of Climate*, **25 (6)**, 1916–1944, doi: 10.1175/JCLI-D-11-00004.1.

Dee, D. P., et al., 2011: The ERA-Interim reanalysis: Configuration and performance of the data assimilation system. *Quarterly Journal of the Royal Meteorological Society*, **137 (656)**, 553–597, doi: 10.1002/qj.828.

Della-Marta, P. M., M. A. Liniger, C. Appenzeller, D. N. Bresch, P. Köllner-Heck, and V. Muccione, 2010: Improved Estimates of the European Winter Windstorm Climate and the Risk of Reinsurance Loss Using Climate Model Data. *Journal of Applied Meteorology and Climatology*, **49 (10)**, 2092–2120, doi: 10.1175/2010JAMC2133.1.

Doblas-Reyes, F., R. Hagedorn, T. Palmer, and J.-J. Morcrette, 2006: Impact of increasing greenhouse gas concentrations in seasonal ensemble forecasts. *Geophysical Research Letters*, **33 (7)**, doi: 10.1029/2005GL025061.

Doblas-Reyes, F., V. Pavan, and D. Stephenson, 2003: The skill of multi-model seasonal forecasts of the wintertime North Atlantic Oscillation. *Climate Dynamics*, **21 (5-6)**, 501–514, doi: 10.1007/s00382-003-0350-4.

Doblas-Reyes, F., et al., 2013a: Initialized near-term regional climate change prediction. *Nature communications*, **4**, 1715, doi: 10.1038/ncomms2704.

Doblas-Reyes, F. J., J. García-Serrano, F. Lienert, A. P. Biescas, and L. R. L. Rodrigues, 2013b: Seasonal climate predictability and forecasting: status and prospects. *Wiley Interdisciplinary Reviews: Climate Change*, **4 (4)**, 245–268, doi: 10.1002/wcc.217.

Doblas-Reyes, F. J., R. Hagedorn, and T. N. Palmer, 2005: The rationale behind the success of multi-model ensembles in seasonal forecasting - II. Calibration and combination. *Tellus A*, **57 (3)**, 234–252, doi: 10.1111/j.1600-0870.2005.00104.x.

Donat, M. G. and L. V. Alexander, 2012: The shifting probability distribution of global daytime and night-time temperatures. *Geophysical Research Letters*, **39 (14)**, 1–5, doi: 10.1029/2012GL052459.

Duan, W. and J. Hu, 2016: The initial errors that induce a significant "spring predictability barrier" for El Niño events and their implications for target observation: results from an earth system model. *Climate Dynamics*, **46 (11-12)**, 3599–3615, doi: 10.1007/s00382-015-2789-5.

Dutra, E., G. Balsamo, P. Viterbo, P. M. Miranda, A. Beljaars, C. Schär, and K. Elder, 2010: An improved snow scheme for the ECMWF land surface model: Description and offline validation. *Journal of Hydrometeorology*, **11 (4)**, 899–916, doi: 10.1175/2010JHM1249.1.

Dutra, E., et al., 2014: Global meteorological drought–part 2: Seasonal forecasts. *Hydrology and Earth System Sciences*, **18 (7)**, 2669–2678, doi: 10.5194/hess-18-2669-2014.

E

Eden, J., G. J. Van Oldenborgh, E. Hawkins, and E. B. Suckling, 2015: A global empirical system for probabilistic seasonal climate prediction. *Geoscientific Model Development*, **8 (12)**, 3947–3973, doi: 10.5194/gmd-8-3947-2015.

Edwards, P. N., 2011: History of climate modeling. *Wiley Interdisciplinary Reviews: Climate Change*, **2 (1)**, 128–139, doi: 10.1002/wcc.95.

Eichler, T. and W. Higgins, 2006: Climatology and ENSO-related variability of North American extratropical cyclone activity. *Journal of Climate*, **19 (10)**, 2076–2093, doi: 10.1175/JCLI3725.1.

Elmore, K. L., 2005: Alternatives to the chi-square test for evaluating rank histograms from ensemble forecasts. *Weather and forecasting*, **20 (5)**, 789–795, doi: 10.1175/WAF884.1.

England, M. H., et al., 2014: Recent intensification of wind-driven circulation in the Pacific and the ongoing warming hiatus. *Nature Clim. Change*, **4 (3)**, 222–227, doi: 10.1038/NCLIMATE2106.

Epstein, E. S., 1969: A scoring system for probability forecasts of ranked categories. *Journal of Applied Meteorology*, **8 (6)**, 985–987, doi: 10.1175/1520-0450(1969)008<0985:ASSFPF>2.0.CO;2.

F

Fan, Y., S.-J. Lin, S. M. Griffies, and M. A. Hemer, 2014: Simulated global swell and wind-sea climate and their responses to anthropogenic climate change at the end of the twenty-first century. *Journal of Climate*, **27 (10)**, 3516–3536, doi: 10.1175/JCLI-D-13-00198.1.

Fant, C., C. Adam Schlosser, and K. Strzepek, 2016: The impact of climate change on wind and solar resources in southern Africa. *Applied Energy*, **161**, 556–564, doi: 10.1016/j.apenergy.2015.03.042.

Fereday, D. R., J. R. Knight, A. A. Scaife, C. K. Folland, and A. Philipp, 2008: Cluster analysis of North Atlantic–European circulation types and links with tropical Pacific sea surface temperatures. *Journal of Climate*, **21 (15)**, 3687–3703, doi: 10.1175/2007JCLI1875.1.

Ferranti, L., S. Corti, and M. Janousek, 2015: Flow-dependent verification of the ECMWF ensemble over the Euro-Atlantic sector. *Quarterly Journal of the Royal Meteorological Society*, **141 (688)**, 916–924, doi: 10.1002/qj.2411.

Ferro, C. A. T., 2014: Fair scores for ensemble forecasts. *Quarterly Journal of the Royal Meteorological Society*, **140 (683)**, 1917–1923, doi: 10.1002/qj.2270.

Fil, C. and L. Dubus, 2005: Winter climate regimes over the North Atlantic and European region in ERA40 reanalysis and DEMETER seasonal hindcasts. *Tellus A*, **57 (3)**, 290–307, doi: 10.1111/j.1600-0870.2005.00127.x.

Flato, G. M., 2011: Earth system models: an overview. *Wiley Interdisciplinary Reviews: Climate Change*, **2 (6)**, 783–800, doi: 10.1002/wcc.148.

Foley, A. M., P. G. Leahy, A. Marvuglia, and E. J. McKeogh, 2012: Current methods and advances in forecasting of wind power generation. *Renewable Energy*, **37 (1)**, 1–8, doi: 10.1016/j.renene.2011.05.033.

Ford, D., S. Kay, R. McEwan, I. Totterdell, and M. Gehlen, 2018: Marine biogeochemical modelling and data assimilation for operational forecasting, reanalysis, and climate research. *GODAE Oceanview International School in "New Frontiers in Operational Oceanography", EP Chassignet, A. Pascual, J. Tintore, and J. Verron, Eds*, doi: 10.17125/gov2018.ch22.

Fricker, T. E., C. A. T. Ferro, and D. B. Stephenson, 2013: Three recommendations for evaluating climate predictions. *Meteorological Applications*, **20 (2)**, 246–255, doi: 10.1016/j.renene.2011.05.033.

Füss, R., S. Mahringer, and M. Prokopczuk, 2013: Electricity derivatives pricing with forward-looking information. *University of St. Gallen, School of Finance Research Paper*, doi: 10.2139/ssrn.2219855.

G

Garcia-Morales, M. B. and L. Dubus, 2007: Forecasting precipitation for hydroelectric power management: how to exploit GCM's seasonal ensemble forecasts. *International*

Journal of Climatology, **27 (12)**, 1691, doi: 10.1002/joc.1608.

García-Serrano, J. and F. Doblas-Reyes, 2012: On the assessment of near-surface global temperature and North Atlantic multi-decadal variability in the ENSEMBLES decadal hindcast. *Climate Dynamics*, **39 (7-8)**, 2025–2040, doi: 10.1007/s00382-012-1413-1.

Gershunov, A. and D. R. Cayan, 2003: Heavy daily precipitation frequency over the contiguous United States: Sources of climatic variability and seasonal predictability. *Journal of Climate*, **16 (16)**, 2752–2765, doi: 10.1175/1520-0442(2003)016<2752: HDPFOT>2.0.CO;2.

GFCS, 2014: Annex to the Implementation Plan of the Global Framework for Climate Services – User Interface Platform Component. Tech. rep., World Meteorological Association.

Goddard, L., 2016: From science to service. *Science*, **353 (6306)**, 1366–1367, doi: 10.1126/science.aag3087.

Goddard, L., S. J. Mason, S. E. Zebiak, C. F. Ropelewski, R. Basher, and M. A. Cane, 2001: Current approaches to seasonal to interannual climate predictions. *International Journal of Climatology*, **21 (9)**, 1111–1152, doi: 10.1002/joc.636.

Goddard, L., et al., 2010: Providing seasonal-to-interannual climate information for risk management and decision-making. *Procedia Environmental Sciences*, **1**, 81–101, doi: 10.1016/j.proenv.2010.09.007.

Graff, M., R. Peña, A. Medina, and H. J. Escalante, 2014: Wind speed forecasting using a portfolio of forecasters. *Renewable Energy*, **68**, 550–559, doi: 10.1016/j.renene.2014.02.041.

Graham, N. E., J. Michaelsen, and T. P. Barnett, 1987: An investigation of the El Niño-Southern Oscillation cycle With statistical models: 2. Model results. *Journal of Geophysical Research: Oceans*, **92 (C13)**, 14 271–14 289, doi: 10.1029/JC092iC13p14271.

Grams, C. M., R. Beerli, S. Pfenninger, I. Staffell, and H. Wernli, 2017: Balancing Europe's wind-power output through spatial deployment informed by weather regimes. *Nature climate change*, **7 (8)**, 557, doi: 10.1038/nclimate3338.

Gregow, H., et al., 2015: User awareness concerning feedback data and input observations used in reanalysis systems. *Advances in Science and Research*, **12 (1)**, 63–67, doi: 10.5194/asr-12-63-2015.

Guemas, V., M. Chevallier, M. Déqué, O. Bellprat, and F. Doblas-Reyes, 2016: Impact of sea ice initialization on sea ice and atmosphere prediction skill on seasonal timescales. *Geophysical Research Letters*, **43 (8)**, 3889–3896, doi: 10.1002/2015GL066626.

H

Hamill, T. M., 2001: Interpretation of rank histograms for verifying ensemble forecasts. *Monthly Weather Review*, **129 (3)**, 550–560, doi: 10.1175/1520-0493(2001)129<0550:IORHFV>2.0.CO;2.

Hamilton, E., R. Eade, R. J. Graham, A. A. Scaife, D. M. Smith, A. Maidens, and C. MacLachlan, 2012: Forecasting the number of extreme daily events on seasonal timescales. *Journal of Geophysical Research: Atmospheres*, **117 (D3)**, doi: 10.1029/2011JD016541.

Hamlington, B. D., P. E. Hamlington, S. G. Collins, S. R. Alexander, and K.-Y. Kim, 2015: Effects of climate oscillations on wind resource variability in the United States. *Geophysical Research Letters*, **42 (1)**, 145–152, doi: 10.1002/2014GL062370.

Hannachi, A., D. M. Straus, C. L. E. Franzke, S. Corti, and T. Woollings, 2017: Low Frequency Nonlinearity and Regime Behavior in the Northern Hemisphere Extra-Tropical Atmosphere. *Reviews of Geophysics*, doi: 10.1002/2015RG000509.

Harmel, R. D., C. W. Richardson, C. L. Hanson, and G. L. Johnson, 2002: Evaluating the adequacy of simulating maximum and minimum daily air temperature with the normal distribution. *Journal of Applied Meteorology*, **41 (7)**, 744–753, doi: 10.1175/1520-0450(2002)041<0744:Etaosm>2.0.Co;2.

Hartigan, J. A. and M. A. Wong, 1979: Algorithm AS 136: A k-means clustering algorithm. *Journal of the Royal Statistical Society. Series C (Applied Statistics)*, **28 (1)**, 100–108, doi: 10.2307/2346830.

Helfand, H. M. and S. D. Schubert, 1995: Climatology of the simulated great plains low-level jet and its contribution to the continental moisture budget of the united states. *Journal of Climate*, **8 (4)**, 784–806.

Hering, J. G., D. A. Dzombak, S. A. Green, R. G. Luthy, and D. Swackhamer, 2014: Engagement at the science-policy interface. ACS Publications, 11031-11033 pp., doi: 10.1021/es504225t.

Hewitt, C., C. Buontempo, and P. Newton, 2013: Using climate predictions to better serve society's needs. *Eos, Transactions American Geophysical Union*, **94 (11)**, 105–107, doi: 10.1002/2013EO110002.

Hewitt, C., S. Mason, and D. Walland, 2012: The global framework for climate services. *Nature Climate Change*, **2 (12)**, 831, doi: 10.1038/nclimate1745.

Hirschi, M., et al., 2011: Observational evidence for soil-moisture impact on hot extremes in southeastern europe. *Nature Geoscience*, **4 (1)**, 17, doi: 10.1038/ngeo1032.

Hobday, A. J., C. M. Spillman, P. Eveson, J. Hartog, X. Zhang, and S. Brodie, 2018: A framework for combining seasonal forecasts and climate projections to aid risk management for fisheries and aquaculture. *Frontiers in Marine Science*, **5**, 137, doi: 10.3389/fmars.2018.00137.

Hoskins, B. J. and D. J. Karoly, 1981: The steady linear response of a spherical atmosphere to thermal and orographic forcing. *Journal of the Atmospheric Sciences*, **38 (6)**, 1179–1196, doi: 10.1175/1520-0469(1981)038<1179:TSLROA>2.0.CO;2.

Hueging, H., R. Haas, K. Born, D. Jacob, and J. G. Pinto, 2013: Regional changes in wind energy potential over Europe using regional climate model ensemble projections. *Journal of Applied Meteorology and Climatology*, **52 (4)**, 903–917, doi: 10.1175/JAMC-D-12-086.1.

Hurrell, J. W., 1995: Decadal trends in the North Atlantic Oscillation: regional temperatures and precipitation. *Science*, **269 (5224)**, 676–679, doi: 10.1126/science.269.5224.676.

Hurrell, J. W. and C. Deser, 2010: North Atlantic climate variability: the role of the North Atlantic Oscillation. *Journal of Marine Systems*, **79 (3-4)**, 231–244, doi: 10.1016/j.jmarsys.2009.11.002.

Hurrell, J. W., Y. Kushnir, G. Ottersen, and M. Visbeck, 2003: An overview of the North Atlantic Oscillation. *The North Atlantic Oscillation: climatic significance and environmental impact*, 1–35, doi: 10.1029/134GM01.

I

IEA, 2017: Energy Access Outlook 2017. Tech. rep., International Energy Agency. URL https://webstore.iea.org/weo-2017-special-report-energy-access-outlook.

IEA, 2018: Global Energy & CO2 Status Report 2017. Tech. rep., International Energy Agency. URL https://www.iea.org/publications/freepublications/publication/GECO2017.pdf.

J

Jerez, S., R. M. Trigo, S. M. Vicente-Serrano, D. Pozo-Vázquez, R. Lorente-Plazas, J. Lorenzo-Lacruz, F. Santos-Alamillos, and J. P. Montávez, 2013: The impact of the North Atlantic Oscillation on renewable energy resources in southwestern Europe. *Journal of Applied Meteorology and Climatology*, **52 (10)**, 2204–2225, doi: 10.1175/JAMC-D-12-0257.1.

Jia, L., et al., 2015: Improved seasonal prediction of temperature and precipitation over land in a high-resolution gfdl climate model. *Journal of Climate*, **28 (5)**, 2044–2062, doi: 10.1175/JCLI-D-14-00112.1.

Jolliffe, I. T. and C. Primo, 2008: Evaluating rank histograms using decompositions of the chi-square test statistic. *Monthly Weather Review*, **136 (6)**, 2133–2139, doi: 10.1175/2007MWR2219.1.

Jolliffe, I. T. and D. B. Stephenson, 2012: *Forecast verification: a practitioner's guide in atmospheric science*. John Wiley & Sons.

Joseph, P. and S. Sijikumar, 2004: Intraseasonal variability of the low-level jet stream of the Asian summer monsoon. *Journal of Climate*, **17 (7)**, 1449–1458, doi: 10.1175/1520-0442(2004)017<1449%3AIVOTLJ>2.0.CO%3B2.

K

Kezunovic, M., I. Dobson, and Y. Dong, 2008: Impact of extreme weather on power system blackouts and forced outages: New challenges. *7th Balkan Power Conf*, Citeseer, 1–5, URL http://iandobson.ece.iastate.edu/PAPERS/kezunovicBPC08.pdf.

Kidston, J., A. A. Scaife, S. C. Hardiman, D. M. Mitchell, N. Butchart, M. P. Baldwin, and L. J. Gray, 2015: Stratospheric influence on tropospheric jet streams, storm tracks and surface weather. *Nature Geoscience*, **8 (6)**, 433, doi: 10.1038/ngeo2424.

Kim, H.-M., E. K. Chang, and M. Zhang, 2015: Statistical–dynamical seasonal forecast for tropical cyclones affecting New York State. *Weather and Forecasting*, **30 (2)**, 295–307, doi: 10.1175/WAF-D-14-00089.1.

Kim, H.-M., P. J. Webster, and J. A. Curry, 2012: Seasonal prediction skill of ECMWF System 4 and NCEP CFSv2 retrospective forecast for the Northern Hemisphere Winter. *Climate Dynamics*, **39 (12)**, 2957–2973, doi: 10.1007/s00382-012-1364-6.

King, M. P., I. Herceg-Bulić, I. Bladé, J. García-Serrano, N. Keenlyside, F. Kucharski, C. Li, and S. Sobolowski, 2018: Importance of late fall ENSO teleconnection in the Euro-Atlantic sector. *Bulletin of the American Meteorological Society*, doi: 10.1175/BAMS-D-17-0020.1.

Kirchner-Bossi, N., R. García-Herrera, L. Prieto, and R. M. Trigo, 2015: A long-term perspective of wind power output variability. *International Journal of Climatology*, **35 (9)**, 2635–2646, doi: 10.1002/joc.4161.

Kirtman, B. and A. Pirani, 2009: The state of the art of seasonal prediction: Outcomes and recommendations from the First World Climate Research Program Workshop on Seasonal Prediction. *Bulletin of the American Meteorological Society*, **90 (4)**, 455–458, doi: 10.1175/2008BAMS2707.1.

Kirtman, B., et al., 2013: Chapter 11 - near-term climate change: Projections and predictability. *Climate Change 2013: The Physical Science Basis. IPCC Working Group I Contribution to AR5*, IPCC, Ed., Cambridge University Press, Cambridge, doi: 10.1017/CBO9781107415324.023.

Kiss, P. and I. M. Jánosi, 2008: Comprehensive empirical analysis of ERA-40 surface wind speed distribution over Europe. *Energy Conversion and Management*, **49 (8)**, 2142–2151, doi: 10.1016/j.enconman.2008.02.003.

Kobayashi, S., et al., 2015: The JRA-55 Reanalysis: General Specifications and Basic Characteristics. *Journal of the Meteorological Society of Japan. Ser. II*, **93 (1)**, 5–48, doi: 10.2151/jmsj.2015-001.

Kushnir, Y., W. A. Robinson, P. Chang, and A. W. Robertson, 2006: The physical basis for predicting Atlantic sector seasonal-to-interannual climate variability. *Journal of Climate*, **19 (23)**, 5949–5970, doi: 10.1175/JCLI3943.1.

L

Lane, J.-e., 2016: Implementation success or failure: the COP21 agreement for the 21rest century. *Journal of Multidisciplinary Engineering Science and Technology*, **2**, 158–166, URL http://journalijcms.com/sites/default/files/issue-files/0076.pdf.

Legates, D. R. and C. J. Willmott, 1990: Mean seasonal and spatial variability in global surface air temperature. *Theoretical and applied climatology*, **41 (1)**, 11–21.

Lemos, M. C., C. J. Kirchhoff, and V. Ramprasad, 2012: Narrowing the climate information usability gap. *Nature climate change*, **2 (11)**, 789, doi: 10.1038/nclimate1614.

Leung, L. R., A. F. Hamlet, D. P. Lettenmaier, and A. Kumar, 1999: Simulations of the ENSO Hydroclimate Signals in the Pacific Northwest Columbia River Basin. *Bulletin of the American Meteorological Society*, **80 (11)**, 2313–2329, doi: 10.1175/1520-0477(1999)080<2313:SOTEHS>2.0.CO;2.

Ligges, U., et al., 2015: Package 'signal'. *R Foundation for Statistical Computing*, URL https://cran.r-project.org/web/packages/signal/signal.pdf.

Liniger, M., H. Mathis, C. Appenzeller, and F. Doblas-Reyes, 2007: Realistic greenhouse gas forcing and seasonal forecasts. *Geophysical Research Letters*, **34 (4)**, doi: 10.1029/2006GL028335.

Lorenz, C. and H. Kunstmann, 2012: The hydrological cycle in three state-of-the-art reanalyses: Intercomparison and performance analysis. *Journal of Hydrometeorology*, **13 (5)**, 1397–1420, doi: 10.1175/JHM-D-11-088.1.

Lorenz, E. N., 1963: Section of planetary sciences: The predictability of hydrodynamic flow. *Transactions of the New York Academy of Sciences*, **25 (4 Series II)**, 409–432, doi: 10.1111/j.2164-0947.1963.tb01464.x.

Lowe, R., M. García-Díez, J. Ballester, J. Creswick, J.-M. Robine, F. R. Herrmann, and X. Rodó, 2016: Evaluation of an early-warning system for heat wave-related mortality in Europe: implications for sub-seasonal to seasonal forecasting and climate services. *International journal of environmental research and public health*, **13 (2)**, 206, doi: 10.3390/ijerph13020206.

Luo, D., X. Chen, and S. B. Feldstein, 2018: Linear and nonlinear dynamics of north atlantic oscillations: A new thinking of symmetry breaking. *Journal of the Atmospheric Sciences*, **75 (6)**, 1955–1977, doi: 10.1175/JAS-D-17-0274.1.

M

MacLachlan, C., et al., 2015: Global Seasonal forecast system version 5 (GloSea5): a high-resolution seasonal forecast system. *Quarterly*

Journal of the Royal Meteorological Society, **141 (689)**, 1072–1084, doi: 10.1175/JCLI-D-15-0067.1.

MacLeod, D., V. Torralba, M. Davis, and F. Doblas-Reyes, 2018: Transforming climate model output to forecasts of wind power production: how much resolution is enough? *Meteorological Applications*, **25 (1)**, 1–10, doi: 10.1002/met.1660.

Magnusson, L., M. Alonso-Balmaseda, S. Corti, F. Molteni, and T. Stockdale, 2013: Evaluation of forecast strategies for seasonal and decadal forecasts in presence of systematic model errors. *Climate Dynamics*, **41 (9-10)**, 2393–2409, doi: 10.1007/s00382-012-1599-2.

Mahlstein, I., C. Spirig, M. A. Liniger, and C. Appenzeller, 2015: Estimating daily climatologies for climate indices derived from climate model data and observations. *Journal of Geophysical Research: Atmospheres*, **120 (7)**, 2808–2818, doi: 10.1002/2014JD022327.

Manubens, N., et al., 2018: An R package for climate forecast verification. *Environmental Modelling & Software*, **103**, 29–42, doi: 10.1016/j.envsoft.2018.01.018.

Manzanas, R. and J. Gutiérrez, 2018: Process-conditioned bias correction for seasonal forecasting: a case-study with ENSO in Peru. *Climate Dynamics*, 1–11, doi: 10.1007/s00382-018-4226-z.

Manzanas, R., J. M. Gutiérrez, J. Bhend, S. Hemri, F. J. Doblas-Reyes, V. Torralba, E. Penabad, and A. Brookshaw, 2019: Bias adjustment and ensemble recalibration methods for seasonal forecasting: a comprehensive intercomparison using the C3S dataset. *Climate Dynamics*, doi: 10.1007/s00382-019-04640-4.

Marcos, R., N. González-Reviriego, V. Torralba, A. Soret, and F. J. Doblas-Reyes, 2018: Characterization of the near surface wind speed distribution at global scale: ERA-Interim reanalysis and ECMWF seasonal forecasting System 4. *Climate Dynamics*, 1–13, doi: 10.1007/s00382-018-4338-5.

Mariotti, A., P. M. Ruti, and M. Rixen, 2018: Progress in subseasonal to seasonal prediction through a joint weather and climate community effort. *npj Climate and Atmospheric Science*, **1 (1)**, 4, doi: 10.1038/s41612-018-0014-z.

Mason, S. J. and O. Baddour, 2008: *Statistical modelling*, 163–201. Springer, doi: 10.1007/978-1-4020-6992-5_7.

Matsueda, M. and T. N. Palmer, 2018: Estimates of flow-dependent predictability of wintertime Euro-Atlantic weather regimes in medium-range forecasts. *Quarterly Journal of the Royal Meteorological Society*, **16**, 12 945, doi: 10.1002/qj.3265.

McPhaden, M. J., S. E. Zebiak, and M. H. Glantz, 2006: ENSO as an integrating concept in earth science. *Science*, **314 (5806)**, 1740–1745, doi: 10.1126/science.1132588.

McVicar, T. R., et al., 2012: Global review and synthesis of trends in observed terrestrial near-surface wind speeds: Implications for evaporation. *Journal of Hydrology*, **416-417**, 182–205, doi: 10.1016/j.jhydrol.2011.10.024.

Meehl, G. A., et al., 2009: Decadal prediction: Can it be skillful? *Bulletin of the American Meteorological Society*, **90 (10)**, 1467–1486, doi: 10.1175/2009BAMS2778.1.

Michelangeli, P.-A., R. Vautard, and B. Legras, 1995: Weather regimes: Recurrence and quasi stationarity. *Journal of the atmospheric sciences*, **52 (8)**, 1237–1256, doi: 10.1175/1520-0469(1995)052<1237:WRRAQS>2.0.CO;2.

Molod, A., L. Takacs, M. Suarez, and J. Bacmeister, 2015: Development of the GEOS-5 atmospheric general circulation model: Evolution from MERRA to MERRA2. *Geoscientific Model Development*, **8 (5)**, 1339–1356, doi: 10.5194/gmd-8-1339-2015.

Molteni, F., T. N. Stockdale, and F. Vitart, 2015: Understanding and modelling extra-tropical teleconnections with the indo-pacific region during the northern winter. *Climate Dynamics*, **45 (11-12)**, 3119–3140, doi: 10.1007/s00382-015-2528-y.

Molteni, F., et al., 2011: The new ECMWF seasonal forecast system (System 4). Tech. Rep. November, European Centre for Medium-Range Weather Forecasts. doi: 10.21957/4nery093i.

Monahan, A. H., 2006: The probability distribution of sea surface wind speeds. Part II: Dataset intercomparison and seasonal variability. *Journal of Climate*, **19 (4)**, 521–534, doi: 10.1175/JCLI3641.1.

N

Najafi, A., H. Falaghi, J. Contreras, and M. Ramezani, 2016: Medium-term energy hub management subject to electricity price and wind uncertainty. *Applied Energy*, **168**, 418–433, doi: 10.1016/j.apenergy.2016.01.074.

National Academies of Sciences, E. and Medicine, 2016: *Next Generation Earth System Prediction: Strategies for Subseasonal to Seasonal Forecasts*. National Academies Press, doi: 10.17226/21873.

National Research Council, N., 2010: *Assessment of intraseasonal to interannual climate prediction and predictability*. National Academies Press, URL http://www.nap.edu/catalog/12878.html.

Nchaba, T., M. Mpholo, and C. Lennard, 2016: Long-term austral summer wind speed trends over southern Africa and the surrounding oceans. *International Journal of Climatology*, doi: 10.1002/joc.4883.

Neal, R., D. Fereday, R. Crocker, and R. E. Comer, 2016: A flexible approach to defining weather patterns and their application in weather forecasting over Europe. *Meteorological Applications*, **23 (3)**, 389–400, doi: 10.1002/met.1563.

O

Ogutu, G. E. O., W. H. P. Franssen, I. Supit, P. Omondi, and R. W. Hutjes, 2017: Skill of ECMWF system-4 ensemble seasonal climate forecasts for East Africa. *International Journal of Climatology*, **37 (5)**, 2734–2756, doi: 10.1002/joc.4876.

Ouarda, T. B. M. J., C. Charron, and F. Chebana, 2016: Review of criteria for the selection of probability distributions for wind speed data and introduction of the moment and L-moment ratio diagram methods, with a case study. *Energy Conversion and Management*, **124**, 247–265, doi: 10.1016/j.enconman.2016.07.012.

P

Palin, E. J., A. A. Scaife, E. Wallace, E. C. Pope, A. Arribas, and A. Brookshaw, 2016: Skillful seasonal forecasts of winter disruption to the UK transport system. *Journal of Applied Meteorology and Climatology*, **55 (2)**, 325–344, doi: 10.1175/JAMC-D-15-0102.1.

Palmer, T. N. and D. L. Anderson, 1994: The prospects for seasonal forecasting—a review paper. *Quarterly Journal of the Royal Meteorological Society*, **120 (518)**, 755–793, doi: 10.1002/qj.49712051802.

Pepler, A. S., L. B. Díaz, C. Prodhomme, F. J. Doblas-Reyes, and A. Kumar, 2015: The ability of a multi-model seasonal forecasting ensemble to forecast the frequency of warm, cold and wet extremes. *Weather and Climate Extremes*, **9**, 68–77, doi: 10.1016/j.wace.2015.06.005.

Petersen, J., D. Sack, and R. E. Gabler, 2010: *Fundamentals of physical geography*. Cengage Learning.

Philander, S. G., 1990: *El Nino, La Nina, and the Southern Oscillation*. Academic Press.

Pinson, P., 2012: Adaptive calibration of (u, v)-wind ensemble forecasts. *Quarterly Journal of the Royal Meteorological Society*, **138 (666)**, 1273–1284, doi: 10.1002/qj.1873.

Pinson, P., 2013: Wind energy: Forecasting challenges for its operational management. *Statistical Science*, **28 (4)**, 564–585, doi: 10.1002/qj.1873.

Prodhomme, C., F. Doblas-Reyes, O. Bellprat, and E. Dutra, 2016: Impact of land-surface initialization on sub-seasonal to seasonal forecasts over Europe. *Climate Dynamics*, **47 (3-4)**, 919–935, doi: 10.1007/s00382-015-2879-4.

Pryor, S. and R. Barthelmie, 2013: Assessing the vulnerability of wind energy to climate change and extreme events. *Climatic change*, **121 (1)**, 79–91, doi: 10.1007/s10584-013-0889-y.

Pryor, S. C. and R. J. Barthelmie, 2010: Climate change impacts on wind energy: A review. *Renewable and sustainable energy reviews*, **14 (1)**, 430–437, doi: 10.1016/j.rser.2009.07.028.

Q

Quan, X., M. Hoerling, J. Whitaker, G. Bates, and T. Xu, 2006: Diagnosing sources of US seasonal forecast skill. *Journal of Climate*, **19 (13)**, 3279–3293, doi: 10.1175/JCLI3789.1.

Quesada, B., R. Vautard, P. Yiou, M. Hirschi, and S. I. Seneviratne, 2012: Asymmetric European summer heat predictability from wet and dry southern winters and springs. *Nature Climate Change*, **2 (10)**, 736, doi: 10.1038/nclimate1536.

R

Raynaud, D., B. Hingray, B. Francois, and J. Creutin, 2018: Energy droughts from variable renewable sources in European climates. *Renewable Energy*, **125**, doi: 10.1016/j.renene.2018.02.130.

Reichler, T. and J. Kim, 2008: Uncertainties in the climate mean state of global observations, reanalyses, and the GFDL climate model. *Journal of Geophysical Research: Atmospheres*, **113 (D5)**, doi: 10.1029/2007JD009278.

Reyers, M., J. G. Pinto, and J. Moemken, 2015: Statistical–dynamical downscaling for wind energy potentials: evaluation and applications to decadal hindcasts and climate change projections. *International Journal of Climatology*, **35 (2)**, 229–244, doi: 10.1002/joc.3975.

Robertson, A. W., A. Kumar, M. Peña, and F. Vitart, 2015: Improving and promoting subseasonal to seasonal prediction. *Bulletin of the American Meteorological Society*, **96 (3)**, ES49–ES53, doi: 10.1175/BAMS-D-14-00139.1.

Rodriguez, D., P. de Voil, D. Hudson, J. Brown, P. Hayman, H. Marrou, and H. Meinke, 2018: Predicting optimum crop designs using crop models and seasonal climate forecasts. *Scientific reports*, **8 (1)**, 2231, doi: 10.1038/s41598-018-20628-2.

Rodríguez-Fonseca, B., et al., 2016: A review of ENSO influence on the North Atlantic. A non-stationary signal. *Atmosphere*, **7 (7)**, 87, doi: 10.3390/atmos7070087.

Rose, S. and J. Apt, 2016: Quantifying sources of uncertainty in reanalysis derived wind speed. *Renewable Energy*, **94**, 157–165, doi: 10.1016/j.renene.2016.03.028.

Royston, J., 1982: An extension of Shapiro and Wilk's W test for normality to large samples. *Applied Statistics*, **31 (2)**, 115–124, doi: 10.2307/2347973.

S

Saha, S., et al., 2014: The NCEP climate forecast system version 2. *Journal of Climate*, **27 (6)**, 2185–2208, doi: 10.1175/JCLI-D-12-00823.1.

Santos, J., C. Rochinha, M. Liberato, M. Reyers, and J. Pinto, 2015: Projected changes in wind energy potentials over Iberia. *Renewable Energy*, **75**, 68–80, doi: 10.1016/j.renene.2014.09.026.

Scaife, A., et al., 2014: Skillful long-range prediction of european and north american winters. *Geophysical Research Letters*, **41 (7)**, 2514–2519, doi: 10.1002/2014GL059637.

Scaife, A., et al., 2016: Seasonal winter forecasts and the stratosphere. *Atmospheric Science Letters*, **17 (1)**, 51–56, doi: 10.1002/asl.598.

Seager, R., N. Naik, M. Ting, M. A. Cane, N. Harnik, and Y. Kushnir, 2010: Adjustment of the atmospheric circulation to tropical Pacific SST anomalies: Variability of transient eddy propagation in the Pacific–North America sector. *Quarterly Journal of the Royal Meteorological Society*, **136 (647)**, 277–296, doi: 10.1002/qj.588.

Semenov, V. A. and M. Latif, 2015: Nonlinear winter atmospheric circulation response to Arctic sea ice concentration anomalies for different periods during 1966–2012. *Environmental Research Letters*, **10 (5)**, 054 020, doi: 10.1088/1748-9326/10/5/054020.

Shapiro, S. S. and M. B. Wilk, 1965: An analysis of variance test for normality (complete samples). *Biometrika*, **52 (3-4)**, 591–611, doi: 10.2307/2333709.

Shapiro, S. S. and M. B. Wilk, 1968: Approximations for the Null Distribution of the W Statistic. *Technometrics*, **10 (4)**, 861–866, doi: 10.1080/00401706.1968.10490638.

Shaw, T. A., et al., 2016: Storm track processes and the opposing influences of climate change. *Nature Geoscience*, **9**, 656–664, doi: 10.1038/ngeo2783.

Siegert, S., 2014: Variance estimation for brier score decomposition. *Quarterly Journal of the Royal Meteorological Society*, **140 (682)**, 1771–1777, doi: 10.1002/qj.2228.

Sigmond, M., J. Fyfe, G. Flato, V. Kharin, and W. Merryfield, 2013: Seasonal forecast skill of Arctic sea ice area in a dynamical forecast system. *Geophysical Research Letters*, **40 (3)**, 529–534, doi: 10.1002/grl.50129.

Sillmann, J., et al., 2017: Understanding, modeling and predicting weather and climate extremes: Challenges and opportunities. *Weather and climate extremes*, **18**, 65–74, doi: 10.1016/j.wace.2017.10.003.

Simmons, A. J., P. Poli, D. P. Dee, P. Berrisford, H. Hersbach, S. Kobayashi, and C. Peubey, 2014: Estimating low-frequency variability and trends in atmospheric temperature using ERA-Interim. *Quarterly Journal of the Royal Meteorological Society*, **140 (679)**, 329–353, doi: 10.1002/qj.2317.

Sinden, G., 2007: Characteristics of the UK wind resource: Long-term patterns and relationship to electricity demand. *Energy Policy*, **35 (1)**, 112–127, doi: 10.1016/j.enpol.2005.10.003.

Slingo, J. and T. Palmer, 2011: Uncertainty in weather and climate prediction. *Philosophical Transactions of the Royal Society of London A: Mathematical, Physical and Engineering Sciences*, **369 (1956)**, 4751–4767, doi: 10.1098/rsta.2011.0161.

Smith, D. M., S. Cusack, A. W. Colman, C. K. Folland, G. R. Harris, and J. M. Murphy, 2007: Improved surface temperature prediction for the coming decade from a global climate model. *Science*, **317 (5839)**, 796–799, doi: 10.1126/science.1139540.

Smith, D. M., A. A. Scaife, and B. P. Kirtman, 2012: What is the current state of scientific knowledge with regard to seasonal and decadal forecasting? *Environmental Research Letters*, **7 (1)**, 015 602, doi: 10.1088/1748-9326/7/1/015602.

Soares, M. B. and S. Dessai, 2016: Barriers and enablers to the use of seasonal climate forecasts amongst organisations in europe. *Climatic Change*, **137 (1-2)**, 89–103, doi: 10.1007/s10584-016-1671-8.

Solomon, S., 2007: *Climate change 2007-the physical science basis: Working group I contribution to the fourth assessment report of the IPCC*, Vol. 4. Cambridge University Press.

Staffell, I. and S. Pfenninger, 2016: Using bias-corrected reanalysis to simulate current and future wind power output. *Energy*, **114**, 1224–1239, doi: 10.1016/j.energy.2016.08.068.

Steinskog, D. J., D. B. Tjøstheim, and N. G. Kvamstø, 2007: A Cautionary Note on the Use of the Kolmogorov–Smirnov Test for Normality. *Monthly Weather Review*, **135 (3)**, 1151–1157, doi: 10.1175/MWR3326.1.

Sterl, A., A. M. Bakker, H. W. van den Brink, R. Haarsma, A. Stepek, I. L. Wijnant, and R. C. de Winter, 2015: Large-scale winds in the southern North Sea region: the wind part of the KNMI'14 climate change scenarios. *Environmental Research Letters*, **10 (3)**, 035 004.

Stockdale, T. N., D. L. Anderson, J. O. S. Alves, and M. A. Balmaseda, 1998: Global seasonal rainfall forecasts using a coupled ocean–atmosphere model. *Nature*, **392 (6674)**, 370, doi: 10.1038/32861.

Stockdale, T. N., F. Molteni, and L. Ferranti, 2015: Atmospheric initial conditions and the predictability of the Arctic Oscillation. *Geophysical Research Letters*, **42 (4)**, 1173–1179, doi: 10.1002/2014GL062681.

Stockdale, T. N., et al., 2011: ECMWF seasonal forecast system 3 and its prediction of sea surface temperature. *Climate Dynamics*, **37 (3)**, 455–471, doi: 10.1007/s00382-010-0947-3.

Stopa, J. E., K. F. Cheung, H. L. Tolman, and A. Chawla, 2013: Patterns and cycles in the Climate Forecast System Reanalysis wind and wave data. *Ocean Modelling*, **70**, 207–220, doi: 10.1016/j.ocemod.2012.10.005.

Street, R. B., 2016: Towards a leading role on climate services in europe: a research and innovation roadmap. *Climate Services*, **1**, 2–5, doi: 10.1016/j.cliser.2015.12.001.

Stryhal, J. and R. Huth, 2017: Classifications of winter Euro-Atlantic circulation patterns: an intercomparison of five atmospheric reanalyses. *Journal of Climate*, **30 (19)**, 7847–7861, doi: 10.1175/JCLI-D-17-0059.1.

T

Terrado, M., N. González-Reviriego, L. Lledó, V. Torralba, A. Soret, and F. J. Doblas-Reyes, 2017: Climate services for affordable wind energy. *WMO Bulletin*, **66 (2)**, URL https://public.wmo.int/en/resources/bulletin/climate-services-affordable-wind-energy.

Themeßl, M. J., A. Gobiet, and A. Leuprecht, 2011: Empirical-statistical downscaling and error correction of daily precipitation from regional climate models. *International Journal of Climatology*, **31 (10)**, 1530–1544, doi: 10.1002/joc.2168.

Thompson, D. W., M. P. Baldwin, and J. M. Wallace, 2002: Stratospheric connection to Northern Hemisphere wintertime weather: Implications for prediction. *Journal of Climate*, **15 (12)**, 1421–1428, doi: 10.1175/JCLI-D-15-0067.1.

Torralba, V., F. J. Doblas-Reyes, and N. Gonzalez-Reviriego, 2017a: Uncertainty in recent near-surface wind speed trends: a global reanalysis intercomparison. *Environmental Research Letters*, **12 (11)**, 114 019, doi: 10.1088/1748-9326/aa8a58.

Torralba, V., F. J. Doblas-Reyes, D. MacLeod, I. Christel, and M. Davis, 2017b: Seasonal climate prediction: A new source of information for the management of wind energy resources. *Journal of Applied Meteorology and Climatology*, **56 (5)**, 1231–1247, doi: 10.1175/JAMC-D-16-0204.1.

Trenberth, K. E., 1991: Storm tracks in the Southern Hemisphere. *Journal of the Atmospheric Sciences*, **48 (19)**, 2159–2178, doi: 10.1175/1520-0469(1991)048<2159:STITSH>2.0.CO;2.

Trenberth, K. E., 1997: The definition of el Niño. *Bulletin of the American Meteorological Society*, **78 (12)**, 2771–2777, doi: 10.1175/1520-0477(1997)078<2771:TDOENO>2.0.CO;2.

Trenberth, K. E., G. W. Branstator, D. Karoly, A. Kumar, N.-C. Lau, and C. Ropelewski, 1998: Progress during TOGA in understanding and modeling global teleconnections associated with tropical sea surface temperatures. *Journal of Geophysical Research: Oceans*, **103 (C7)**, 14 291–14 324, doi: 10.1029/97JC01444.

U

Ulbrich, U., J. G. Pinto, H. Kupfer, G. C. Leckebusch, T. Spangehl, and M. Reyers, 2008: Changing Northern Hemisphere storm tracks in an ensemble of IPCC climate change simulations. *Journal of Climate*, **21 (8)**, 1669–1679, doi: 10.1175/2007JCLI1992.1.

V

Vaillancourt, K., et al., 2014: A Canadian 2050 energy outlook: Analysis with the multi-regional model TIMES-Canada. *Applied Energy*, **132**, 56–65, doi: 10.1016/j.apenergy.2014.06.072.

Van den Dool, H., 1994: Searching for analogues, how long must we wait? *Tellus A*, **46 (3)**, 314–324, doi: 10.1034/j.1600-0870.1994.t01-2-00006.x.

Van den Dool, H., 2007: *Empirical methods in short-term climate prediction*. Oxford University Press.

Van Den Dool, H. M. and Z. Toth, 1991: Why do forecasts for "near normal" often fail? *Weather and forecasting*, **6 (1)**, 76–85, doi: 10.1175/1520-0434(1991)006<0076:WDFFNO>2.0.CO;2.

Van Oldenborgh, G. J., M. A. Balmaseda, L. Ferranti, T. N. Stockdale, and D. L. Anderson, 2005: Did the ECMWF seasonal forecast model outperform statistical ENSO forecast models over the last 15 years? *Journal of Climate*, **18 (16)**, 3240–3249, doi: 10.1175/JCLI3420.1.

Van Oldenborgh, G. J., F. J. Doblas-Reyes, B. Wouters, and W. Hazeleger, 2012: Decadal prediction skill in a multi-model ensemble. *Climate Dynamics*, **38 (7-8)**, 1263–1280, doi: 10.1007/s00382-012-1313-4.

Vaughan, C. and S. Dessai, 2014: Climate services for society: origins, institutional arrangements, and design elements for an evaluation framework. *Wiley Interdisciplinary Reviews: Climate Change*, **5 (5)**, 587–603, doi: 10.1002/wcc.290.

Vautard, R., 1990: Multiple weather regimes over the North Atlantic: Analysis of precursors and successors. *Monthly weather review*, **118 (10)**, 2056–2081, doi: 10.1175/1520-0493(1990)118<2056:MWROTN>2.0.CO;2.

Vautard, R., J. Cattiaux, P. Yiou, J.-N. Thépaut, and P. Ciais, 2010: Northern Hemisphere atmospheric stilling partly attributed to an increase in surface roughness. *Nature Geoscience*, **3 (11)**, 756–761, doi: 10.1038/ngeo979.

Vautard, R., F. Thais, I. Tobin, F.-M. Bréon, J.-G. D. de Lavergne, A. Colette, P. Yiou, and P. M. Ruti, 2014: Regional climate model simulations indicate limited climatic impacts by operational and planned European wind farms. *Nature communications*, **5**, doi: 10.1038/ncomms4196.

Vitart, F., 2004: Monthly forecasting at ECMWF. *Monthly Weather Review*, **132 (12)**, 2761–2779, doi: 10.1175/MWR2826.1.

Vitart, F., A. W. Robertson, and D. L. Anderson, 2012: Subseasonal to seasonal prediction project: Bridging the gap between weather and climate. *WMO Bulletin*, **61 (2)**, 23, URL https://public.wmo.int/en/resources/bulletin/subseasonal-seasonal-prediction-project-bridging-gap-between-weather-and-climate.

Von Storch, H., 1999: On the use of "inflation" in statistical downscaling. *Journal of Climate*, **12 (12)**, 3505–3506, doi: 10.1175/1520-0442(1999)012<3505:OTUOII>2.0.CO;2.

Von Storch, H. and F. W. Zwiers, 2002: *Statistical analysis in climate research*. Cambridge university press.

Vose, R. S., S. Applequist, M. J. Menne, C. N. Williams, and P. Thorne, 2012: An intercomparison of temperature trends in the U.S. Historical Climatology Network and recent atmospheric reanalyses. *Geophysical Research Letters*, **39 (10)**, 1–6, doi: 10.1029/2012GL051387.

W

Walker G.T., B. W., 1932: World weather v. *Memorial Royal Meteorological Society*, **4 (36)**, 53–84.

Wallace, J. M. and D. S. Gutzler, 1981: Teleconnections in the geopotential height field during the Northern Hemisphere winter. *Monthly Weather Review*, **109 (4)**, 784–812, doi: 10.1175/1520-0493(1981)109<0784:TITGHF>2.0.CO;2.

Walz, M. A., M. G. Donat, and G. C. Leckebusch, 2018: Large-Scale Drivers and Seasonal Predictability of Extreme Wind Speeds Over the North Atlantic and Europe. *Journal of Geophysical Research: Atmospheres*, **123 (20)**, 11–518, doi: 10.1029/2017JD027958.

Wang, C., C. Deser, J.-Y. Yu, P. DiNezio, and A. Clement, 2017a: *El Niño and southern oscillation (ENSO): a review*, 85–106. Springer, doi: 10.1007/978-94-017-7499-4_4.

Wang, L., M. Ting, and P. Kushner, 2017b: A robust empirical seasonal prediction of winter NAO and surface climate. *Scientific reports*, **7 (1)**, 279, doi: 10.1038/s41598-017-00353-y.

Weigel, A. P., M. Liniger, and C. Appenzeller, 2008: Can multi-model combination really enhance the prediction skill of probabilistic ensemble forecasts? *Quarterly Journal of the Royal Meteorological Society*, **134 (630)**, 241–260, doi: 10.1002/qj.210.

Weisheimer, A., S. Corti, T. Palmer, and F. Vitart, 2014: Addressing model error through atmospheric stochastic physical parametrizations: impact on the coupled ECMWF seasonal forecasting system. *Phil. Trans. R. Soc. A*, **372 (2018)**, 20130 290.

Weisheimer, A. and T. N. Palmer, 2014: On the reliability of seasonal climate forecasts. *Journal of The Royal Society Interface*, **11 (96)**, 20131 162, doi: 10.1098/rsif.2013.1162.

Weisheimer, A., T. N. Palmer, and F. J. Doblas-Reyes, 2011: Assessment of representations of model uncertainty in monthly and seasonal forecast ensembles. *Geophysical Research Letters*, **38 (16)**, doi: 10.1029/2011GL048123.

Wilks, D. S., 2011: *Statistical methods in the atmospheric sciences*, Vol. 100. Academic press.

WMO, 2017: Energy Exemplar to the User Interface Platform of the Global Framework for Climate Services. Tech. rep., World Meteorological Organization. URL http://www.wmo.int/gfcs/sites/default/files/Priority-Areas/Energy/GFCS_Energy%20Exemplar_JN17453.pdf.

WWEA, 2016: Wind Bulletin. Tech. rep., World Wind Energy Association. URL https://wwindea.org/wp-content/uploads/filebase/wwea_quaterly_bulletin/Bulletin_2_2016_reduced.pdf.

Y

Yang, X. and T. DelSole, 2012: Systematic comparison of ENSO teleconnection patterns between models and observations. *Journal of Climate*, **25 (2)**, 425–446, doi: 10.1175/JCLI-D-11-00175.1.

Yang, X., et al., 2015: Seasonal predictability of extratropical storm tracks in GFDL's high-resolution climate prediction model. *Journal of Climate*, **28 (9)**, 3592–3611, doi: 10.1175/JCLI-D-14-00517.1.

Yin, J. H., 2005: A consistent poleward shift of the storm tracks in simulations of 21st century climate. *Geophysical Research Letters*, **32 (18)**, 1–4, doi: 10.1029/2005GL023684.

Yiou, P., K. Goubanova, Z. X. Li, and M. Nogaj, 2008: Weather regime dependence of extreme value statistics for summer temperature and precipitation. *Nonlinear Processes in Geophysics*, **15 (3)**, 365–378, doi: 10.5194/npg-15-365-2008.

Young, I. R., J. Vinoth, S. Zieger, and A. V. Babanin, 2012: Investigation of trends in extreme value wave height and wind speed. *Journal of Geophysical Research: Oceans*, **117 (3)**, 1–13, doi: 10.1029/2011JC007753.

Young, I. R., S. Zieger, and A. V. Babanin, 2011: Global Trends in Wind Speed and Wave Height. *Science*, **332 (6028)**, 451–455, doi: 10.1126/science.1197219.

Z

Zebiak, S. E. and M. A. Cane, 1987: A Model El Niño-Southern Oscillation. *Monthly Weather Review*, **115 (10)**, 2262–2278, doi: 10.1175/1520-0493(1987)115<2262:AMENO>2.0.CO;2.

Zhao, M. and H. H. Hendon, 2009: Representation and prediction of the indian ocean dipole in the poama seasonal forecast model. *Quarterly Journal of the Royal Meteorological Society*, **135 (639)**, 337–352, doi: 10.1002/qj.370.

Zhao, T., J. C. Bennett, Q. Wang, A. Schepen, A. W. Wood, D. E. Robertson, and M.-H. Ramos, 2017: How Suitable is Quantile Mapping For Postprocessing GCM Precipitation Forecasts? *Journal of Climate*, **30 (9)**, 3185–3196, doi: 10.1175/JCLI-D-16-0652.1.

Zheng, C. W., J. Pan, and C. Y. Li, 2016: Global oceanic wind speed trends. *Ocean & Coastal Management*, **129 (667)**, 15–24, doi: 10.1016/j.ocecoaman.2016.05.001.

Zhou, Y. and S. J. Smith, 2013: Spatial and temporal patterns of global onshore wind speed distribution. *Environmental Research Letters*, **8 (3)**, 034 029, doi: 10.1088/1748-9326/8/3/034029.

Zhu, J., B. Huang, A. Kumar, and J. L. Kinter III, 2015: Seasonality in prediction skill and predictable pattern of tropical Indian Ocean SST. *Journal of Climate*, **28 (20)**, 7962–7984, doi: 10.1175/JCLI-D-15-0067.1.

Zubiate, L., F. McDermott, C. Sweeney, and M. O'Malley, 2017: Spatial variability in winter NAO–wind speed relationships in western Europe linked to concomitant states of the East Atlantic and Scandinavian patterns. *Quarterly Journal of the Royal Meteorological Society*, **143 (702)**, 552–562, doi: 10.1002/qj.2943.